Synthesis of onion-like nanocarbons from cooking oil for the adsorptive and photocatalytic removal of Cr(VI) and methyl orange from aqueous solutions

A thesis submitted to the faculty of science, at the University of the Witwatersrand, Johannesburg, in fulfilment of the requirements for the degree of Doctor of Philosophy

By: Themba Dominic Ntuli

Supervisor: Dr Manoko S. Maubane-Nkadimeng

Co-supervisors: Prof Neil J. Coville and Prof Edward N. Nxumalo

Johannesburg, 2022

Declaration

I declare that this thesis which I submit for the degree of Doctor of Philosophy in the University of the Witwatersrand, Johannesburg, is apart from the recognized assistance of my supervisor Dr M.S. Maubane-Nkadimeng, co-supervisors Prof N.J. Coville and Prof E.N. Nxumalo and my Erasmus Mundus mobility host Prof C Palet Ballús, my own, unaided work. It has not been submitted before for any degree or examination in any other institution.

Signed (Candidate)

On this 31 day of October 2022

Abstract

Rapid industrialization and urbanization have coincided with increased concentrations of organic and inorganic pollutants in wastewater. These include trace metal ions and dyes such as Cr(VI) ions and methyl orange, respectively. Such pollutants tend to bioaccumulate in living organisms, resulting in toxic effects for humans and biota alike and they should thus, be removed from water streams. Two of the common and widely applied technologies for the removal of pollutants from wastewater are adsorption and photocatalysis, typically using carbon materials. This is because carbonaceous materials can serve as adsorbents and/or support materials for semiconductor nanoparticles.

This study explores the use of onion-like nanocarbons (OLNCs) as the material of interest for the removal of pollutants in water. The synthesis of OLNCs was achieved by the flame pyrolysis of vegetable cooking oil (olive oil) and waste cooking oil. First, the OLNCs synthesized from olive oil and waste cooking oil were used as adsorbents for the removal of Cr (VI). It was found that the optimum condition for the removal of Cr(VI) ions took place at pH = 2 and C_O = 10 mg/L. The values found were t = 720 min and Q^0_{max} = 26.53 mg/g for the olive oil OLNCs and t = 360 min and Q^0_{max} = 47.62 mg/g for the waste cooking oil OLNCs. The improved removal of Cr(VI) ions by the OLNCs from waste cooking oil was attributed to increased surface oxygen moieties as a result of the oxygenation that took place during the cooking process. The removal mechanism for both adsorbents was consistent with the adsorption coupled reduction removal pathway as indicated by the presence of Cr(III) on the surface of the adsorbent and the presence of Cr(VI) ions in the solution. The experimental data followed the pseudo-second-order (PSO) model and the Langmuir adsorption isotherm. The OLNCs from waste cooking oil demonstrated higher adsorption efficiency than the OLNCs from olive oil, an indication of how waste material could be converted into a useful material.

Oxygen functional groups play a role in the surface adherence of chromium ions. Therefore, H_2O_2 and KOH were used as oxidizing agents for the OLNCs from olive oil. The OLNCs were chemically modified with 10% and 25% of H2O2 and 0.1 M and 0.2M of KOH respectively to improve their adsorption efficiency. Generally, the H_2O_2-treated adsorbents showed higher adsorption efficiency than the KOH-treated adsorbents. The Q^0_{max} values of the chemically modified adsorbents were significantly higher than

that of the unmodified OLNCs from olive oil (26.53 mg/g) but relatively lower than those of waste cooking oil (47.62 mg/g). The Freundlich adsorption isotherm fitted both adsorbents indicating heterogeneous surface coverage of the surface. The PSO kinetic model was followed by both adsorbents predicting the possible chemisorption mechanism.

TiO_2 is a well know and widely used photocatalyst, and to further explore the effect of OLNCs in photocatalysis, nanocomposites of OLCNs and TiO_2 nanoparticles (TiO_2/OLNCs) were prepared via hydrothermal synthesis. This was achieved by varying the mass of the OLNCs (10, 20, 30, and 50 mg) added to 100 mg of TiO_2. The materials were labelled as TC-10, TC-20, TC-30, and TC-50 corresponding to the OLNCs mass. The nanocomposites were then used as photocatalysts in the photocatalytic degradation of methyl orange (MO). It was found that the photocatalytic degradation rate of MO using the TiO_2/OLNCs was more rapid than TiO_2 alone in this order TC-10 > TC-20 > TC-30 >TC-50.

The waste cooking oil OLNCs were also used as a support material for iron oxide nanoparticles to form iron oxide/OLNCs nanocomposite. The mass of the OLNCs was varied as follows (25, 50, 100, and 170 mg) the materials were labelled FeC-25, FeC-50, FeC-100, and FeC-170. The nanocomposites were then used as photocatalysts for the photocatalytic reduction of Cr(VI) ions to Cr(III) ions. The reduction of Cr(VI) ions to Cr(III) ions was rapid, taking place in the first 15 min. This was followed by subsequent adsorption of the Cr(III) ions through the carbonyl groups of the nanocomposite.

Overall the results showed that the flame pyrolysis method was successfully used to convert vegetable cooking oil to carbon nanomaterials (OLNCs). The OLNCs showed promise in the removal of Cr(VI) and (MO). The results are comparable with other carbon nanomaterials, an indication that the as-synthesized OLNCs have potential applications in adsorption, reduction and photocatalysis.

Dedication

I dedicate this work to the following people

My parents Mr Malevu P. Ntuli and Mrs Zodwa V. Ntuli

My brothers Sibusiso M. Ntuli and Mthobisi W. Ntuli

My sister Thabile G. Ntuli

Motho-Waka Ms Matsie E. Mofokeng

To the Zulu (Mom’s side) and the Ntuli (Dad’s side) families

To those who walked with us and now no are more, you shall never be forgotten

Maye Simakadze mukhulu

Acknowledgements

I would like to thank the University of the Witwatersrand, the DSI-NRF Centre of Excellence in Strong Materials (CoESM), the National Research Foundation of South Africa (Grant number: 138075 and number: 99196), Universitat Autònoma de Barcelona, Spanish research projects (Grant number: CTM2015-65414-C2-1-R and number: AGL2015-70393-R), the Erasmus+ KA107 mobility grant, Microscopy and Microanalysis Unit (MMU) at the University of the Witwatersrand, and the Instituto de Ciencia de Materiales de Barcelona (ICMAB-CSIC) for my studies.

I am grateful for the opportunities that have directly resulted in me being where I am at this stage and thank you to everyone that played a part. Others are no longer alive to witness what their contribution has led to. Their memories will live with me forever. I would like to thank my parents, brothers and sister (Mr Malevu Ntuli and Mrs Zodwa Ntuli, Sibusiso Ntuli, Mthobisi Ntuli and Thabile Ntuli for all your sacrifices, encouragement, and never-ending support. To every member of the Zulu and Ntuli family ngibonga angiwuvali umlomo bo Mageba nani Mazingili.

Dr MS Maubane-Nkadimeng, words fail me in showing my gratitude for what you have done, at a time when I almost gave up you were there as a beacon of light. As a supervisor, you were incredible and thank you for the freedom of going through the maze without being forced into doing what I did not want to do. Thank you for introducing me to Prof NJ Coville and Prof EN Nxumalo as co-supervisors. It is a humbling experience to have had the unique experience of drinking from the well of knowledge flowing from the river of my supervision team. As I set on the bank's principles of chemistry and solving everyday problems come to life. Truly a once in a lifetime experience one that will stay with me for aeons to come. To my supervisors thank you for the time and knowledge shared with me, ‘ut diu permanere’ long may it continue.

I would like to thank Mr Siyasanga Mpelane (University of Johannesburg, Auckland Park) for the high-magnification TEM analysis and Mr Patrick Nguyen (Vaal University of Technology) for the AAS analysis. To the members of the CATMAT and CarboCatalysis, groups at Wits and GTS group at Universitat Autònoma de Barcelona to mention a few, Mr LL Sikeyi, Dr TH Mongwe, and Dr TP Mofokeng thank you for the inputs, outputs, a continual exchange of ideas, and science communications.

To Prof Cristina Palet Ballus my host at Universitat Autònoma de Barcelona, thank you for your contribution and the extra mile to ensure that my stay at UAB was not only productive but enjoyable. To the Alliance church in Barberton, the Seventh-day Adventist church in Barberton and the Seventh-day Adventist church student movement at Wits thank you for the invaluable fellowship.

A special mention to ‘Motho-Waka’ Ms Matsie Mofokeng thank you so much for being there for me more than most you know the depths of what I went through to be at this point now. Our studies have been the central point in our relationship and brought us even closer, thank you for your patience, and never-ending support wayawaya.

To everyone in Barberton ‘Barberton forever we shall not be moved just like the tree standing on the waterside we shall not be moved at the foot of the Makhonjwa mountains we shall not be moved’ Magenge thank you so much, dreams do come true

All the glory to the almighty God, Jesus Christ the Lord of the Sabbath

A luta continua

Research outputs

Publications

Published manuscript

1. Ntuli, T.D., Mongwe, T.H., Sikeyi, L.L., Mkhari, O., Coville, N.J., Nxumalo, E.N. and Maubane-Nkadimeng, M.S. **(2021) '**Removal of hexavalent chromium via an adsorption coupled reduction mechanism using olive oil derived carbon nano-onions', *Environmental Nanotechnology, Monitoring & Management.* **16**, pp. 1-8

   Author contribution

   T.D. Ntuli: Conceptualization, Methodology, Writing – original draft, Investigation, Formal analysis, Writing - review & editing. T.H. Mongwe: Data curation, Formal analysis, Investigation. L.L. Sikeyi: Data curation, Formal analysis, Investigation. O. Mkhari: Data curation, Formal analysis, Investigation. N.J. Coville: Supervision, Resources, Writing - review & editing. E.N. Nxumalo: Supervision, Resources, Writing - review & editing, Software, Validation. M.S. Maubane-Nkadimeng: Conceptualization, Supervision, Resources, Project adminis- tration, Writing - review & editing.

Submitted manuscript

1. Themba D. Ntuli, Ludwe L. Sikeyi, Thomas H. Mongwe, Orlette Mkhari, Neil J. Coville, Edward N. Nxumalo, Manoko S. Maubane-Nkadimeng **(2022)** 'From waste cooking oil to oxygen-rich onion-like nanocarbons for the removal of hexavalent chromium from aqueous solution', *South African Journal of Science*. **Ref: SAJS 14006**

Manuscript to be submitted

1. Themba D. Ntuli, Ludwe L. Sikeyi, Thomas H. Mongwe, Orlette Mkhari, Neil J. Coville, Edward N. Nxumalo, Manoko S. Maubane-Nkadimeng **(2022)** *'Oxygen functionalized onion-like nanocarbons for the sequestration of hexavalent chromium from aqueous solutions'*

2. T.D. Ntuli, L.L. Sikeyi, F. Dziike, N.J. Coville, E.N. Nxumalo, M.S. Maubane-Nkadimeng **(2022)** '*Photocatalytic degradation of methyl orange by onion-like nanocarbon/TiO_2 nanocomposites under solar radiation'*

3. T.D. Ntuli, L.L. Sikeyi, T.H. Mongwe, O. Mkhari, C. Palet, N.J. Coville, E.N. Nxumalo, M.S. Maubane-Nkadimeng **(2022)** '*Rapid removal of Cr(VI) and Cr(III) via adsorption coupled photoreduction systems using iron oxide/onion-like nanocarbon composites'*

Manuscripts from collaborations with similar materials (OLNCs)

1. Sikeyi, L. L., **Ntuli, T. D**., Mongwe, T. H., Maxakato, N. W., Coville, N. J. and Maubane-Nkadimeng, M. S. **(2022)** 'Platinum Nanoparticles Loaded on Pristine and Boron Oxide Modified Carbon Nano-Onions for Enhanced Ammonia Electrooxidation in Alkaline Direct Ammonia Fuel Cells'. Journal of Electroanalytical Chemistry. **917**, pp. 1-12

2. Mongwe, T. H., **Ntuli, T. D**., Sikeyi, L. L., Coville, N. J., Mamo, M. A., Serbena, José P. M. and Maubane-Nkadimeng, M. S. **(2022)** 'The use of ex-situ nitrogen-doped olive oil-derived carbon nano-onions for application in chemi-resistive gas sensors to detect acetone at room temperature, *South African Journal of Chemistry*. **76**, pp. 38-48

3. Mkhari, O., **Ntuli, T. D**., Coville, N. J., Nxumalo, E. N. and Maubane-Nkadimeng, M. S. **(2021)** 'A comparison of fluorescent N-doped carbon dots supported on the surface of hollow and solid carbon spheres, and solid silica spheres'. *Diamond and Related Materials.* **118**, pp. 1-11

4. Sikeyi, L. L., **Ntuli, T. D**., Mongwe, T. H., Maxakato, N. W., Carleschi, E. D., Bryan P., Coville, N. J. and Maubane-Nkadimeng, M. S. **(2021)** 'Microwave assisted synthesis of nitrogen doped and oxygen functionalized carbon nano onions supported palladium nanoparticles as hybrid anodic electrocatalysts for direct alkaline ethanol fuel cells', *International Journal of Hydrogen Energy*. **46**, pp. 10862-10875

My contribution to each collaboration was data curation, formal analysis and investigation.

Manuscript from other collaborations

1. Nchoe, O.B., **Ntuli, T.D**., Klink, M.J., Mtundzi, F.M. and Pakade, V.E. **(2020)** 'A comparative study of acid, base and Fenton-like reagent treated biomass for Cr(VI) sequestration from aqueous solutions', *Water Environment Research*. **93**, pp. 370-383

My contribution - Data curation, formal analysis and investigation.

Presentations

1. Ntuli, T.D., Coville, N.J., Nxumalo, E.N., Maubane-Nkadimeng, M.S. Adsorptive removal of hexavalent chromium from wastewater using carbon nano-onions, Wits 10th Cross Faculty Postgraduate Symposium, 2019, September, The University of the Witwatersrand, Johannesburg, South Africa. *Oral presentation (*3rd position best presenter)

2. Ntuli, T.D., Coville, N.J., Nxumalo, E.N., Maubane-Nkadimeng, M.S. Adsorptive removal of hexavalent chromium from wastewater using carbon nano-onions, Wits 10th Faculty of Science Postgraduate Symposium, 2019, September, The University of the Witwatersrand, Johannesburg, South Africa. *Oral presentation* (2nd position best presenter)

3. Ntuli, T.D., Mongwe, T.H., Coville, N.J., Nxumalo, E.N., Maubane-Nkadimeng, M.S. The Annual CoE-SM/AMSEN Student Presentation Workshop, 2019, May, The University of the Witwatersrand, Johannesburg, South Africa. *Poster presentation.*

4. Ntuli, T.D., Coville, N.J., Nxumalo, E.N., Maubane-Nkadimeng, M.S. Class in session 'carbon nanomaterials?', FameLab South Africa, Wits regional finals, 2020, February, British Council South Africa Events, Johannesburg, South Africa. *Oral presentation* (2nd position best presenter)

5. Ntuli, T.D., Coville, N.J., Nxumalo, E.N., Maubane-Nkadimeng, M.S. Class freshwater for all, FameLab South Africa, National semifinals, 2020, February, British Council South Africa Events, Johannesburg, South Africa. *Oral presentation*

6. Themba D. Ntuli, Ludwe L. Sikeyi, Thomas H. Mongwe, Orlette Mkhari, Neil J. Coville, Edward N. Nxumalo, Manoko S. Maubane-Nkadimeng. Closing the gap between waste and value, 10th NYRS-2020/21 National symposium, 2021, October, The University of the Witwatersrand, Johannesburg, South Africa. *Oral presentation*

7. Ntuli, T.D., Coville, N.J., Nxumalo, E.N., Maubane-Nkadimeng, M.S. Engineering of carbon nanomaterials for the removal of pollutants in water, Wits Science Slam, 2019, 29 July to 2 August, The University of the Witwatersrand, Johannesburg, South Africa. *Oral presentation*

8. Ntuli, T.D., Mongwe, T.H., Coville, N.J., Nxumalo, E.N., Maubane-Nkadimeng, M.S. Carbon quantum dots from sucrose for the detection of Cr(VI) ions from aqueous solution, NANOSMAT international conference, 2018, November, The University of South Africa, Somerset west, Cape Town, South Africa. *Poster presentation*

9. Themba D. Ntuli, Ludwe L. Sikeyi, Thomas H. Mongwe, Orlette Mkhari, Neil J. Coville, Edward N. Nxumalo, Manoko S. Maubane-Nkadimeng. One man's waste is another man's treasure, Wits 12th Cross Faculty Postgraduate Symposium, 2022, May. The University of the Witwatersrand, Johannesburg, South Africa. *Oral presentation.* (3rd position best presenter)

10. Ntuli, T.D., Coville, N.J., Nxumalo, E.N., Maubane-Nkadimeng, M.S. Adsorption coupled photocatalytic systems for the removal of organic and inorganic binary mixers, using carbon dot Materials functionalized with ionic liquids. Proposal presentation, 2018, May, CATMAT weekly seminars, Wits, Johannesburg, South Africa. *Oral presentation*

11. Ntuli, T.D., Coville, N.J., Nxumalo, E.N., Maubane-Nkadimeng, M.S. What's with the onions? Well, they can remove heavy metals from solutions, Exit talk, 2022, April, The University of the Witwatersrand, Johannesburg, South Africa. *Oral presentation*

12. Ntuli, T.D., Mongwe, T.H., Sikeyi, L.L., Mkhari, O., Coville, N.J., Nxumalo, E.N. and Maubane-Nkadimeng, M.S. 'Removal of hexavalent chromium via an adsorption coupled reduction mechanism using olive oil derived carbon nano-onions', 8th NanoAfrica conference, 2022, October, The University of South Africa, Somerset west, Cape Town, South Africa. *Oral presentation*

13. Ntuli, T.D., Sikeyi, L.L., Coville, N.J., Nxumalo, E.N. and Maubane-Nkadimeng, M.S. 'From waste to value: The use of waste cooking oil as a starting material for the synthesis of onion-like nanocarbons for the photocatalytic degradation of methyl orange', 32nd CATSA international conference, 2022, November, The University of the Witwatersrand, Central Drakensberg, KwaZulu Natal, South Africa. *Oral presentation*

Awards

1. **3rd positions** oral presenter at Wits 10th Cross Faculty Postgraduate Symposium, 2019
2. **2nd position** oral presenter at Wits 10th Faculty of Science Postgraduate Symposium, 2019
3. **2nd position** oral presenter at FameLab South Africa regional finals 2020
4. **3rd position** oral presenter at Wits 12th Cross Faculty Postgraduate Symposium, 2022,

5. DSI-NRF Centre of Excellence in Strong Materials (CoESM), **bursary**
6. Erasmus+ KA107 mobility grant **scholarship**

Visits

3 months at the Universitat Autònoma de Barcelona, Barcelona, Spain. Hosted by Prof Cristina Palet under GTS Research Group, Department of Chemistry, and Faculty of Science. From 16 September 2021 to 25 December 2021.

Contents

List of figures

List of Tables

Chapter 1: *Background*

Chapter 1 presents the background and the introduction of the key concepts of the study. Those concepts include trace metal and dye pollution of water streams due to inadequate disposal. This includes the effects of the presence of such pollutants in water streams. Different methods of pollutant removal are outlined culminating in adsorption and photocatalysis being the chosen removal methods for this study. The problem statement, motivation of the study, aim and objectives are also presented.

1.1. Introduction

The past decade has seen a rise in the concentration of heavy metals and dyes in freshwater streams. This can be linked to the poor disposal of heavy metals and dyes associated with increased industrialization and urbanization [1]. Industries that produce heavy metals and dyes in large quantities comprise but are not limited to mining [2], lather tanning [3], textile [4], steel production [5] and electrochemical industries [6]. These anthropogenic activities result in heavy metals and dyes such as Cr(VI), Cu(II), Ni(II) and methyl orange (MO) finding their way to the food and water sources leading to human and animal ingestion. These pollutants are toxic and carcinogenic even at trace concentrations. The aforementioned pollutants have a slow bio-accumulation rate making them accumulate in living organisms [7,8]. Consequently, they must be removed or reduced from freshwater streams before they get disposed of from industrial effluent.

Several technologies have been developed over the years to remediate heavy metals and dyes from aqueous systems. These technologies include chemical precipitation [9], ion–exchange [10], photocatalysis [11], membrane technology [11] and adsorption [12]. Though the methods can remove pollutants and offer a variety and suitable

operation conditions they have shortcomings such as the high volume of chemicals used and the high consumption of electricity and the generation of secondary toxins [13]. Nevertheless, the adsorption technique comes with the advantage of using adsorbents that are abundantly obtainable. Adsorbents such as agricultural waste [14], as well as natural and synthetic polymers [15], have been used and the common denominator with the mentioned adsorbents is that they are carbonaceous materials. Due to their carbonaceous nature, they provide an opportunity to modify the surface of the adsorbent. This means their adsorption capacity can be improved through chemical [16] and physical modification [17].

Equivalent to the use of carbonaceous materials, nanomaterials such as CuO, ZnO, and MgO have also been used as adsorbents since the emergence of nanoscience and nanotechnology [18]. Nanomaterials come with the advantage of smaller sizes and unique chemical and physical properties [19]. However, the challenge with these traditional nanomaterials is that they are predominantly synthesized from heavy metal salts as precursors. Conversely, these materials have been reported to leach into the environment thus, resulting in the contamination of freshwater streams [20]. Carbon nanomaterials such as carbon nanotubes CNTs [21], carbon nanofibers (CNFs) [22], carbon nanodiamonds [23] and fullerenes [24] have found use in the removal of heavy metals and dyes from different water streams. In the family of fullerenes, carbon nano-onions (CNOs) are a type of carbon nanomaterial that has gained attraction. They have a quasi-spherical morphology with several layers, they consist of sp^2 graphene sheets organisation in like manner to an onion thus, their name [25]. Different authors give CNOs various names such as carbon onions [26], cross-linked nano-onions [27], onion-like carbon [28], hollow carbon nanospheres [29], and carbon multi-cages [30]. In this study, they will be referred to as onion-like nanocarbons (OLNCs). This material

has in this study been explored for its potential to be used in the removal of trace metals and dyes.

The OLNCs originated with striking physical and chemical properties such as quasi-spherical morphology, concentric graphene layers, organic functional groups and tuneable solubility [31]. Due to such properties, the use of OLNCs as potential adsorbents for heavy metals has been reported by many authors [32,33]. Methods of synthesizing OLNCs include electron–beam irradiation of carbon soot [34], annealing of nanodiamonds [35], arc-discharge [36], chemical vapour deposition [37], laser irradiation [38] and pyrolysis [39].

The literature on using OLNCs as adsorbents for heavy metals and dyes is not extensive. Therefore, the current work seeks to expand the body of knowledge of OLNCs in terms of pyrolysis synthesis, modification of surface functional groups via chemical modification and application in the removal of Cr(VI), Cu(II), Ni(II), and methyl orange from aqueous solutions. This is because the metal plating industry usually has Cr(VI), Cu(II), and Ni(II) in their effluent [40] and the textile industry generates Cr(VI) and methyl orange to name but a few examples, in effluent streams [41]. Thus, the removal of Cr(VI) in the presence of the aforementioned cations and anions is an important problem. The adsorption method typically has a low adsorption capacity and incomplete removal of pollutants. The OLNCs were incorporated with TiO_2 and iron oxide nanoparticles to form nanocomposites that were applied as photocatalysts for the removal of Cr(VI) ions and methyl orange.

1.2. Problem statement

The increasing concentration levels of heavy metals and dyes are proving to be persistent and contributing to the decreasing availability of freshwater. The adsorption

method has been developed to remedy the situation. However, the use of abundantly available adsorbents such as agricultural waste, and natural and synthetic polymers has shown that such materials come with shortcomings such as incomplete removal and leaching of organic compounds which results in the creation of secondary pollutants. This has led to the use of nanomaterials such as metal oxides as alternative adsorbents. These materials work best when they are in combination with carbon-rich materials to form composites. The use of such materials has improved the removal of pollutants but issues of incomplete removal and the generation of secondary toxic sludge through the leaching of metallic nanomaterials persist. Independently photocatalysis has been used to mitigate the presence of trace metals and dyes in solutions. Metal oxide nanoparticles have been applied as a photocatalyst, however, their lack of adsorption sites requires an extended amount of time for expectable removal percentages. In this study, we propose the use of nanocomposites synthesized by the addition of carbon-rich materials in the form of OLNCs and metal oxide nanoparticles such as anatase TiO_2 and iron oxide. To be used as adsorbents/photocatalysts in the removal of Cr(VI) and MO. Therefore, exploring the use of the carbonyl functional groups present on the surface of the OLNCs. This could provide an opportunity to take advantage of this carbon nanomaterial's adsorption sites and the photocatalytic ability of the metal oxide could prove fruitful in the removal of Cr(CVI) and MO from solutions. The chemical modification of the OLNCs is anticipated to mitigate the leaching of organic compounds and prevent the generation of toxic sludge.

1.3. The motivation for the study

The removal of heavy metals and dyes from water bodies remains a widespread challenge in the 21st century [42]. At present, there is a comprehensive range of adsorbents that are used ranging from chemically modified agricultural waste materials, and polymers, to sophisticated nanocomposite materials [43].

It has been proposed that the chemical modification of OLNCs presents an exciting methodology for enhancing the chemical and physical properties of the synthesized OLNCs [46]. The improved OLNCs are anticipated to result in increased adsorption capacity and not leach organic compounds into the solution. In this study, the removal and degradation of heavy metals and dyes will be investigated. The selected pollutants (Cr(VI), and methyl orange) have been chosen because they are used in combination with Cr(VI) industries such as steel, electroplating [47] and leather tanning industry [48] and therefore, are most likely to be in a single matrix in industrial wastewater. The use of OLNCs as an adsorbent for Cr(VI) ions is not widely available. However, researchers such as Sakulthaew et al. [33] and Ko et al. [32] have used similar materials to remove Cr(VI) ions. What was not presented in their studies was how the removal of Cr(VI) ions is affected by the presence of cationic and anionic dyes and the used materials were not chemically modified with milder chemicals than H_2SO_4 a strong acid used by Ko et al. [32]. It is for this reason that the current study was conducted. This study used a readily available carbon source for the synthesis of OLNCs to study the removal of Cr(VI) and methyl orange in singular and multiple matrices. A removal mechanism, in the presence of competing ions from dyes was determined. Further, the exploration of multiple ions was studied using Cu(II) and Ni(II) since they are found in matrix with Cr(VI) in the steel and electroplating industry.

1.4. Aim

This study aims to synthesize OLNCs from vegetable cooking oil via flame pyrolysis for the adsorptive and photocatalytic removal of Cr(VI) and methyl orange from aqueous solutions.

1.5. Objectives

The objectives of the study were as follows:

i. Synthesis of OLNCs from olive oil and waste cooking oil using the flame pyrolysis technique.
ii. The synthesized OLNCs were chemically modified with different concentrations of H_2O_2 and KOH followed by subsequent characterisation with conventional techniques.
iii. Application of OLNCs in the adsorption process by varying adsorption conditions such as pH, contact time, initial concentration, adsorbent mass and temperature.
iv. Equilibrium studies such as adsorption isotherms, kinetic modelling and thermodynamics will be conducted.
v. Synthesizing TiO_2/ OLNCs and iron oxide/ OLNCs nanocomposites to be used in the photocatalytic degradation of methyl orange and photocatalytic reduction of Cr(VI) ions.
vi. Adsorbent/photocatalyst regeneration studies.

The synthesized materials will be characterised using various techniques such as Fourier transform infrared (FTIR) spectroscopy, thermogravimetric analysis (TGA), BET analysis, carbon, hydrogen, nitrogen and sulphur (CHNS) analysis, Raman spectroscopy, ultraviolet-visible (UV-visible) spectroscopy, scanning electron

microscopy (SEM), transition electron microscopy (TEM) and X-ray photoelectron spectroscopy (XPS).

1.6. References

[1] G. Huang, M. Zhang, C. Liu, L. Li, Z. Chen, Heavy metal(loid)s and organic contaminants in groundwater in the Pearl River Delta that has undergone three decades of urbanization and industrialization: Distribution, sources, and driving force, Sci. Total Environ. 635 (2018) 913–925.

[2] R. Akhbarizadeh, M.R. Shayestefar, E. Darezereshki, Konkurrierende Entfernung von Metallen aus Abwasser mit Hilfe von Maghemit- Nanopartikeln: Ein Vergleich zwischen künstlichem Abwasser und Sauerwasser, Mine Water Environ. 33 (2014) 89–96. https://doi.org/10.1007/s10230-013-0255-3.

[3] G. Lofrano, S. Meriç, G.E. Zengin, D. Orhon, Chemical and biological treatment technologies for leather tannery chemicals and wastewaters: A review, Sci. Total Environ. 461–462 (2013) 265–281. https://doi.org/10.1016/j.scitotenv.2013.05.004.

[4] N. Halimoon, S. Yin, Rachel, Goh, Removal of Heavy Metals from Textile Wastewater using Zeolite, EnvironmentAsia. 3 (2014) 124–130.

[5] Y. Tong, Q. Zhang, J. Cai, C. Gao, L. Wang, P. Li, Water consumption and wastewater discharge in China’s steel industry, Ironmak. Steelmak. 45 (2018) 868–877. https://doi.org/10.1080/03019233.2018.1538180.

[6] M. Sala, M.C. Gutiérrez-Bouzán, Electrochemical treatment of industrial wastewater and effluent reuse at laboratory and semi-industrial scale, J. Clean. Prod. 65 (2014) 458–464. https://doi.org/10.1016/j.jclepro.2013.08.006.

[7] P. Mahadappa, N. Krishnaswamy, M. Karunanidhi, A.G. Bhanuprakash, B. V. Bindhuja, S. Dey, Effect of plastic foreign body impaction on rumen function and heavy metal concentrations in various body fluids and tissues of buffaloes, Ecotoxicol. Environ. Saf. 189 (2020) 1–9. https://doi.org/10.1016/j.ecoenv.2019.109972.

[8] F. Yu, C. Yang, Z. Zhu, X. Bai, J. Ma, Adsorption behavior of organic pollutants and metals on micro/nanoplastics in the aquatic environment, Sci. Total Environ. 694 (2019) 1–11. https://doi.org/10.1016/j.scitotenv.2019.133643.

[9] Q. Chen, Y. Yao, X. Li, J. Lu, J. Zhou, Z. Huang, Comparison of heavy metal removals from aqueous solutions by chemical precipitation and characteristics of precipitates, J. Water Process Eng. 26 (2018) 289–300. https://doi.org/10.1016/j.jwpe.2018.11.003.

[10] S.M. Hosseini, H. Alibakhshi, E. Jashni, F. Parvizian, J.N. Shen, M. Taheri, M. Ebrahimi, N. Rafiei, A novel layer-by-layer heterogeneous cation exchange membrane for heavy metal ions removal from water, J. Hazard. Mater. 381 (2020). https://doi.org/10.1016/j.jhazmat.2019.120884.

[11] K. Santha kumar, B. Vellaichamy, T. Paulmony, Visible light active metal-free photocatalysis: N-doped graphene covalently grafted with g-C_3N_4 for highly robust degradation of methyl orange, Solid State Sci. 94 (2019) 99–105. https://doi.org/10.1016/j.solidstatesciences.2019.06.003.

[12] N.D. Shooto, E.B. Naidoo, M. Maubane, Sorption studies of toxic cations on ginger root adsorbent, J. Ind. Eng. Chem. 76 (2019) 133–140. https://doi.org/10.1016/j.jiec.2019.02.027.

[13] H. Qin, T. Hu, Y. Zhai, N. Lu, J. Aliyeva, The improved methods of heavy metals

removal by biosorbents: A review, Environ. Pollut. 258 (2020). https://doi.org/10.1016/j.envpol.2019.113777.

[14] M. Moyo, V.E. Pakade, S.J. Modise, Biosorption of lead(II) by chemically modified Mangifera indica seed shells: Adsorbent preparation, characterization and performance assessment, Process Saf. Environ. Prot. 111 (2017) 40–51. https://doi.org/10.1016/j.psep.2017.06.007.

[15] V. Pakade, L. Chimuka, Polymeric sorbents for removal of Cr(VI) from environmental samples, 85 (2013) 2145–2160.

[16] M. Lesaoana, R.P.V. Mlaba, F.M. Mtunzi, M.J. Klink, P. Edijike, V.E. Pakade, Influence of inorganic acid modification on Cr(VI) adsorption performance and the physicochemical properties of activated carbon, South African J. Chem. Eng. 28 (2019) 8–18. https://doi.org/10.1016/j.sajce.2019.01.001.

[17] L. Zhang, J. Pan, L. Liu, K. Song, Q. Wang, Combined physical and chemical activation of sludge-based adsorbent enhances Cr(Ⅵ) removal from wastewater, J. Clean. Prod. 238 (2019). https://doi.org/10.1016/j.jclepro.2019.117904.

[18] S. Wadhawan, A. Jain, J. Nayyar, S.K. Mehta, Role of nanomaterials as adsorbents in heavy metal ion removal from waste water: A review, J. Water Process Eng. 33 (2020). https://doi.org/10.1016/j.jwpe.2019.101038.

[19] A. Jawed, V. Saxena, L.M. Pandey, Engineered nanomaterials and their surface functionalization for the removal of heavy metals: A review, J. Water Process Eng. 33 (2020) 101009. https://doi.org/10.1016/j.jwpe.2019.101009.

[20] Y. Zhu, X. Liu, Y. Hu, R. Wang, M. Chen, J. Wu, Y. Wang, S. Kang, Y. Sun, M.

Zhu, Behavior, remediation effect and toxicity of nanomaterials in water environments, Environ. Res. 174 (2019) 54–60. https://doi.org/10.1016/j.envres.2019.04.014.

[21] M. Chandrashekhar Nayak, A.M. Isloor, Inamuddin, B. Lakshmi, H.M. Marwani, I. Khan, Polyphenylsulfone/multiwalled carbon nanotubes mixed ultrafiltration membranes: Fabrication, characterization and removal of heavy metals Pb^{2+}, Hg^{2+}, and Cd^{2+} from aqueous solutions, Arab. J. Chem. 13 (2019) 4661–4672. https://doi.org/10.1016/j.arabjc.2019.10.007.

[22] P.S. Kumar, K. Venkatesh, E.L. Gui, S. Jayaraman, G. Singh, G. Arthanareeswaran, Electrospun carbon nanofibers/TiO_2-PAN hybrid membranes for effective removal of metal ions and cationic dye, Environ. Nanotechnology, Monit. Manag. 10 (2018) 366–376. https://doi.org/10.1016/j.enmm.2018.08.006.

[23] V. Vatanpour, E. Salehi, N. Sahebjamee, M. Ashrafi, Novel chitosan/polyvinyl alcohol thin membrane adsorbents modified with detonation nanodiamonds: Preparation, characterization, and adsorption performance, Arab. J. Chem. 13 (2020) 1731–1740. https://doi.org/10.1016/j.arabjc.2018.01.010.

[24] S.S. Rikame, A.A. Mungray, A.K. Mungray, Synthesis, characterization and application of phosphorylated fullerene/sulfonated polyvinyl alcohol (PFSP) composite cation exchange membrane for copper removal, Sep. Purif. Technol. 177 (2017) 29–39. https://doi.org/10.1016/j.seppur.2016.12.011.

[25] V. Dhand, M. Yadav, S.H. Kim, K.Y. Rhee, A comprehensive review on the prospects of multi-functional carbon nano onions as an effective, high-performance energy storage material, Carbon N. Y. 175 (2021) 534–575.

https://doi.org/10.1016/j.carbon.2020.12.083.

[26] J.K. McDonough, Y. Gogotsi, Carbon onions: Synthesis and electrochemical applications, Electrochem. Soc. Interface. 22 (2013) 61–66. https://doi.org/10.1149/2.F05133if.

[27] L. Hultman, S. Stafström, Z. Czigány, J. Neidhardt, N. Hellgren, I.F. Brunell, K. Suenaga, C. Colliex, Cross-Linked Nano-onions of Carbon Nitride in the Solid Phase: Existence of a Novel $C_{48}N_{12}$ Aza-Fullerene, Phys. Rev. Lett. 87 (2001) 225503-225503–4. https://doi.org/10.1103/PhysRevLett.87.225503.

[28] D. Satyabola, T. Ahuja, S. Bose, B. Mondal, P. Srikrishnarka, M.P. Kannan, B.K. Spoorthi, T. Pradeep, Transformation of Nanodiamonds to Onion-like Carbons by Ambient Electrospray Deposition, J. Phys. Chem. C. 125 (2021) 10998–11006. https://doi.org/10.1021/acs.jpcc.1c00166.

[29] F. Xu, Z. Tang, S. Huang, L. Chen, Y. Liang, W. Mai, H. Zhong, R. Fu, D. Wu, Facile synthesis of ultrahigh-surface-area hollow carbon nanospheres for enhanced adsorption and energy storage, Nat. Commun. 6 (2015). https://doi.org/10.1038/ncomms8221.

[30] M. V. Diudea, A. Bende, C.L. Nagy, Carbon multi-shell cages, Phys. Chem. Chem. Phys. 16 (2014) 5260–5269. https://doi.org/10.1039/c3cp55309d.

[31] O. Mykhailiv, H. Zubyk, M.E. Plonska-Brzezinska, Carbon nano-onions: Unique carbon nanostructures with fascinating properties and their potential applications, Inorganica Chim. Acta. 468 (2017) 49–66. https://doi.org/10.1016/j.ica.2017.07.021.

[32] Y.J. Ko, K. Choi, S. Lee, J.M. Cho, H.J. Choi, S.W. Hong, J.W. Choi, H.

Mizuseki, W.S. Lee, Chromate adsorption mechanism on nanodiamond-derived onion-like carbon, J. Hazard. Mater. 320 (2016) 368–375. https://doi.org/10.1016/j.jhazmat.2016.08.041.

[33] C. Sakulthaew, C. Chokejaroenrat, A. Poapolathep, Hexavalent chromium adsorption from aqueous solution using carbon nano-onions (CNOs), Chemosphere. 184 (2017) 1168–1174. https://doi.org/10.1016/j.chemosphere.2017.06.094.

[34] D. Ugarte, Curling and closure of graphitic networks under electron-beam irradiation, Nature. 359 (1992) 707–710.

[35] M. Zeiger, N. Jäckel, M. Aslan, D. Weingarth, V. Presser, Understanding structure and porosity of nanodiamond-derived carbon onions, Carbon N. Y. 84 (2015) 584–598. https://doi.org/10.1016/j.carbon.2014.12.050.

[36] R. Borgohain, J. Yang, J.P. Selegue, D.Y. Kim, Controlled synthesis, efficient purification, and electrochemical characterization of arc-discharge carbon nano-onions, Carbon N. Y. 66 (2014) 272–284. https://doi.org/10.1016/j.carbon.2013.09.001.

[37] C. Ruan, Z. Li, D. Zhang, X. Yuan, C. Liang, Y. Chang, H. Huang, L. Xu, M. Chen, A scalable chemical vapor deposition synthesis of high purity hollow carbon onions, Carbon N. Y. 161 (2020) 622–628. https://doi.org/10.1016/j.carbon.2020.01.074.

[38] J.H. Yeon, S.J. Park, I. Choi, M. Choi, Generation of carbon nano-onions by laser irradiation of gaseous hydrocarbons for high durability catalyst support in proton exchange membrane fuel cells, J. Ind. Eng. Chem. 80 (2019) 65–73. https://doi.org/10.1016/j.jiec.2019.07.032.

[39] V. Dhand, J.S. Prasad, M.V. Rao, S. Bharadwaj, Y. Anjaneyulu, P.K. Jain, Flame synthesis of carbon nano onions using liquefied petroleum gas without catalyst, Mater. Sci. Eng. C. 33 (2013) 758–762. https://doi.org/10.1016/j.msec.2012.10.029.

[40] F. Akbal, S. Camcidotless, Copper, chromium and nickel removal from metal plating wastewater by electrocoagulation, Desalination. 269 (2011) 214–222. https://doi.org/10.1016/j.desal.2010.11.001.

[41] C. Hu, Y.C. Chu, Y.R. Lin, H.C. Yang, K.H. Wang, Photocatalytic dye and Cr(VI) degradation using a metal-free polymeric g-C_3N_4 synthesized from solvent-treated urea, Polymers (Basel). 11 (2019) 1–14. https://doi.org/10.3390/polym11010182.

[42] V.E. Pakade, T.D. Ntuli, A.E. Ofomaja, Biosorption of hexavalent chromium from aqueous solutions by Macadamia nutshell powder, Appl. Water Sci. 6 (2016) 1–16. https://doi.org/10.1007/s13201-016-0412-5.

[43] V.E. Pakade, N.T. Tavengwa, L.M. Madikizela, Recent advances in hexavalent chromium removal from aqueous solutions by adsorptive methods, RSC Adv. 9 (2019) 26142–26164. https://doi.org/10.1039/c9ra05188k.

[44] M.M. Hossain, I.M. Scott, B.D. Mcgarvey, K. Conn, L. Ferrante, F. Berruti, C. Briens, Journal of Analytical and Applied Pyrolysis Toxicity of lignin , cellulose and hemicellulose-pyrolyzed bio-oil combinations : Estimating pesticide resources, J. Anal. Appl. Pyrolysis. 99 (2013) 211–216. https://doi.org/10.1016/j.jaap.2012.07.008.

[45] L. Miao, C. Wang, J. Hou, P. Wang, Y. Ao, Y. Li, N. Geng, Y. Yao, B. Lv, Y. Yang, G. You, Y. Xu, Bioresource Technology Aggregation and removal of

copper oxide (CuO) nanoparticles in wastewater environment and their effects on the microbial activities of wastewater biofilms, Biomass and Bioenergy. 216 (2016) 537–544. https://doi.org/10.1016/j.biortech.2016.05.082.

[46] O. Butsyk, P. Olejnik, E. Romero, M.E. Plonska-Brzezinska, Postsynthetic treatment of carbon nano-onions: Surface modification by heteroatoms to enhance their capacitive and electrocatalytic properties, Carbon N. Y. 147 (2019) 90–104. https://doi.org/10.1016/j.carbon.2019.02.063.

[47] I. Heidmann, W. Calmano, Removal of Zn(II), Cu(II), Ni(II), Ag(I) and Cr(VI) present in aqueous solutions by aluminium electrocoagulation, J. Hazard. Mater. 152 (2008) 934–941. https://doi.org/10.1016/j.jhazmat.2007.07.068.

[48] Y.C. Zhou, X.Y. Xu, P. Wang, H. Fu, C. Zhao, C.C. Wang, Facile fabrication and enhanced photocatalytic performance of visible light responsive UiO-66-$NH_{2/}Ag_2CO_3$ composite, Chinese J. Catal. 40 (2019) 1912–1923. https://doi.org/10.1016/S1872-2067(19)63433-9.

Chapter 2: Literature review

This chapter expands on the background information that was introduced in Chapter 1. It gives a more detailed review of the literature, starting with the nature and problems associated with water pollutants, in particular, heavy metals and dyes. The different methods currently in use, to remove these contaminants, with emphasis on adsorption and the type of adsorbents used are also discussed. The last part of the chapter gives a review of the adsorbent of choice [onion-like nanocarbons (OLNCs)] and their use in the removal of Cr(VI) ions from water.

2.1. Chosen pollutants

The World Health Organization (WHO) lists hexavalent chromium [Cr(VI)] as one of the common heavy metal pollutants [1]. The focus of this study is based on the application of onion-like nanocarbons (OLNCs) in the removal of Cr(VI) ions from an aqueous medium. Cr has a wide range of oxidation states, with Cr(VI) and Cr(III) being the most stable When it comes to toxicity, Cr(VI) is more toxic than Cr(III), due to its higher mobility. In terms of the (WHO) classification, Cr(VI) is in group 1 (most toxic) as a human carcinogen, and Cr(III) is in group 3 [1].

In the environment Cr(VI) is present as diverse anionic species, depending on the pH and concentration of the solution, The species include chromate, hydrogen chromate, dichromate, and hydrogen dichromate (CrO_4^{2-}, $HCrO_4^-$, $Cr_2O_7^{2-}$, and $HCr_2O_7^{2-}$) respectively (Figure 2.1). In the presence of a strong acid, Cr(VI) ions tend to be reduced to their less toxic form, namely Cr(III) ions. The reduction of Cr(VI) ions can also be enabled by electron-donating groups in the presence of carbonaceous materials [2]. In drinking water, the maximum permissible limit of Cr(VI) is 0.05 mg/L, the same as the total Cr[1].

The existence of dyes and trace metals in water streams contributes to a lack of plant growth and decreased photosynthesis for aquatic plants. Such pollutants also increase biological oxygen demand (BOD) and chemical oxygen demand (COD), resulting in increased toxicity harmful to humans, animals, and biota [7]. Thus, there is a need for

the development of techniques that can adequately remediate heavy metals and dyes or break them down into less harmful compounds from water bodies. Freshwater scarcity is a universal problem, the solution should be accessible to second and third-world countries as much as they are available in first-world countries. Thus, issues such as availability, economic implication, and the reusability of the adsorbent or photocatalyst should be taken into consideration during system development.

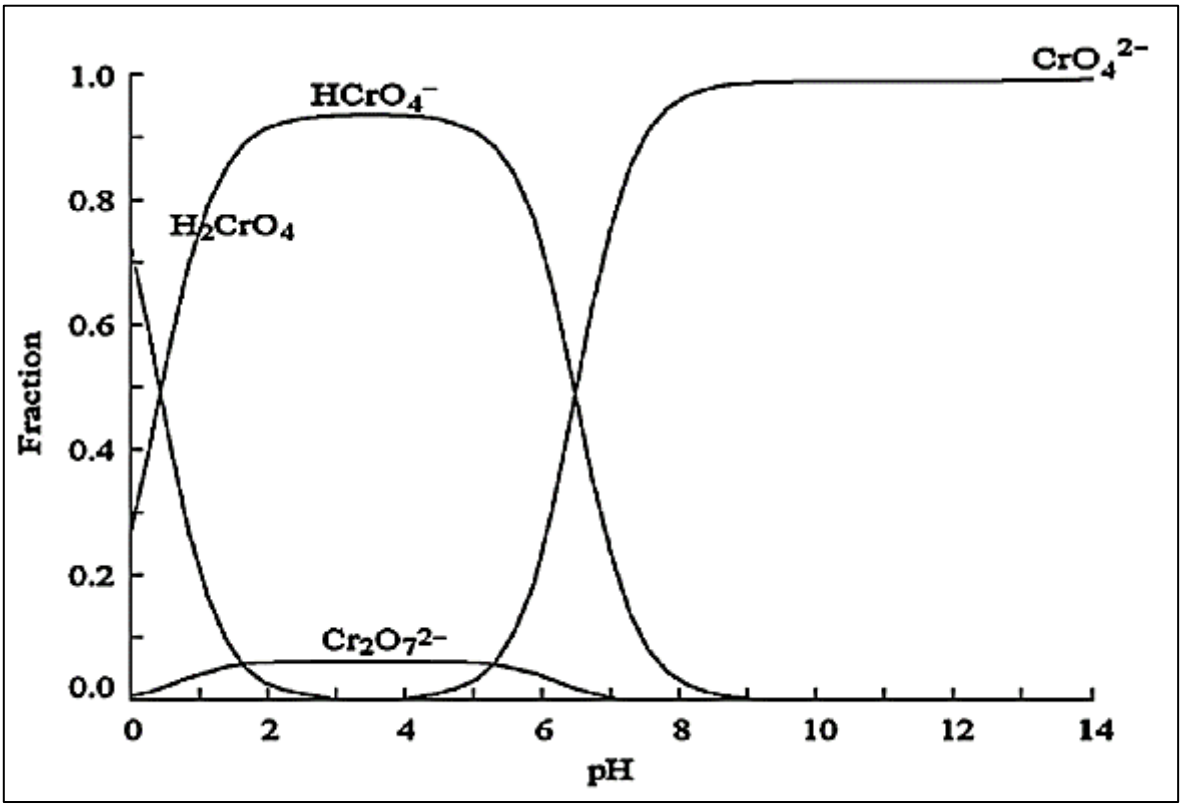

Figure 2. 1: The speciation diagram for Cr(VI) ions [8]

2.2. Methods for the removal of Cr(VI) ions

The commonly used methods for the removal of Cr(VI) include electrochemical reduction-precipitation [9], ion–exchange [10], electrocoagulation [11], photocatalytic reduction [12], and microbial reduction [13]. They do, however, employ elaborate equipment, high volumes of chemicals, and the generation of secondary toxic sludge as presented in Table 2.1. Importantly, they can reduce Cr(VI) ions to their less toxic form; Cr(III) ions. Among removal methods adsorption has found attractiveness since the method addresses some of the shortcomings of the aforementioned technologies.

Table 2. 1: Summary of Cr(VI) ions removal methods

Method	Reduction to Cr(III)	Extra chemicals	Special equipment	Sludge	References
Electrochemical reduction-precipitation	Complete	Strong base	electrochemical cell	Yes	[9]
Ion – exchange		Nitrates, sulphates, carbonates	None		[10]
Electrocoagulation		Fe	Fuel cell		[11]
Photocatalytic reduction		Catalyst support	Ultraviolet light		[12]
Microbial reduction		Fe(II),nutrients	Reductase cell		[13]

2.2. Removal of Cr(VI) ions using adsorption technology

Among the Cr(VI) removal methods, adsorption is one of the favourable methods. Adsorption technology involves the adherence of the adsorbate ions onto the surface of the adsorbent via physical adsorption or chemical adsorption, as demonstrated in Figure 2.4 [14].

Physical adsorption (physisorption) can be described as the accumulation of the adsorbate ions on the surface of the adsorbent via physical attachment facilitated by weak intermolecular forces such as Van der Waals forces. These bonds can be easily broken by vigorous agitation of the adsorption environment and by an increase in the temperature of the reaction. The physisorption mechanism is reversible and requires low energy consumption taking place at temperatures that are more or less that of the critical temperature of the adsorbate. Since the critical temperatures of the adsorbate ions are less than 100°C and that of the adsorbents are above 100°C [14]. In contrast, chemical adsorption (chemisorption) is the accumulation of the adsorbate ions on the surface of the adsorbent that involves the formation of a chemical bond between the adsorbate and adsorbent. The chemical bond can either be an ionic bond or a covalent bond and is not easily broken. Chemisorption can take place in all temperatures and

is normally irreversible [14]. Several adsorption parameters are involved in a typical adsorption experiment that contributes to the optimum removal of the adsorbate ions.

The use of adsorbents mitigates the use of the large volume of chemicals, the generation of toxic sludge, and the use of specialized equipment. Another advantage of adsorption is the abundance and availability of many carbonaceous materials.

A wide range of adsorbents has been used in the removal of Cr(VI) ions via the adsorption technique. These include agricultural waste [15], activated carbon[16], natural and synthetic polymers[17], and metal nanoparticles [18]. Recently novel carbon-based nanomaterials such as carbon nanotubes [19], carbon nanofibers [20], and carbon nano-onions [21], have been used as adsorbents for the removal of Cr(VI) ions via the adsorption technique [18]. In this thesis study, the adsorbate will be [Cr(VI) ions] and the adsorbent will be OLNCs.

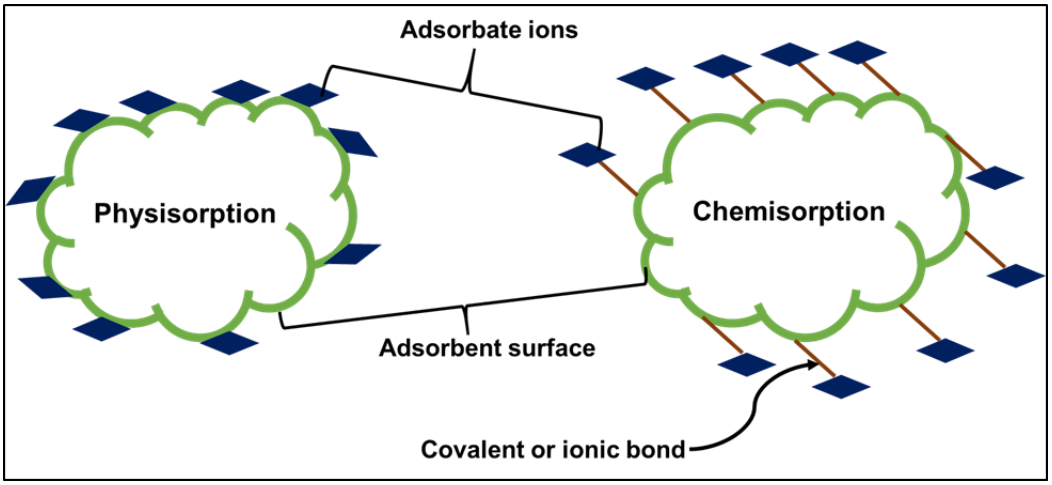

Figure 2.4: Illustration of physisorption and chemisorption

2.3. Different types of adsorbents used for the removal of Cr(VI) ions

2.3.1. Agricultural waste

Agricultural waste (AW) materials are abundantly available and tend to take up space needed for agricultural activity. Therefore implementing AW materials as adsorbents for the removal of Cr(VI) ions and other water-contaminating pollutants adds value to this disregarded carbon-rich source [22]. A wide range of AW materials that have been used as absorbents for the removal of Cr(VI) includes, but is not restricted to, rice husk [23], groundnut hull [24], and pomelo peel [25]. (Table 2.2). It could be seen from Table 2.2 that all the maximum removal of Cr(VI) took place at pH 2 and 1 with the experimental data explained by the Langmuir adsorption isotherm. It is to be noted

that the different adsorbents showed varying maximum adsorption capacities. This indicates the impact of the chemical treatment of the adsorbent. The chemically treated adsorbents showed increased adsorption capacity for the removal of Cr(VI) ions. It could be seen from Table 2.2 that the adsorbents do not respond similar with similar chemical treatment. For example the Macadamia nutshells showed higher adsorption capacity for the HCl treated material than the NaOH treated material. This was contrary to higher adsorption capacity for the NaOH treated material than the HCl treated material. However, for the Macadamia nutshells showed that different types of chemical treatments resulted in decreased adsorption capacity compared to the non-treated material. This was attributed to the HCl and NaOH ability to extract acid and base-soluble material, which could result in the loss of active sites [22].

Table 2.2: Comparison of different adsorbents, treatment and adsorption capacity

Adsorbent	Treatment	pH	Q_{max}	Isotherm	Reference
Rice husk	Boiled	2	8.50	Langmuir	[26]
	CH_2O		10.40		
Groundnut hull	Pristine		90.00		[24]
	$C_{10}H_2O_6$		131.00		
Pomelo peel	Pristine		0.57		[27]
	$FeCl_3$		21.55		
Macadamia nutshells	Pristine		45.23		[22]
	HCl		44.83		
	NaOH		42.44		
Harpagophytum procumbens roots	HCl	1	77.24		[28]
	NaOH		102.64		

2.3.2. Activated carbon

Activated carbon (AC) has been one of the most used adsorbents for the removal of Cr(VI) ions from an aqueous solution [16,29,30]. One of the most attractive features of AC is the diverse landscape such as wood, macadamia nutshells [16], Bermuda grass [31], prawn shells [32], apple peel [33], etc. AC comes with surface functional groups such as carbonyl, hydroxyl, and thiol functional groups which serve as a pathway for the removal of Cr(VI) ions making it attractive as an adsorbent [16].

Lesaoana et al. [16] reported the use of pristine and acid-treated AC for the removal of Cr(VI) ions. The chosen acids were H_2SO_4, HNO_3, and H_3PO_4 at varying concentrations of the respective acid. The AC modification or treatment was done in anticipation of improved adsorption capacity for the AC in the removal of Cr(VI) ions. The adsorption capacity was reported to have increased for the H_3PO_4 and the HNO_3 treatments, due to the increased protonation of the surface of the AC. This gave an improvement in adsorption capacity from 22.3 mg/g (pristine) to 25.75 mg/g (H_3PO_4) and 40.99 mg/g (HNO_3). However, the modification with H_2SO_4 showed a drop in adsorption capacity to 9.66 mg/g attributed to the Cr(VI) ions having a lower affinity for sulphur-containing functional groups and that the acid extracted more organic functional groups from the activated carbon [16].

Although acid modification may increase the adsorption capacity of the adsorbent, the concentration and type of acid needed has to be varied to find the best conditions, without destroying the backbone structure of the adsorbent. In the preparation of AC, several activating agents have been used such as $ZnCl_2$ and $FeCl_3$ under different temperatures for optimum activation [34]. The AC is activated by the removal of surface debris, the extraction of soluble materials, an increase in the surface area, and the improvement of metal or dye active sites or adsorption sites that improves the chelation of targeted adsorbates [16,34]. The activating agent may result in the generation of toxic sludge and high temperatures may contribute to the higher operational cost for industrial applications.

2.3.3. Natural polymers

Nature has been a gift that keeps on giving to the area of adsorption technology by supplying many new adsorbents. Natural occurring polymers such as cellulose [27], chitosan [35], and natural rubber [36] have been generally used as adsorbents for the removal of Cr(VI) ions. This has been achieved with pristine polymer as well as physical, and chemically modified polymers. Rubberwood sawdust (RWS) a waste by-product from the timber manufacturing industry was used without any chemical modification for the removal of Cr(VI) ions. The RWS was reported to have the potential to remove Cr(VI) ions. The results showed that most of the Cr(VI) ions were removed at $pH < 2$ while a decrease in removal percentages was observed at $pH > 3$.

This was attributed to the protonation of surface functional groups such as COO^- and NH_2 to $COOH^+$ and NH_3^+, which attract the adsorbate anions, at acidic pH. Under alkaline conditions, the surface functional groups are deprotonated, resulting in the repulsion of the adsorbate anions. The decrease in adsorption at pH > 3 was attributed to the point of zero charge of the adsorbent (pH 4.90) level [36].

The removal of Cr(VI) ions has been improved via chemical modification of the surface groups on a polymer. Awang et al. [37] modified the surface of extracted cellulose by grafting with acrylonitrile under alkaline conditions. The grafted cellulose showed a higher adsorption capacity (15, 12 mg/g) compared to that of the pristine cellulose (8, 11 mg/g). The improved performance was attributed to the successful grafting of the nitrile functional group onto the surface of the cellulose, as observed from the FTIR spectra [37].

2.3.4. Synthetic polymers for the removal of Cr(VI) ions

Synthetic polymers with amine functional groups (as part of their backbone) such as polypyrrole and polyaniline have gained momentum as adsorbents for the removal of Cr(VI) ions. It has been reported that the amine groups are protonated under acidic conditions making it a potent Cr(VI) ion chelate [38]. An ion-imprinted polymer (IIP) synthesized by the incorporation of 1,5-diphenylcarbazide (ligand), 4-vinyl pyridine, ethylene glycol dimethacrylate (functional monomers), and β-cyclodextrin was used as an adsorbent for Cr(VI) ions removal by Nchoe et al. [39]. The materials' adsorption capacity was higher compared to that of the corresponding non-imprinted polymer (NIP) without the ligand 1, 5 dipheynylcarbazide. This was attributed to the higher surface area of the IIP to that of the NIP and a higher complexation affinity of the IIP towards Cr(VI) ions due to the presence of the ligand providing added active sites [17].

2.3.5. Carbon nanomaterials as an adsorbent for the removal of Cr(VI) ions

The use of carbon nanomaterials such as graphene oxide (GO) [40], carbon nanotubes (CNTs) [19], carbon nanofibers (CNFs) [41] and fullerenes [42] have found applications as adsorbents. Another type of carbon, often called carbon nano-onions

(CNOs) has also been used for the removal of metal ions [21]. In this study, we will refer to these as onion-like nanocarbons (OLNCs) and the reason for this name change is discussed in Section 2.3.6. Some of the appealing properties of carbon nanomaterials as adsorbents are that they generally show an increase in surface area, hydrophobicity, insolubility, and surface functional groups relative to carbons that have macro dimensions. All these properties combine to provide increased chelation to metal ions, making carbon nanomaterials an attractive material for the removal of Cr(VI) ions. It is to be noted that apart from CNOs and CNTs, the other carbon nanomaterials have been mainly used in composites or placed on some type of support. In a study by Hu et al. [43], multi-walled carbon nanotubes (MWCNT) were oxidized using HNO_3 and used for the removal of Cr(VI) ions from the aqueous solution. It was found that the oxidation resulted in an increased concentration of COOH and OH groups on the surface of the MWCNT which were assumed to serve as adsorption sites.

The MWCNT studies showed that the removal of Cr(VI) was not only due to adsorption but also due to the reduction of Cr(VI) ions to Cr(III) ions. This was attributed to electron donor groups present on the surface of the MWCNTs. The reduction mechanism was proposed to take place in one of two ways, where firstly the Cr(VI) ions were reduced by direct interaction with the surface of the adsorbent. This occurs whilst the adsorbate is still in solution and is followed by adsorption of the Cr(III) ions. The second mechanism involves the adsorption of Cr(VI) ions on the surface of the adsorbent then before the Cr(VI) ions are reduced to Cr(III) ions by the adjacent electron donor group[43]. The challenge in using MWCNTs is their removal without breaking the structure of the carbon[18]. As such, the MWCNTs may promote the generation of secondary toxic sludge. Subsequently, adsorbent regeneration or recycling remains a challenge, depending on the leaching agent used.

In other studies, fullerenes have been applied as adsorbents for the adsorption of Cu(II) ions. They were found to have an affinity towards the Cu(II) ions with an adsorption capacity of 14.6 mmol/g [44]. Though fullerenes have the potential as adsorbents for heavy metals their synthesis is expensive making them more suitable for use in composites or surface decoration [45].

2.3.6. Onion-like nanocarbons (OLNCs) as adsorbents for Cr(VI)

Over the years many carbons in the nanoscale range have been made with a spherical shape. The smallest member of this family is fullerene (C60) [46]. It has a perfectly symmetrical structure with a complete surface made only of carbon atoms. A family of fullerenes have been made since its discovery in 1985. This includes (i) carbon structures with elongated shapes and (ii) fullerenes embedded in other fullerenes (Russian doll structure) [47].

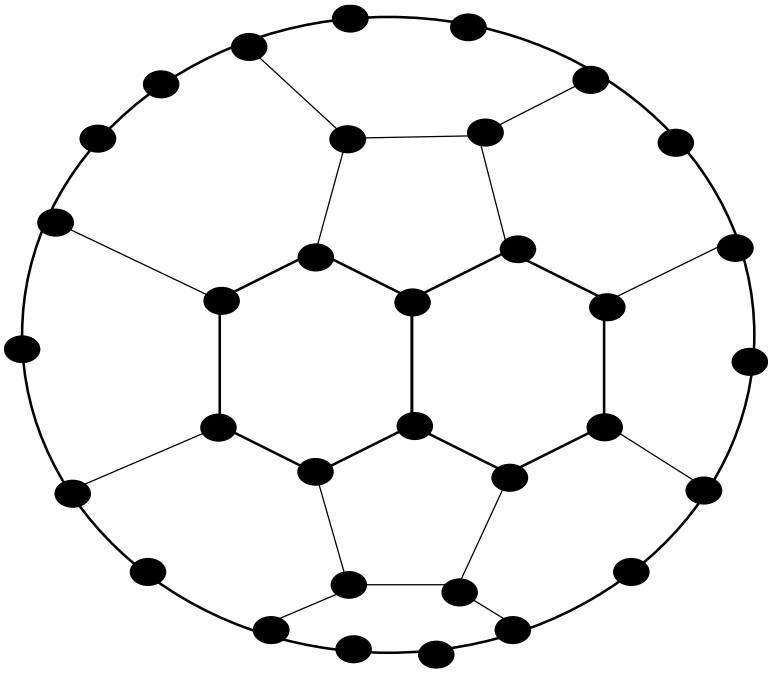

Figure 2.1: Typical structure of fullerene

When fullerenes that are embedded within other fullerenes reach a large size of 2 to 100 nm they are called carbon nano-onions (CNOs) [48,49]. This name is given to them because they have a structure that resembles an onion with layers within layers. (Figure 2.2) While small fullerenes embedded within fullerenes have a molecular structure the CNOs tend to accrete.

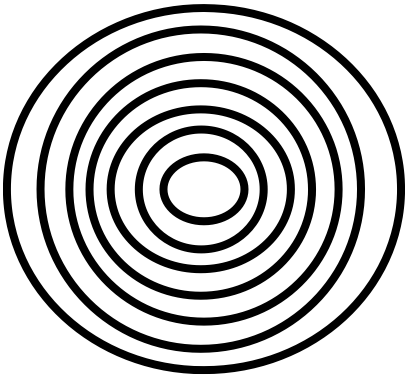

Figure 2.2: Typical structure of CNOs (fullerenes embedded within fullerenes

It is also to be noted that the CNOs and fullerenes are made by different paths. Indeed the first recognised CNO was made by irradiation in an electron microscope [50]. Again, these carbons have only been known in the last few decades. Since then most syntheses route to make the 'true' CNOs involve starting from nanodiamond. Where nanodiamonds are converted to CNOs through annealing at different temperatures in an inert environment using argon, hydrogen, helium, or nitrogen [51]. This method produces CNOs on a large scale with high purity and homogeneity having a particle size that is between 5 nm to 10 nm [48].

Other methods include arc discharge of graphite in a liquid environment [52], chemical vapour deposition [53], and ozonolysis [54]. It is to be noted that most of the synthesis routes involve the use of a metal catalyst [55]. Carbon nano-onions (CNOs) are a type of carbon nanomaterial that belong to the fullerene family of carbon. They encompass quasi-spherical several layers, archetypal they have sp^2 graphene sheets organisation in like manner to an onion thus, their name [56]. Different authors give CNOs various names such as carbon onions [57], cross-linked Nano-onions [58], onion-like carbon [59], hollow carbon nanospheres [60], and carbon multi-cages [61], for this study we call them onion-like nanocarbons (OLNCs).

We have had to use this terminology as these types of carbons have been described by many authors as being OLCs. In many cases, the carbons described are spherical and in the nano range but more closely resemble a carbon black/soot structure. We have also incorrectly used this terminology in our early studies when we first made the OLNCs [62]. Another method for large-scale production of OLNCs that is gaining momentum is flame pyrolysis [63]. This method of synthesis mainly produces materials that have multiple shells and are quasi-spherical resembling an onion. With the

deference in the morphology of an incomplete cycle or broken cycle compared to traditional CNOs (see Figure 2.3) [62]. Be that as it may, several authors are not in harmony when it comes to the naming of such materials. Names such as chain-like carbon nano-onions (chain-like CNOs) [64], CNOs [65], onion-like carbon nanostructures (OLCs) [66], and carbon onions [67] have been used and the synthesis methods are different (see Table 2.1).

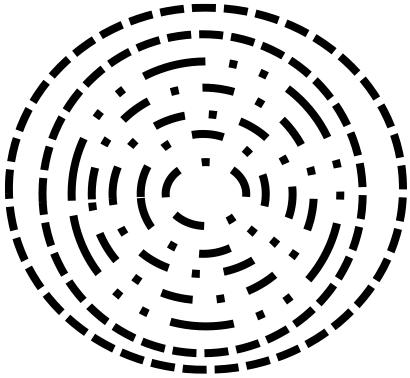

Figure 2.3: Typical structure of OLNCs synthesized by flame pyrolysis

OLNCs have been explored as adsorbents for the removal of Cr(VI) ions as well as other heavy metals such as Cu(II), Ni(II), Zn(II), Pb(II), and Cd(II) [21,68]. The process of removing Cr(VI) ions from an aqueous solution using OLNCs is similar to the methods discussed above and involves the adsorption of Cr(VI) ion followed by reduction of Cr(III) ions and subsequent adsorption of Cr(III). The evidence for the reduction on the surface of the adsorbent is often shown by XPS analysis [21]. Such a phenomenon was attributed to the presence of electron donor groups present on the surface of the OLNCs which are more dominant under acidic conditions. The surface of the OLNCs was able to adsorb multiple elements such as Pb(II), Cu(II), Zn(II), and Cr(VI) with the downside being the decrease in the removal efficiency of Cr(VI) ions in the presence of competing cations [21].

Ko et al. [69] reported the use of a similar material as an adsorbent for chromate ions (chromate was mainly removed by C–O–H functional groups on the surface of the adsorbent under acidic conditions [69].

2.4. Chemical modification of carbon nanomaterials for improved removal of Cr(VI) ions

Nano-carbons such as CNFs, CNTs, GO, and OLNCs have different shapes and sizes depending on the synthesis method. What remains common is that they have carbon in their backbone structure and contain oxygen (O), nitrogen (N), and sulphur (S) related surface moieties. Several researchers have attributed the metal ion chelation as directly related to the presence of O, N, and S moieties [22,69–71]. Therefore, the appropriate functionalization of the surface of the carbon nanoparticles with heteroatoms such as O, N, and S may increase the adsorption capacity of the adsorbent [72].

The modification can be physical or chemical, however, it should be noted that modification is not directly proportional to an increase in adsorption capacity. Pakade et al. [22] reported a decrease in the adsorption capacity of pristine macadamia nutshells when modified with HCl and NaOH respectively. The decrease in the adsorption capacity was attributed to the loss of active sites that may have been extracted by the respective acid and base used [22]. Chemical modification via oxidation, sulphonation, nitration, hydrocarbon addition, and metal nanoparticle incorporation has been widely favoured because of the availability of cheap chemicals [72].

In a comparison study, the pristine and NHO_3-modified AC and CNTs were tested for the removal of Cr(VI) ions from an aqueous solution. It was found that the adsorption capacity of the pristine AC increased from 3.46 mg/g to 18.52 mg/g after modification. The increase in the adsorption capacity was attributed to an increase in surface area from 1126.00 m^2/g to 1420.00 m^2/g and the increase in surface-active groups. However, for the CNTs, the adsorption capacity was reported to be similar before and after modification. The inability to increase the adsorption capacity was attributed to the minimal increase in the surface area from 156.00 m^2/g to 170.00 m^2/g, and the addition of surface negative moieties. It was further indicated that the negative moieties may have contributed to the repulsion of the Cr(VI) anions [73]. The modification of the AC and the CNTs with HNO_3 showed that different materials

respond differently to modification. Therefore, appropriate characterization of the adsorbent plays an important role in how the material is to be chemically modified.

Lesaoana et al. [16] modified the surface of AC with three inorganic acids H_2SO_4, HNO_3, and H_3PO_4, respectively, and the materials were applied for the removal of Cr(VI) ions. The AC modified with 20% H_2SO_4 showed a lower adsorption capacity of 8.73 mg/g compared to 20% H_3PO_4 (23.05 mg/g) and 20% HNO_3 (48.56 mg/g). The lower adsorption capacity was attributed to H_2SO_4 extracting more active sites and the lack of attraction between Cr(VI) ions and the sulphur moieties on the surface of the adsorbent. On the other hand, the highest adsorption of 48.56 mg/g for the HNO_3 was due to the increased affinity between Cr(VI) ions and the amino groups on the surface of the adsorbent [16].

There is a lack of literature available on the removal of Cr(VI) ions using pristine or modified OLNCs.

2.4.1. Chemical modification of OLNCs

The difficulty in dispersing CNOs in aqueous solutions leads to poor performance as adsorbents. Such occurrences can be mitigated by subjecting the CNOs to chemical modification designed to increase their dispensability for increased adsorption. The motivation for chemically modifying the OLNCs has been adopted from earlier modifications of other carbon nanoparticles such as AC and CNTs [73].

Seymour et al. [68] used two different modifying agents for the addition of carboxylate moieties to the surface of OLNCs via HNO_3 and NaOCl treatment respectively. The oxidized OLNCs were used to adsorb Cu(II), Pb(II), Cd(II), Zn(II), and Ni(II) ions. The adsorption capabilities of the oxidized OLNCs were compared with those of C_{60} which was oxidized in a similar to which the OLNCs were oxidized. It was found that the OLNCs showed a higher adsorption capacity than the C_{60}. This was attributed to the addition of –COOH functional groups on the surface of the adsorbents, with a larger effect taking place on the OLNCs than on the C_{60}. Even though the C_{60} showed lower adsorption than the OLNCs, the NaOCl-modified C_{60} showed a higher adsorption capacity than the HNO_3-modified C_{60} for all the metal ions. However, the NaOCl-modified CNOs were more selective towards Cu(II), Cd(II), Ni(II), and Zn(II) ions

whereas the HNO_3 modified CNOs were selective towards Pb(II) ions only, this was attributed to NaOCl having advanced oxidizing aptitude than HNO_3 [68].

The aforementioned study gives a clear indication of the selective nature of the modifying agent and the selectivity of the surface-attached functional groups towards certain metal ions. Not all modifying agents or surface moieties will increase the adsorption capacity of an adsorbent relating to a specific metal ion that is being targeted.

2.5. Parameters that influence the interaction between adsorbent and adsorbate ions

The adsorption capacity of an adsorbent is not only dependent on the type of moieties present on the surface of the adsorbent, but also on the reaction parameters such as solution pH, contact time, initial concentration of adsorbate, and temperature. Also, the mass of the adsorbent plays a major role in the adsorption capacity. The current study explores how these features affect the chelation of metal ions on the surface of the adsorbent.

2.5.1. The effect of solution pH

One of the major factors in adsorption is the pH of the adsorbate solution since it affects the nature of the adsorbent and the adsorbate ions. The surface functional groups of the adsorbent will be protonated (more H^+ ions) in a more acidic medium and deprotonated (more OH^- ions) in an alkaline solution. Even though Cr(VI) exists as oxyanions in an aqueous medium as discussed earlier, the type of Cr(VI) species is influenced by pH (Figure 2.1) [8,70]. It is for this reason that Cr(VI) anions are attracted to the surface of an adsorbent under acidic conditions and repelled under alkaline conditions.

The exception is when the adsorbent has a permanent positive charge throughout the entire pH range. For example, Pakade et al. showed that when activated carbon was treated with epichlorohydrin, diethylenetriamine, and trimethylamine the modification resulted in a permanent positive charge on the surface of the adsorbent., [29]. The pH_{PZC} of Macadamia nutshells was reported to be at pH 6.25 indicating that at a pH

below 6.25, the material is mainly protonated and at a pH above 6.25 it is mainly deprotonated. Therefore, more Cr(VI) ions were removed at pH <6.25 due to electrostatic attraction. [22].

2.5.2. The effect of the initial concentration of adsorbate

The initial adsorbate concentration plays an important role in the removal of adsorbate ions. Under normal circumstances, it is expected that as the initial adsorbate concentration is increased, the removal of the adsorbate ions would decrease. This is because, at a low initial adsorbate concentration, the number of moles of the adsorbate would match the number of active sites of the adsorbent. Then, the decrease in the removal of the adsorbate ions as the initial concentration of adsorbate is increased is due to the complete saturation of active sites of the adsorbent [74].

On the other hand, an increase in the initial concentration of the adsorbate may result in overcoming the mass transfer resistance owed to more coverage of active sites by the adsorbate molecules as the concentration of the adsorbate is increased [15]. These occurrences could be explained by the adsorption capacity equation where the initial concentration of the adsorbate ions is proportional to the adsorption capacity (Equation 3.). Therefore, it is important to determine at which point or concentration where the mass transfer resistance could be overcome resulting in maximum adsorption capacity.

2.5.3. The effect of the adsorbent mass

Generally, the number of active sides increases with the increase in the mass of the adsorbent which increases the removal of the adsorbate ions. However, this could result in a decrease in the adsorption capacity of the adsorbent. This can be further elaborated by the adsorption capacity equation where the mass of the adsorbate is proportional to the adsorption capacity. Therefore, for maximum coverage of the adsorbent surface, the influence of the initial concentration of adsorbate ions and the mass of the adsorbent needs to be known.

2.5.4. The effect of contact time

Maximum surface coverage of the adsorbent by the adsorbate ions takes place at equilibrium. It is a general trend that when the contact time has increased the removal of adsorbate ions will increase [16]. The increase in contact time is directly proportional to the surface coverage of the adsorbent by adsorbate ions, resulting in an increased adsorption capacity [16].

Pakade et al. reported the use of Macadamia nutshells as an adsorbent for the removal of Cr(VI) ions from aqueous solutions. It was found that the removal of Cr(VI) was more rapid within the first 200 min of contact time due to the linear progression of the Cr(VI) uptake. After a further 30 min, the removal slowed down and reached equilibrium in 600 min. However, not all the Cr(VI) ions were removed and this was attributed to repulsion between surface-bounded Cr(VI) ions and the unbounded Cr(VI) ions [75].

2.5.5. The effect of the reaction temperature

The reaction temperature plays an important role in determining the interaction between the adsorbent surface and the adsorbate, in line with Le Chateleir's principle. One factor that relates to the reaction temperature is an increase in the viscosity of the solvent results in an increased diffusion rate of reactants. The temperature increase affects the adsorption capacity in that an endothermic process favours an adsorption capacity increase with the increase in reaction temperature[18].

It is to be noted that an increase in reaction temperature could result in a decrease in the activity of the adsorbent active sites, leading to decreased removal of adsorbate ions [76].

2.6. Equilibrium studies

An adsorption process is not complete without equilibrium studies, this can be performed by the investigation of adsorption isotherms, kinetics, and thermodynamics at equilibrium. This type of information provides a more detailed understanding of the adsorption capacity of the adsorbent and the type of interaction taking place between

the adsorbent and adsorbate ions. Most studies are analysed in terms of pseudo-first-order (PFO) and pseudo-second-order (PSO) models as kinetic models. Typical adsorption isotherms used are the Langmuir and Freundlich isotherms. The thermodynamic parameters that were considered are the Gibbs energy change (ΔG°), entropy change (Δ*S*°), and enthalpy change (Δ*H*°) [77].

2.6.1. Adsorption kinetics

The effect of contact time is used to estimate the adsorption kinetics of the adsorption process. Adsorption kinetics determine the rate at which the adsorbate ions migrate from the solution to the surface of the adsorbent, the time it takes for the adsorption process to come to completion, and the mass transfer data [78]. When the migration of adsorbate ions is mainly based on a linear driving force, the adsorption process is said to be better described by the PFO kinetic model, also known as the Lagergren first-order rate equation. This model was originally proposed by Lagergren in 1898 when oxalic acid and malonic acid were adsorbed onto the surface of charcoal [79]. Gupta et al. [80] used red mud as an adsorbent for the removal of Cr(VI) ions from an aqueous solution. It was found that the adsorption kinetics followed that of a pseudo-first-order kinetic model. The adsorption capacity reached about 45% within the first hour and attained equilibrium in about 8 h. Furthermore, the rate of removal was directly proportional to the initial concentration of Cr(VI) ions within the first hour [80]. The adsorption kinetic was described by the pseudo-first-order with the interaction between the adsorbate ions and the adsorbent surface being reversible. Such an interaction indicates physical adsorption or physisorption [81].

Often when adsorption kinetic data are reported in the literature, the pseudo-first-order is complimented with the pseudo-second-order model [77,82,83]. The adsorption process is said to be described better by the PSO model when the interaction between the adsorbent surface and the adsorbate ions indicates chemical bond formation, that is facilitated by the sharing or the exchange of electrons between the adsorbate ions and the adsorbent surface [84,85].

Lesaoana et al. [16] used different acids H_2SO_4, HNO_3, and H_3PO_4 at varying concentrations to modify the surface of an AC used as an adsorbent for the removal of Cr(VI) ions. The PFO and PSO kinetic models were used to describe the adsorption

process, where it was found that the materials modified with H_2SO_4 and H_3PO_4 followed the PSO model indicating chemisorption, whilst materials modified with HNO_3 followed the PFO model indicating physisorption. This was attributed to the strength of the acid and the different surface properties of the AC after the acid reaction [16].

2.6.2. Adsorption isotherms

Adsorption isotherm studies are conducted at equilibrium by control of the solution pH, initial adsorbate concentration, adsorbent mass, and contact time. The Langmuir [86] and Freundlich [87] adsorption isotherms are the isotherms used in most adsorption studies.

The Langmuir adsorption isotherm indicates that the adsorption process takes place on a homogeneous surface of an adsorbent and that for every sorbate ion, one sorbent active site will be covered or occupied [88]. The process can be reversible and the sorbate species do not interact with each other and the energy of interaction between the adsorbent and the active sites is the same [77]. Hall et al. reported that it was important to determine the separation factor (R_L) which is dimensionless. It provides the adsorption process with the following information; $R_L = 0$ (irreversible), $0 < R_L < 1$ (favourable), $R_L > 1$ (unfavourable), and $R_L = 1$ (linear) [89].

The Freundlich adsorption isotherm can involve multiple-layer adsorption processes. The Freundlich intensity parameter (n) (dimensionless) describes the magnitude of the adsorption driving force. The values for n can be $n = 0$ (irreversible), $0 < n > 1$ (favourable), $n > 1$ (unfavourable), and $n = 1$ (linear) [90]. On their own, the adsorption isotherms are not conclusive in describing the adsorption mechanism but they do provide valuable insight into the nature of the adsorption process. The nonlinear and linear forms of the Langmuir and Freundlich equations are presented and discussed in chapter 3.

2.6.3. Adsorption thermodynamics

The adsorption mechanism can be correlated with thermodynamic parameters such as the Gibbs energy change (ΔG°), the enthalpy change (ΔH°), and the entropy change (ΔS°). The sign and the magnitude of the aforementioned thermodynamic parameters

provide important information relating to the mechanism, where a negative value for the Gibbs energy change indicates that the reaction is feasible and spontaneous and positive values indicate a non-feasible and non-spontaneous reaction. Negative values of enthalpy indicate an exothermic process and could be physisorption or chemisorption. Whilst positive ones indicate an endothermic process and chemisorption. Negative values of entropy indicate an associative mechanism and positive values indicate a dissociative mechanism.

2.7. Photocatalysis

Photocatalysis is another method for pollutant removal that has gained prominence, mainly due to its ability to completely degrade targeted pollutants in a reasonable reaction time. It is a method rooted in green chemistry particularly degrading dyes to CO_2 and H_2O or less toxic substances. The method takes advantage of oxidative processes to govern radical formation under radiation in the presence of a catalyst. Most of the widely used catalysts are semiconductors such as ZnO, TiO_2, ZnS, CdS, ZrO_2, and Fe_2O_3 [91]. Though semiconductors may be economically viable and have a bandgap most appropriate for visible light absorption, challenges such as photo corrosion and stability derail their application as photocatalysts [92]. Other challenges include fast recombination of photo-generated electron/hole, lack of adsorption sites, low surface area, and limited access to visible light absorption [93].

Due to abundance, chemical inertness, less toxicity, and the strong oxidizing prowess of photo-induced holes TiO_2 remain one of the mostly applied semiconductors for photocatalytic reactions for the removal of wastewater pollutants [94]. However, the aforementioned challenges of recombination, lack of surface coverage of pollutants, and absorption of visible light still prevail. Thus, efforts to improve the photo-activity of the photocatalysts include doping with heteroatoms, anions, and cations to channel their absorption towards longer wavelengths [95].

The decrease or inhibition of the recombination of photo-generated e^-/h^+ was made possible by doping Pd on the surface of TiO_2. Attributed to accelerated mobility of e^-/h^+ which increased the photocatalytic activity of the TiO_2/Pd photocatalyst. This was reported to be the result of lowering the bandgap of pure anatase (~3.10 eV) to (~2.25 eV) [96]. The e^-/h^+ recombination inhibition was proposed to take place as followed. The electrons move from the valence band (VB) to the conduction band (CB) of the

semiconductor (TiO_2). Without the Pd the e^- return to the VB but in the presence of the Pd, the e^- get trapped or captured through the Pd allowing more free radicals available for advanced oxidation as shown in Figure 2.4 [96]. The doping of TiO_2 with Pd was reported to affect the bandgap of TiO_2 where the adsorption edge was shifted from 380 nm to 400 nm and towards the near-infrared region of the spectrum. Thus, allowing more visible light to be absorbed by the TiO_2/Pd photocatalyst [96].

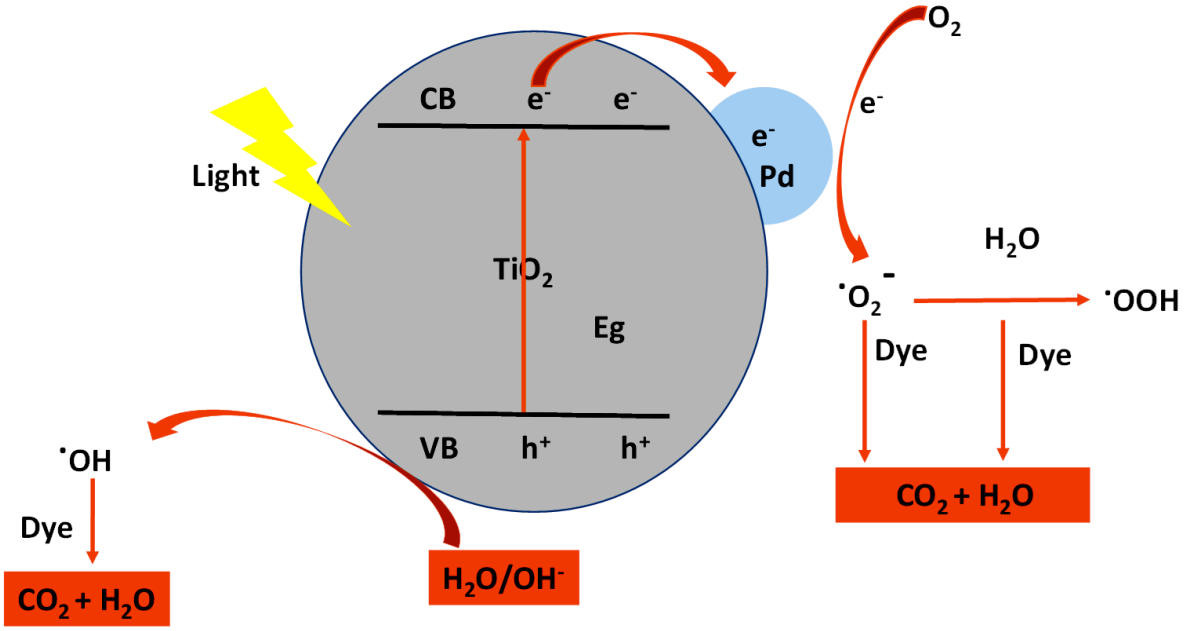

Figure 2.4: Illustration of the inhibition of e^-/h^+ recombination using Pd doped TiO_2

Another method of enhancing visible light absorption of TiO_2 by decreasing its bandgap was doping with heteroatoms. It was reported by Hwang et al. that doping TiO_2 with nitrogen shifted the bandgap from 3.0 eV to 1.93 eV attributed to the formation of oxygen and Ti^{3+} defects on the surface of the photocatalyst [97]. As effective as the dopping with metals and heteroatoms is, such photocatalysts suffer from the lack of adsorption sites on the surface thus, limiting their use in the photocatalytic degradation of pollutants [93].

Surface adsorption sites play a supportive role in the photocatalytic degradation of pollutants. Photocatalytic mineralization of phenolic compounds was reportedly enhanced by the adsorption of the pollutants on the surface of the photocatalyst. Where the photocatalyst that retained the highest adsorption capacity was the one that showed the fastest degradation rate [98]. However, instability and self-etching remain a problem. Thus, nanocomposites of metal oxides (TiO_2, WO_x, and ZnO) and

carbon nanomaterials such as carbon nanotubes (CNTs) have gained momentum as preferred candidates for the photocatalytic degradation of dyes. This is due to their high surface area, chemical tenability, and ability to enhance visible light absorption of semiconductors [99].

The combination of metal oxides/CNTs (TiO_2/CNTs) nanocomposites results in a synergistic effect for the photocatalytic degradation of dye. The synergistic photocatalytic degradation mechanism is represented in Figure 2.5. Firstly the dye is adsorbed to the surface of the photocatalyst. Followed by light irradiation which sparks the excitation of photo-generated e^- and they migrate from the VB to the CB creating h^+ in the VB. Recombination of the e^- and h^+ would quickly take place in the absence of the CNTs, but since they are present the TiO_2 would act as an e^- donor whilst the CNTs act as an e^- acceptor. This will then trigger the formation of highly reactive oxide radicals ($O2^{\bullet -}$) that are responsible for the oxidation of the dye. Simultaneously, hydroxyl radicals ($^{\bullet}OH$) are formed in the VB as a result of the h^+, these radicals are responsible for the degradation of the dye (Figure 2.5). The process of forming nanocomposites of metal oxide and carbon nanomaterial is not only effective in dye degradation but can also convert Cr(VI) compound to Cr(III) and its derivatives [100].

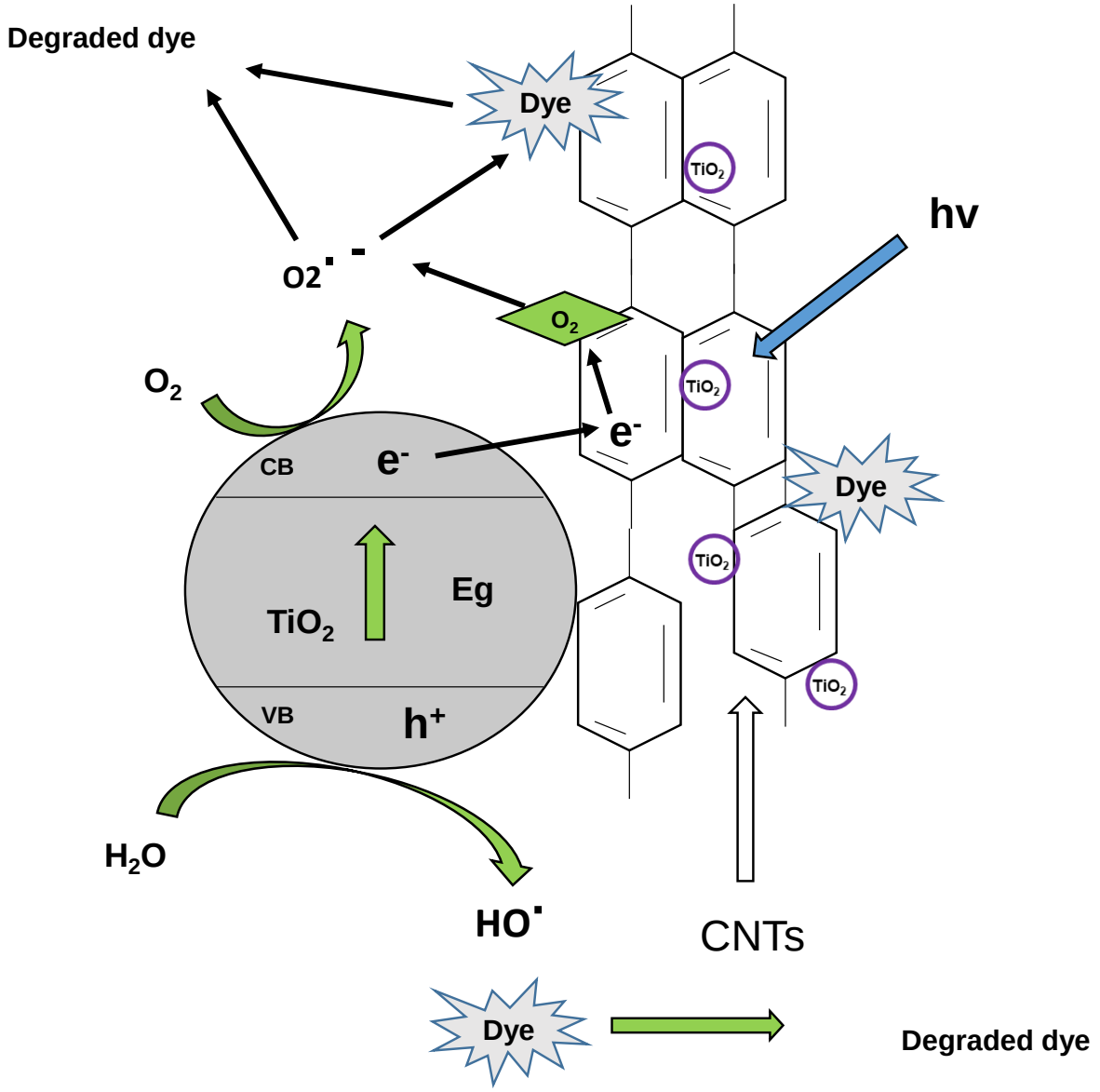

Figure 2.5: Schematic representation of the synergistic effect of TiO_2/CNTs photocatalytic degradation of dyes.

In summary limitations of semiconducting photocatalysts include low surface area, lack of adsorption sites, limited absorption of visible light, chemical instability, and rapid recombination of photo-generated e^-/h^+. Could be overcome by the formation of nanocomposites based on metal oxides and carbon nanomaterials. Where the metal oxide acts as an electron donor and the carbon material as an electron acceptor thus, hindering rapid recombination of e^-/h^+. Resulting in a more effective photocatalytic system.

2.8. Adsorbent/photocatalyst regeneration

Adsorbent regeneration is another important aspect used to evaluate the performance and the reusability of an adsorbent. In general, regeneration involves the leaching of adsorbate ions from the surface of the adsorbent and sustaining the original adsorption capacity of the adsorbent.

Three major steps describe the desorption process, (i) soaking the adsorbent after adsorption in a suitable leaching agent for a particular time; (ii) rinsing the adsorbent with a solvent, to revive the active site and removing excess leaching agent; (iii) drying and reuse Typically the adsorbent losses active sites during the process of regeneration, resulting in a decreased adsorption capacity as the cycle of regeneration is repeated [22].

For example, Guo et al. [101] used 1 M HCl as a leaching agent for the desorption of Cr(VI) ions from the surface of activated carbon. It was reported that about 80% of the adsorption capacity was retained after five cycles of desorption with acid [101]. On the contrary, Sun et al. used 0.1 M NaOH as a leaching agent for Cr(VI) ions bound on the surface of a carbon nanocomposite. It was reported that after five cycles of desorption, more than 80% of the Cr was removed. This limited result was attributed to the metal hydrolysing due to the increased OH ions in the solution [102].

In summary, the literature survey indicated that currently, the most effective method of Cr(VI) ions removal involves reducing it to Cr(III). This is appealing because the toxicity of Cr(III) ions is much less than that of Cr(VI) ions. Apart from adsorption the other discussed methods reported involve the use of special equipment e.g. a fuel cell or electrochemical cell, the use of large volumes of chemicals, and the generation of toxic sludge. Other reasons include the use of abundantly available adsorbents, easily tuneable adsorbent surface, adsorbent reusability, and the incorporation of nanotechnology.

2.9. References

[1] World Health Organization, Guidelines for drinking-water quality, 2008. https://doi.org/10.1016/S1462-0758(00)00006-6.

[2] D. Park, S.R. Lim, Y.S. Yun, J.M. Park, Reliable evidences that the removal mechanism of hexavalent chromium by natural biomaterials is adsorption-

coupled reduction, Chemosphere. 70 (2007) 298–305. https://doi.org/10.1016/j.chemosphere.2007.06.007.

[3] F. Akbal, S. Camcidotless, Copper, chromium and nickel removal from metal plating wastewater by electrocoagulation, Desalination. 269 (2011) 214–222. https://doi.org/10.1016/j.desal.2010.11.001.

[4] UNIDO, Pollutants in tannery effluents Sources, description, environmental impact, 2003.

[5] J.D. Cuppett, S.E. Duncan, A.M. Dietrich, Evaluation of copper speciation and water quality factors that affect aqueous copper tasting response, Chem. Senses. 31 (2006) 689–697. https://doi.org/10.1093/chemse/bjl010.

[6] L.F. Huang, M.J. Hutchison, R.J. Santucci, J.R. Scully, J.M. Rondinelli, Improved Electrochemical Phase Diagrams from Theory and Experiment: The Ni-Water System and Its Complex Compounds, J. Phys. Chem. C. 121 (2017) 9782–9789. https://doi.org/10.1021/acs.jpcc.7b02771.

[7] B. Lellis, C.Z. Fávaro-Polonio, J.A. Pamphile, J.C. Polonio, Effects of textile dyes on health and the environment and bioremediation potential of living organisms, Biotechnol. Res. Innov. 3 (2019) 275–290. https://doi.org/10.1016/j.biori.2019.09.001.

[8] C.V. Gherasim, G. Bourceanu, R.I. Olariu, C. Arsene, A novel polymer inclusion membrane applied in chromium (VI) separation from aqueous solutions, J. Hazard. Mater. 197 (2011) 244–253. https://doi.org/10.1016/j.jhazmat.2011.09.082.

[9] A.K. Golder, A.K. Chanda, A.N. Samanta, S. Ray, Removal of hexavalent chromium by electrochemical reduction-precipitation: Investigation of process performance and reaction stoichiometry, Sep. Purif. Technol. 76 (2011) 345–350. https://doi.org/10.1016/j.seppur.2010.11.002.

[10] A. Korak, Julie, R. Huggins, M. Arias-Paic, Regeneration of Pilot-Scale Ion Exchange Columns for Hexavalent Chromium Removal Supplemental Information, Water Res. 118 (2017) 141–151.

[11] S.U. Khan, D.T. Islam, I.H. Farooqi, S. Ayub, F. Basheer, Hexavalent chromium

removal in an electrocoagulation column reactor: Process optimization using CCD, adsorption kinetics and pH modulated sludge formation, Process Saf. Environ. Prot. 122 (2019) 118–130. https://doi.org/10.1016/j.psep.2018.11.024.

[12] C. Bao, M. Chen, X. Jin, D. Hu, Q. Huang, Efficient and stable photocatalytic reduction of aqueous hexavalent chromium ions by polyaniline surface-hybridized ZnO nanosheets, J. Mol. Liq. 279 (2019) 133–145. https://doi.org/10.1016/j.molliq.2019.01.122.

[13] D. Pradhan, L.B. Sukla, M. Sawyer, P.K.S.M. Rahman, Recent bioreduction of hexavalent chromium in wastewater treatment: A review, J. Ind. Eng. Chem. 55 (2017) 1–20. https://doi.org/10.1016/j.jiec.2017.06.040.

[14] Dąbrowski.A, Adsorption - from theory to practice, Adv. Colloid Interface Sci. 93 (2001) 135–224.

[15] M. Moyo, V.E. Pakade, S.J. Modise, Biosorption of lead(II) by chemically modified Mangifera indica seed shells: Adsorbent preparation, characterization and performance assessment, Process Saf. Environ. Prot. 111 (2017) 40–51. https://doi.org/10.1016/j.psep.2017.06.007.

[16] M. Lesaoana, R.P.V. Mlaba, F.M. Mtunzi, M.J. Klink, P. Edijike, V.E. Pakade, Influence of inorganic acid modification on Cr(VI) adsorption performance and the physicochemical properties of activated carbon, South African J. Chem. Eng. 28 (2019) 8–18. https://doi.org/10.1016/j.sajce.2019.01.001.

[17] O.B. Nchoe, M.J. Klink, F.M. Mtunzi, V.E. Pakade, Synthesis, characterization, and application of β-cyclodextrin-based ion-imprinted polymer for selective sequestration of Cr(VI) ions from aqueous media: Kinetics and isotherm studies, J. Mol. Liq. 298 (2020). https://doi.org/10.1016/j.molliq.2019.111991.

[18] S. Wadhawan, A. Jain, J. Nayyar, S.K. Mehta, Role of nanomaterials as adsorbents in heavy metal ion removal from waste water: A review, J. Water Process Eng. 33 (2020). https://doi.org/10.1016/j.jwpe.2019.101038.

[19] M.H. Dehghani, M.M. Taher, A.K. Bajpai, B. Heibati, I. Tyagi, M. Asif, S. Agarwal, V.K. Gupta, Removal of noxious Cr(VI) ions using single-walled carbon nanotubes and multi-walled carbon nanotubes, Chem. Eng. J. 279 (2015) 344–

352. https://doi.org/10.1016/j.cej.2015.04.151.

[20] P.S. Kumar, K. Venkatesh, E.L. Gui, S. Jayaraman, G. Singh, G. Arthanareeswaran, Electrospun carbon nanofibers/TiO_2-PAN hybrid membranes for effective removal of metal ions and cationic dye, Environ. Nanotechnology, Monit. Manag. 10 (2018) 366–376. https://doi.org/10.1016/j.enmm.2018.08.006.

[21] C. Sakulthaew, C. Chokejaroenrat, A. Poapolathep, Hexavalent chromium adsorption from aqueous solution using carbon nano-onions (CNOs), Chemosphere. 184 (2017) 1168–1174. https://doi.org/10.1016/j.chemosphere.2017.06.094.

[22] V.E. Pakade, T.D. Ntuli, A.E. Ofomaja, Biosorption of hexavalent chromium from aqueous solutions by Macadamia nutshell powder, Appl. Water Sci. 6 (2016) 1–16. https://doi.org/10.1007/s13201-016-0412-5.

[23] M. Bansal, U. Garg, D. Singh, V.K. Garg, Removal of Cr(VI) from aqueous solutions using pre-consumer processing agricultural waste: A case study of rice husk, J. Hazard. Mater. 162 (2009) 312–320. https://doi.org/10.1016/j.jhazmat.2008.05.037.

[24] S.O. Owalude, A.C. Tella, Removal of hexavalent chromium from aqueous solutions by adsorption on modified groundnut hull, Beni-Suef Univ. J. Basic Appl. Sci. 5 (2016) 377–388. https://doi.org/10.1016/j.bjbas.2016.11.005.

[25] Q. Wang, C. Zhou, Y. jie Kuang, Z. hui Jiang, M. Yang, Removal of hexavalent chromium in aquatic solutions by pomelo peel, Water Sci. Eng. 13 (2020) 65–73. https://doi.org/10.1016/j.wse.2019.12.011.

[26] M. Bansal, D. Singh, V.K. Garg, A comparative study for the removal of hexavalent chromium from aqueous solution by agriculture wastes' carbons, J. Hazard. Mater. 171 (2009) 83–92. https://doi.org/10.1016/j.jhazmat.2009.05.124.

[27] X. Peng, Z. Yan, L. Hu, R. Zhang, S. Liu, A. Wang, X. Yu, L. Chen, Adsorption behavior of hexavalent chromium in aqueous solution by polyvinylimidazole modified cellulose, Int. J. Biol. Macromol. 155 (2020) 1184–1193.

https://doi.org/10.1016/j.ijbiomac.2019.11.086.

[28] N.D. Shooto, Removal of lead(II) and chromium(VI) ions from synthetic wastewater by the roots of harpagophytum procumbens plant, J. Environ. Chem. Eng. 8 (2020) 104541. https://doi.org/10.1016/j.jece.2020.104541.

[29] V.E. Pakade, L.C. Maremeni, T.D. Ntuli, N.T. Tavengwa, Application of quaternized activated carbon derived from Macadamia nutshells for the removal of hexavalent chromium from aqueous solutions, South African J. Chem. 69 (2016) 180–188. https://doi.org/http://dx.doi.org/10.17159/0379-4350/2016/v69a22.

[30] L. Hlungwane, E.L. Viljoen, V.E. Pakade, Macadamia nutshells-derived activated carbon and attapulgite clay combination for synergistic removal of Cr(VI) and Cr(III), Adsorpt. Sci. Technol. 36 (2018) 713–731. https://doi.org/10.1177/0263617417719552.

[31] B. Tu, R. Wen, K. Wang, Y. Cheng, Y. Deng, W. Cao, K. Zhang, H. Tao, Efficient removal of aqueous hexavalent chromium by activated carbon derived from Bermuda grass, J. Colloid Interface Sci. 560 (2020) 649–658. https://doi.org/10.1016/j.jcis.2019.10.103.

[32] M. Arulkumar, K. Thirumalai, P. Sathishkumar, T. Palvannan, Rapid removal of chromium from aqueous solution using novel prawn shell activated carbon, Chem. Eng. J. 185–186 (2012) 178–186. https://doi.org/10.1016/j.cej.2012.01.071.

[33] I. Enniya, L. Rghioui, A. Jourani, Adsorption of hexavalent chromium in aqueous solution on activated carbon prepared from apple peels, Sustain. Chem. Pharm. 7 (2018) 9–16. https://doi.org/10.1016/j.scp.2017.11.003.

[34] Y.H. Chiu, L.Y. Lin, Effect of activating agents for producing activated carbon using a facile one-step synthesis with waste coffee grounds for symmetric supercapacitors, J. Taiwan Inst. Chem. Eng. 101 (2019) 177–185. https://doi.org/10.1016/j.jtice.2019.04.050.

[35] A.M. Abdel-Mohsen, J. Jancar, L. Kalina, A.F. Hassan, Comparative study of chitosan and silk fibroin staple microfibers on removal of chromium (VI):

Fabrication, kinetics and thermodynamic studies, Carbohydr. Polym. 234 (2020) 115861. https://doi.org/10.1016/j.carbpol.2020.115861.

[36] Z. Akmar Zakaria, M. Suratman, N. Mohammed, W. Azlina Ahmad, Chromium(VI) removal from aqueous solution by untreated rubber wood sawdust, Desalination. 244 (2009) 109–121. https://doi.org/10.1016/j.desal.2008.05.018.

[37] N. Asikin Awang, W. Norharyati Wan Salleh, A. Fauzi Ismail, H. Hasbullah, Synthesis, Characterization and Adsorption Properties of Grafted Cellulose for Cr(VI) Removal, Mater. Today Proc. 19 (2019) 1777–1786. https://doi.org/10.1016/j.matpr.2019.11.216.

[38] V. Pakade, L. Chimuka, Polymeric sorbents for removal of Cr(VI) from environmental samples, 85 (2013) 2145–2160.

[39] O.B. Nchoe, T.D. Ntuli, M.J. Klink, F.M. Mtunzi, V.E. Pakade, A comparative study of acid, base and Fenton-like reagent treated biomass for Cr(VI) sequestration from aqueous solutions, Water Environ. Fed. 93 (2020) 370–383. https://doi.org/10.1002/wer.1421.

[40] A. Sheikhmohammadi, S.M. Mohseni, R. Khodadadi, M. Sardar, M. Abtahi, S. Mahdav, H. Keramati, Z. Dahaghin, S. Rezaei, M. Almasian, M. Sarkhosh, M. Faraji, S. Nazari, Application of grapheoxide modified with 8-hydroxyquinoline for the adsorption of Cr(VI) from wastewater: Optimization, kinetic, thermodynamic and equilibrium studies, J. Mol. Liq. 233 (2017) 75–88.

[41] X. Jin, H. Wang, X. Jin, H. Wang, L. Chen, W. Wang, T. Lin, Z. Zhu, Preparation of keratin/PET nanofiber membrane and its high adsorption performance of Cr(VI), Sci. Total Environ. 710 (2020). https://doi.org/10.1016/j.scitotenv.2019.135546.

[42] T. Nakagawa, K. Kokubo, H. Moriwaki, Application of fullerenes-extracted soot modified with ethylenediamine as a novel adsorbent of hexavalent chromium in water, J. Environ. Chem. Eng. 2 (2014) 1191–1198. https://doi.org/10.1016/j.jece.2014.05.003.

[43] J. Hu, C. Chen, X. Zhu, X. Wang, Removal of chromium from aqueous solution

by using oxidized multiwalled carbon nanotubes, J. Hazard. Mater. 162 (2009) 1542–1550. https://doi.org/10.1016/j.jhazmat.2008.06.058.

[44] O. V. Alekseeva, N.A. Bagrovskaya, A. V. Noskov, Sorption of heavy metal ions by fullerene and polystyrene/fullerene film compositions, Prot. Met. Phys. Chem. Surfaces. 52 (2016) 443–447. https://doi.org/10.1134/S2070205116030035.

[45] R. Baby, B. Saifullah, Z.M. Hussein, Carbon Nanomaterials for the Treatment of Heavy Metal-Contaminated Water and Environmental Remediation, Nanoscale Res. Lett. 14 (2019) 1–17. https://doi.org/https://doi.org/10.1186/s11671-019-3167-8 NANO.

[46] H.W. Kroto, A.W. Allaf, S.P. Balm, C60: Buckminsterfullerene, Chem. Rev. 91 (1991) 1213–1235. https://doi.org/10.1021/cr00006a005.

[47] O. Mykhailiv, H. Zubyk, M.E. Plonska-Brzezinska, Carbon nano-onions: Unique carbon nanostructures with fascinating properties and their potential applications, Inorganica Chim. Acta. 468 (2017) 49–66. https://doi.org/10.1016/j.ica.2017.07.021.

[48] M. Zeiger, N. Jäckel, V.N. Mochalin, V. Presser, Review: Carbon onions for electrochemical energy storage, J. Mater. Chem. A. 4 (2016) 3172–3196. https://doi.org/10.1039/c5ta08295a.

[49] M.E. Plonska-Brzezinska, Carbon Nano-Onions A Review of Recent Progress in Synthesis and Applications, Chem. Nanomater. Energy, Biol. More. 5 (2019) 568–580. https://doi.org/10.1002/cnma.201800583.

[50] D. Ugarte, Curling and closure of graphitic networks under electron-beam irradiation, Nature. 359 (1992) 707–710.

[51] J. Bartelmess, S. Giordani, Carbon nano-onions (multi-layer fullerenes): Chemistry and applications, Beilstein J. Nanotechnol. 5 (2014) 1980–1998. https://doi.org/10.3762/bjnano.5.207.

[52] C. Wang, D. Li, Z. Lu, M. Song, W. Xia, Continuous preparation of carbon nano-onions in a non-thermal plasma process, Mater. Lett. 272 (2020) 127808. https://doi.org/10.1016/j.matlet.2020.127808.

[53] N. Luo, H. Jing, Z. Ma, R. Chen, Gaseous detonation chemical synthesis of

onion-like carbons, Mendeleev Commun. 27 (2017) 195–197. https://doi.org/10.1016/j.mencom.2017.03.030.

[54] M.E. Plonska-Brzezinska, A. Lapinski, A.Z. Wilczewska, A.T. Dubis, A. Villalta-Cerdas, K. Winkler, L. Echegoyen, The synthesis and characterization of carbon nano-onions produced by solution ozonolysis, Carbon N. Y. 49 (2011) 5079–5089. https://doi.org/10.1016/j.carbon.2011.07.027.

[55] A. Makhongoana, B.J. Matsoso, T.H. Mongwe, N.J. Coville, D. Wamwangi, M.S. Maubane-Nkadimeng, The role of oxygen in a carbon source (castor oil versus paraffin oil) in the synthesis of carbon nano-onions, Nanotechnology. 32 (2021). https://doi.org/10.1088/1361-6528/abd0b1.

[56] V. Dhand, M. Yadav, S.H. Kim, K.Y. Rhee, A comprehensive review on the prospects of multi-functional carbon nano onions as an effective, high-performance energy storage material, Carbon N. Y. 175 (2021) 534–575. https://doi.org/10.1016/j.carbon.2020.12.083.

[57] J.K. McDonough, Y. Gogotsi, Carbon onions: Synthesis and electrochemical applications, Electrochem. Soc. Interface. 22 (2013) 61–66. https://doi.org/10.1149/2.F05133if.

[58] L. Hultman, S. Stafström, Z. Czigány, J. Neidhardt, N. Hellgren, I.F. Brunell, K. Suenaga, C. Colliex, Cross-Linked Nano-onions of Carbon Nitride in the Solid Phase: Existence of a Novel $C_{48}N_{12}$ Aza-Fullerene, Phys. Rev. Lett. 87 (2001) 225503-225503–4. https://doi.org/10.1103/PhysRevLett.87.225503.

[59] D. Satyabola, T. Ahuja, S. Bose, B. Mondal, P. Srikrishnarka, M.P. Kannan, B.K. Spoorthi, T. Pradeep, Transformation of Nanodiamonds to Onion-like Carbons by Ambient Electrospray Deposition, J. Phys. Chem. C. 125 (2021) 10998–11006. https://doi.org/10.1021/acs.jpcc.1c00166.

[60] F. Xu, Z. Tang, S. Huang, L. Chen, Y. Liang, W. Mai, H. Zhong, R. Fu, D. Wu, Facile synthesis of ultrahigh-surface-area hollow carbon nanospheres for enhanced adsorption and energy storage, Nat. Commun. 6 (2015). https://doi.org/10.1038/ncomms8221.

[61] M. V. Diudea, A. Bende, C.L. Nagy, Carbon multi-shell cages, Phys. Chem.

Chem. Phys. 16 (2014) 5260–5269. https://doi.org/10.1039/c3cp55309d.

[62] T.D. Ntuli, T.H. Mongwe, L.L. Sikeyi, O. Mkhari, N.J. Coville, E.N. Nxumalo, M.S. Maubane-Nkadimeng, Removal of hexavalent chromium via an adsorption coupled reduction mechanism using olive oil derived carbon nano-onions, Environ. Nanotechnology, Monit. Manag. 16 (2021) 100477. https://doi.org/10.1016/j.enmm.2021.100477.

[63] L.L. Sikeyi, T.D. Ntuli, T.H. Mongwe, N.W. Maxakato, E. Carleschi, B.P. Doyle, N.J. Coville, M.S. Maubane-Nkadimeng, Microwave assisted synthesis of nitrogen doped and oxygen functionalized carbon nano onions supported palladium nanoparticles as hybrid anodic electrocatalysts for direct alkaline ethanol fuel cells, Int. J. Hydrogen Energy. 46 (2021) 10862–10875. https://doi.org/10.1016/j.ijhydene.2020.12.154.

[64] T.H. Mongwe, B.J. Matsoso, B.K. Mutuma, N.J. Coville, M.S. Maubane, Synthesis of chain-like carbon nano-onions by a flame assisted pyrolysis technique using different collecting plates, Diam. Relat. Mater. 90 (2018) 135–143. https://doi.org/10.1016/j.diamond.2018.10.002.

[65] M.R. Pallavolu, Y.A. Kumar, N. Ramesh reddy, M. Dhananjaya, B.A. Al-Asbahi, A. Sreedhar, S.W. Joo, Design and synthesis of highly efficient nitrogen-doped carbon nano-onions for asymmetric supercapacitors, J. Alloys Compd. 918 (2022) 165609. https://doi.org/10.1016/j.jallcom.2022.165609.

[66] A.V. Ramya, R. Thomas, M. Balachandran, Mesoporous onion-like carbon nanostructures from natural oil for high-performance supercapacitor and electrochemical sensing applications: Insights into the post-synthesis sonochemical treatment on the electrochemical performance, Ultrason. Sonochem. 79 (2021) 105767. https://doi.org/10.1016/j.ultsonch.2021.105767.

[67] M. Choucair, J.A. Stride, The gram-scale synthesis of carbon onions, Carbon N. Y. 50 (2012) 1109–1115. https://doi.org/10.1016/j.carbon.2011.10.023.

[68] M.B. Seymour, C. Su, Y. Gao, Y. Lu, Y. Li, Characterization of carbon nano-Onions for heavy metal ion remediation, J. Nanoparticle Res. 14 (2012) 1–14. https://doi.org/10.1007/s11051-012-1087-y.

[69] Y.J. Ko, K. Choi, S. Lee, J.M. Cho, H.J. Choi, S.W. Hong, J.W. Choi, H. Mizuseki, W.S. Lee, Chromate adsorption mechanism on nanodiamond-derived onion-like carbon, J. Hazard. Mater. 320 (2016) 368–375. https://doi.org/10.1016/j.jhazmat.2016.08.041.

[70] T.D. Ntuli, V.E. Pakade, Hexavalent chromium removal by polyacrylic acid-grafted Macadamia nutshell powder through adsorption–reduction mechanism: Adsorption isotherms, kinetics and thermodynamics, Chem. Eng. Commun. 207 (2019) 1–16. https://doi.org/10.1080/00986445.2019.1581619.

[71] C. Jung, J. Heo, J. Han, N. Her, S.J. Lee, J. Oh, J. Ryu, Y. Yoon, Hexavalent chromium removal by various adsorbents: Powdered activated carbon, chitosan, and single/multi-walled carbon nanotubes, Sep. Purif. Technol. 106 (2013) 63–71. https://doi.org/10.1016/j.seppur.2012.12.028.

[72] S. Lal, A. Singhal, P. Kumari, Exploring carbonaceous nanomaterials for arsenic and chromium removal from wastewater, J. Water Process Eng. 36 (2020) 101276. https://doi.org/10.1016/j.jwpe.2020.101276.

[73] Ihsanullah, F.A. Al-Khaldi, B. Abu-Sharkh, A.M. Abulkibash, M.I. Qureshi, T. Laoui, M.A. Atieh, Effect of acid modification on adsorption of hexavalent chromium (Cr(VI)) from aqueous solution by activated carbon and carbon nanotubes, Desalin. Water Treat. 57 (2016) 7232–7244. https://doi.org/10.1080/19443994.2015.1021847.

[74] E.N. Zare, A. Motahari, M. Sillanpää, Nanoadsorbents based on conducting polymer nanocomposites with main focus on polyaniline and its derivatives for removal of heavy metal ions/dyes: A review, Environ. Res. 162 (2018) 173–195. https://doi.org/10.1016/j.envres.2017.12.025.

[75] V.E. Pakade, T.D. Ntuli, A.E. Ofomaja, Biosorption of hexavalent chromium from aqueous solutions by Macadamia nutshell powder, Appl. Water Sci. 7 (2017) 3015–3030. https://doi.org/10.1007/s13201-016-0412-5.

[76] L. Joseph, B.M. Jun, J.R.V. Flora, C.M. Park, Y. Yoon, Removal of heavy metals from water sources in the developing world using low-cost materials: A review, Chemosphere. 229 (2019) 142–159. https://doi.org/10.1016/j.chemosphere.2019.04.198.

[77] H.N. Tran, S.J. You, A. Hosseini-Bandegharaei, H.P. Chao, Mistakes and inconsistencies regarding adsorption of contaminants from aqueous solutions: A critical review, Water Res. 120 (2017) 88–116. https://doi.org/10.1016/j.watres.2017.04.014.

[78] J. Wang, X. Guo, Adsorption kinetic models: Physical meanings, applications, and solving methods, J. Hazard. Mater. 390 (2020) 122156. https://doi.org/10.1016/j.jhazmat.2020.122156.

[79] S. Lagergren, “Zur Theorie der Sogenannten Adsorption GelosterStoffe”, Kungliga Svenska Vetenskapsakademiens., Handl. Band. 24 (1898) 1–39.

[80] V.K. Gupta, M. Gupta, S. Sharma, Process development for the removal of lead and chromium from aqueous solutions using red mud - An aluminium industry waste, Water Res. 35 (2001) 1125–1134. https://doi.org/10.1016/S0043-1354(00)00389-4.

[81] S. Sen Gupta, K.G. Bhattacharyya, Kinetics of adsorption of metal ions on inorganic materials: A review, Adv. Colloid Interface Sci. 162 (2011) 39–58. https://doi.org/10.1016/j.cis.2010.12.004.

[82] Y. Xie, H. Li, X. Wang, I.S. Ng, Y. Lu, K. Jing, Kinetic simulating of Cr(VI) removal by the waste Chlorella vulgaris biomass, J. Taiwan Inst. Chem. Eng. 45 (2014) 1773–1782. https://doi.org/10.1016/j.jtice.2014.02.016.

[83] M. Barkat, D. Nibou, S. Chegrouche, A. Mellah, Kinetics and thermodynamics studies of chromium(VI) ions adsorption onto activated carbon from aqueous solutions, Chem. Eng. Process. 48 (2009) 38–47. https://doi.org/10.1016/j.cep.2007.10.004.

[84] G. Blanchard, M. Maunaye, G. Martin, Removal of heavy metals from waters by means of natural zeolites, Water Res. 18 (1984) 1501–1507. https://doi.org/10.1016/0043-1354(84)90124-6.

[85] Y. Ho, G. McKay, Pseudo-second order model for sorption processes, Process Biochem. 34 (1999) 451–651.

[86] I. Langmuir, The adsorption of gases on plane surfaces of glass, mica and platinum., J. Am. Chem. Soc. 40 (1918) 1361–1403. https://doi.org/doi:

10.1021/ja02242a004.

[87] H. Freundlich, Über die Adorption in Lösungen, Z Phys.Chem. 57 (1906) 385–471.

[88] Y.S. Ho, C.T. Huang, H.W. Huang, Equilibrium sorption isotherm for metal ions on tree fern, Process Biochem. 37 (2002) 1421–1430. https://doi.org/10.1016/S0032-9592(02)00036-5.

[89] K.R. Hall, L.C. Eagleton, A. Acrivos, T. Vermeulen, Pore- and solid-diffusion kinetics in fixed-bed adsorption under constant-pattern conditions, Ind. Eng. Chem. Fundam. 5 (1966) 212–223. https://doi.org/10.1021/i160018a011.

[90] E. Worch, Adsorption Technology in Water Treatment: Fundamentals, Processes, and Modeling, 2nd rev. e, De Gruyter, 2012. https://doi.org/https://doi.org/10.1515/9783110715507.

[91] M.K.H.M. Nazri, N. Sapawe, A short review on photocatalytic toward dye degradation, Mater. Today Proc. 31 (2020) A42–A47. https://doi.org/10.1016/j.matpr.2020.10.967.

[92] A. Mills, S. Le Hunte, An overview of semiconductor photocatalysis, J. Photochem. Photobiol. A Chem. 108 (1997) 1–35. https://doi.org/10.1126/science.12.296.346-a.

[93] D. Zhu, Q. Zhou, Action and mechanism of semiconductor photocatalysis on degradation of organic pollutants in water treatment: A review, Environ. Nanotechnology, Monit. Manag. 12 (2019) 100255. https://doi.org/10.1016/j.enmm.2019.100255.

[94] K.M. Reddy, S. V. Manorama, A.R. Reddy, Bandgap studies on anatase titanium dioxide nanoparticles, Mater. Chem. Phys. 78 (2003) 239–245. https://doi.org/10.1016/S0254-0584(02)00343-7.

[95] N. Serpone, A. V. Emeline, Semiconductor photocatalysis - Past, present, and future outlook, J. Phys. Chem. Lett. 3 (2012) 673–677. https://doi.org/10.1021/jz300071j.

[96] W. Zhou, Y. Guan, D. Wang, X. Zhang, D. Liu, H. Jiang, J. Wang, X. Liu, H. Liu, S. Chen, PdO/TiO_2 and Pd/TiO_2 heterostructured nanobelts with enhanced

photocatalytic activity, Chem. - An Asian J. 9 (2014) 1648–1654. https://doi.org/10.1002/asia.201301638.

[97] Y.J. Hwang, S. Yang, H. Lee, Surface analysis of N-doped TiO_2 nanorods and their enhanced photocatalytic oxidation activity, Appl. Catal. B Environ. 204 (2017) 209–215. https://doi.org/10.1016/j.apcatb.2016.11.038.

[98] P. Shandilya, D. Mittal, M. Soni, P. Raizada, J.H. Lim, D.Y. Jeong, R.P. Dewedi, A.K. Saini, P. Singh, Islanding of $EuVO_4$ on high-dispersed fluorine doped few layered graphene sheets for efficient photocatalytic mineralization of phenolic compounds and bacterial disinfection, J. Taiwan Inst. Chem. Eng. 93 (2018) 528–542. https://doi.org/10.1016/j.jtice.2018.08.034.

[99] T.A. Saleh, The Role of Carbon Nanotubes in Enhancement of Photocatalysis, in: Satoru Suzuki (Ed.), Synth. Appl. Carbon Nanotub. Their Compos., INTECH, 2013: pp. 479–493. https://doi.org/10.5772/51050.

[100] S.J. Park, G.S. Das, F. Schütt, R. Adelung, Y.K. Mishra, K.M. Tripathi, T.Y. Kim, Visible-light photocatalysis by carbon-nano-onion-functionalized ZnO tetrapods: degradation of 2,4-dinitrophenol and a plant-model-based ecological assessment, NPG Asia Mater. 11 (2019). https://doi.org/10.1038/s41427-019-0107-0.

[101] Z. Guo, J. Zhang, H. Liu, Y. Kang, Development of a nitrogen-functionalized carbon adsorbent derived from biomass waste by diammonium hydrogen phosphate activation for Cr(VI) removal, Powder Technol. 318 (2017) 459–464. https://doi.org/10.1016/j.powtec.2017.06.024.

[102] Z. Sun, B. Liu, M. Li, C. Li, S. Zheng, Carboxyl-rich carbon nanocomposite based on natural diatomite as adsorbent for efficient removal of Cr (VI), J. Mater. Res. Technol. 9 (2020) 948–959. https://doi.org/10.1016/j.jmrt.2019.11.034.

Chapter 3: Methodology

This chapter presents the research methodology comprising materials, chemicals, and experimental procedures such as synthesis and adsorption experiments. The chapter is rounded up by presenting the instrumentation and techniques used in the study.

3.1.1. Materials and chemicals

Olive oil (Hercules) used for the synthesis of OLNCs was purchased from a local supermarket and was used as received, without any other treatment. The waste cooking oil was collected from a local restaurant. The waste cooking oil was filtered using 0.45 μL to remove solid particles and used without any other treatment. All the chemicals used were obtained from Sigma-Aldrich, South Africa; and were used as received unless otherwise stated. The pH adjustment of the solutions was achieved by dropwise addition of 0.1 M HCl (ACS reagent, 37%) and 0.1 M NaOH (ACS reagent, 97%). Stock solutions were prepared in the laboratory by dissolving calculated amounts of $K_2Cr_2O_7$ (ACS reagent, 99%), $CuCl_2$.$2H_2O$ (ACS reagent, 99%), $NiCl_2.6H_2O$ (bioreagent) and methyl orange (ACS reagent, 85%) accordingly in 1000 mL deionized water. For purification and chemical modification appropriate amounts of hexane (laboratory reagent, 95%), H_2O_2 (ACS reagent, 30%) and KOH (ACS reagent, 85%) were used and for complexing 1,5 – diphenylcarbazide (reagent grade, 98%) and H_2SO_4 (ACS reagent, 98%) were used. TiO_2 (anatase) (nanopowder, 99.7%) and $FeCl_3.6H_2O$ (ACS reagent, 97%) were used for the respective nanocomposites.

3.1.2. Synthesis of the adsorbent (OLNCs)

The OLNCs were synthesized using a modified method that was adopted by Mongwe et al. [7]. A wick was soaked in olive oil and ignited over a nozzle to give a flame, and the adsorbent (OLNCs) was collected on a brass plate. This was done repeatedly until a satisfactory amount of the OLNCs was adequate for all the adsorption experiments. The same procedure was followed when using waste cooking oil as a carbon processor. The percentage conversion of 100 mL oil was found to be 4% (olive oil) and 8% (waste cooking oil) as shown by equation 1

$$\%Conversion = \frac{Total\ CNO's\ collected\ (g)}{Total\ oil\ used\ (g)} \times 100 \quad (1)$$

3.1.3. Purification and chemical modification of the OLNCs

The synthesized OLNCs were purified with hexane. In a standard procedure, 2 g of the OLNCs was added into a round bottom flask containing 100 mL of hexane and refluxed for 6 h at 60°C. The procedure was repeated three times pending the yellow solution turning colourless. Thereafter, the material was rinsed with deionized water until a neutral pH was achieved. This was followed by filtration using a Millipore filter and dried in an oven for 24 h at 70°C. The material was stored in a desiccator for use. This procedure was also followed for the modification with 25% and 10% of H_2O_2 and 0.1 M and 0.2 M KOH solutions.

3.1.4. Synthesis of nanocomposites

The OLNCs were incorporated with TiO_2 (anatase), where 10 mg of OLNCs was added to 100 mg of TiO_2 (anatase) in a 5 M solution of 50 mL NaOH. The mixture was refluxed for 6 h at 100 °C, the nanocomposites were separated from the solution by using centrifugation. Then rinsed with ethanol and HCl to remove unreacted materials and

regeneration. The material was rinsed with distilled water and vacuum dried at 60°C for 24 h.

Then the materials were subjected to calcination at 450°C for 4 h in an inert environment. The material was called TC-50, TC-30, TC20, and TC-10 according to the mass (mg) of OLNCs added to the TiO_2. In summary two powdered materials were mixed, but they were mixed in a solution of a hot strong base. Such a synthesis method promotes crystal growth of the TiO_2 due to the NaOH.

For the iron oxide/OLNCs nanocomposites, 25 mg of OLNCs were mixed with 100 mg $FeCl_3.6H_2O$ in 50 mL of 5 M NaOH solution. The mixture was refluxed at 150°C for 12 h, followed by centrifugation to separate the solid and the solution. The material was rinsed with deionised water to a stable pH of 9 and then rinsed with ethanol until a pH of 7 was achieved. The material was dried in a vacuum oven at 80°C for 24 h and then calcined at 450°C under a flow of N_2 (g) for 4 h. The mass of the OLNCs was varied as follows (25, 50, 100, 170 mg) and the synthesized materials were labelled FeC-25, FeC-50, FeC-100, and FeC-170, corresponding to the mass of the OLNCs.

3.1.5. Batch adsorption experiments

Parameters that were varied for the adsorption experiments include solution pH, contact time, initial concentration, the temperature of the solution, and the mass of the adsorbent. The effect of solution pH was used as an example for all other adsorption experiments that were conducted. Firstly the pH range was selected to be (2, 3, 4, 5, 6, 7, and 8) where 0.02 g of the adsorbent was transferred in a series of 100 mL conical flasks containing 10 mL of 10 mg/L adsorbates at different solution pH. The mixture was agitated using an OrbiShake for 720 min and the adsorbent and adsorbate were separated using a Millipore filter. The adsorbate's concentration was determined with

the AA-7000 atomic absorption spectrometer (AAS) (total Cr, Cu(II), and Ni(II). The aforementioned AAS was only used for Chapter 4 samples and subsequent Chapters the atomic absorption spectrometer (200 Series AA). The 1,5-diphenylcarbazade was used as a complexing agent for the determination of the concentration of Cr(VI) at a wavelength of 540 nm using the Cary 100 ultraviolet-visible spectroscopy. The same instrument was used to determine the concentration of methyl orange at a wavelength of 464 nm.

The concentration of Cr(III) was determined by subtraction of Cr(VI) from total chromium. To calculate the percent removal and adsorption capacity equations 2 and 3 were used respectively.

$$\%R = \frac{C_o - C_e}{C_o} \times 100 \qquad 2$$

$$q_e = \frac{(C_o - C_e)V}{m} \qquad 3$$

Where: C_o is the initial concentration (mg/L), C_e is the equilibrium concentration (mg/L), q_e is the adsorption capacity (mg/g) $\%R$ is the percent removal, V is the volume of solution (L) and m is the mass of the adsorbent (g).

3.1.6. Photocatalysis experiments

The adsorption of methyl orange using OLNCs and the nanocomposites was performed at a pH of 7, solution volume of 50 mL and mass of 100 mg for 120 min. Aliquots were withdrawn from the solution at appropriate intervals. The reaction was conducted in a 100 mL silica glass tube and agitated at 200 rpm.

The photodegradation of methyl orange was conducted in a 100 mL quartz tube. The quartz tube was connected to a 300 W Xe short arc lamp (solar simulator equivalent to 1 sun radiation) as a source of light. The quartz tube and the lamp were placed 20 cm apart to enable 1000 W m^{-2} t radiation. Where 100 mg of the nanocomposites/catalyst was introduced into 50 mL of 10 mg/L of methyl orange solution at pH 7.

The experiment was first conducted in the dark for 30 min for adsorption-desorption homogeneity. Then the lamp was switched on and 2 mL of aliquots were withdrawn from the reaction mixture at 5, 10, 15, 20, 30, 60, and 120 min intervals. The concentration of methyl orange was determined by the Cary 100 ultraviolet-visible (UV–vis) spectrometer at a wavelength of 465 nm. The rate of degradation of methyl orange ions was presented by a plot of C_e/C_o against time (t; min). Where C_e (mg/L) was the equilibrium concentration, C_O (mg/L) was the initial concentration and t (min) was the time taken for the reaction.

A similar pattern was followed for the photocatalytic reduction of Cr(VI) ions where methyl orange was replaced with a Cr(VI) solution. The concentration of Cr(VI) ions was determined by using the aforementioned UV-vis spectrometer and AAS for total Cr. The rate of reduction of Cr(VI) ions to Cr(III) ions was presented by a plot of C_e/C_o against time (t; min). Where C_e (mg/L) was the equilibrium concentration, C_O (mg/L) was the initial concentration and t (min) was the time taken for the reaction.

3.1.7. Adsorbent regeneration or desorption

In a typical desorption experiment, firstly an adsorption experiment was conducted at optimum conditions with 0.1 M HCl and 0.1 M NaOH solutions chosen as regeneration agents. After the adsorption was conducted the adsorbate and adsorbent were separated using a Millipore filter, and the adsorbent was rinsed with deionized water until a neutral pH. Then, the adsorbent was dried for 24 h in an oven at 70°C. The

adsorbent was then transferred into a conical flask containing 0.1 M HCl and 0.1 M NaOH respectively, for 2880 min and the concentration of the adsorbate was determined. After the desorption experiment, the adsorbate was again rinsed with deionized water until a neutral pH, filtered and dried in an oven for 24 h at 70°C. The desorption cycle was repeated five times.

3.2. Equilibrium studies

3.2.1. Kinetic modelling

The experimental data was tested against the Lagergren pseudo-first-order (PFO) [8] and pseudo-second-order (PSO) [9] kinetic model. The nonlinear and linear forms of the PFO are represented by equations 4 and 5 respectively.

$$q_t = q_e(1 - e^{k_1 t}) \quad (4)$$

$$\log(q_e - q_t) = \frac{k_1}{2.303} t + \log(q_e) \quad (5)$$

Where q_e (mg/g) and q_t (mg/g) are the amounts of adsorbate uptake per mass of adsorbent at equilibrium and at any time t (min) respectively, k_1 (1/min) represents the rate constant of the PFO model.

The nonlinear and linear forms of the PSO and the initial adsorption rate (*h*) proposed by Ho et al.[9] are presented by equations 6, 7 and 8 respectively.

$$q_t = \frac{q_e^2 k_2 t}{1 + k_2 q_e t} \quad (6)$$

$$\frac{t}{q_t} = \left(\frac{1}{q_e}\right)t + \frac{1}{k_2 q_e^2} \quad (7)$$

$$h = k_2 = k_2 q_e^2 \quad (8)$$

Where q_e (mg/g) and q_t (mg/g) are the amounts of adsorbate uptake per mass of adsorbent at equilibrium and at any time t (min) respectively, k_2 (g/mg x min) is the rate constant of the PSO model.

3.2.2. Adsorption isotherms

The experimental data was tested against the Langmuir [10] and Freundlich [11] isotherm to determine whether the adsorption process proceeded via monolayer or multilayer adsorption. The nonlinear and linear forms of the Langmuir isotherm can be represented by equations 9 and 10 respectively. The dimensionless separation factor R_L is represented by equation 11.

$$q_e = \frac{Q_{max}^O K_L C_e}{1 + K_L C_e} \quad (9)$$

$$\frac{C_e}{q_e} = \left(\frac{1}{Q_{max}^O}\right)C_e + \frac{1}{Q_{max}^O K_L} \quad (10)$$

$$R_L = \frac{1}{1 + K_L C_0} \quad (11)$$

Where Q_{max}^{O} (mg/g) and q_e (mg/g) represents the maximum adsorption capacity for the Langmuir model and adsorption capacity for the experimental data at equilibrium respectively, C_O (mg/L) and C_e (mg/L) are the initial and equilibrium concentration of the adsorbate, K_L (L/mg) is the Langmuir equilibrium constant that is related to the affinity between the adsorbent and adsorbate.

The nonlinear and linear forms of the Freundlich isotherms are represented by equations 12 and 13 respectively.

$$q_e = K_F C_e^n \quad (12)$$

$$\log q_e = n \log C_e + \log K_F \quad (13)$$

Where q_e (mg/g) is the amount of adsorbate uptake at equilibrium, K_F (mg/g)/(mg/L)^n is the Freundlich constant, C_e (mg/L) is the concentration of the adsorbate at equilibrium, n is the dimensionless Freundlich intensity parameter.

For determination of the best fitting model the chi-squared (χ^2) and the coefficient of determination (R^2) has been used as shown by equations 14 and 15 respectively.

$$\mathcal{X}^2 = \sum \frac{(q_{e,exp} - q_{e,exp})^2}{q_{e,cal}} \quad (14)$$

$$R^2 = 1 - \frac{\sum(q_{e,exp} - q_{e,cal})^2}{\sum(q_{e,exp} - q_{e,mean})^2} \quad (15)$$

Where, $q_{e,\,exp}$ (mg/g), and $q_{e,\,cal}$ (mg/g) are the adsorption capacity of the experimental data and model respectively, the $q_{e,\,mean}$ (mg/g) is the mean adsorption capacity of the $q_{e,exp}$ values.

3.2.3. Thermodynamics

The thermodynamic parameters have been computed by using equations 16 to 19

$$\Delta G° = -RT\ln K_C \quad (16)$$

The equilibrium constant (K_C) was made dimensionless by multiplying the Langmuir constant (K_L) by a factor of 10^6 the density of the solution with the assumption that the density of pure water is 1.0 g/mL as shown by equation 17.

$$K_C = 10^6 K_L \quad (17)$$

Substitute equation 17 into 16 to obtain equation 18, then the relationship of the Gibbs energy change (ΔG°) to the enthalpy change (ΔH°) and the entropy change (ΔS°) can be described by equation 19.

$$\Delta G° = - RT\ln(10^6 K_L) \quad (18)$$

$$\Delta G° = \Delta H° - T\Delta S° \quad (19)$$

By substituting equation 18 into 19, the van't Hoff equation can be obtained as shown by equation 20.

$$\text{Ln}(10^6 K_L) = \frac{-\Delta H°}{R} \times \frac{1}{T} + \frac{\Delta S°}{R} \quad (20)$$

Where T is the absolute temperature (K) and R is the universal gas constant (8.3144 J/mol x K). The (ΔG°) can be calculated from equation 18, with (ΔH°) and (ΔS°)

obtained from the slope and intercept of the plot of $\ln K_C$ v/s 1/T from equation 20 respectively.
Microsoft excel and the KyPlot were used in the computation of the data obtained.

3.3. Instrumentation and characterization techniques

The surface morphology of materials used in Chapter 4 was determined by using transmission electron microscopy (TEM); (Tecnai G2 30ST), along with scanning electron microscopy (SEM); (FEI Nova). The samples were prepared by dispersing a tip of a spatula of the sample in 4 mL of distilled water and sonicated for 5 min. Then the sample was drop cast on a copper grid and allowed to dry, the sample was kept in a dry place for use. For SEM the samples were prepared in the same way that the TEM samples were prepared but were drop-cast in an aluminium stub and coated with palladium. For subsequent Chapters the JEOL JEM-2100F transmission electron microscope (TEM) at 200 kV and ZEISS GeminiSEM 560 scanning electron microscopy (SEM) utilizing sub 1 kV resolution below 1 nm. The surface area, average pore size and pore volume of all the materials were determined by using a Micrometrics Tristar 3000, where the samples were used as synthesized by weighing 300 mg of each sample. The surface configurations of the materials were determined by using the Thermo ESCAlab 250Xi X-ray photoelectron spectroscopy (XPS) and a Bruker Tensor 27 Fourier transform infrared (FTIR) spectroscopy for Chapter 4 materials and the FTIR spectroscopy (PerkinElmer Spectrum 100) for subsequent Chapters. The thermal analysis of all the materials was determined by using a Perkin Elmer 6000 thermogravimetric analyzer. The samples were used as synthesized and the thermal analysis was conducted under oxygen. A Horiba Jobin Yvon Raman spectrometer equipped with a laser wavelength of $\lambda = 514$ nm, was used for all Raman spectral analyses to determine the surface defects. The crystallinity of the materials was evaluated using the Bruker D2 Phaser Powder X-Ray Diffractometer (PXRD), using monochromatic Cu K_{alpha} radiation generated at 30 kV and 10 mA. For other instruments, the samples were used as synthesized by weighing the appropriate amounts.

3.4. References

[1] T.P. Mofokeng, Z.N. Tetana, K.I. Ozoemena, Defective 3D nitrogen-doped carbon nanotube-carbon fibre networks for high-performance supercapacitor: Transformative role of nitrogen-doping from surface-confined to diffusive kinetics, Carbon N. Y. 169 (2020) 312–326. https://doi.org/10.1016/j.carbon.2020.07.049.

[2] M. Lesaoana, R.P.V. Mlaba, F.M. Mtunzi, M.J. Klink, P. Edijike, V.E. Pakade, Influence of inorganic acid modification on Cr(VI) adsorption performance and the physicochemical properties of activated carbon, South African J. Chem. Eng. 28 (2019) 8–18. https://doi.org/10.1016/j.sajce.2019.01.001.

[3] P.S. Kumar, K. Venkatesh, E.L. Gui, S. Jayaraman, G. Singh, G. Arthanareeswaran, Electrospun carbon nanofibers/TiO_2-PAN hybrid membranes for effective removal of metal ions and cationic dye, Environ. Nanotechnology, Monit. Manag. 10 (2018) 366–376. https://doi.org/10.1016/j.enmm.2018.08.006.

[4] A.S. Rad, S.M. Aghaei, E. Aali, M. Peyravi, Study on the electronic structure of Cr- and Ni-doped fullerenes upon adsorption of adenine: A comprehensive DFT calculation, Diam. Relat. Mater. 77 (2017) 116–121. https://doi.org/10.1016/j.diamond.2017.06.013.

[5] P. Dong, T. Maneerung, W.C. Ng, X. Zhen, Y. Dai, Y.W. Tong, Y.P. Ting, S.N. Koh, C.H. Wang, K.G. Neoh, Chemically treated carbon black waste and its potential applications, J. Hazard. Mater. 321 (2017) 62–72. https://doi.org/10.1016/j.jhazmat.2016.08.065.

[6] T.D. Ntuli, T.H. Mongwe, L.L. Sikeyi, O. Mkhari, N.J. Coville, E.N. Nxumalo, M.S. Maubane-Nkadimeng, Removal of hexavalent chromium via an adsorption coupled reduction mechanism using olive oil derived carbon nano-onions, Environ. Nanotechnology, Monit. Manag. 16 (2021) 100477. https://doi.org/10.1016/j.enmm.2021.100477.

[7] T.H. Mongwe, B.J. Matsoso, B.K. Mutuma, N.J. Coville, M.S. Maubane, Synthesis of chain-like carbon nano-onions by a flame assisted pyrolysis technique using different collecting plates, Diam. Relat. Mater. 90 (2018) 135–143. https://doi.org/10.1016/j.diamond.2018.10.002.

[8] S. Lagergren, “Zur Theorie der Sogenannten Adsorption GelosterStoffe”, Kungliga Svenska Vetenskapsakademiens., Handl. Band. 24 (1898) 1–39.

[9] Y.S. Ho, G. McKay, The Kinetics of Sorption of Basic Dyes from Aqueous Solution by Sphagnum Moss Peat, Can. J. Chem. Eng. 76 (1998) 822–827. https://doi.org/10.1002/cjce.5450760419.

[10] I. Langmuir, The adsorption of gases on plane surfaces of glass, mica and platinum., J. Am. Chem. Soc. 40 (1918) 1361–1403. https://doi.org/doi: 10.1021/ja02242a004.

[11] H. Freundlich, Über die Adorption in Lösungen, Z Phys.Chem. 57 (1906) 385–471.

Chapter 4: Removal of hexavalent chromium via an adsorption coupled reduction mechanism using olive oil-derived carbon nano-onions

Published: T.D. Ntuli, T.H. Mongwe, L.L. Sikeyi, O. Mkhari, N.J. Coville, E.N. Nxumalo, M.S. Maubane-Nkadimeng, Removal of hexavalent chromium via an adsorption coupled reduction mechanism using olive oil derived carbon nano-onions, Environmental Nanotechnology, Monitoring & Management, 16 (2021) 100477.

Abstract

Carbon nano-onions (CNOs) were obtained on a gram-scale by a simple flame pyrolysis method using olive oil. The olive oil carbon nano-onions (OCNOs) obtained had a quasi-spherical chain-like onion structure with an average diameter of 46 ± 5.4 nm. Fourier transform infrared spectroscopy and X-ray photoelectron spectroscopy (XPS) analysis were employed to determine the existence of surface functional groups (-OH, -COOH) on the OCNOs. The OCNOs were applied as adsorbents for the elimination of Cr(VI) ions from aqueous solutions using batch experiments. The ideal conditions for the sequestration of Cr(VI) ensued at pH = 2, T = 25°C, m = 0.05 g, t = 720 min, and C_O = 10 mg/L. The XPS data for Cr after adsorption on the OCNOs revealed that Cr(III) ions were produced in the reaction, consistent with the adsorption-coupled reduction mechanism. The sequestration of Cr(VI) proceeded via monolayer surface coverage (Langmuir isotherm), with the kinetic information in line with the pseudo-second-order model. The thermodynamic features showed that the removal progression was viable, exothermic, and involved an associative mechanism. After the adsorbent regeneration, the removal of Cr(VI) ions was improved owing to the -OH ions added by the NaOH (regeneration solution). The CNOs produced by flame pyrolysis gave similar Cr(VI) removal data to that observed using more sophisticated CNO synthesis methods.

Keywords:
Adsorption; carbon nano-onions; flame pyrolysis; hexavalent chromium

4.1. Introduction

Multiple anthropogenic activities in the 21st century have resulted in an increased accumulation of trace metal ions in water bodies [1]. The foremost problems associated with trace metal ions are that they contribute to the contamination of water sources, are toxic and persistent in the environment, and bio-accumulate in living organisms [2]. Frequent exposure to trace metal ions by humans can have detrimental health effects such as skin problems, mutilation of internal organs, and can cause cancer [3]. Hexavalent chromium, [Cr(VI)], is one such toxic trace metal and exists as H_2CrO_4, $HCr_2O_4^-$, CrO_4^{2-} and $Cr_2O_7^{2-}$ in an aqueous solution [4]. Industries that use chromium (in particular mining, leather tanning, textile, and electroplating [5]) can generate Cr(VI) ions. Due to the detrimental effects of Cr(VI) ions, even low concentrations of Cr(VI) need to be removed from water systems, with the World Health Organization (WHO) setting the exposure limit in drinking water at 0.05 mg/L [6].

Numerous approaches have been applied for the remediation of trace metal ions from the aquatic environment. These comprise electrocoagulation [7], photoreduction [8], membrane technologies [9], precipitation [10], ion–exchange [11], electrodialysis [12], and adsorption [13]. The chemical reduction of Cr(VI) ions to Cr(III) has played a pivotal role in the remediation of Cr(VI) ions and typical reducing agents that have been used include H_2S, H_2O_2, SO_2, and Fe^{2+}. However, these aforementioned reducing agents can themselves contribute to toxicity and thus their use should be limited if possible [14]. Moreover, adsorption has attracted considerable attention among researchers because of the use of inexpensive and abundantly available materials, in particular carbonaceous materials, as adsorbents [15]. Carbonaceous materials such as agricultural waste material [16,17], natural and synthetic polymers [18], biochar [19], sawdust [20], fly ash [21], and activated carbon [22,23], have all been used as adsorbent materials. The evolution of studies on the aforementioned carbon materials has led to the synthesis of micro or macro-carbon nanoparticles [24]. These carbon nanoparticles include graphene flakes [25], graphene [26,27], carbon nanotubes [28], carbon nanofibers [29], thin carbon structures [30] and fullerenes [31]. Another class of carbon nanoparticles that have been studied is that of the carbon nano-onions (CNOs), which belong to the family of fullerenes. These nanoparticles

have a graphitic morphology with a quasi-spherical or polyhedral shape with carbon layers packed close to each other [32]. The CNOs have been synthesized by chemical vapour deposition [33], arc-discharge [34], ozonolysis [35], laser ablation [36], and pyrolysis [37]. For example, the pyrolysis of propane has been reported to make CNOs in a process that is low cost and sustainable [38]. The pyrolysis technique was reported to have yielded CNOs in gram scale quantity. The advantage of this method is that no catalyst is used and as a result, it produces carbon materials that are relatively free of impurities [39].

The CNOs have been used for energy conversion and storage, catalysis, and environmental applications [40]. In particular, CNOs found attraction as adsorbents for the elimination of Cr(VI) ions [41,42]. While CNOs used in these studies were successfully employed as adsorbents, the CNOs were made by either a laser resonant excitation method [42] or by the annealing of nanodiamonds [41]. The setback with these synthetic methods is that they require sophisticated instruments such as a laser and high consumption of electricity for annealing, which can be costly. In this study, we have made CNOs by a simple and cheap process (flame pyrolysis of olive oil). Olive oil was chosen for this study as it has a carbon-rich structure and contains mostly oleic acid (monosaturated fatty acid) which is less accessible to thermal oxidation than many other vegetable oils. It is also available in ‘used or waste’ form, and the conversion of the used olive oil to more useful products is needed to reduce the impact of the used oil on the environment. Herein we only report on the conversion of the ‘pure’ oil, to provide a basic understanding of its conversion to CNOs.

This study was to establish if (i) the CNOs synthesis method was viable and (ii) to determine if the CNOs produced by this simple methodology would give similar Cr(VI) removal data to that observed with more sophisticated synthesis methods. This was achieved by studying the effect of adsorption constraints at a pH range (2 – 8) at a particular time (t), mass (m) of OCNOs, and initial concentration (C_O) of Cr(VI) ions. The sequestration of Cr(VI) ions was considered by fitting the experimental data to the Lagergren pseudo-first-order (PFO) [43] and the pseudo-second-order (PSO) models [44] and adsorption isotherms such as the Langmuir [45] and Freundlich [46] isotherms.

4.2. Experimental

4.2.1. Materials and chemicals

Olive oil (Hercules) used for the synthesis of CNOs was purchased from a local supermarket and was used without any further treatment. All chemicals used were acquired from Sigma-Aldrich, South Africa; and were used as received unless otherwise stated. The pH adjustment of the solutions was achieved by the dropwise accumulation of 0.1 M HCl or 0.1 M NaOH. The stock solution comprising Cr(VI) ions was prepared in the laboratory by dissolving appropriate amounts of $K_2Cr_2O_7$ in 1000 mL of deionized water. 1,5-Diphenylcarbazade was used as a complexing agent with Cr(VI) to determine the Cr(VI) concentrations in the solution.

4.2.2. Preparation of adsorbent

The CNOs were synthesized via the flame pyrolysis method that was adapted from [32]. A wick was dipped in olive oil and kindled to give fire, and the adsorbent (CNOs) was collected on a brass plate which was placed 3 cm from the top of the wick. This was repeated until a satisfactory amount of the CNOs was collected. About 4 g of the CNOs per 100 g of oil was collected (1 h) and the percentage conversion was found to be 4% (equation 1). The black carbonaceous material was used as-synthesized and called olive oil carbon nano-onions (OCNOs).

4.2.3. Characterization of the adsorbent

A Micrometrics Tristar 3000 surface area and porosity analyzer were utilized to elucidate the surface area, pore-volume, and pore size of the OCNOs. The thermal analysis of the samples was conducted using a Perkin Elmer 6000 thermogravimetric analyzer. A Bruker Tensor 27 Fourier transform infrared (FTIR) spectrometer and a Thermo ESCAlab 250Xi X-ray photoelectron spectrometer were used to determine the surface composition of the OCNOs. Scanning electron microscopy (SEM), (FEI Nova), and transmission electron microscopy (TEM) (Tecnai G2 30ST) were used to study the morphological properties of the OCNOs.

4.2.4. Batch adsorption experiments

In a typical adsorption experiment, 0.025 g of OCNOs was transferred into flasks comprising 10 mL of 10 mg/L Cr(VI) ions. This was done at a pH range of (2 – 8) and agitated using an OrbiShake for 720 min. This was followed by filtration for the separation of the adsorbate and the absorbent. The final concentration of total chromium remaining in the solution was determined using the AA-7000 atomic absorption spectrometer (AAS). The Cary 100 ultraviolet-visible (UV-Vis) spectrometer was employed to measure the concentration of Cr(VI) ions, using 1,5-diphenylcarbazade at a wavelength of 540 nm. The concentration of Cr(III) was calculated by subtraction between the Cr(VI) from the total chromium. This was followed for all other adsorption experiments. To calculate the percent removal and adsorption capacity, equations 2 and 3 were used, correspondingly.

The desorption experiments were done similarly to the adsorption experiment with 0.1 M HCl and 0.1 NaOH as leaching agents. After the adsorption experiment, the adsorbent was rinsed with deionized water and dried for 24 h at 100°C in an oven. Then the adsorbent was used for the desorption of Cr(VI) ions.

4.2.5. Equilibrium studies

Equilibrium studies (adsorption isotherms, kinetic modelling, and thermodynamic) were all performed using standard procedures. The equations used in the calculations are given in section 3 (equations 2 to 20). The equilibrium data were computed by using Microsoft excel and the KyPlot.

4.3. Results and discussion

4.3.1. Characterization of the OCNOs

The surface area of OCNOs was found to be 81.8 m^2/g, while the pore volume and average pore size were found to be 0.08 cm^3/g and 4.2 nm in that order (Table S4.1.). The TEM micrographs revealed that the as-synthesized OCNOs had quasi-spherical shapes with average particle sizes of 46 ± 5 nm (Figure 4.1 a). The average particle size of the OCNOs was within the range of those reported by [32] (37 nm) and [42] (35 nm). The carbon nanomaterial consisted of particles that were mostly connected in an accreted form (insert in Figure 4.1a). Furthermore, the high magnification micrographs displayed OCNOs that have concentric multi-layers with an onion-like structure, with a lattice fringe spacing of 0.35 nm [39].

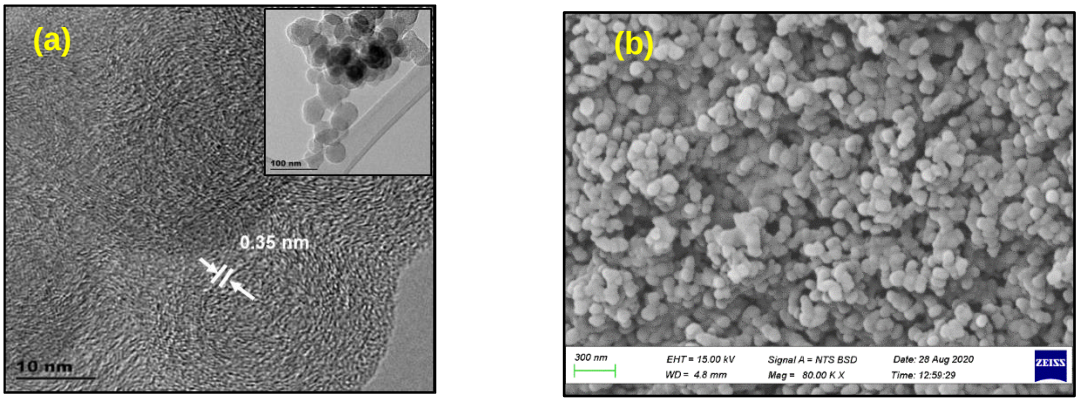

Figure 4.1: TEM (a) and SEM (b) micrographs of OCNOs.

The external morphology of OCNOs was further deliberated using SEM as shown in Figure 4.1(b) The SEM micrographs of the OCNOs confirmed that these nanomaterials are connected and form agglomerates/conglomerates that exhibited multiple quasi-spherical shapes [39].

Figure 4.2 (a) shows that the OCNOs have a single decomposition temperature at 505°C, owing to the oxidation of graphitic carbon. The broad derivative peak can be attributed to structural defects present on the surfaces of OCNOs [32]. It was reported that a single decomposition step between 450 to 550°C for CNOs synthesized via the annealing of nanodiamonds [47]. The thermogravimetric analysis (TGA) and the differential thermal analysis (DTA) confirm that the OCNOs synthesized had no

residue. Signifying that a pure carbon nanomaterial had been produced without any by-products or impurities [Figure 4.2 (a)].

The FTIR spectra of the OCNO sample are depicted in Figure 4.2 (b). Strong broad O-H stretching peaks are seen at 3441 cm^{-1} and 3151 cm^{-1} representing OH groups associated with alcohol or absorbed water respectively. The weak peak at 1633 cm^{-1} is related to an alkene C=C stretch and the strong, broad peak at 1400 cm^{-1} represents the C-O-H bending mode. The aforementioned functional groups are in agreement with those found in CNOs derived from the annealing of nanodiamonds [41] and the carbonization of tomatoes [48]. It should be mentioned that a peak associated with a carboxylic acid group around 1700 cm^{-1} (C=O) was not present in the FTIR spectra of the OCNOs. It can be noted that the FTIR spectra of olive oil and the OCNOs are different indicating that the chemical structure of the olive oil has changed from what it was, to that of new material (OCNOs) (Figure S4.2.).

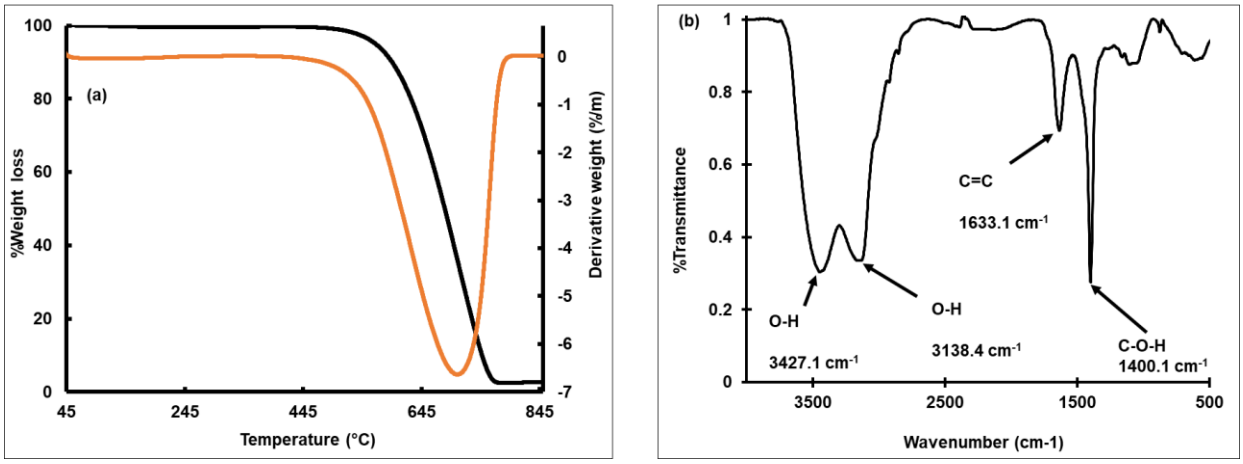

Figure 4.2: TGA and DTA (a) and FTIR spectra (b) for the as-synthesized OCNOs.

The XPS analysis of the OCNOs depicted in Figure 4.3, showed peaks of *C1s* (88.2 %) and *O1s* (11.8 %) at 284.1 eV and 532.3 eV. The *C1s* peak was de-convoluted into four peaks. Two represented C-C sp2 and sp3 carbons at 283.8 eV and 284.9 eV with atomic% of 48.2% and 25.0% respectively. The other two peaks were for C-O and O-C=O functional groups at 286.1 eV and 288.6 eV with an atomic% of 8.9% and 5.9% respectively. The *O1s* peak was de-convoluted into three peaks at 530.1, 531.9, and

533.3 eV for C-O, C-O, and C=O functional moieties with atomic% of 0.5%, 6.1%, and 5.4% respectively (Figure 4.3.). The surface functional groups were consistent with those reported by Ko et al. for CNOs produced via the annealing of nanodiamonds [41]. The FTIR results are supportive of the elemental composition from XPS analysis (Table S4.1.).

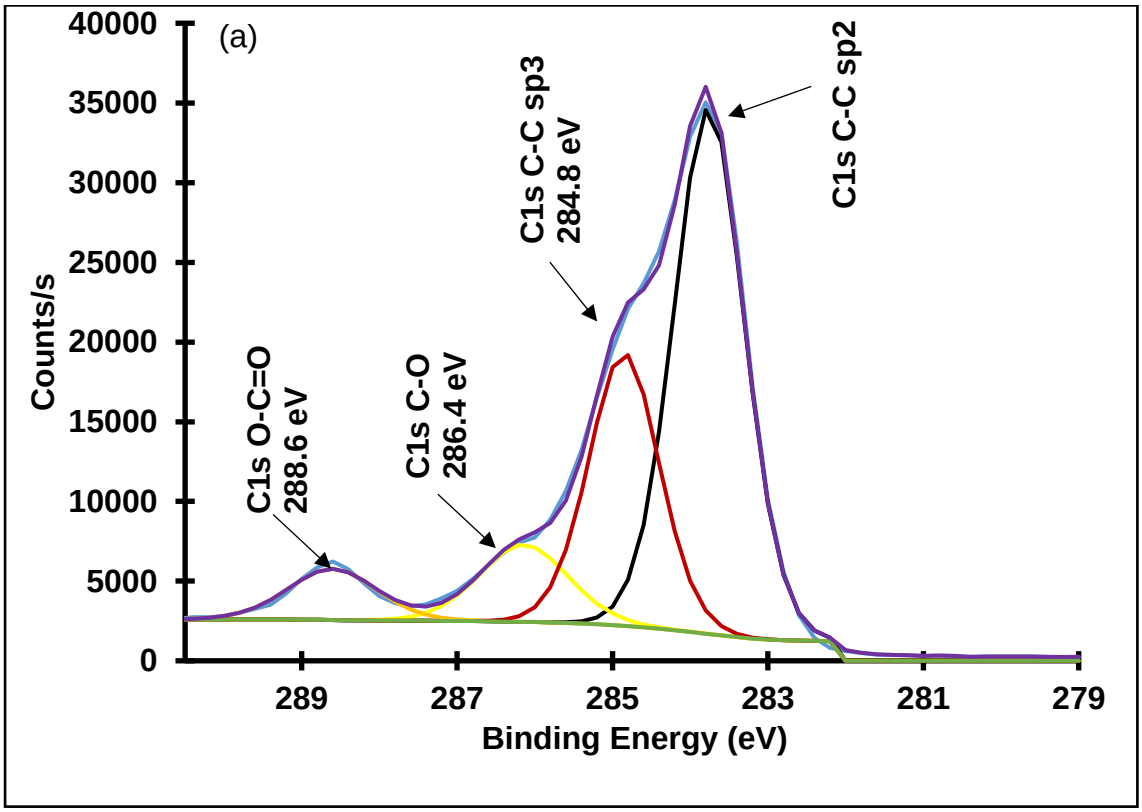

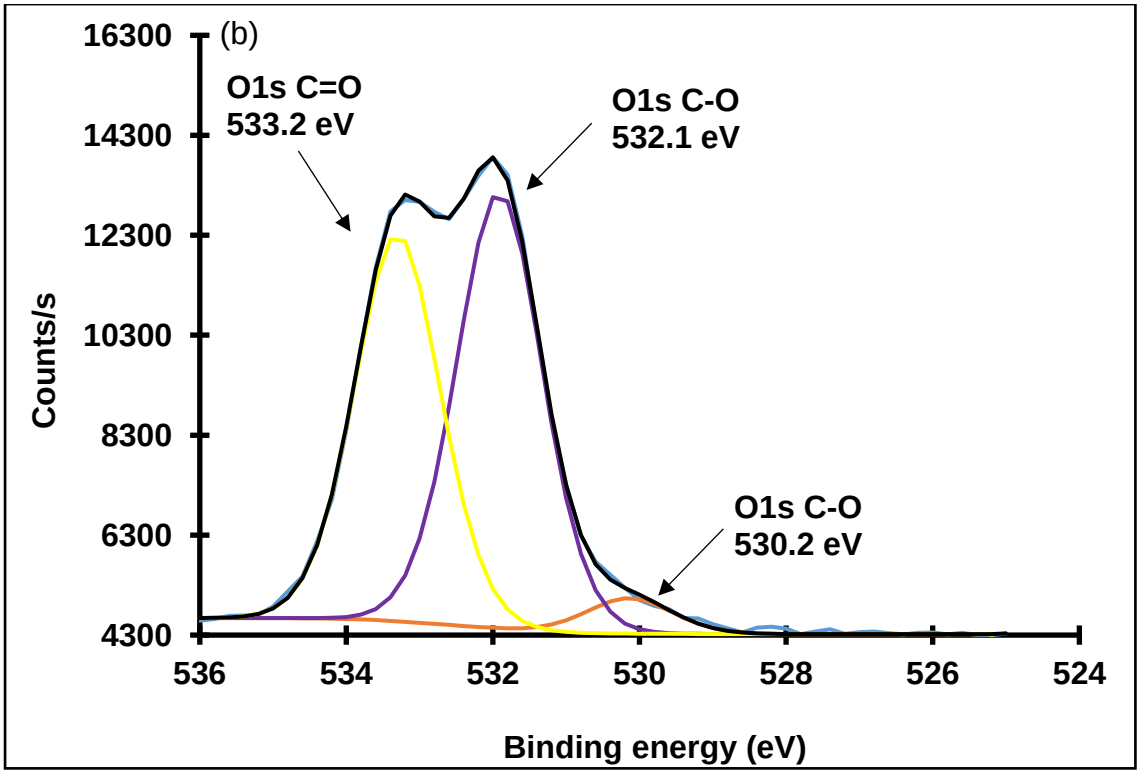

Figure 4.3: De-convoluted XPS peaks of C1s (a) and O1s (b) from the as-synthesized OCNOs before adsorption.

4.3.2. Removal of Cr(VI) ions from aqueous solution

4.3.2.1. Remediation depending on pH

Figure 4.4. portrays how the remediation of Cr(VI) ions using OCNOs as adsorbent was heavily dependent on the pH of the Cr(VI) solution. Most of the removal occurred at pH 2, with 96% removal. The increase in pH from 3 to 8 promoted a decrease in the removal of Cr(VI) significantly; to 65% and lower. This can be attributed to two factors: (i) the nature of the OCNOs and (ii) the type of chromium species in solution between pH 2 and 8.

The $pH_{(PZC)}$ of OCNOs was found to be at pH 5.2 (Table S4.1.), and thus below pH 5.2, the OCNOs surface will be positively charged. The type of Cr species at low pH exists as CrO_4^{2-}, $HCrO_4^-$, $Cr_2O_7^{2-}$ and Cr^{3+} depending on the solution pH and concentration. This is shown in the chromium speciation diagram, Figure S4.1. [49]. At pH = 2, the $Cr_2O_7^{2-}$ species readily hydrolyze to form $HCrO_4^-$, making $HCrO_4^-$ the most dominant Cr(VI) species [50,51].

Cr(VI) removal would thus be due to an electrostatic lure amid the oxyanions of chromium and the positively charged surface of the OCNOs at pH 2 [52]. Therefore, a decreased removal of Cr(VI) ions as the pH was increased from pH 3 to 8 would be due to electrostatic repulsion. The removal of all Cr ions in an aqueous solution is shown in Figure 4.4. The highest removal of total Cr was 96% at pH 2, as was for Cr(VI), consistent with literature which indicates higher removal of Cr(VI) ions under acidic conditions [53] The percent removal of total Cr decreased from pH 3 to pH 5 this could be correlated to the elimination of Cr(VI).

The percent removal of Cr(VI) and total Cr is equal at pH 2 and suggests that only Cr(VI) is present at pH 2. As the pH increased between pH 3 and pH 8 the total Cr removed decreased and then remained near-constant as does the Cr(IV) removal. The results indicate that some of the Cr(VI) ions have been converted to other Cr species. Literature reports suggest that the removal of Cr(VI) ions using carbon material involves a reduction to Cr(III) [16,53,54]. Thus, the data in Figure 4.4 could be explained by the conversion of Cr(VI) to Cr(III) due to the reducing power of the OCNOs. The reduction of Cr(VI) to Cr(III) was found by other researchers to be noticeable in both acidic and alkaline media, indicating that the reduction was not due to the acidic strength of the solution, but rather due to the electron donor moieties on the surface of the adsorbent [53].

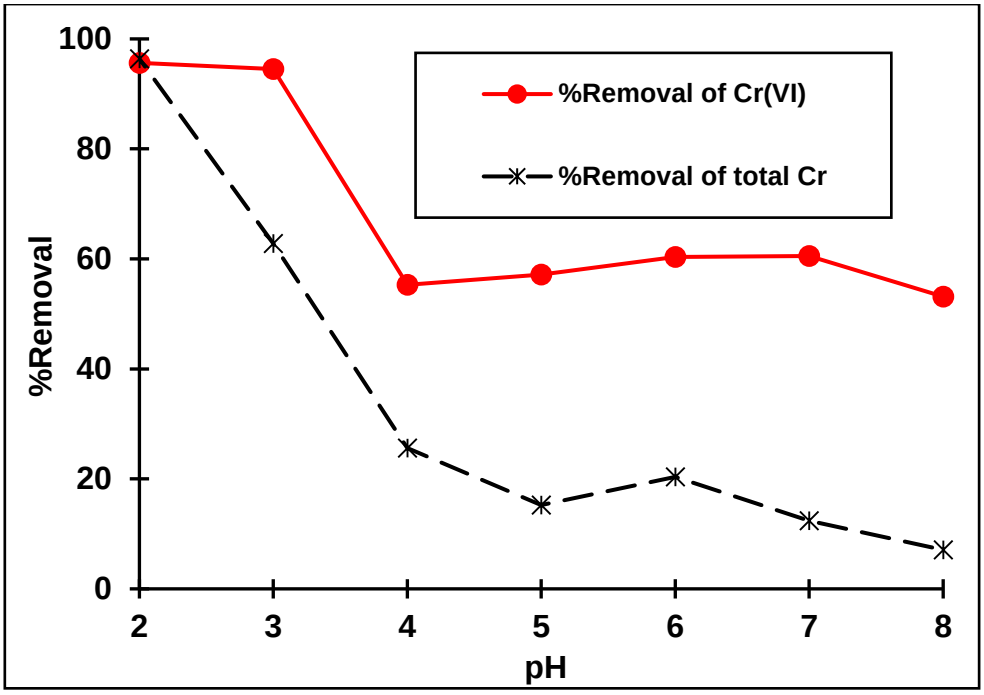

Figure 4.4: The influence of solution pH on the adsorption of Cr(VI) ions and total Cr on OCNOs (adsorption conditions: pH range (2 to 8), t = 720 min, m = 0.05 g and C_O = 10 mg/L).

The removal mechanism is consistent with adsorption coupled with reduction, resulting in the formation of Cr(III), a less toxic form of chromium, remaining in the solution [6]. This was supported by the presence of the Cr_{2p} peak after the removal of Cr(VI) ions shown in the XPS spectrum at 577.4 eV, which was absent before the removal [Figures 4.5 (a)]. The peak was de-convoluted to give the two peaks due to $2p_{3/2}$ and $2p_{1/2}$ at 586.8 eV and 577.6 eV respectively [Figure 4.5 (b)], representing Cr(III); this indicates chemical bond formation between the adsorbent and the adsorbate [41]. The occurrence of Cr(III) ions on the surface of the OCNOs indicates that reduction took place.

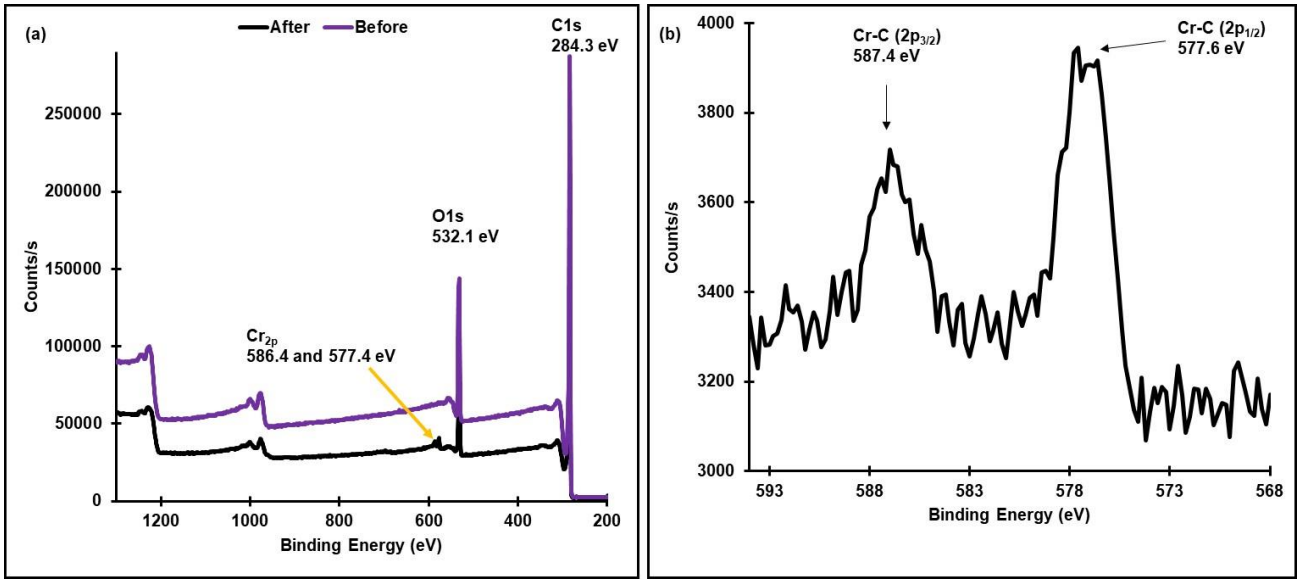

Figure 4.5: XPS survey spectrum for OCNOs before and after adsorption (a) and the Cr_{2p} XPS spectrum of the as-synthesized OCNOs after adsorption of Cr(VI) ions (b).

4.3.3. Kinetics

Figure 4.6. shows the influence of time on Cr(VI) ions removal by the OCNOs. From 30 min to 2880 min, the removal increased linearly with time. Erratic behaviour was noted in the first 15 mins of the reaction and this can be attributed to the hydrophobic nature of the OCNOs and the low density of the OCNOs. A comparable trend was observed for the adsorption capacity as well (Figure 4.6.). The trend was expected since the contact time can be used to determine the rate at which the Cr(VI) ions cover the surface of the adsorbent [55]. Kinetic data modelling of the data was undertaken assuming pseudo-first-order (PFO) and pseudo-second-order (PSO) kinetic models. Nonlinear forms of the PFO and PSO did not yield any meaningful R^2 values, but the linear forms showed R^2 values of 0.4535 and 0.9734, and q_e values of 2.60 and 4.16 mg/g for the PFO and PSO models respectively. The q_e for the PSO model (4.16 mg/g) was close to the experimental value of q_e (4.00 mg/g) (Figure 4.6 and Table 4.1). Therefore, the removal of Cr(VI) ions appears to follow a PSO model, indicating possible chemical bond formation amid Cr(VI) ions and the surface of the OCNOs (i.e. chemisorption). The removal of Cr(VI) ions was slower for the first 20 min and become more rapid from 30 min as indicated by the rate constant (k_2) and the initial adsorption

rate (*h*) (Figure 4.6 and Table 4.1). This could be a result of the hydrophobicity nature of the adsorbent.

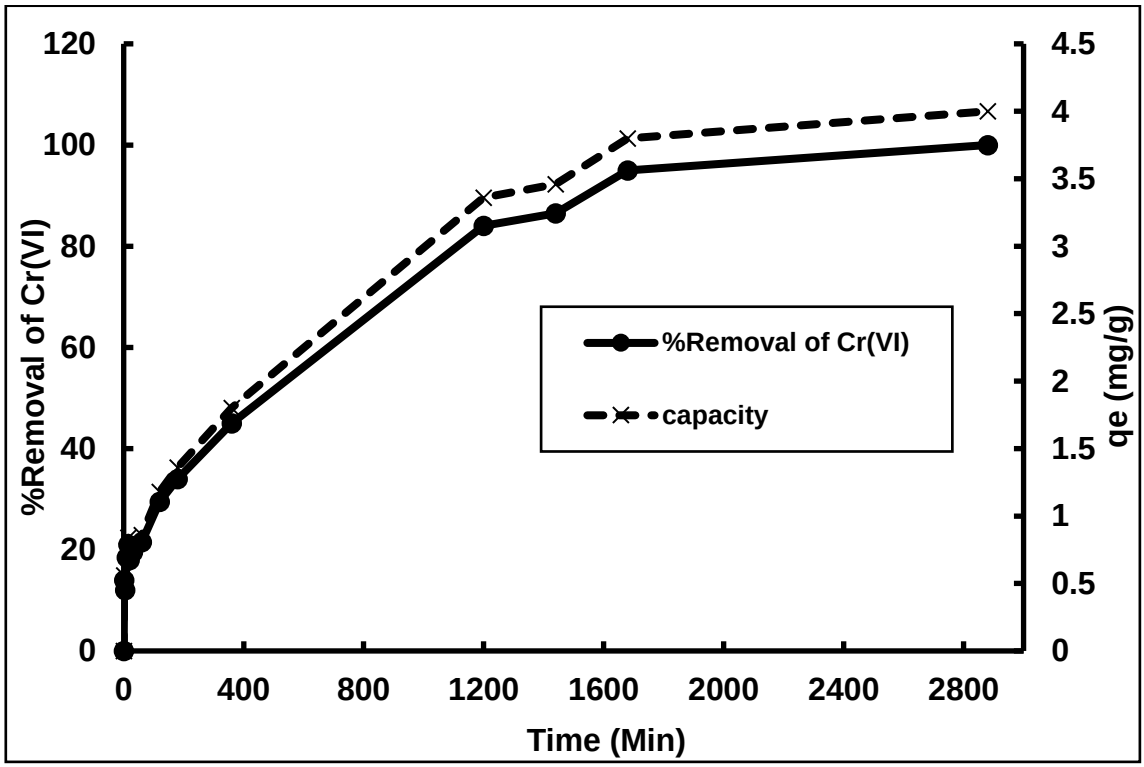

Figure 4.6: The influence of time on the adsorption of Cr(VI) on OCNOs (adsorption factors: t = (1 to 2880 min), pH = 2, m = 0.025 g, and C_O = 10 mg/L).

Table 4.1: Parameters of adsorption kinetic models for the removal of Cr(VI) ions

Model			**Parameters**		
PFO	**Time (min)**	**q_e (mg/g)**	**k_1 (1/min)**	**R^2**	
	1 to 2880	2.6	0.001	0.454	
PSO	**Time (min)**	**q_e (mg/g)**	**k_2 (g/mg x min)**	**R^2**	***h* (mg/g x min)**
	1 to 2880	4.16	0.0014	0.973	0.0248
	1 to 20	0.81	0.8996	0.958	0.5914
	30 to 2880	4.44	0.0007	0.984	0.0147

4.3.4. Adsorption isotherms

Figure 4.7. shows the removal of Cr(VI) ions from an aqueous solution as a function of the initial concentration of Cr(VI) ions (10 to 100 mg/g). The adsorption capacity was observed to increase as the initial concentration was increased, with the highest capacity of 26.24 mg/g at 100 mg/L. The adsorption sites of the adsorbent are limited at elevated concentration values [56]. The Langmuir and Freundlich adsorption isotherms were selected to study the progression of the Cr(VI) ions removal using the OCNOs (Table 4.2.). Different model factors were used to establish the best model: the coefficient of determination (R^2), the maximum adsorption capacity Q_{max} (mg/g) compared to the experimental adsorption capacity (q_e mg/g), the chi-squared $\mathcal{X}^2$ values and the R^2 values determined using equations 14 and 15 respectively.

The coefficient of determination (R^2) value for the linear Langmuir isotherm was higher and closer to unity. The maximum adsorption capacity Q_{max} was found to be 26.53 mg/g which was close to the experimental adsorption capacity (26.24 mg/g). The linear Langmuir model showed a value of chi-squared $(\mathcal{X}^2)$ close to zero, indicating that the model data were close to the experimental data. Furthermore, the R^2 values calculated from equation 15 showed that the linear Langmuir isotherm was close to unity. Overall the experimental data was better explained by the linear Langmuir isotherm indicating a monolayer coverage.

The separation factor (R_L) values obtained from the Langmuir isotherm and the Freundlich exponent (n) depicted values $0<R_L>1$ and $0<n>1$ respectively, indicating favourable adsorption of Cr(VI) ions by the OCNOs. The R_L values decreased as the initial concentration of Cr(VI) ions was increased from 10 mg/L to 100 mg/L (Table S4.2.). This can be attributed to stronger bond formation between the sorbate ions and the sorbent surface indicating possible chemisorption [16,53].

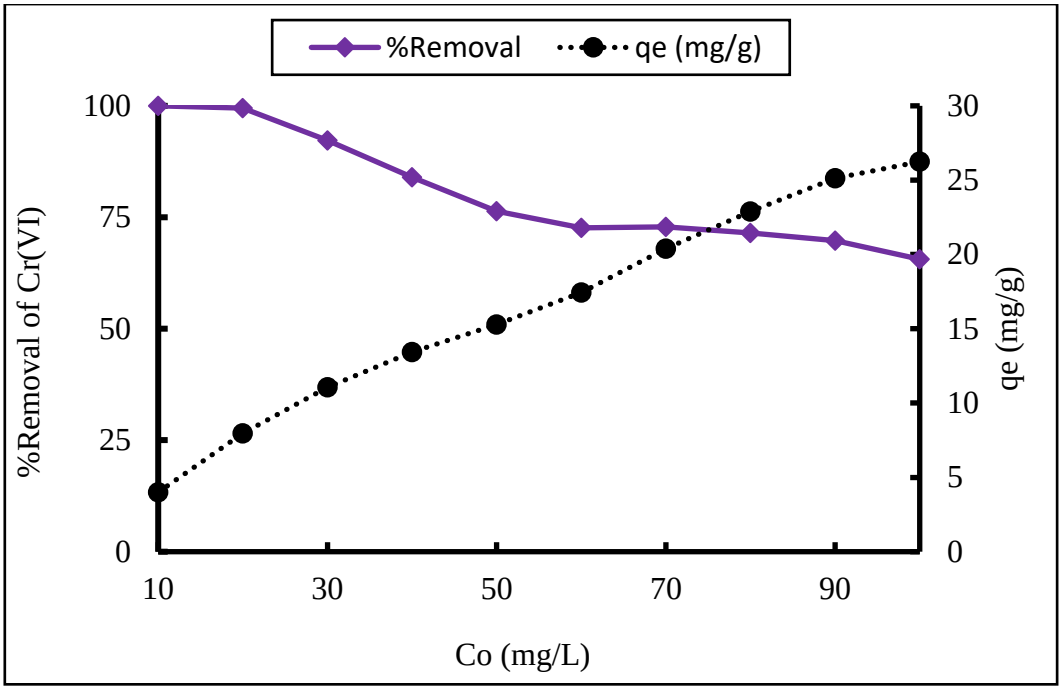

Figure 4.7: The influence of initial concentration on the adsorption of Cr(VI) on OCNOs (adsorption conditions: pH = 2, t = 720 min, m = 0.025 g, and C_O range (10 to 100 mg/L).

Table 4.2: Factors of adsorption isotherms for the removal of Cr(VI) ions

Isotherm	**R^2**	***R^2**	**Q_{max} (mg/g)**	**K_L (L/mg)**	****χ^2**
Langmuir linear	0.9276	0.992	26.53	0.261806	0.0031
Langmuir nonlinear	0.7686	0.9285	29.84	0.130749	0.493
	R^2	***R^2**	**K_F (mg/g)/(mg/L)^n**	**n**	****χ^2**
Freundlich linear	0.687	0.1296	163.38	0.383774	716.749
Freundlich nonlinear	0.8952	-0.392	8.29	0.313216	12.277

**χ^2 and *R^2 calculated from equations 14 and 15

4.3.5. Removal mechanism for Cr(VI) ions

The removal mechanism of Cr(VI) ions in the past have been reported to be either by adsorption or by adsorption-coupled reduction [54,57,58]. Data from this study support the adsorption coupled reduction removal mechanism. Thus, it can be observed from Figure 4.4 that the elimination of all Cr ions was not achieved. This was attributed to the Cr(VI) ions being reduced to Cr(III) ions. The XPS data analysis showed that the

metal present on the surface of the OCNOs after adsorption was Cr(III) and this finding supported the adsorption-coupled reduction mechanism (Figure 4.5). The kinetic modelling gave a good fit with the PSO model, an indication of possible chemisorption between the surface of the adsorbent and the adsorbate (Table 4.1). The isotherm data fitted the Langmuir isotherm indicating monolayer coverage of the adsorbent active sites by the adsorbate. The aforementioned data shows that indeed Cr ions were on the surface of the OCNOs in the form of Cr(III) ions. The data do not however allow one to determine the sequence of reactions viz. is a reduction in solution followed by adsorption on the surface (direct) or is adsorption followed by reduction on the surface (indirect) [16,53,54,59].

The removal mechanism was further described by the use of thermodynamic parameters presented in Table 4.3. It can be seen that the removal of Cr(VI) ions was spontaneous and favoured (- ΔG° value). The - ΔH° indicates that the reaction was exothermic, in line with the decrease in adsorption capacity at higher temperatures (Figure S4.3.). The removal of Cr(VI) ions by the as-synthesized OCNOs involved the associative mechanism, as indicated by the - ΔS° value [60].

Table 4.3: Thermodynamic features computed via the Langmuir constant (K_L)

T (K)	van't Hoff equation	K_C	ΔG° (kJ/mol)	ΔH° (kJ/mol)	ΔS° (J/mol)
298.15	y = 27903x -77.842	14853333.33	-40.94	-232.00	-647.21
303.15	R^2 = 0.8395	454174.51	-32.83		
308.15		330684.12	-32.56		
313.15		116384.18	-30.37		

4.3.6. Comparison of adsorption capacity

Table 4.4. shows the contrasting q_e for the removal of Cr(VI) ions from diverse carbon materials. It can be perceived that the adsorption capacity of the as-synthesized OCNOs was similar to that found for other carbon-based materials. More importantly, the OCNOs produced from olive oil gave very similar results to the data obtained from a laser and nanodiamond-produced CNOs. The study thus shows that the method used to make the CNOs is not significant. Thus, the use of CNOs produced from waste

carbon materials could provide a facile method of removing Cr (IV) from polluted waterways. Since the surface interaction is key, the way forwards will be to (i) create more surface groups to bind to the Cr ions and (ii) enhance the surface area of the CNOs

Table 4.4: Evaluation of adsorption capacities for Cr(VI) ions removal

Adsorbent	Isotherm	pH	q_e (mg/g)	References
OCNOs	Langmuir	2	26.53	This study
Magnetic pine cone	Langmuir	3	15.24	(Pholosi et al., 2020)
Jatropha oil cake	Freundlich	2	11.75	(Garg et al., 2007)
CNOs	Langmuir	3.4	27.86	(Sakulthaew et al., 2017)
Onion-like-carbon (OLC)	Langmuir	3.6-3.9	27.29	(Ko et al., 2016)
SWCNTs	Langmuir	4	20.3	(Jung et al., 2013)
MWCNTs	Langmuir	4	2.48	(Jung et al., 2013)
Nanofiber	Langmuir	3	27.27	(Jin et al., 2020)
Activated carbon	Langmuir	4	25.75	(Lesaoana et al., 2019)
Wheat bran	Freundlich	2	4.53	(Kaya et al., 2014)

4.3.7. Effect of Ni(II) and Cu(II) on the removal of Cr(VI)

Normally in steel production, the Cr(VI) ions exist in a mixture with Ni(II) and Cu(II) ions. Therefore, the removal of Cr(VI) ions was tested in the trinary system with Ni(II) and Cu(II) ions, and the results are shown in Figure 4.8. The OCNOs showed a higher affinity towards Cr(VI) ions (98% adsorption) at pH 2, followed by Cu(II) ions (87%) at pH 6 and lastly Ni(II) ions (45%) at pH 6 (Figure 4.8.). However, the sequestration of Cr(VI) ions at pH 2 was not affected negatively by the presence of Cu(II) and Ni(II) ions. It can be noted that as the pH was increased from 3 to 8 and the removal of Cr(VI) ions was d by the occurrence of the contending ions. Where the Cr(VI) ions removal was lowered in the presence of competing ions (Figure 4.4.). This could be due to the affinity of the Cu(II) and Ni(II) cations towards the negatively charged surface of the adsorbent due to electrostatic attraction as the adsorbent surface becomes more negative, as the solution pH was increased.

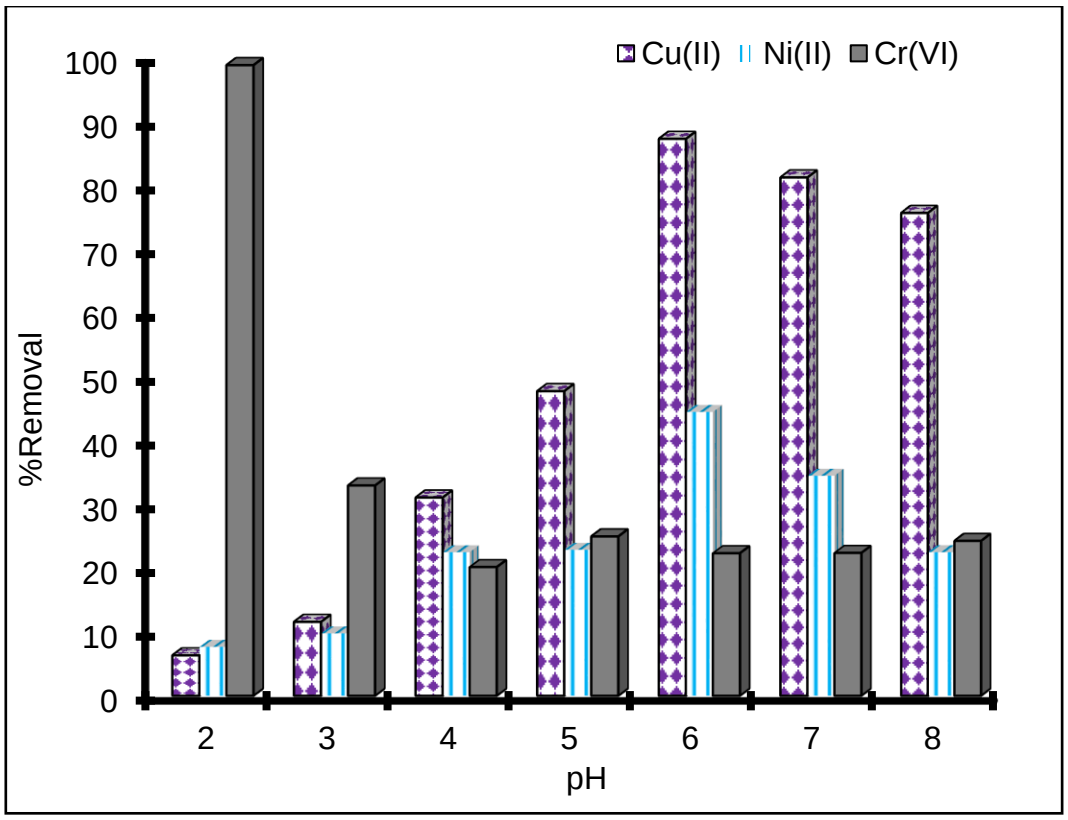

Figure 4.8: The influence of counter ions on the removal of Cr(VI) ions in a trinary matrix on OCNOs by varying the solution pH (adsorption conditions: pH range 2 to 8, t = 720 min, m = 0.05 g and C_O = 10 mg/L).

4.3.8. Adsorbent regeneration

Desorption or adsorbent regeneration studies were performed to determine if the adsorbent could be reused. The removal of Cr(VI) ions using the OCNOs was done as described in section 4.2.4. The desorption solutions used were 0.1 M NaOH and 0.1 M HCl and the data is presented in Figure S4.4. The acid did not yield any desorption of Cr(VI) ions after two desorption cycles. This could be attributed to the protonation of the adsorbent surface resulting in the Cr(VI) ions bonding more strongly to the surface of the adsorbent. However, the use of NaOH gave better desorption of Cr(VI) ions for the first cycle (6.1 mg/g) while for the second and third cycles, it was 0.8 and 0.4 mg/g respectively. This may be a result of the deprotonation of the surface of the adsorbent due to the OH^- ions. It can be noted that the Cr(VI) ions removed were

7.3 mg/g. This indicated that not all the Cr(VI) ions were desorbed, and would relate to the reduction of Cr(VI) ions to Cr(III) ions (Figure 4). After the three desorption cycles, the adsorbent was taken for re-adsorption of Cr(VI) ions. The percent removal was shown to be 99%, which was an increase from 88% when the OCNOs were used for the first time. The increase in the removal of the Cr(VI) ions can be attributed to the surface modification by the NaOH.

4.4. Conclusions

Carbon nano-onions were successfully synthesized via the pyrolysis of olive oil. The as-synthesized OCNOs were of quasi-spherical morphology with an average particle size of 46 ± 5.4 nm and a comparable surface area of 81.8 m^2/g. The optimum conditions for the elimination of Cr(VI) ions from the aqueous solutions were found to occur at pH = 2, t = 2880 min, C_O = 10 mg/L. When the mass of the adsorbent was kept at 0.025 g. The removal process was shown to involve a spontaneous, exothermic reaction owing to the interaction of the Cr(VI) ions with the interface of the OCNOs involving an associative mechanism. The removal mechanism was shown to be adsorption coupled with reduction, resulting in the formation of Cr(III). This was supported by the presence of a Cr_{2p3} peak due to Cr(III) in the XPS spectrum. The chemisorption process was observed and the experimental data was explained by the PSO model. The removal was more rapid for the first 20 min and slower after 30 min with an adsorption rate of 0.59144 mg/g x min and 0.01469 mg/g x min respectively. This took place on the surface (monolayer) of the OCNOs as indicated by the Langmuir adsorption isotherm with a maximum adsorption capacity of 26.53 mg/g. The OCNOs showed affinity towards Cr(VI) ions at pH 2 and Cu(II), and Ni(II) ions at pH 6. The adsorbent was regenerated with NaOH and showed improved Cr(VI) ion removal after regeneration. Our data have demonstrated that CNOs derived from olive oil via flame pyrolysis have opened opportunities to explore cooking oils as a simple and cheap method to make CNOs for the adsorption of Cr(VI) ions from aqueous solution. The as-synthesized CNOs were comparable with those produced via more sophisticated approaches such as the laser resonant extraction method and the annealing of nanodiamonds.

4.5. References

[1] P.A. Kobielska, A.J. Howarth, O.K. Farha, S. Nayak, Metal–organic frameworks for heavy metal removal from water, Coord. Chem. Rev. 358 (2018) 92–107. https://doi.org/10.1016/j.ccr.2017.12.010.

[2] Y. Zhao, M. Xu, Q. Liu, Z. Wang, L. Zhao, Y. Chen, Study of heavy metal pollution , ecological risk and source apportionment in the surface water and sediments of the Jiangsu coastal region , China : A case study of the Sheyang Estuary, Mar. Pollut. Bull. 137 (2018) 601–609.

[3] S. Zuo, S. Dai, Y. Li, J. Tang, Y. Ren, Analysis of Heavy Metal Sources in the Soil of Riverbanks Across an Urbanization Gradient, Int. J. Environ. Res. Public Health. 15 (2018) 2175. https://doi.org/10.3390/ijerph15102175.

[4] L. Hlungwane, E.L. Viljoen, V.E. Pakade, Macadamia nutshells-derived activated carbon and attapulgite clay combination for synergistic removal of Cr(VI) and Cr(III), Adsorpt. Sci. Technol. 36 (2018) 713–731. https://doi.org/10.1177/0263617417719552.

[5] J.A. Arcos, M.R. Cruz, J. Cardoso, J. Vázquez, F. Caballero, Chromium adsorption into a macroporous resin based on vinylpyridine – divinylbenzene copolymers : thermodynamics , kinetics , and process dynamic in a fixed bed column, Adsorption. 24 (2018) 105–120. https://doi.org/10.1007/s10450-017-9925-y.

[6] World Health Organization, Guidelines for drinking-water quality, 2008. https://doi.org/10.1016/S1462-0758(00)00006-6.

[7] S.U. Khan, D.T. Islam, I.H. Farooqi, S. Ayub, F. Basheer, Hexavalent chromium removal in an electrocoagulation column reactor: Process optimization using CCD, adsorption kinetics and pH modulated sludge formation, Process Saf. Environ. Prot. 122 (2019) 118–130. https://doi.org/10.1016/j.psep.2018.11.024.

[8] H.O.N. Tugaoen, P. Herckes, K. Hristovski, P. Westerhoff, Influence of ultraviolet wavelengths on kinetics and selectivity for N-gases during TiO_2 photocatalytic reduction of nitrate, Appl. Catal. B Environ. 220 (2018) 597–606. https://doi.org/10.1016/j.apcatb.2017.08.078.

[9] V. Saucedo-Rivalcoba, A.L. Martínez-Hernández, G. Martínez-Barrera, C. Velasco-Santos, J.L. Rivera-Armenta, V.M. Castaño, Removal of hexavalent chromium from water by polyurethane-keratin hybrid membranes, Water. Air. Soil Pollut. 218 (2011) 557–571. https://doi.org/10.1007/s11270-010-0668-6.

[10] C.R. Ramakrishnaiah, B. Prathima, Hexavalent chromium removal from industrial watsewater by chemical precipitation method, Int. J. Eng. Res. Appl. 2 (2012) 599–603.

[11] A. Korak, Julie, R. Huggins, M. Arias-Paic, Regeneration of Pilot-Scale Ion Exchange Columns for Hexavalent Chromium Removal Supplemental Information, Water Res. 118 (2017) 141–151.

[12] Y. Zhao, D. Kang, Z. Chen, J. Zhan, X. Wu, Removal of chromium using electrochemical approaches: A review, Int. J. Electrochem. Sci. 13 (2018) 1250–1259. https://doi.org/10.20964/2018.02.46.

[13] N.D. Shooto, E.B. Naidoo, M. Maubane, Sorption studies of toxic cations on ginger root adsorbent, J. Ind. Eng. Chem. 76 (2019) 133–140. https://doi.org/10.1016/j.jiec.2019.02.027.

[14] X.R. Xu, H. Bin Li, X.Y. Li, J.D. Gu, Reduction of hexavalent chromium by ascorbic acid in aqueous solutions, Chemosphere. 57 (2004) 609–613. https://doi.org/10.1016/j.chemosphere.2004.07.031.

[15] M. Moyo, V.E. Pakade, S.J. Modise, Biosorption of lead(II) by chemically modified Mangifera indica seed shells: Adsorbent preparation, characterization and performance assessment, Process Saf. Environ. Prot. 111 (2017) 40–51. https://doi.org/10.1016/j.psep.2017.06.007.

[16] V.E. Pakade, T.D. Ntuli, A.E. Ofomaja, Biosorption of hexavalent chromium from aqueous solutions by Macadamia nutshell powder, Appl. Water Sci. 7 (2017) 3015–3030. https://doi.org/10.1007/s13201-016-0412-5.

[17] T.A.H. Nguyen, H.H. Ngo, W.S. Guo, J. Zhang, S. Liang, Q.Y. Yue, Q. Li, T. V. Nguyen, Applicability of agricultural waste and by-products for adsorptive removal of heavy metals from wastewater, Bioresour. Technol. 148 (2013) 574–585. https://doi.org/10.1016/j.biortech.2013.08.124.

[18] Y. Jiang, Z. Liu, G. Zeng, Y. Liu, B. Shao, Z. Li, Y. Liu, W. Zhang, Q. He, Polyaniline-based adsorbents for removal of hexavalent chromium from aqueous solution: a mini review, Environ. Sci. Pollut. Res. 25 (2018) 6158–6174. https://doi.org/10.1007/s11356-017-1188-3.

[19] S. Varjani, G. Kumar, E.R. Rene, Developments in biochar application for pesticide remediation: Current knowledge and future research directions, J. Environ. Manage. 232 (2019) 505–513. https://doi.org/10.1016/j.jenvman.2018.11.043.

[20] M.S. Alhumaimess, I.H. Alsohaimi, A.A. Alqadami, M.M. Kamel, M. Naushad, T. Ahamad, H. Alshammari, Synthesis of phosphorylated raw sawdust for the removal of toxic metal ions from aqueous medium: Adsorption mechanism for clean approach, J. Sol-Gel Sci. Technol. 89 (2019) 602–615. https://doi.org/10.1007/s10971-018-4870-0.

[21] E.D. Cason, P.J. Williams, E. Ojo, J. Castillo, M.F. DeFlaun, E. van Heerden, Hexavalent chromium bioreduction and chemical precipitation of sulphate as a treatment of site-specific fly ash leachates, World J. Microbiol. Biotechnol. 33 (2017) 1–9. https://doi.org/10.1007/s11274-017-2243-4.

[22] J.K. Kim, T. Jiang, Z. Li, S. Mayadevi, K. Bharat, J.C. Joo, L.C. Campos, Degradation of Metaldehyde in Aqueous Solution by Nano-Sized Photocatalysts and Granular Activated Carbon, J. Nanosci. Nanotechnol. 20 (2020) 4505–4508. https://doi.org/10.1166/jnn.2020.17595.

[23] B. Fernández-Reyes, S. Morales-Jiménez, J.C. Muñoz-Senmache, D.R. Vega-Santander, A.J. Hernández-Maldonado, Single- and multi-component adsorption of selected contaminants of emerging concern from water and some of their metabolites onto hierarchical porous copper(II)-zeolite -activated carbon composite, Microporous Mesoporous Mater. 312 (2021) 24–32. https://doi.org/10.1016/j.micromeso.2020.110355.

[24] B.B. Wang, X.L. Qu, M.K. Zhu, I. Levchenko, M. Keidar, X.X. Zhong, S. Xu, K. Ostrikov, Carbon nanoflake-nanoparticle interface: A comparative study on structure and photoluminescent properties of carbon nanoflakes synthesized on nanostructured gold and carbon by hot filament CVD, Carbon N. Y. 124 (2017) 391–402. https://doi.org/10.1016/j.carbon.2017.08.078.

[25] J. Liu, C.K. Poh, D. Zhan, L. Lai, S.H. Lim, L. Wang, X. Liu, N. Gopal Sahoo, C. Li, Z. Shen, J. Lin, Improved synthesis of graphene flakes from the multiple electrochemical exfoliation of graphite rod, Nano Energy. 2 (2013) 377–386. https://doi.org/10.1016/j.nanoen.2012.11.003.

[26] Š. Ervin, G. Dra, I. Jerman, Solar Energy Materials and Solar Cells Graphene nanoplatelets as an anticorrosion additive for solar absorber coatings, 176 (2018) 19–29. https://doi.org/10.1016/j.solmat.2017.11.016.

[27] Y. Yao, S. Miao, S. Liu, L.P. Ma, H. Sun, S. Wang, Synthesis, characterization, and adsorption properties of magnetic Fe_3O_4@graphene nanocomposite, Chem. Eng. J. 184 (2012) 326–332. https://doi.org/10.1016/j.cej.2011.12.017.

[28] V. Sridhar, H. Park, Zeolitic imidazolate frameworks as novel precursors for microwave synthesis of carbon nanotubes, J. Alloys Compd. 781 (2019) 166–173. https://doi.org/10.1016/j.jallcom.2018.12.123.

[29] S. Kovivchak, Vladimir, G. Kryazhev, Yurii, V. Trenikhin, Mikhail, B. Arbuzov, Aleksey, S. Zapevalova, Evgenia, A. Likholobov, Vladimir, Ultrafast catalytic synthesis of carbon nanofibers on a surface of commercial chlorinated polymers under the action of a high power ion beam of nanosecond duration, Appl. Surf. Sci. 448 (2018) 642–645. https://doi.org/10.1088/1742-6596/1115/3/032088.

[30] L. Zhang, M. Wang, Y. Lai, X. Li, Oil/molten salt interfacial synthesis of hybrid thin carbon nanostructures and their composites, J. Mater. Chem. A. 6 (2018) 4988–4996. https://doi.org/10.1039/c7ta10692k.

[31] A. Pramanik, S. Sarkar, S. Pal, P. Sarkar, Pentacene-fullerene bulk-heterojunction solar cell: A computational study, Phys. Lett. Sect. A Gen. At. Solid State Phys. 379 (2015) 1036–1042. https://doi.org/10.1016/j.physleta.2015.01.040.

[32] T.H. Mongwe, B.J. Matsoso, B.K. Mutuma, N.J. Coville, M.S. Maubane, Synthesis of chain-like carbon nano-onions by a flame assisted pyrolysis technique using different collecting plates, Diam. Relat. Mater. 90 (2018) 135–143. https://doi.org/10.1016/j.diamond.2018.10.002.

[33] N. Luo, H. Jing, Z. Ma, R. Chen, Gaseous detonation chemical synthesis of onion-like carbons, Mendeleev Commun. 27 (2017) 195–197. https://doi.org/10.1016/j.mencom.2017.03.030.

[34] R. Borgohain, J. Yang, J.P. Selegue, D.Y. Kim, Controlled synthesis, efficient purification, and electrochemical characterization of arc-discharge carbon nano-onions, Carbon N. Y. 66 (2014) 272–284. https://doi.org/10.1016/j.carbon.2013.09.001.

[35] M.E. Plonska-Brzezinska, A. Lapinski, A.Z. Wilczewska, A.T. Dubis, A. Villalta-Cerdas, K. Winkler, L. Echegoyen, The synthesis and characterization of carbon nano-onions produced by solution ozonolysis, Carbon N. Y. 49 (2011) 5079–5089. https://doi.org/10.1016/j.carbon.2011.07.027.

[36] D. Dorobantu, P.M. Bota, I. Boerasu, D. Bojin, M. Enachescu, Pulse laser ablation system for carbon nano-onions fabrication, Surf. Eng. Appl. Electrochem. 50 (2014) 390–394. https://doi.org/10.3103/s1068375514050044.

[37] V. Dhand, J.S. Prasad, M.V. Rao, S. Bharadwaj, Y. Anjaneyulu, P.K. Jain, Flame

synthesis of carbon nano onions using liquefied petroleum gas without catalyst, Mater. Sci. Eng. C. 33 (2013) 758–762. https://doi.org/10.1016/j.msec.2012.10.029.

[38] T. Garcia-Martin, P. Rincon-Arevalo, G. Campos-Martin, Method to obtain carbon nano-onions by pyrolisys of propane, Cent. Eur. J. Phys. 11 (2013) 1548–1558. https://doi.org/10.2478/s11534-013-0294-1.

[39] M. Choucair, J.A. Stride, The gram-scale synthesis of carbon onions, Carbon N. Y. 50 (2012) 1109–1115. https://doi.org/10.1016/j.carbon.2011.10.023.

[40] O. Mykhailiv, H. Zubyk, M.E. Plonska-Brzezinska, Carbon nano-onions: Unique carbon nanostructures with fascinating properties and their potential applications, Inorganica Chim. Acta. 468 (2017) 49–66. https://doi.org/10.1016/j.ica.2017.07.021.

[41] Y.J. Ko, K. Choi, S. Lee, J.M. Cho, H.J. Choi, S.W. Hong, J.W. Choi, H. Mizuseki, W.S. Lee, Chromate adsorption mechanism on nanodiamond-derived onion-like carbon, J. Hazard. Mater. 320 (2016) 368–375. https://doi.org/10.1016/j.jhazmat.2016.08.041.

[42] C. Sakulthaew, C. Chokejaroenrat, A. Poapolathep, Hexavalent chromium adsorption from aqueous solution using carbon nano-onions (CNOs), Chemosphere. 184 (2017) 1168–1174. https://doi.org/10.1016/j.chemosphere.2017.06.094.

[43] S. Lagergren, “Zur Theorie der Sogenannten Adsorption GelosterStoffe”, Kungliga Svenska Vetenskapsakademiens., Handl. Band. 24 (1898) 1–39.

[44] Y.S. Ho, G. McKay, The Kinetics of Sorption of Basic Dyes from Aqueous Solution by Sphagnum Moss Peat, Can. J. Chem. Eng. 76 (1998) 822–827. https://doi.org/10.1002/cjce.5450760419.

[45] I. Langmuir, The adsorption of gases on plane surfaces of glass, mica and platinum., J. Am. Chem. Soc. 40 (1918) 1361–1403. https://doi.org/doi: 10.1021/ja02242a004.

[46] H. Freundlich, Über die Adorption in Lösungen, Z Phys.Chem. 57 (1906) 385–471.

[47] M. Frasconi, V. Maffeis, J. Bartelmess, L. Echegoyen, S. Giordani, Highly surface functionalized carbon nano-onions for bright light bioimaging, Methods Appl. Fluoresc. 3 (2015). https://doi.org/10.1088/2050-6120/3/4/044005.

[48] G.H.G. Ahmed, R.B. Laíño, J.A.G. Calzón, M.E.D. García, Facile synthesis of

water-soluble carbon nano-onions under alkaline conditions, Beilstein J. Nanotechnol. 7 (2016) 758–766. https://doi.org/10.3762/bjnano.7.67.

[49] H. Hagendorfer, W. Goessler, Separation of chromium(III) and chromium(VI) by ion chromatography and an inductively coupled plasma mass spectrometer as element-selective detector, Talanta. 76 (2008) 656–661. https://doi.org/10.1016/j.talanta.2008.04.010.

[50] M. Lesaoana, R.P.V. Mlaba, F.M. Mtunzi, M.J. Klink, P. Edijike, V.E. Pakade, Influence of inorganic acid modification on Cr(VI) adsorption performance and the physicochemical properties of activated carbon, South African J. Chem. Eng. 28 (2019) 8–18. https://doi.org/10.1016/j.sajce.2019.01.001.

[51] J. Jeřábková, V. Tejnecký, L. Borůvka, O. Drábek, Chromium in Anthropogenically Polluted and Naturally Enriched Soils: A Review, Sci. Agric. Bohem. 49 (2018) 297–312. https://doi.org/10.2478/sab-2018-0037.

[52] M.K. Miyittah, F.W. Tsyawo, K.K. Kumah, C.D. Stanley, J.E. Rechcigl, Suitability of Two Methods for Determination of Point of Zero Charge (PZC) of Adsorbents in Soils, Commun. Soil Sci. Plant Anal. 47 (2016) 101–111. https://doi.org/10.1080/00103624.2015.1108434.

[53] T.D. Ntuli, V.E. Pakade, Hexavalent chromium removal by polyacrylic acid-grafted Macadamia nutshell powder through adsorption–reduction mechanism: Adsorption isotherms, kinetics and thermodynamics, Chem. Eng. Commun. 207 (2019) 1–16. https://doi.org/10.1080/00986445.2019.1581619.

[54] D. Park, S.R. Lim, Y.S. Yun, J.M. Park, Reliable evidences that the removal mechanism of hexavalent chromium by natural biomaterials is adsorption-coupled reduction, Chemosphere. 70 (2007) 298–305. https://doi.org/10.1016/j.chemosphere.2007.06.007.

[55] J. Wang, X. Guo, Adsorption kinetic models: Physical meanings, applications, and solving methods, J. Hazard. Mater. 390 (2020) 122156. https://doi.org/10.1016/j.jhazmat.2020.122156.

[56] V.E. Pakade, L.C. Maremeni, T.D. Ntuli, N.T. Tavengwa, Application of quaternized activated carbon derived from Macadamia nutshells for the removal of hexavalent chromium from aqueous solutions, South African J. Chem. 69 (2016) 180–188. https://doi.org/http://dx.doi.org/10.17159/0379-4350/2016/v69a22.

[57] D.C. Sharma, C.F. Forster, A preliminary examination into the adsorption of

hexavalent chromium using low-cost adsorbents, Bioresour. Technol. 47 (1994) 257–264. https://doi.org/10.1016/0960-8524(94)90189-9.

[58] D.C. Sharma, C.F. Forster, The treatment of chromium wastewaters using the sorptive potential of leaf mould, Bioresour. Technol. 49 (1994) 31–40. https://doi.org/10.1016/0960-8524(94)90170-8.

[59] D. Park, Y.-S. Yun, J.H. Jo, J.M. Park, Mechanism of hexavalent chromium removal by dead fungal biomass of Aspergillus niger, Water Res. 39 (2005) 533–540.

[60] H.N. Tran, S.J. You, H.P. Chao, Thermodynamic parameters of cadmium adsorption onto orange peel calculated from various methods: A comparison study, J. Environ. Chem. Eng. 4 (2016) 2671–2682. https://doi.org/10.1016/j.jece.2016.05.009.

Chapter 5: From waste cooking oil to oxygen-rich onion-like nanocarbons for the removal of hexavalent chromium from aqueous solution

Submitted: Themba D. Ntuli, Ludwe L. Sikeyi, Thomas H. Mongwe, Orlette Mkhari, Neil J. Coville, Edward N. Nxumalo, Manoko S. Maubane-Nkadimeng, From waste cooking oil to oxygen-rich onion-like nanocarbons for the removal of hexavalent chromium from aqueous solution, South African Journal of Science **Ref: SAJS 14006**

Abstract

Vegetable cooking oil has been used in domestic and commercial kitchens owing to its ability to modify and enhance the taste of the food through the frying process. However, as the oil is used through several frying cycles it changes colour to dark brown and has an unpleasant smell. This change in the oil results in food that is less palatable and at this point, the waste oil (WO) is usually discarded, typically finding its way into freshwater streams as a contaminant. To provide an alternative 'green' route to WO disposal, herein we report on the metal-free synthesis of onion-like nanocarbons (OLNCs) made from waste cooking oil (WCO) via flame pyrolysis. The WCO pyrolysis produced OLNCs functionalized with oxygen, due to the oxygenation process that takes place during the cooking process. The as-synthesised OLNCs were then applied in the removal of hexavalent chromium ions from aqueous solutions. The as-synthesized OLNCs were found to have similar properties (size, onion-like structure, and quasi-spherical shape) to those OLNCs synthesized from pure cooking oils. The Fourier transform infrared (FTIR) spectroscopy data showed that the OLNCs contained C-O-type moieties. The OLNCs from WO were applied as adsorbent for Cr(VI) and showed optimal removal conditions at pH 2, t = 360 min, Co = 10 mg/L and Q^0_{max} = 47.62 mg/g, superior to data obtained from pristine cooking oil. The results showed that the OLNCs derived from waste cooking oil with their high oxygen functionalized carbon content were effective in the removal of hexavalent chromium.

5.1. Introduction

Urbanization has seen a rise in industries manufacturing chemicals and oil [1–3]. Some of these manufacturing industries produce or make use of compounds that include vegetable cooking oils which eventually enter freshwater streams via anthropogenic processes resulting in aquatic environmental pollution [4]. Another toxic pollutant that can contaminate water systems is the Cr(VI) ion. It is known to be toxic to biota and humans alike due to its high mobility and biological accumulation [5]. Herein we provide a methodology to address these two issues.

Contamination of water with waste oil also leads to unsightly immiscible mixtures that are a threat to the environment and the ecosystem. This later issue arises from the lack of systems for the disposal of these oils [6]. Vegetable oil, which is mainly used in both industrial and household kitchens, is one such oil. This oil is often discarded in municipal drains, and as such, finds its way into groundwater or rivers. These oils increase the biological oxygen demand (BOD) and chemical oxygen demand (COD) of water which could be detrimental to humans, micro-organisms and the quality of the water through de-oxygenation [2,3].

One of the most utilized methods for trace metal removal is adsorption. Adsorption is typically achieved by using abundantly available carbonaceous materials which have functional groups comprising of oxygen, nitrogen, and sulfur moieties on their surface that attach to the trace metal ions [7]. One class of carbonaceous material that has been recently used for this purpose are based on nanomaterials of carbon. These include carbon nanofibers [8], carbon nanotubes [9], carbon dots [10], carbon spheres [11], graphene [12], carbon nano-onions (CNOs; Mykhailiv et al., 2017), and onion-like nanocarbons (OLNCs) [14]. Their use is owed to their high surface-to-volume ratio, thermal stability, chemical robustness, and tunable surface functional groups [15]. CNOs and OLNCs can be viewed as fullerene types of carbon and have found application in numerous adsorption processes, in particular for the removal of Cr(VI) ions [16]. The high operational costs, high consumption of energy and the use of a metal catalyst to synthesize such carbons have to date limited their use in water application processes [17].

Removal techniques for oils are different and include in-situ burning, containment booms, dispersants, and biodegradation, but all show an incomplete separation of oil

from the water [18]. An alternative process is to convert these oils into useful carbonaceous products that could be used in various applications, thus putting value to waste. The use of oil for the synthesis of nano-carbons such as CNOs has been well documented [19]. For example, Shaku et.al used flame pyrolysis of grapeseed oil to synthesize CNOs that were applied in supercapacitors [20]. This method was used by Sikeyi et al. to make CNOs using olive oil as a starting material for CNOs that were applied in fuel cells [21].

The current study seeks to simultaneously address the aquatic environmental problem of trace metals (specifically Cr) and oil pollution (specifically cooking oil) in water streams. This was achieved by (i) using waste cooking oil as a precursor for the synthesis of OLNCs and, (ii) using the OLNCs for the removal of Cr(VI) ions from an aqueous solution.

Khalisanni et al. reported that the chemical compounds found in waste cooking oils consist mainly of carboxylic acid derivatives [22]. This makes waste cooking oil attractive as a carbon and oxygen-rich source for the synthesis of OLNCs via flame pyrolysis. As will be shown, the cooking process generates more oxygen groups than found in pure oil and this leads to better Cr-OLNCs interactions. The OLNCs produced in this study were applied as adsorbents for the removal of Cr(VI) ions from aqueous solutions. The results were compared with those from our previous study where we reported the use of olive oil as a starting material to make OLNCs for the removal of Cr(VI) in water [23]. For methodology and instrumentation please refer to Chapter 3

5.2. Results and discussion

5.2.1. Characterization of the waste cooking oil and adsorbents

The waste cooking oil was obtained from a local restaurant that used a mixture of vegetable oils for the cooking of potato chips and fat cakes. Compounds contained in the waste cooking oil were identified using gas chromatography-mass spectrometry (GC-MS) and the results were compared to different waste cooking oils found in the literature.

Table 5.1. and Figure 5.1. presents the major chemical compounds found in the waste cooking oil. This data is sin agreement with data reported by Khalisanni et al. who noted that oleic acid and *n*-hexadecanoic acid were the two major compounds found in waste cooking oil obtained from the Universiti Teknologi MARA, Malaysia [22], and similar to data reported by Zayed et al. [24] for waste oils obtained from sunflower, cotton, and soybean oils. This indicates that our study can be generalised to the synthesis of OLNCs from many similar waste oils.

During the cooking process, cooking oil undergoes three major processes which include hydrogenation, oxidation and polymerization which can result in the formation of volatile organic compounds (VOCs) [25]. Some of these VOCs detected in the current study were nonanal, hexanoic acid, 2,4-decadienal, farnesene, propanoic acid, heptane, 2.4-heptadienal, and 2-decenal compounds similar to those reported by Mannu et al. in their waste oil [25]. We also found oleic acid, hexadecenoic acid , palmitoleic acid, and 9-octadecenoic acid (Z)- in our waste oil, compounds, reported to be present in waste sunflower oil and waste cotton oil by Zayed et al. [24]. This indicated that our data are similar to those observed in the literature.

Zhang et al. reported that VOCs such as furan, nonanal, hexanal, heptanal, octanal, and benzene are highly carcinogenic and that more VOCs are produced as the temperature of the oil are increased [26]. These carcinogenic compounds could be harmful to humans and biota should they find their way into water streams. Therefore, this study was motivated by seeking a method to convert waste cooking oil into a more valuable material. In our study, oil was used as a starting material for the metal-free synthesis of useful carbon nanomaterials via flame pyrolysis. The soot produced was collected in good yield (8%) by a procedure described previously (Equation 1) [23]. The OLNCs were then applied in the removal of Cr(VI) ions from the solution.

Table 5.1: List of chemical compounds detected in different waste cooking oil

This study	Zayed et al., 2017		Mannu et al., 2019
Unknown	**Waste sunflower oil**	**Waste cotton**	**Unknown**
Oleic acid	Oleic acid	Oleic acid	
Hexadecenoic acid	Hexadecenoic acid	Hexadecenoic acid	
Palmitoleic acid	Palmitoleic acid	Palmitoleic acid	
9 -Octadecenoic acid (Z)-	9 -Octadecenoic acid (Z)-	9 -Octadecenoic acid (Z)-	

2-Pentanone	2-Pentacosanone		
2-Heptanone	2-Heptacosanone		2-Heptanone
Eeicosatetraenoic acid	Eicosanoic acid		
Quinoline		Quinoline	
1-Cyclohexyldimethylsilyloxybutane		1Cyclohexyldimethylsiyoxybutane	
Nonanal			Nonanal
Cyclopropane			
9,12-Octadecadienoic acid (Z,Z)-			
Heptane			Heptane
Hexanoic acid			Hexanoic acid
2-Decenal, (E)-			2-Decenal, (E)-
Farnesene			Farnesene
2-Undecenal			2-Undecenal
2,4-Decadienal			2,4-Decadienal
2-Decenal, (E)-			2-Decenal, (E)-
Propanoic acid			Propanoic acid
2,4-Heptadienal			2,4-Heptadienal

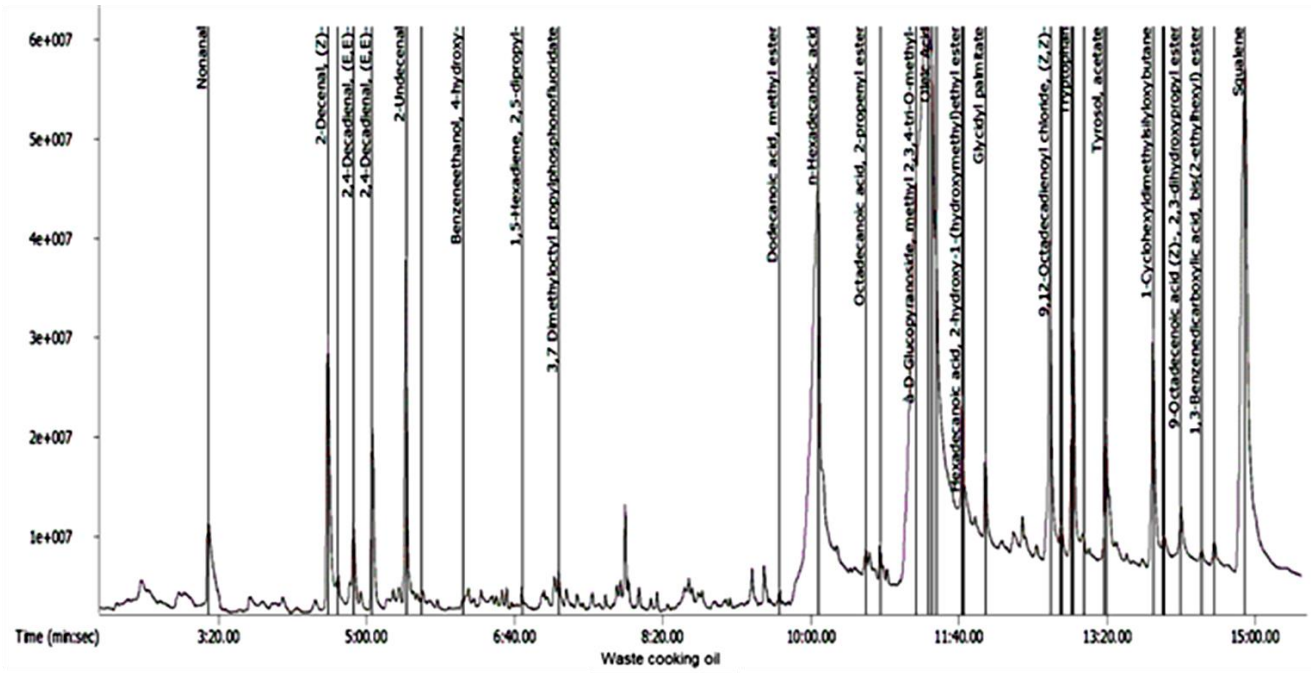

Figure 5.1: Chromatogram for the waste cooking oil

SEM micrographs of the adsorbent showed that the materials are quasi-spherical and closely packed together (Figure 5.2a). The TEM micrographs showed that the adsorbent consisted of interlinked spheres resembling a cut onion-like structure with multiple shells with an average external diameter of 41 nm Figure 5.2b. The OLNCs

showed similar morphological characteristics and diameter with similar materials derived from pure oil [17]. The BET results indicated that the synthesized material had a surface area of 69 m^2/g, a pore volume of 0.20 cm^3/g, and an average pore size of 11 nm. The as-synthesized materials had surface areas that were in the range of those reported previously (60–85 m^2/g) [21,23]. A closer look reveals the presence of cavities, another attribute for adsorption processes as the cavities could encapsulate adsorbate ions.

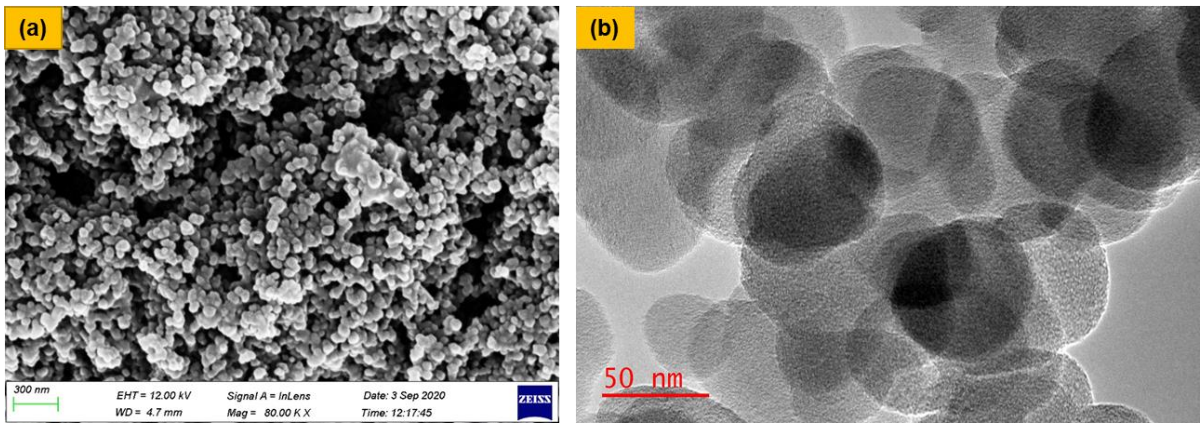

Figure 5.2: (a) SEM micrographs of the OLNCs and (b) TEM micrographs of the OLNCs.

Thermal analysis showed a single decomposition step between 500 and 800°C (Figure 5.3a), which indicated that the material was thermally stable and contained no impurities [19]. The FTIR spectra showed that the adsorbent consisted mainly of carbon and oxygen-containing functional groups and some O-H groups (Figure 5.3 b). For example, the spectrum indicated O–H peaks at 3437 cm^{-1} representing O-H stretching modes for alcohol moieties and a peak at 3153 cm^{-1} for carboxylic acid moieties [27]. The O-H bending peaks at 1400 and 1100 cm^{-1} are also consistent with the presence of carboxylic acid functional groups. The peak at 1635 cm^{-1} signifies the C=C stretching mode for conjugated alkenes. The predicted surface moieties were similar to those reported previously (Venkatesan and Balachandran) on similar material synthesized via flame pyrolysis using a liquid paraffin precursor [28]. The Raman spectra of the OLNCs before and after the adsorption of Cr(VI) ions are depicted in Figure 5.2 c. Two major peaks could be identified between 1300 to 1650 cm^{-1}, due to the D band and G band. The presence of the D bands in the aforementioned range can be attributed to the amorphous nature of the carbon

material with graphitic layers [29,30]. The I_D/I_G ratio computed from the respective peak areas of the D and G bands were similar indicating that the presence of Cr on the surface of the adsorbent did not disrupt the characteristics of the adsorbent. However, the peak position shifted indicating possible Cr interaction with the surface (Table 5.2). The Raman spectra for the current material were similar to those produced via flame pyrolysis of olive oil [21].

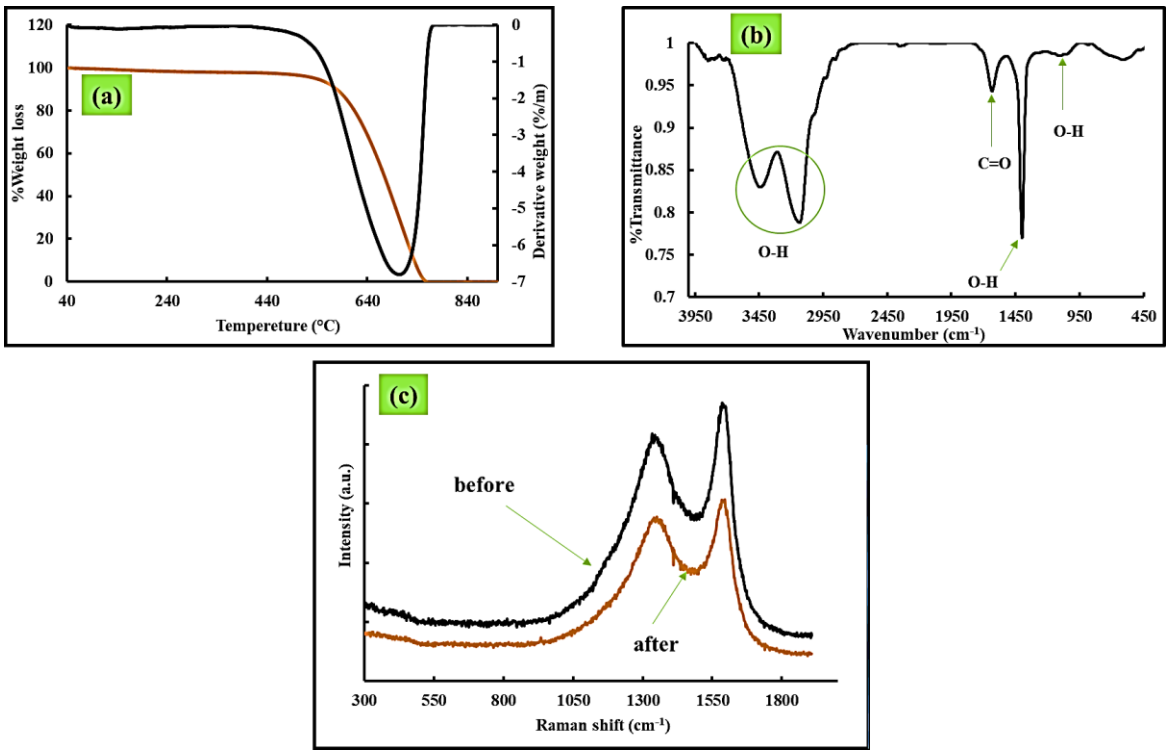

Figure 5.3: The TGA and DTA thermograms for OLNCs (a), the FTIR spectra of OLNCs (b), and the Raman spectra of OLNCs before and after adsorption of [Cr(VI)] (c).

Table 5.2: Raman spectroscopy data of the OLNCs before and after Cr(VI) ions removal

Adsorbent	D-band		G-band		
	Raman shift (cm^{-1})	Area	Raman shift (cm^{-1})	Area	I_D/I_G
OLNCs	1352.6	409981	1600.3	143752	2.9
OLNC-Cr	1344.1	272281	1593.7	97375	2.8

The XPS analysis of the adsorbent is depicted in Figure 5.4. It can be observed that the adsorbent surface contained mainly carbon and oxygen atoms. The material showed four peaks for C1s representing carbon bonded to oxygen at 288.8 eV, 288.4 eV, and 286.2 eV for O–C=O, C=O, and C–O moieties. The sp^3 and sp^2 hybridized carbon peaks were observed at 284.6 eV and 284.2 eV respectively (Figure 5.4a). The material also showed two peaks for O1s representing carbon bonded to oxygen. These peaks were observed at 531.8 eV and 533.2 eV, as expected for carboxylic acid C=O and C–O moieties (Figure 5.4b).

It is to be noted that the adsorbent had a higher oxygen content (13.5%) [see Table 5.3.] than OLNCs (11.8%) derived from olive oil [23]. This can be attributed to the oxidation of the starting material (waste cooking oil) during cooking. The surface moieties shown in the XPS data were similar to those reported by Ko et al. for carbon nano-onions (CNOs) synthesized after the annealing of nanodiamonds [31].
Overall the OLNCs synthesized via flame pyrolysis of waste cooking oil showed similar characteristics to OLNCs produced from pure oils such as olive oil, castor oil, paraffin oil, and ghee oil [17,19,21]. The results showed that the hydrogenation, oxidation and polymerization reactions taking place during the frying process did not negatively affect the quality of the OLNCs that were synthesized using the waste cooking oil. This offers the possibility of using waste oils in place of pure oils for the synthesis of OLNCs. More importantly, the as-synthesized OLNCs also showed similar characteristics to CNOs synthesized from more expensive methods such as the annealing of nanodiamonds and laser irradiation [16,31]. The synthesized OLNCs showed similar characteristics (quasi-spherical, multi-shells, size diameter >100 nm, disordered and having surface defects) to carbon nano-onions and carbon black [32].

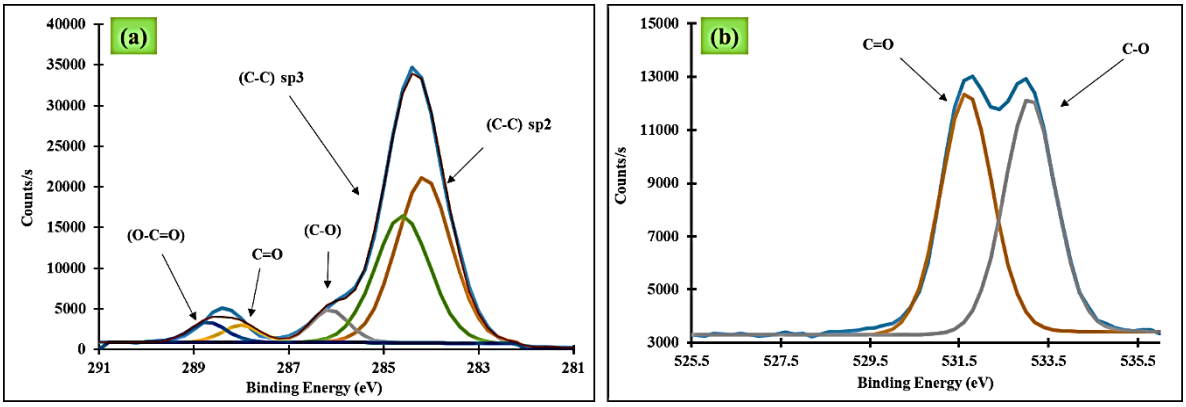

Figure 5.4: The XPS spectra of OLNCs adsorbent for C1s and O1s peaks (a and b).

Table 5.3: Elemental identification and quantification for the OLNCs

Material	Name	Peak BE	Atomic %
OLNCs	C1s	284.1	86.5
	O1s	532.2	13.5

5.2.2. Effect of solution pH on the Cr(VI) ions removal

The removal of Cr(VI) ions is interrelated with the solution pH of the Cr(VI) ions. The solution pH affects the speciation of Cr(VI) ions as well as the nature of the surface moieties on the adsorbent. Figure 5.5. presents the performance of the OLNCs for the removal of the Cr(VI) ions in the pH range of 2 – 8. The removal efficiency decreased as the pH of the solution was increased from 2 to 8 (48 to 81%). This, as mentioned in the literature, can readily be attributed to an electrostatic attraction as a result of the nature of the adsorbate and adsorbent. since Cr(VI) ions are present as anionic species (chromate and dichromate) in a basic and acidic environment [33]. In more acidic conditions, $Cr_2O_7^-$ species are formed and undergo hydrolysis to form $HCrO_4^-$ while the surface moieties of the adsorbent predominantly undergo protonation. This results in an electrostatic attraction between the adsorbate and the adsorbent producing good metal ion removal under acidic conditions [34].

The electrostatic attraction was supported by the pH_{PZC} of the adsorbent which was found to be at pH 7.2. The pH_{PZC} was determined by measuring the initial pH and the final pH where the change in pH was plotted against the initial pH. The point at which the graph intersects the x-axis was taken as the pH_{PZC}. The adsorbent undergoes protonation at the pH below the pH_{PCZ} and deprotonation above it. This arises since Cr ions have hard acid characteristics and may be bound to the surface of the adsorbent as a result of the hard base characteristics of the oxygen moieties [7]. The high removal of Cr(VI) ions under acidic media has also been extensively reported by other authors who have used carbon-rich adsorbents, and our data are in full agreement with the earlier studies [35–38].

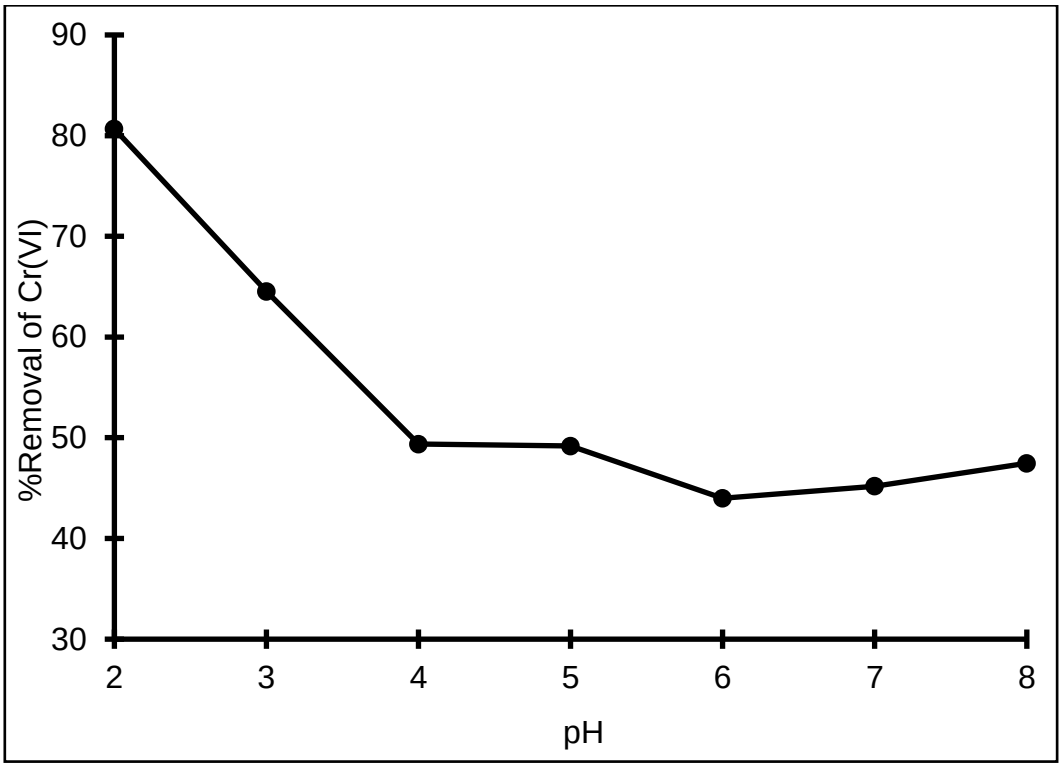

Figure 5.5: Performance of the OLNCs as a function of solution pH [Conditions: m = 0.05 g, t = 720 min and C_O = 10 mg/L).

5.2.3. Effect of adsorbent mass

The performance of the OLNCs as a function of adsorbent mass is depicted in Figure 5.6. From Figure 5.6. it can be seen that an increase in the mass of the adsorbent leads to an increase in efficiency. This arises since more adsorption sites are available [39]. However, the efficiency profile did not reach equilibrium at the selected adsorbent mass range. This could be an indication that the surface of the adsorbent was not fully covered by the adsorbate ions and thus still had vacant active sites available for binding with the Cr ions.

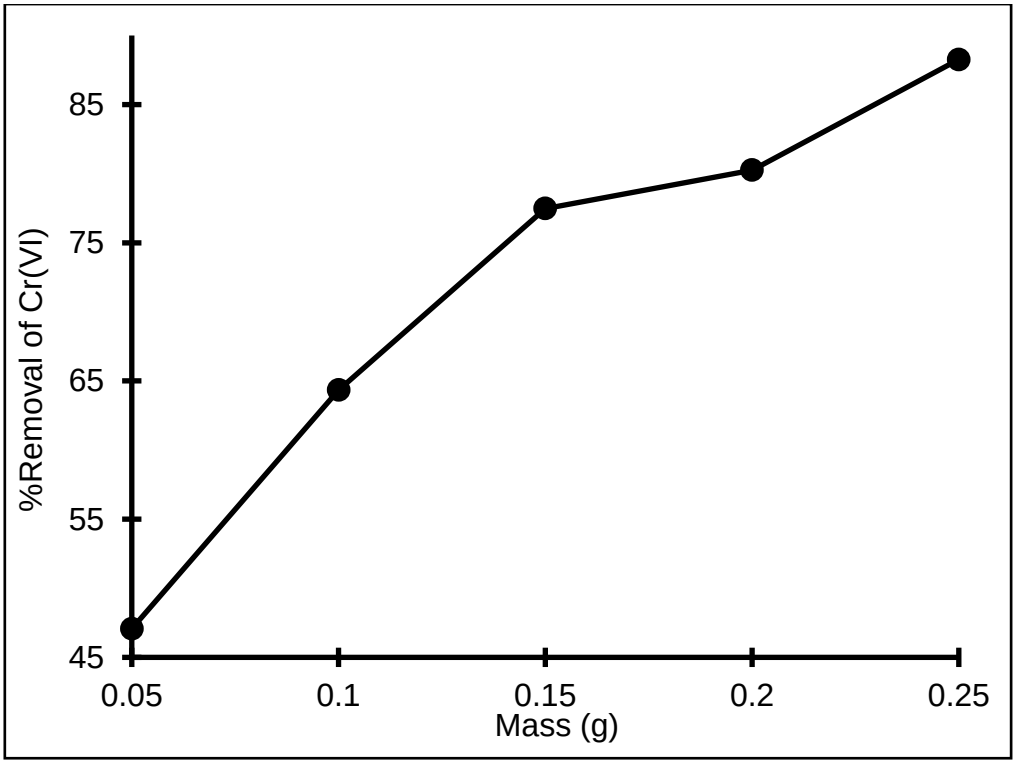

Figure 5.6: Performance of the OLNCs as a function of adsorbent mass [Conditions: pH 2, t = 30 min, and C_O = 10 mg/L].

5.2.4. Effect of contact time

The amount of time that the adsorbent and adsorbate are in contact plays a major role in the migration of the adsorbate ions to the surface of the adsorbent [35]. Figure 5.7a shows the performance of the adsorbent as a function of time (15 min to 720 min). This adsorption capacity (qe) changed from 0.96 mg/g (15 min) to 6.4 mg/g (720 min) with increasing time. It was also observed that the total Cr removal was not equal to the removal of Cr(VI). This can be attributed to the reduction of Cr(VI) to Cr(III) as has been observed previously with carbon-rich materials [40].

The removal of Cr(VI) ions was further tested as a function of time using two adsorbent masses (0.05 g and 0.1 g) (Figure 5.7 b). As expected, as the adsorbent mass increased, the removal improved from 15.3 mg/g after 15 min to 48.0 mg/g after 180 min. This was attributed to the availability of more active sites as the adsorbent mass was increased since the number of active sites could be linked to the amount of the adsorbent.

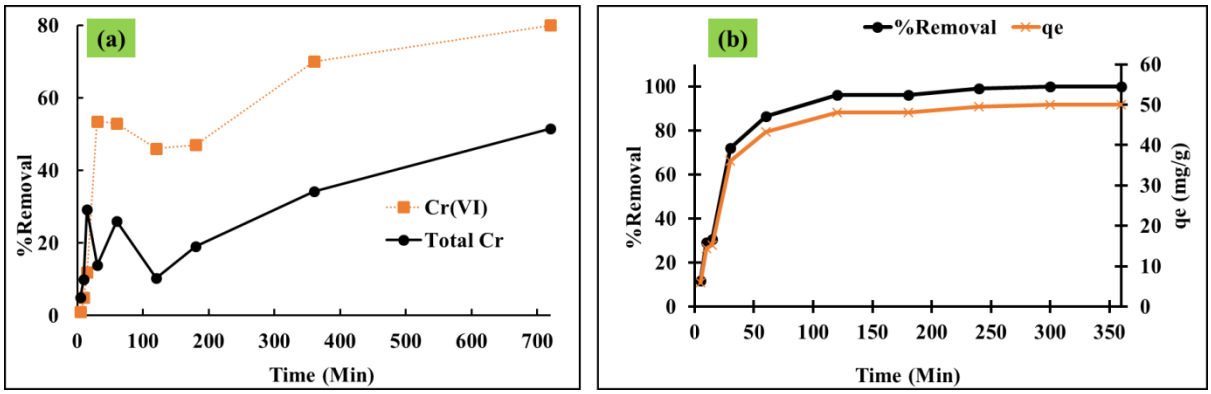

Figure 5.7: Performance of the OLNCs as a function of time for (a) 0.05 g and (b) 0.1 g absorbent [Conditions: pH 2 and C_O = 10 mg/L].

5.2.5. Kinetics

A summary of the adsorption kinetics for the removal of Cr(VI) ions using the as-synthesized OLNCs is presented in Table 5.4. The removal of Cr(VI) ions for the initial 30 min followed the pseudo-first-order (PFO) kinetic model. This could be attributed to a removal process taking place through interface diffusion with a rate constant (k_1) of 0.0345 1/min [41]. However, after 30 min of contact time, the adsorption kinetics followed a pseudo-second-order (PSO) route indicating a chemisorption process with the rate constant (k_2) of 0.0024 g/mg x min [42]. Some researchers (Ho and McKay, 1998;[44] have suggested that the PFO may not be suitable for the whole range of contact times used and that only the first 20 to 30 min can be attributed to chemical bond formation between the adsorbate ions and the adsorbate surface. The initial adsorption rate (*h*) for the reaction was found to be 2.074 mg/g x min and 0.190 mg/g x min from 30 to 360 min (Table 5.4.). This could be attributed to the surface coverage with more exposed sites filled first.

Table 5.4: A summary of the adsorption kinetics parameters

PFO			PSO			
k_1	q_e	R^2	k_2	q_e	*h*	R^2
Overall						
0.012	22.60	0.7965	0.00069	54.65	2.074	0.9951
5 to 30 min						

0.046	58.92	0.9545	344.379	1.24	526.316	0.0278
30 to 360 min						
0.002	2.60	0.7050	0.00235	6.80	0.190	0.9881

5.2.6. Initial concentration

The performance of the OLNCs for the removal of Cr(VI) ions was tested as a function of the initial concentration of the Cr(VI) ions (Figure 5.8.). It can be observed that as the initial concentration of the Cr(VI) ions increased (10 mg/L to 100 mg/L) the removal percentage decreased. However, the adsorption capacity (q_e) increased from 7.92 mg/g to 50.40 mg/g, attributed to the possibility of enhanced interactions at the surface of the adsorbate as the initial concentration was increased [45]. This phenomenon is in agreement with data that showed that the initial concentration is directly proportional to the adsorption capacity (see Equation 3).

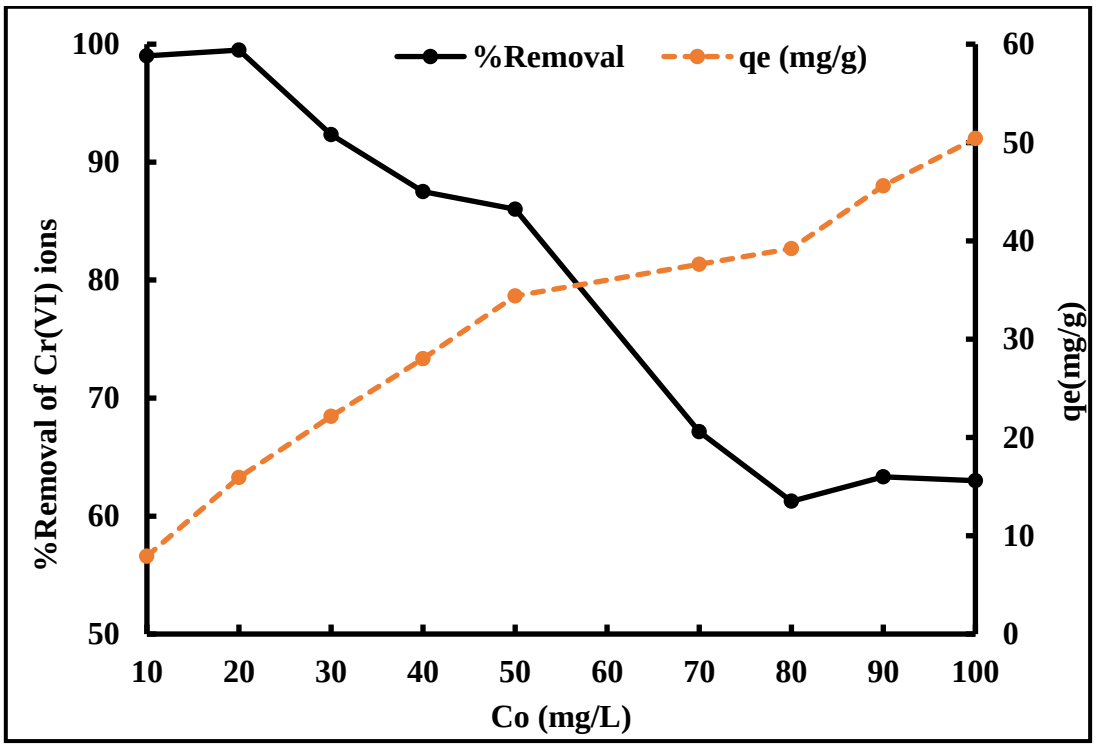

Figure 5.8: Performance of the OLNCs as a function of the initial concentration of Cr(VI) ions [@ pH 2, t = 120 min, m = 0.025g, and C_o = (10 – 100 mg/L)].

5.2.7. Adsorption isotherms

The linear forms of the Langmuir and Freundlich adsorption isotherms were selected for modelling the Cr(VI) ions removal pathway using OLNCs as an adsorbent, with the data presented in Table 5.5. Both the dimensionless constants separation factor (R_L) and Freundlich intensity parameter (n) were between zero and one indicating a favourable removal of Cr(VI) ions. The coefficient of determination (R^2) values for the Langmuir adsorption isotherm were nearer to unity compared to those of the Freundlich isotherm. This corresponded with the chi-squared (χ^2) values which were nearer to zero for the Langmuir isotherm and not the Freundlich isotherm. This suggests that the removal pathway was through a monolayer surface coverage of the adsorbent [46]. Moreover, the maximum adsorption capacity was 47.62 mg/g, which was close to the experimental adsorption capacity of 50.40 mg/g, in agreement with a Langmuir isotherm or monolayer surface coverage. The adsorption capacity of the adsorbent was significantly higher than similar material produced from olive oil (26.53 mg/g) [23]. This could be due to the added adsorbent oxygen content due to oxidation through cooking. The results discussed thus far, indicate that different oils (olive and waste cooking oil) that undergo flame pyrolysis yield carbon nanomaterials with similar characteristics. However, due to the difference in the oils, the surface moieties may be slightly different. Such differences may result in significant changes in the application of the materials.

Table 5.5: Adsorption isotherm parameters

Langmuir				Freundlich		
Q_{max} (mg/g)	**K_L (L/mg)**	**R^2**	**X^2**	**n**	**R^2**	**X^2**
47.62	0.392	0.9453	0.162	0.384	0.8656	142478

C_o (mg/L)	**R_L**
10	0.2033
20	0.1132
30	0.0784
40	0.0600
50	0.0486

70	0.0352
80	0.0309
90	0.0276
100	0.0249

5.3 Removal mechanism of Cr(VI) ions

The XPS analysis of the OLNCs before and after the removal of Cr(VI) ions is presented in Figure 5.9. A new peak was observed at 577.9 eV for Cr_{p2}, which represents Cr(III) ions bound to the surface of the adsorbent (Figure S5.2.). This peak was absent before the material was used as an adsorbent for the removal of Cr(VI) ions. It can be noted that in the process of Cr(VI) ions removal, some ions were reduced to the less toxic Cr(III) ions. Figure 5.7 (a) shows the percent removal of Cr(VI) ions and the total Cr ions. The thermodynamic parameters for the removal of Cr(VI) ions have been depicted in Table 5.6. All the thermodynamic parameters returned negative values and were representative of a favourable and spontaneous (-ΔG) removal of Cr. The removal of Cr(VI) ions at the adsorbate/adsorbent boundary layer involved an associative mechanism (-ΔS) [44]. The -ΔH value could indicate that the removal of Cr(VI) ions involved chemisorption, physisorption, or comprehensive removal (a mixture of chemisorption and physisorption). Therefore, the removal mechanism as described fits the proposed removal that involves an adsorption coupled reduction mechanism between the Cr(VI) ions and the adsorbent.

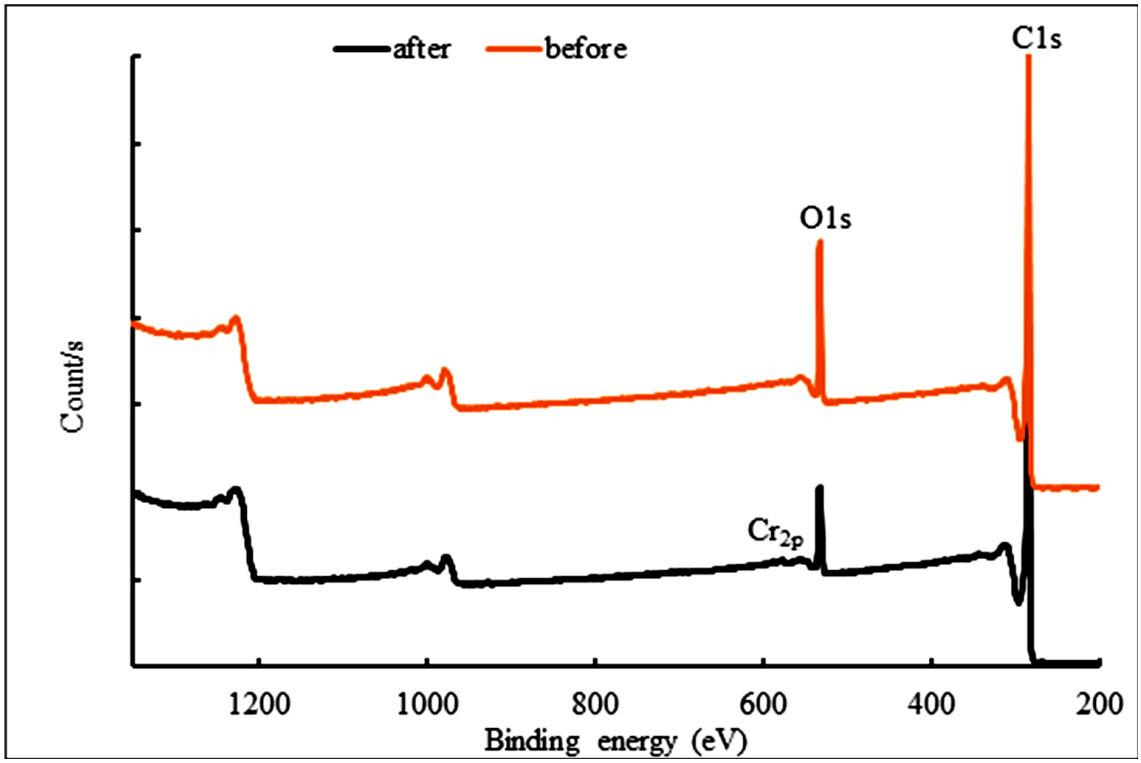

Figure 5.9: The XPS survey spectra for the OLNCs before and after the removal of Cr(VI) ions

Table 5.6: Thermodynamic parameter calculated via the Langmuir constant K_L

T (K)	van't Hoff equation	K_C	ΔG° (kJ/mol)	ΔH° (kJ/mol)	ΔS° (J/mol)
298.15	y = 23092x - 61.419	6213254.8	-38.8	-192.0	-510.6
303.15	R^2 = 0.9333	4082853.0	-38.4		
308.15		957665.7	-35.3		
313.15		160788.5	-31.2		

5.4 Comparison of adsorption capacities for different adsorbents

Direct comparison of different adsorption studies in the literature is challenging due to the different optimum adsorption conditions used in the respective studies. Therefore, as a comparison, the pH, contact time, adsorbent modification, and adsorption capacity have been selected for comparison studies. (Table 5.7.).

It can be observed that the optimum pH for the removal of Cr(VI) ions was under acidic media (pH < 7) Most of the adsorbents in Table 5.7. have undergone functionalization to improve their adsorption capacity. In comparison, the as-synthesized adsorbent was used in its pristine state. Remarkably, the adsorption capacity of the OLNCs was higher than other pristine adsorbents as well as functionalized ones, except for a graphene nanocomposite. (Table 5.7.)

The graphene nanocomposite showed the highest adsorption capacity, an indication of the value of surface modification and the synergy between different materials to form a composite with high adsorption capacity [47]. However, the as-synthesized OLNCs from waste cooking oil showed a comparable adsorption capacity of 48 mg/g at a time of 360 min. This is an indication that the adsorbent has the potential as an adsorbent for the removal of Cr(VI) ions. It is also to be noted that the adsorbent had a higher adsorption capacity (48 mg/g) than those from pure oil (26.53 mg/g) [23]. This was attributed to the higher oxygen content of the OLNCs from waste cooking oil, due to the oxidation process that takes place during cooking.

Table 5.7: Comparison of different adsorbents

Adsorbent	pH	Time (Min)	Modification	qe (mg/g)	Reference
(3D) NiO/Ni	4	120	Composite	25.94	[48]
Activated carbon	4	1440 4320	None Polysulfide	3.47 8.93	[49]
Graphene oxide	2	1440	Manganese ferrite	34.02	[50]
MWCNTs	2	6000	Oxidation	31.95	[51]
CNOs	2	720	None	26.53	[23]
PANI/Ag/ GO CDs	2	60	Composite	59.96	[47]
OLNCs	2	360	None	48	Current study

5.5. Conclusions

This study has shown that waste cooking oil is used as a starting material for the synthesis of high-quality of OLNCs produced. The OLNCs obtained in this work had a higher oxygen content than pure oils due to the cooking process and this led to more sites for binding to metal ions.

The OLNCs were applied as an efficient adsorbent for the removal of Cr(VI) ions from an aqueous solution. With the maximum adsorption capacity of 47.62 mg/g at a pH of 2 and a contact time of 360 min, the OLNCs produced were better than those made from pure oils. The adsorption-coupled reduction mechanism was found to be the pathway for the removal of the Cr(VI) ions as demonstrated by the presence of Cr(VI) and Cr(III) ions in the adsorption media The removal was spontaneous, and exothermic and involved an associative mechanism. The study showed that waste material can be converted into a useful material for application in adsorption processes. In this study this was achieved by taking a toxic material (waste cooking oil) and converting it into a less harmful material that could be used in the removal of toxic Cr(VI) ions thus, putting value to waste. This then provides a means of solving the double aquatic environmental problem of trace metal removal and oil pollution.

5.6. References

[1] V.E. Pakade, T.D. Ntuli, A.E. Ofomaja, Biosorption of hexavalent chromium from aqueous solutions by Macadamia nutshell powder, Appl. Water Sci. 7 (2017) 3015–3030. https://doi.org/10.1007/s13201-016-0412-5.

[2] S. Sridhar, A. Kale, A.A. Khan, Reverse osmosis of edible vegetable oil industry effluent, J. Memb. Sci. 205 (2002) 83–90. https://doi.org/10.1016/S0376-7388(02)00065-0.

[3] T. Ahmad, T. Belwal, L. Li, S. Ramola, R.M. Aadil, Abdullah, Y. Xu, L. Zisheng, Utilization of wastewater from edible oil industry, turning waste into valuable products: A review, Trends Food Sci. Technol. 99 (2020) 21–33. https://doi.org/10.1016/j.tifs.2020.02.017.

[4] M. Mofokeng, L.N. Nthunya, L. Gutierrez, P. Matabola, S. Mishra, E.N. Nxumalo, Perflurooctyltriethoxy silane and carbon nanotubes-modified PVDF superoleophilic nanofibre membrane for oil-in-water adsorption and recovery, J. Environ. Chem. Eng. 8 (2020) 104497. https://doi.org/10.1016/j.jece.2020.104497.

[5] World Health Organization, Guidelines for drinking-water quality, 2008. https://doi.org/10.1016/S1462-0758(00)00006-6.

[6] Z. LF, A. Waadu GDB, Used-Oil Generation and Its Disposal along East-West Road, Port Harcourt Nigeria, Int. J. Waste Resour. 06 (2016) 1–5. https://doi.org/10.4172/2252-5211.1000195.

[7] M. Lesaoana, R.P.V. Mlaba, F.M. Mtunzi, M.J. Klink, P. Edijike, V.E. Pakade, Influence of inorganic acid modification on Cr(VI) adsorption performance and the physicochemical properties of activated carbon, South African J. Chem. Eng. 28 (2019) 8–18. https://doi.org/10.1016/j.sajce.2019.01.001.

[8] A. Kakoria, S. Sinha-Ray, S. Sinha-Ray, Industrially scalable Chitosan/Nylon-6 (CS/N) nanofiber-based reusable adsorbent for efficient removal of heavy metal from water, Polymer (Guildf). 213 (2021) 123333. https://doi.org/10.1016/j.polymer.2020.123333.

[9] S. Deng, X. Liu, J. Liao, H. Lin, F. Liu, PEI modified multiwalled carbon nanotube as a novel additive in PAN nanofiber membrane for enhanced removal of heavy metal ions, Chem. Eng. J. 375 (2019) 122086. https://doi.org/10.1016/j.cej.2019.122086.

[10] O. Mkhari, T.D. Ntuli, N.J. Coville, E.N. Nxumalo, M.S. Maubane-Nkadimeng, A comparison of fluorescent N-doped carbon dots supported on the surface of hollow and solid carbon spheres, and solid silica spheres, Diam. Relat. Mater. 118 (2021) 108500. https://doi.org/10.1016/j.diamond.2021.108500.

[11] P. Mente, V. Mashindi, T.N. Phaahlamohlaka, T.N. Monyatsi, R.P. Forbes, N.J. Coville, Oxidation of Benzyl Alcohol Using Cobalt Oxide Supported Inside and Outside Hollow Carbon Spheres, ChemistryOpen. 10 (2021). https://doi.org/10.1002/open.202000312.

[12] M. Majdoub, A. Amedlous, Z. Anfar, A. Jada, N. El Alem, Engineering of amine-based binding chemistry on functionalized graphene oxide/alginate hybrids for simultaneous and efficient removal of trace heavy metals: Towards drinking water, J. Colloid Interface Sci. 589 (2021) 511–524. https://doi.org/10.1016/j.jcis.2021.01.029.

[13] O. Mykhailiv, H. Zubyk, M.E. Plonska-Brzezinska, Carbon nano-onions: Unique carbon nanostructures with fascinating properties and their potential applications, Inorganica Chim. Acta. 468 (2017) 49–66. https://doi.org/10.1016/j.ica.2017.07.021.

[14] Gunture, C. Dalal, J. Kaushik, A.K. Garg, S.K. Sonkar, Pollutant-Soot-Based Nontoxic Water-Soluble Onion-like Nanocarbons for Cell Imaging and Selective Sensing of Toxic Cr(VI), ACS Appl. Bio Mater. 3 (2020) 3906–3913. https://doi.org/10.1021/acsabm.0c00456.

[15] R. Baby, B. Saifullah, Z.M. Hussein, Carbon Nanomaterials for the Treatment of Heavy Metal-Contaminated Water and Environmental Remediation, Nanoscale Res. Lett. 14 (2019) 1–17. https://doi.org/https://doi.org/10.1186/s11671-019-3167-8 NANO.

[16] C. Sakulthaew, C. Chokejaroenrat, A. Poapolathep, Hexavalent chromium adsorption from aqueous solution using carbon nano-onions (CNOs), Chemosphere. 184 (2017) 1168–1174. https://doi.org/10.1016/j.chemosphere.2017.06.094.

[17] A. Makhongoana, B.J. Matsoso, T.H. Mongwe, N.J. Coville, D. Wamwangi, M.S. Maubane-Nkadimeng, The role of oxygen in a carbon source (castor oil versus paraffin oil) in the synthesis of carbon nano-onions, Nanotechnology. 32 (2021). https://doi.org/10.1088/1361-6528/abd0b1.

[18] H. Singh, N. Bhardwaj, S.K. Arya, M. Khatri, Environmental impacts of oil spills and their remediation by magnetic nanomaterials, Environ. Nanotechnology, Monit. Manag. 14 (2020) 100305. https://doi.org/10.1016/j.enmm.2020.100305.

[19] T.H. Mongwe, B.J. Matsoso, B.K. Mutuma, N.J. Coville, M.S. Maubane, Synthesis of chain-like carbon nano-onions by a flame assisted pyrolysis technique using different collecting plates, Diam. Relat. Mater. 90 (2018) 135–

143. https://doi.org/10.1016/j.diamond.2018.10.002.

[20] B. Shaku, T.P. Mofokeng, T.H. Mongwe, N.J. Coville, K.I. Ozoemena, M.S. Maubane-Nkadimeng, Physicochemical Properties of Nitrogen Doped Carbon Nano-onions Grown by Flame Pyrolysis from Grapeseed Oil for Use in Supercapacitors, Electroanalysis. 32 (2020) 2946–2957. https://doi.org/10.1002/elan.202060383.

[21] L.L. Sikeyi, T.D. Ntuli, T.H. Mongwe, N.W. Maxakato, E. Carleschi, B.P. Doyle, N.J. Coville, M.S. Maubane-Nkadimeng, Microwave assisted synthesis of nitrogen doped and oxygen functionalized carbon nano onions supported palladium nanoparticles as hybrid anodic electrocatalysts for direct alkaline ethanol fuel cells, Int. J. Hydrogen Energy. 46 (2021) 10862–10875. https://doi.org/10.1016/j.ijhydene.2020.12.154.

[22] K. Khalisanni, K. Khalizani, M.S. Rohani, P.O. Khalid, Analysis of Waste Cooking Oil as Raw Material for Biofuel Production, Glob. J. Environ. Res. 2 (2008) 81–83.

[23] T.D. Ntuli, T.H. Mongwe, L.L. Sikeyi, O. Mkhari, N.J. Coville, E.N. Nxumalo, M.S. Maubane-Nkadimeng, Removal of hexavalent chromium via an adsorption coupled reduction mechanism using olive oil derived carbon nano-onions, Environ. Nanotechnology, Monit. Manag. 16 (2021) 100477. https://doi.org/10.1016/j.enmm.2021.100477.

[24] M.A. Zayed, M.S.M. Abd El-Kareem, N.H.S. Zaky, Gas Chromatography-Mass Spectrometry Studies of Waste Vegetable Mixed and Pure Used Oils and Its Biodiesel Products, J. Pharm. Appl. Chem. 3 (2017) 109–116. https://doi.org/10.18576/jpac/030204.

[25] A. Mannu, G. Vlahopoulou, P. Urgeghe, M. Ferro, A. Del Caro, A. Taras, S. Garroni, J.P. Rourke, R. Cabizza, G.L. Petretto, Variation of the chemical composition of waste cooking oils upon bentonite filtration, Resources. 8 (2019) 1–15. https://doi.org/10.3390/resources8020108.

[26] D.C. Zhang, J.J. Liu, L.Z. Jia, P. Wang, X. Han, Speciation of VOCs in the cooking fumes from five edible oils and their corresponding health risk assessments, Atmos. Environ. 211 (2019) 6–17.

https://doi.org/10.1016/j.atmosenv.2019.04.043.

[27] T.D. Ntuli, V.E. Pakade, Hexavalent chromium removal by polyacrylic acid-grafted Macadamia nutshell powder through adsorption–reduction mechanism: Adsorption isotherms, kinetics and thermodynamics, Chem. Eng. Commun. 207 (2019) 1–16. https://doi.org/10.1080/00986445.2019.1581619.

[28] R.A. Venkatesan, M. Balachandran, Novel carbon nano-onions from paraffinum liquidum for rapid and efficient removal of industrial dye from wastewater, Environ. Sci. Pollut. Res. 27 (2020) 43845–43864. https://doi.org/10.1007/s11356-020-09981-w.

[29] J.P. Bartolome, A. Fragoso, Preparation and characterization of carbon nano-onions by nanodiamond annealing and functionalization by radio-frequency Ar/O_2 plasma, Fullerenes Nanotub. Carbon Nanostructures. 25 (2017) 327–334. https://doi.org/10.1080/1536383X.2017.1303604.

[30] M.B. Seymour, C. Su, Y. Gao, Y. Lu, Y. Li, Characterization of carbon nano-Onions for heavy metal ion remediation, J. Nanoparticle Res. 14 (2012) 1–14. https://doi.org/10.1007/s11051-012-1087-y.

[31] Y.J. Ko, K. Choi, S. Lee, J.M. Cho, H.J. Choi, S.W. Hong, J.W. Choi, H. Mizuseki, W.S. Lee, Chromate adsorption mechanism on nanodiamond-derived onion-like carbon, J. Hazard. Mater. 320 (2016) 368–375. https://doi.org/10.1016/j.jhazmat.2016.08.041.

[32] M. Zeiger, N. Jäckel, V.N. Mochalin, V. Presser, Review: Carbon onions for electrochemical energy storage, J. Mater. Chem. A. 4 (2016) 3172–3196. https://doi.org/10.1039/c5ta08295a.

[33] J. Namieśnik, A. Rabajczyk, Speciation Analysis of Chromium in Environmental Samples, Crit. Rev. Environ. Sci. Technol. 42 (2012) 327–377. https://doi.org/10.1080/10643389.2010.518517.

[34] M.C. Qhubu, L.G. Mgidlana, L.M. Madikizela, V.E. Pakade, Preparation, characterization and application of activated clay biochar composite for removal of Cr(VI) in water: Isotherms, kinetics and thermodynamics, Mater. Chem. Phys. 260 (2021) 124165. https://doi.org/10.1016/j.matchemphys.2020.124165.

[35] P.M. Thabede, N.D. Shooto, T. Xaba, E.B. Naidoo, Magnetite Functionalized Nigella Sativa Seeds for the Uptake of Chromium(VI) and Lead(II) Ions from Synthetic Wastewater, Adsorpt. Sci. Technol. 2021 (2021) 1–15. https://doi.org/10.1155/2021/6655227.

[36] N.D. Shooto, Removal of lead(II) and chromium(VI) ions from synthetic wastewater by the roots of harpagophytum procumbens plant, J. Environ. Chem. Eng. 8 (2020) 104541. https://doi.org/10.1016/j.jece.2020.104541.

[37] O.B. Nchoe, T.D. Ntuli, M.J. Klink, F.M. Mtunzi, V.E. Pakade, A comparative study of acid, base and Fenton-like reagent treated biomass for Cr(VI) sequestration from aqueous solutions, Water Environ. Fed. 93 (2020) 370–383. https://doi.org/10.1002/wer.1421.

[38] A. Pholosi, E.B. Naidoo, A.E. Ofomaja, Batch and continuous flow studies of Cr(VI) adsorption from synthetic and real wastewater by magnetic pine cone composite, Chem. Eng. Res. Des. 153 (2020) 806–818. https://doi.org/10.1016/j.cherd.2019.11.004.

[39] N. Gnanasundaram, M. Loganathan, A. Singh, Optimization and Performance parameters for adsorption of Cr6+ by microwave assisted carbon from Sterculia foetida shells, IOP Conf. Ser. Mater. Sci. Eng. 206 (2017). https://doi.org/10.1088/1757-899X/206/1/012065.

[40] D. Park, S.R. Lim, Y.S. Yun, J.M. Park, Reliable evidences that the removal mechanism of hexavalent chromium by natural biomaterials is adsorption-coupled reduction, Chemosphere. 70 (2007) 298–305. https://doi.org/10.1016/j.chemosphere.2007.06.007.

[41] S. Lagergren, “Zur Theorie der Sogenannten Adsorption GelosterStoffe”, Kungliga Svenska Vetenskapsakademiens., Handl. Band. 24 (1898) 1–39.

[42] G. Blanchard, M. Maunaye, G. Martin, Removal of heavy metals from waters by means of natural zeolites, Water Res. 18 (1984) 1501–1507. https://doi.org/10.1016/0043-1354(84)90124-6.

[43] Y.S. Ho, G. McKay, The Kinetics of Sorption of Basic Dyes from Aqueous Solution by Sphagnum Moss Peat, Can. J. Chem. Eng. 76 (1998) 822–827.

https://doi.org/10.1002/cjce.5450760419.

[44] H.N. Tran, S.J. You, A. Hosseini-Bandegharaei, H.P. Chao, Mistakes and inconsistencies regarding adsorption of contaminants from aqueous solutions: A critical review, Water Res. 120 (2017) 88–116. https://doi.org/10.1016/j.watres.2017.04.014.

[45] V.E. Pakade, L.C. Maremeni, T.D. Ntuli, N.T. Tavengwa, Application of quaternized activated carbon derived from Macadamia nutshells for the removal of hexavalent chromium from aqueous solutions, South African J. Chem. 69 (2016) 180–188. https://doi.org/http://dx.doi.org/10.17159/0379-4350/2016/v69a22.

[46] I. Langmuir, The adsorption of gases on plane surfaces of glass, mica and platinum., J. Am. Chem. Soc. 40 (1918) 1361–1403. https://doi.org/doi: 10.1021/ja02242a004.

[47] A. Shokry, A. El Tahan, H. Ibrahim, M. Soliman, S. Ebrahim, The development of a ternary nanocomposite for the removal of Cr(vi) ions from aqueous solutions, RSC Adv. 9 (2019) 39187–39200. https://doi.org/10.1039/c9ra08298k.

[48] Z. Wang, Q. Shen, J. Xue, H. Jia, B. Xu, X. Liu, Q. Li, Annealing temperature effect on 3D hierarchically porous NiO/Ni for removal of trace hexavalent chromium, Mater. Chem. Phys. 240 (2020) 1–10. https://doi.org/10.1016/j.matchemphys.2019.122140.

[49] S. Mortazavian, A. Saber, J. Hong, J.H. Bae, D. Chun, N. Wong, D. Gerrity, J. Batista, K.J. Kim, J. Moon, Synthesis, characterization, and kinetic study of activated carbon modified by polysulfide rubber coating for aqueous hexavalent chromium removal, J. Ind. Eng. Chem. 69 (2019) 196–210. https://doi.org/10.1016/j.jiec.2018.09.028.

[50] S. Shahrin, W.J. Lau, P.S. Goh, J. Jaafar, A.F. Ismaila, Adsorptive removal of Cr(VI) and Cu(II) ions from water solution using graphene oxide–Manganese ferrite (GMF) nanomaterials, Int. J. Eng. Trans. B Appl. 31 (2018) 1341–1346. https://doi.org/10.5829/ije.2018.31.08b.24.

[51] M. Gholipour, H. Hashemipour, Evaluation of multi-walled carbon nanotubes performance in adsorption and dresorption of hexavalent chromium, Chem. Ind. Chem. Eng. Q. 18 (2012) 509–523. https://doi.org/10.2298/CICEQ111104025G.

Chapter 6: Oxygen-functionalized onion-like nanocarbons for the sequestration of hexavalent chromium from aqueous solutions

Abstract

Hexavalent chromium [Cr(VI)] is a priority pollutant in the environment and needs to be removed as it is a major health hazard. As such onion-like nanocarbons (OLNCs) have been developed to act as effective adsorbents for Cr(VI) ion sequestration. We hereby present a simple flame pyrolysis method for the production of the (OLNCs). This was followed by functionalization with oxygen using H_2O_2 (25% and 10%) and KOH (0.2 M and 0.1 M) as oxidising agents at different concentrations. The functionalized OLNCs were then, applied in the sequestration of Cr(VI) via adsorption processes.

The optimum conditions for the sequestration of Cr(VI) from the solution were pH = 2, m = 0.0025 g, V = 10 mL, t = 24 h, and C_o = 10 mg/L. The Q^o_{max} of the functionalised adsorbents was computed to be 41.18 mg/g and 33.80 mg/g for 25H-NC and 0.2K-NC respectively. The experimental data fitted the pseudo-second-order model and the Freundlich isotherm.

The KOH and H_2O_2 treatment did not appear to affect the morphological characteristics of the OLNCs. TEM micrographs confirmed that the quasi-spherical, multi-layered structure with surface cavities was retained. After functionalization, the OLNCs had a diameter size range of 35 to 45 nm. The study showed the importance of maximizing the oxygen content of the carbons to provide binding sites for Cr removal.

6.1. Introduction

The bulk of the surface of the earth is enclosed by water, with a majority of it being saltwater and about 3% of this is freshwater in the form of ice, groundwater, rivers, streams, rainfall, lakes, etc. [1]. Freshwater gets contaminated by trace metal ions due to the inconsiderate dumping of foreign ions/complexes/materials into freshwater streams by industries such as those associated with mining, clothing, electroplating, agriculture, etc. [2]. Natural catastrophes such as volcanic epidemics and earthquakes also contribute to the contamination of freshwater streams [3]. Metal ions, even in trace quantities, have the potential to cause harmful effects on organisms [4]. Chromium is one such trace metal and is labelled as a priority pollutant by the World Health

Organization (WHO). The two most stable forms of chromium are Cr(III) and Cr(VI). Cr(VI) is more toxic than Cr(III) due to its higher mobility [4] and its removal from freshwater streams is important for human health. One of the widely used methods for the sequestration of Cr(VI) is adsorption [5].

This is because of the wide use of carbonaceous materials as adsorbents for the sequestration of trace metal ions from aqueous solutions [6]. These carbonaceous adsorbents are mainly derived from agricultural waste biomass [7] and the diversity of polymer materials due to the wide availability and high carbon content [8]. To increase the adsorption capacity (Q_e) of the carbonaceous materials, functionalization or chemical modification has been employed [9]. The increase in (Q_e) by functionalized carbonaceous materials was attributed to the increase in the surface area and added surface functional groups [10].

Functionalization may include the introduction of a heteroatom or a combination of heteroatoms such as oxygen, sulphur, and nitrogen onto the surface of an adsorbent. For example, Moyo et al. used NaOH and EDTA respectively, for the chemical modification of mango seed shells for the adsorption of Pb(II) ions in solution. The EDTA-modified adsorbent was reported to have five times as high a (Q_e) compared to a NaOH-treated adsorbent. This was attributed to the increase in the oxygen content on the surface of the EDTA-modified adsorbent, confirmed by elemental analysis [7]. In another study, Nchoe et al. treated biomass with NaOH, HNO_3 and H_2O_2 for the effective sequestration of Cr(VI). It was reported that the NaOH-treated adsorbent had a high efficiency due to a higher surface area compared to the other adsorbent [6]. These studies showed that the functionalization of adsorbents enhanced the adsorption capacity of the materials due to an increase in the number of adsorption sites created by the addition of heteroatoms [11].

Nano-carbons (NCs) have emerged as a unique class of carbonaceous materials and be attractive for the adsorption of trace metal ions. This class of NC includes activated carbon (AC) [12], carbon spheres (CS) [13], carbon dots (C-dots) [14], carbon nanofibers (CNFs) [15], carbon nanotubes (CNTs) [10], carbon black (CB) [16], and carbon nano-onions (CNOs) [17]. The aforementioned materials can easily be functionalized with heteroatoms. They are widely used due to their ability to be

chemically modified, their low toxicity, relatively low mass density, chemical stability, high carbon content, and the availability of surface functional groups [18].

Numerous examples of the effect of surface functionalization of carbons for Cr(VI) removal have been reported. AC from Macadamia nutshells was chemically modified with three inorganic acids, H_2SO_4, HNO_3, and H_3PO_4 to enhance the adsorptive performance of the adsorbent in the sequestration of Cr(VI) from solutions. It was reported that after the modification process, the Q^o_{max} of the HNO_3 and H_3PO_4 adsorbents increased to 40.99 mg/g and 25.75 mg/g respectively, compared to the pristine AC (22.30 mg/g). This was attributed to the addition of oxygen and nitrogen moieties on the surface of the adsorbent. However, the Q^o_{max} decreased to 9.66 mg/g due to the loss of organic matter when H_2SO_4 was used as an oxidising agent [9].

Though NCs are employed as adsorbents for the adsorption of trace metals, their application is limited by complex or sophisticated synthesis methods, which include chemical vapour deposition (CVD), laser ablation, and arc discharge methods. Some of the limiting factors to the aforementioned methods are the high consumption of electrical energy, use of a metal catalyst, low yield (excluding the CVD method) and an additional phase for purification [19]. The low Q^o_{max} of NCs has contributed to their limited use in adsorption processes. The Q^o_{max} is used as a standard parameter for evaluating the performance of an adsorbent. With a higher Q^o_{max} translating to a better adsorbent. Therefore the functionalization of NCs has the potential to increase the Q^o_{max} of the material [3].

Carbon nano-onions (CNOs) are a class of onion-like nanocarbons (OLNCs) in the family of fullerenes, due to their structural forms such as porosity and multiple layers [20]. Such material was synthesised from paraffin liquid and was applied as an adsorbent. It was reported that the CNOs were treated by hydrothermal, acid oxidation, and chemical exfoliation methods used for the adsorption of methylene blue [21]. Seymour et al. reported the functionalization of CNOs with HNO_3 and NaOCl as oxidizing agents for the adsorption of Zn(II), Cd(II), Ni(II), Cu(II) and Pb(II) [22]. Though the aforementioned studies used oxidation to functionalize CNOs their targeted pollutants were cationic.

In this study, we present a sustainable flame pyrolysis method for the synthesis of onion-like nanocarbons (OLNCs) using vegetable cooking oil. The simplicity of the

method mitigates the use of a metal catalyst, does not require electricity, has no additional purification step, and produces OLNCs in high yields [23]. H_2O_2 and KOH were used as oxidants for the functionalization of the OLNCs. In this study, the adsorption capacity relating to the sequestration of Cr(VI) from aqueous solutions was studied. , where the matrix of the Cr(VI) was determined in an aqueous solution and also in the presence of methyl orange as a competing ion. Methyl orange was chosen since Cr(VI) and methyl orange are normally found in effluent from the clothing industry [24]. To the best of our knowledge, functionalization of OLNCs by H_2O_2 and KOH respectively for application in the adsorption of Cr(VI) has not been reported previously. The study continues from our earlier studies on the use of OLNCs made by the flame pyrolysis route [23] For methodology and instrumentation please refer to Chapter 3

6.2. Results and discussions

6.2.1. SEM and TEM analysis

Figure 6.1. displays the SEM and TEM micrographs for the functionalized OLNCs. It can be observed from the SEM micrographs that the OLNCs were quasi-spherical and were closely packed together [Figure 6.1 (a & b)], as previously reported by other authors [25]. The adsorbents had an onion-like shape in the form of concentric multiple shells or layers with cavities as seen from the TEM micrographs Figure 6.1 (c & d). The concentric multiple shells were also observed by Makhogoana et al. when they reported on the synthesis of CNOs via the flame pyrolysis of castor oil and paraffin oil [26].

The size diameter of oxygen-functionalized OLNCs was determined, the 25H-NC (43 ± 8.12 nm), 10H-NC (38 ± 9.45 nm), 0.1K-NC (36 ± 8.57 nm) and 0.2K-NC (42 ± 11.20 nm) values similar to the pristine material (46 ± 5.4 nm) (Ntuli et al., 2021) Thus, the treatment with different concentrations of KOH and H_2O_2 did not damage the backbone structure of the adsorbents. Micrographs for the 0.1K-NC and 10H-NC are presented in Figure 6.2.

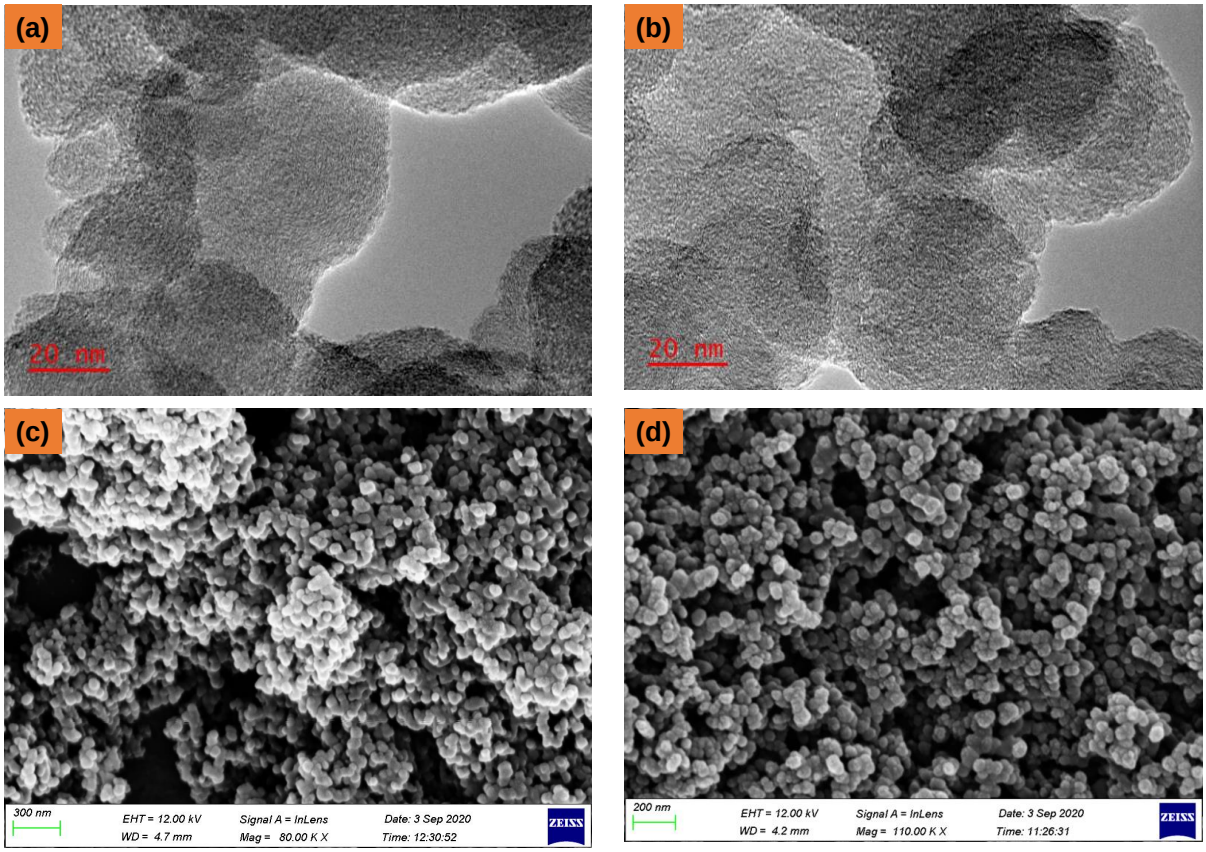

Figure 6.1: SEM micrographs for 0.2K-NC (a), 25H-NC (b) and TEM micrographs for 25H-NC (c) and 0.2K-NC (d).

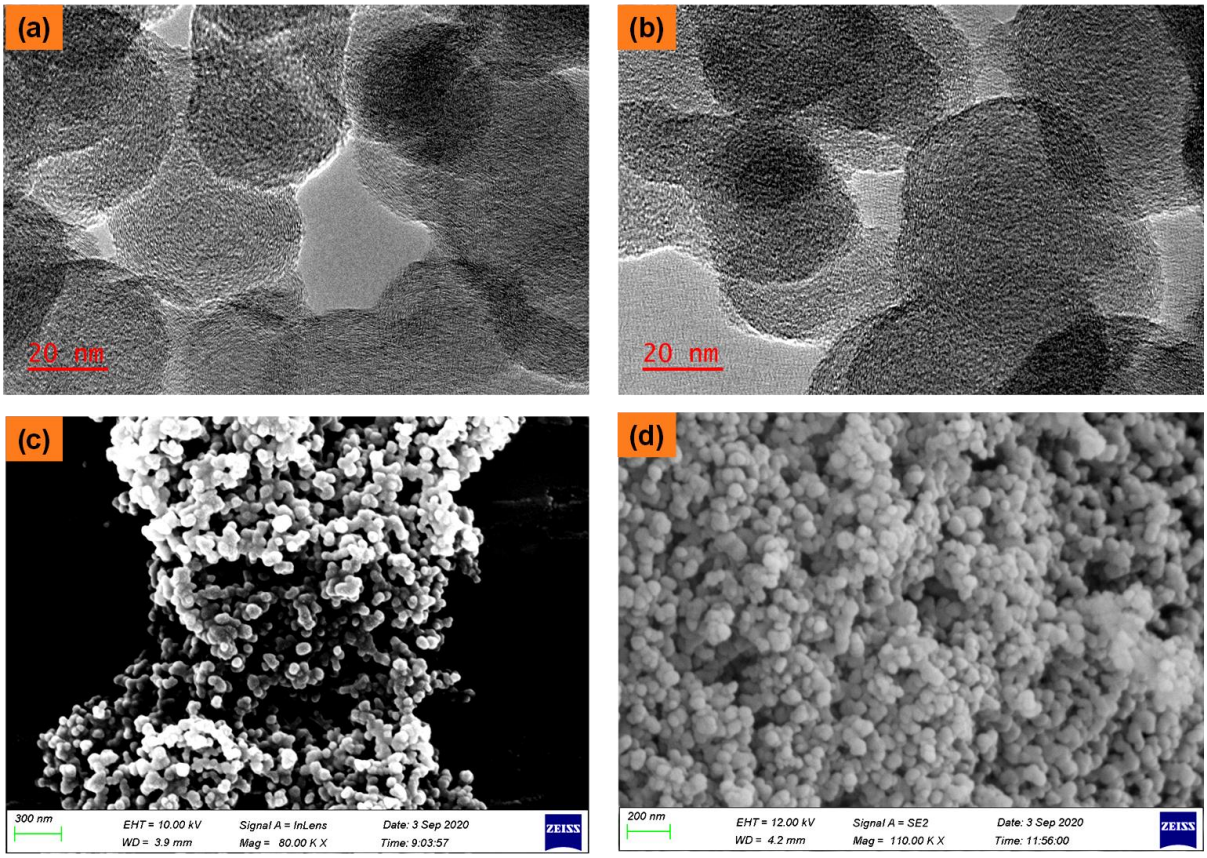

Figure 6.2: TEM micrographs for 0.1K-NC (a), 10H-NC (b) and SEM micrographs for 10H-NC (c) and 0.1K-NC (d).

6.2.2. BET and thermal analysis

The chemical treatment of the adsorbents did not appear to present enormous alterations to the surface properties of the adsorbents (see Table 6.1.). It is to be noted that the surface area increased as the concentration of H_2O_2 was increased due to increased oxygen moieties. On the contrary, the surface area decreased as the concentration of KOH increased. Attributed to the leaching of organic functional groups.

Table 6.1: BET parameters

Adsorbent	Surface area (m^2/g)	Pore volume (cm^3/g)	Average pore size (nm)
10H-NC	78.92	0.68	28.95
25H-NC	91.32	0.75	37.07
0.1K-NC	81.61	0.79	37.96
0.2K-NC	78.1	0.79	39.69

The thermal decomposition of the adsorbents was measured by thermogravimetric analysis (TGA) and differential thermal analysis (DTA) and the data is presented in Figure 6.3. The thermograms for all functionalized adsorbents showed three decomposition steps, at around ~100°C (i), ~200°C (ii), and ~450°C (iii). This was attributed to the evolution of moisture, degradation of functional groups and volatile organic compounds, and lastly the decomposition of the graphitic core [27].

It could be observed from the thermograms that the material treated with H_2O_2 had higher thermal stability than the KOH-treated materials. Showing final decomposition at ~ 650 °C and ~640°C for (25H-NC and 10H-NC) and ~575°C and ~545°C for (0.2K-NC and 0.1K-NC) respectively. The weight loss of the materials at 400°C before the final degradation step was calculated to be 7% and 8% for (10H-NC and 25H-NC) and 10% for both the 0.2K-NC and 0.1K-NC individually. This indicated that the materials underwent different chemical treatments, with the KOH able to remove more carbon material than the H_2O_2.

The data also indicate that the synthesized adsorbents would not decompose during the sequestration of Cr(VI) as the adsorption experiments take place at T < 100 ^oC.

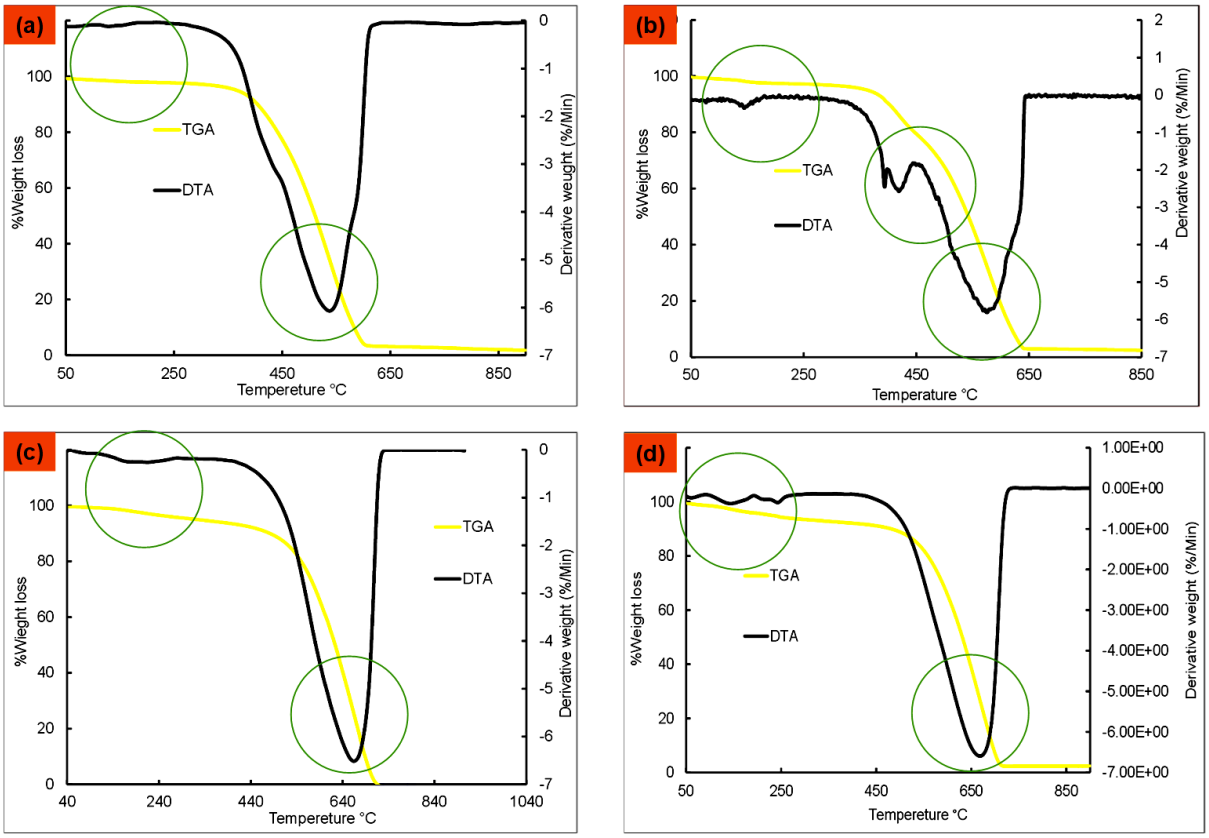

Figure 6.3: Thermograms for all the adsorbents 0.1K-NC (a), 0.2K-NC (b), 10H-NC (c), and 25H-NC (d).

6.2.3. The influence of solution pH

The pH of the solution is an integral parameter in the sequestration of Cr(VI). This is because the pH of the adsorbate affects both the adsorbent and the adsorbate [Cr(VI)] due to protonation and deprotonation of the surface of the adsorbent and the type of adsorbate ions present at the different pH values [28].

Figure 6.4. depicts the influence of pH on the adsorption of Cr(VI) by the functionalized adsorbents. It can be observed that the high elimination of Cr(VI) takes place under acidic conditions with the highest sequestration at pH 2, for all the materials. This pattern was attributed to the electrostatic attraction between the dominant presence of $HCrO_4^{-1}$ which is anionic, and the protonated surface of the adsorbents [29].

The point of zero charge pH_{PZC} was used to elaborate on the aforementioned phenomena. The pH_{PZC} of the materials was found to be at pH 7.2 (10H-NC) and 7.4 (25H-NC) for the H_2O_2-treated materials. Indicating that the adsorbents were mainly protonated below pH 7.2 and 7.4 and deprotonated above the aforementioned solution pH respectively. The pH_{PZC} for the KOH-treated adsorbents was found to be pH 3.9

(0.1K-NC) and pH 3.2 (0.2K-NC) showing that below the aforementioned pH levels, the surface of the adsorbents was mainly protonated and deprotonated above those levels. The indifferences in the pH_{PZC} of the adsorbents were attributed to the decreased buffering capacity of the KOH-treated adsorbents and the increased buffering capacity of the H_2O_2-treated adsorbents [30]. The pH_{PZC} of the adsorbents played a major role in the elimination of Cr(VI), where the adsorbents treated with KOH showed more adsorption at pH < 3. Whereas the adsorbents treated with H_2O_2 showed more adsorption of Cr(VI) at pH < 7 (Figure 6.4). This was attributed to the electrostatic attraction between the adsorbents and the adsorbate at the pH levels below those of their respective pH_{PZC}.

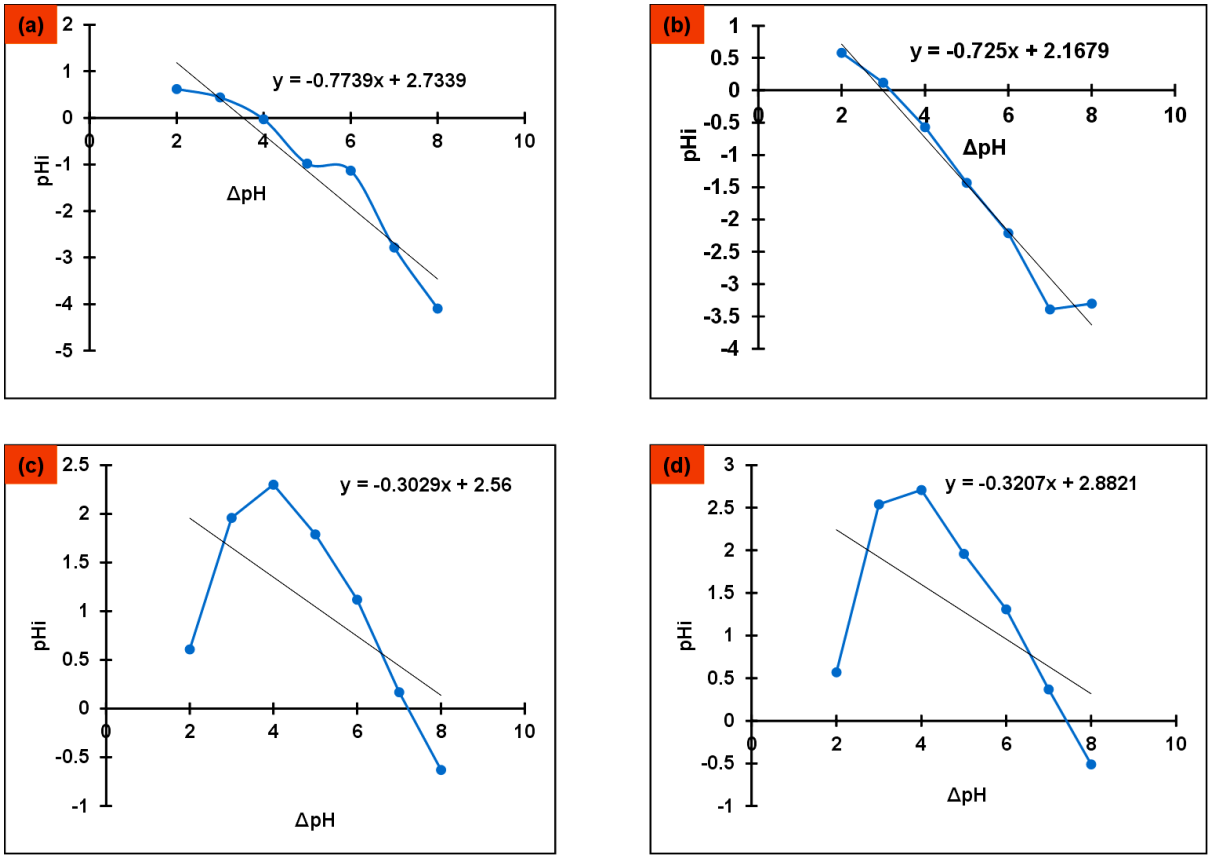

Figure 6.4: pH_{PZC} profile for 10H-NC (a), 25H-NC (b), 0.1K-NC (c), and 0.2K-NC (d).

Generally, the materials treated with KOH showed lower removals of Cr(VI) compared to those treated with H_2O_2. This was attributed to the H_2O_2-treated adsorbents having more oxygen groups on the surface and a higher surface area thus may contribute to increased active sites leading to higher adsorption efficiency [9]. The H_2O_2 treated adsorbents had a higher removal efficiency than the pristine adsorbents and this was

attributed to an increased oxygen content of the H_2O_2 treated adsorbents compared to pristine adsorbents as shown by XPS data (Table 6.2.) [23].

Table 6.2: Elemental identification and quantification

Name	Peak position	Atomic %
C1s	248.2	85.8
O1s	532.1	12.8
Na1s	1072.1	1.1
S2p	168.2	0.2

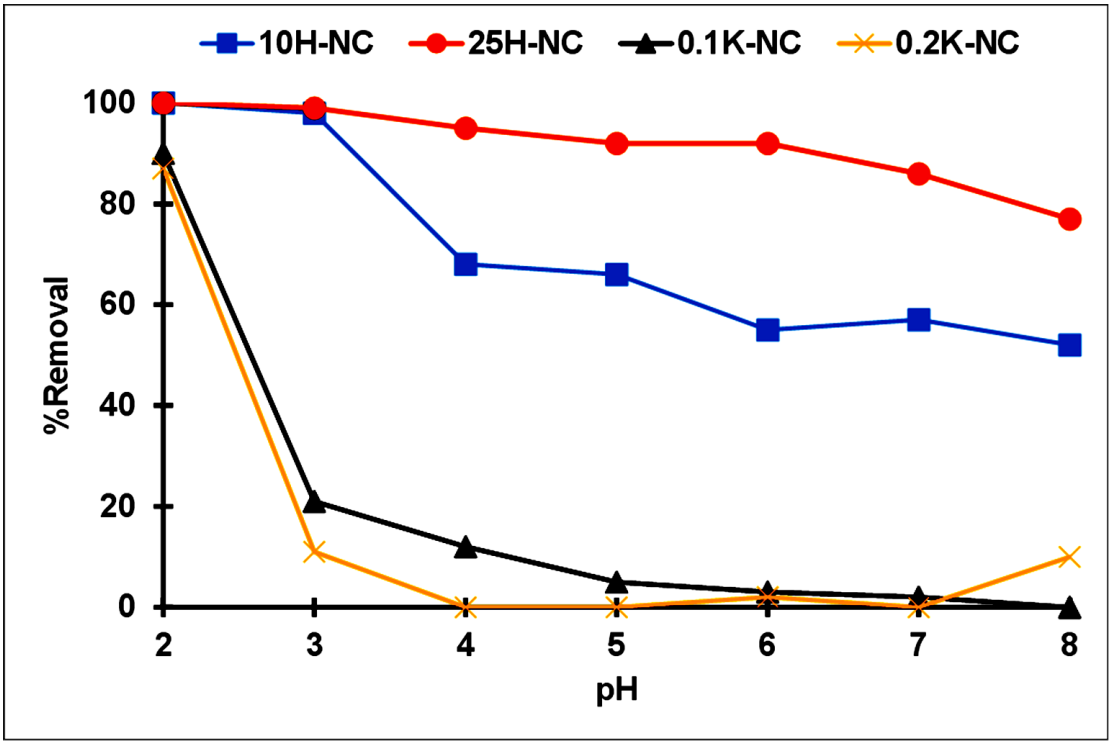

Figure 6.5: Influence of solution pH for the 10H-NC, 25H-NC, 0.1K-NC, and 0.2K-NC (m = 0.025 g, V = 10 mL, C_o = 10 mg/L, t = 12 h, and pH range 2 – 8).

6.2.4. Effect of interaction time and kinetics

Figure 6.5. depicts the interaction time between adsorbate ions and the surface of the adsorbent was measured at the time range of 5 to 1440 min. It can be observed that an increase in the interaction time is directly proportional to the increase in the adsorption capacity (Q_t) at any time (t) for the 25H-NC and the 0.2K-NC respectively. However, the 25H-NC reached equilibrium at 360 min with an adsorption capacity of 4 mg/g compared to the 0.2K-NC which took 1440 min. This was attributed to the higher surface area of the 25H-NC (91.32 m^2/g) adsorbent compared to that of the 0.2K-NC (78.1 m^2/g) adsorbent.

It could be seen that in the experimental data for both adsorbents, the PSO model gave a better fit than the PFO model (Figure 6.5.). The kinetic data for both adsorbents are shown in Table 6.3 where it can be seen that the R^2 value for the PSO model was closer to 1 than the value for the PFO model. This was correlated by the Chi-squared values for the 25H-NC which were closer to zero than those of the 0.2K-NC. The experimental adsorption capacity (Q_e) of 4 mg/g was closer to the PSO adsorption capacity (Q_{mod}) of 4.1 mg/g (25H-NC) and 3.9 mg/g (0.2K-NC) when compared to the

values of 3.7 mg/g (25H-NC) and 3.5 mg/g (0.2K-NC) for the PFO model. This indicates that the experimental data for both adsorbents fitted the PSO model.

This suggests that the rate-limiting step could be the chemisorption of the Cr(VI) on the respective adsorbents [31]. In addition, the kinetic data showed that the sequestration of Cr(VI) was more rapid for the 25H-NC than the 0.2K-NC with the rate constant (k_1) = 0.0302 (1/min) for PFO and (k_2) = 0.0092 g/mg x min with an initial adsorption rate (*h*) = 0.1508 mg/g x min for the 25H-NC. In contrast, the values for the 0.2K-NC were k_1 = 0.0116 (1/min), k_2 = 0.0042 g/mg x min, and *h* = 0.0622 mg/g x min (see Table 6.3). Thus, the 25H-NC reached equilibrium at 360 min compared to the 1440 min for the 0.2K-NC.

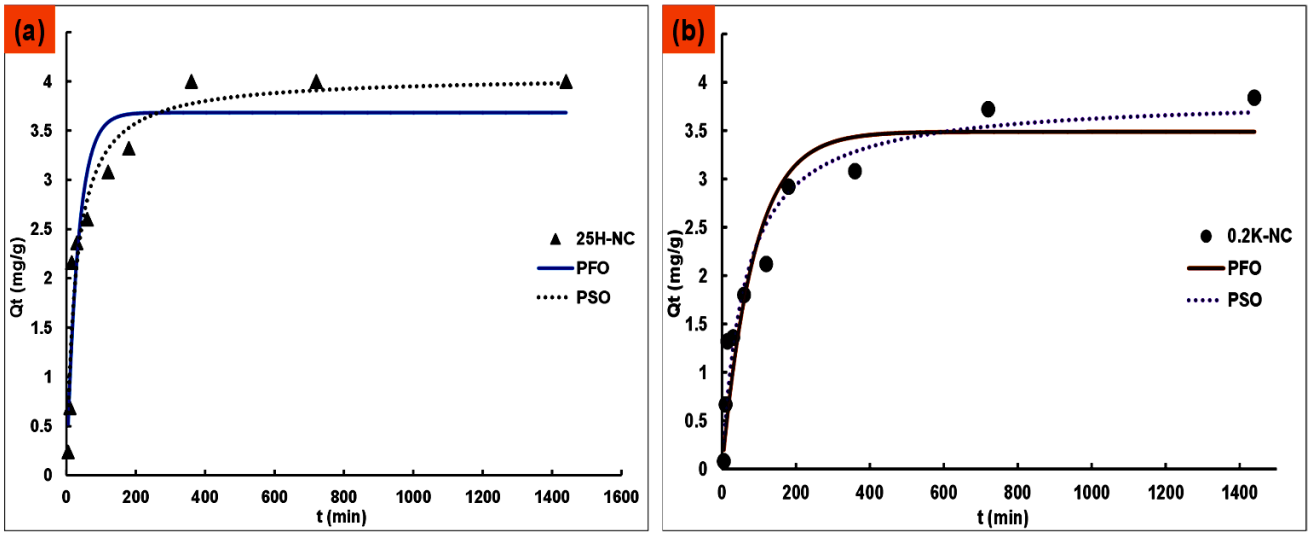

Figure 6.5: Effect of interaction time and adsorption kinetics for (a) 25H-NC and (b) 0.2K-NC (pH = 2, C_o = 10 mg/L, V = 10 mL, m = 0.025 g, time range 5 – 1440 min)

Table 6.3: Adsorption kinetic data

			PSO		
Adsorbent	**R^2**	**$Q_{e\ exp}$ (mg/g)**	**$Q_{e\ mod}$ (mg/g)**	**k_2 (g/mgxmin)**	***h* (mg/gxmin)**
25H-NC	0.9331	4.00	4.06	0.0092	0.1508
0.2K-NC	0.9538	3.84	3.85	0.0042	0.0622
			PFO		
	R^2	**$Q_{e\ exp}$ (mg/g)**	**$Q_{e\ mod}$ (mg/g)**	**k_1 (1/min)**	
25H-NC	0.8908	4.00	3.68	0.0302	
0.2K-NC	0.9070	3.84	3.49	0.0116	

6.2.5 Effect of initial adsorbate concentration and adsorption isotherms

A representation of the effect of the initial adsorbate concentration and the adsorption isotherms for the 25H-NC and the 10H-NC are given in Figure 6.6. and the isotherm data is in Table 6.4. It can be observed from Figure 6.6 (a) that as the initial adsorbate concentration increased the adsorption capacity also increased, for both adsorbents. This was attributed to the availability of active sites that could bind with the adsorbate ions as the concentration of the adsorbate ions was increased.

The sequestration of Cr(VI) by the 0.2K-NC reached equilibrium using initial concentrations of 90 mg/L to 100 mg/L implying that the surface of the 0.2K-NC had been fully covered by the adsorbate ions. In contrast, the 25H-NC did not reach an equilibrium at these concentrations. This was accredited to the addition of oxygen moieties and higher surface area by the 25H-NC adsorbent compared to the 0.2K-NC adsorbent.

It could be observed from Figures 6.6 (b and c) that the experimental data gave a modest fitting to the Freundlich adsorption isotherm for both adsorbents. This was supported by the adsorption isotherm data. The R^2 values from the Freundlich isotherm fit were greater than that of the Langmuir isotherm for both adsorbents. Furthermore, the adsorption capacity of the 25H-NC was found to be 41.2 mg/g and 34.0 mg/g for the 0.2K-NC when extrapolated from the Freundlich model. The aforementioned adsorption capacities were closer to the experimental data of 41.6 mg/g for 25H-NC and 35.2 mg/g for the 0.2K-NC.

Therefore, the experimental data was better explained by the Freundlich isotherm. This suggests that the sequestration of Cr(VI) proceeded via a heterogeneous surface coverage mechanism [32]. The sequestration of Cr(VI) using the 25H-NC and the 0.2K-NC was established to be favourable and spontaneous as the values of the separation factor (R_L) and the Freundlich exponent (n) were $1 < 0$ (Table 6.4) [33]. The R_L values for both adsorbents decreased as the initial adsorbate concentration was increased, indicating that the adsorbate-adsorbent binding force was enhanced as the concentration was increased [34].

The favourable sequestration conditions were supported by the lower values of the Langmuir equilibrium constant (K_L) of 0.2445 L/mg (25H-NC) and 0.0716 L/mg (0.2K-

NC). This indicated a greater affinity between the respective adsorbents and the adsorbate ions [35].

Lastly, the Freundlich constant (K_F) value for the 25H-NC 17.4915 [(mg/g) (L/mg)^n] was higher than that of the 0.2K-NC 9.3313 [(mg/g) (L/mg)n]. An indication that the Cr(VI) had a greater affinity toward the 25H-NC. This was supported by the higher adsorption capacity for the Freundlich model 41.18 mg/g (25H-NC) compared to 33.80 mg/g (0.2K-NC) [35].

Park et al. suggested that the sequestration mechanism of Cr(VI) takes place in one of two ways: (I) complete reduction of Cr(VI) ion in solution to Cr(III) ions due to electron donor group from the adsorbate followed by subsequent adsorption of the Cr(III) or(II) Cr(VI) adsorption to the surface of the adsorbent followed by reduction to Cr(III) ions due to adjacent electron donor groups. This would result in both Cr(III) and Cr(VI) being on the adsorbent surface with some of the Cr(III) ions leaching back into the solution [28]. In this study, the data are consistent with an adsorbate-adsorbate interaction due to Cr(VI) binding with Cr(III) ions or vice versa on the surface of the oxygen-functionalised adsorbents.

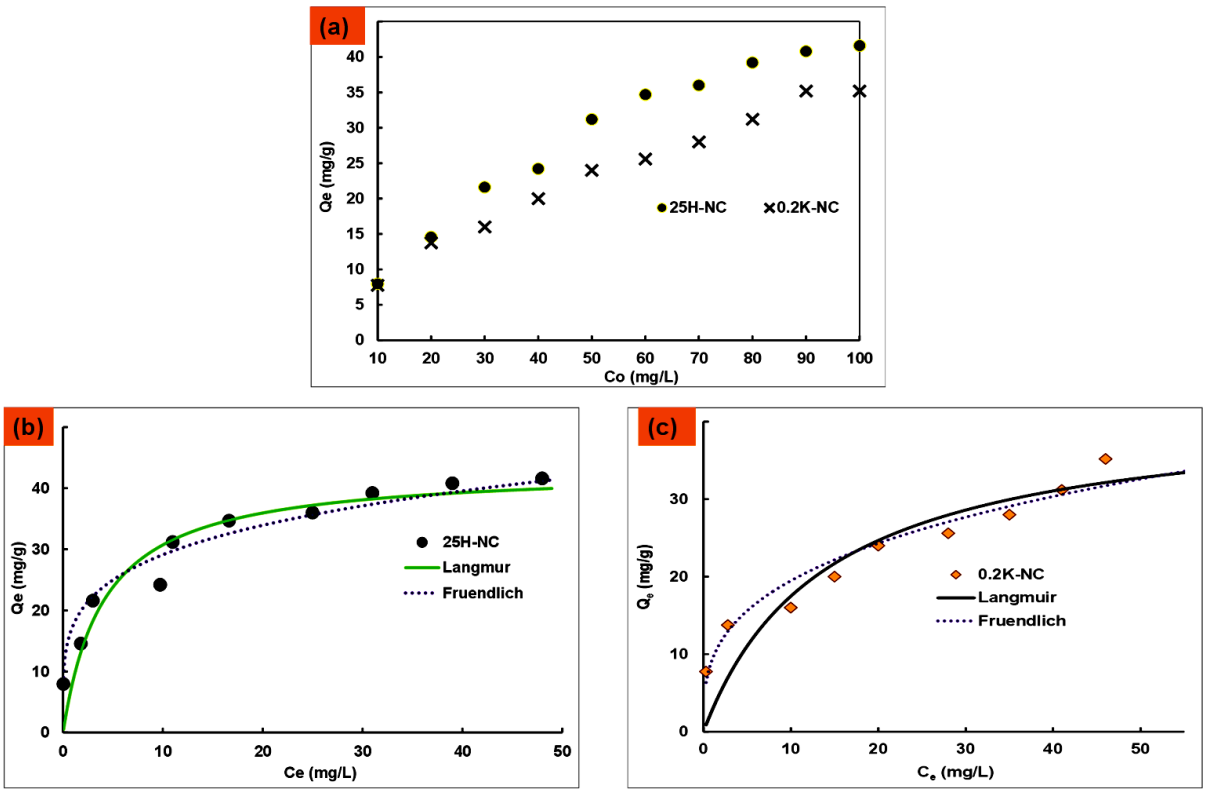

Figure 6.6: Effect of initial Cr(VI) (a), and the adsorption isotherm data (b and c): (pH = 2, t = 1440 min, m = 0.0025 g, V = 10 mL, C_O range 10 to 100 mg/g).

Table 6.4: Adsorption isotherm parameters for the 25H-NC and the 0.2K-NC.

Langmuir isotherm					
Adsorbent	**R^2**	**$Q_{e\ exp}$ (mg/g)**	**$Q_{e\ mod}$ (mg/g)**	**K_L (L/mg)**	
25H-NC	0.9053	41.60	43.29	0.2445	
0.2K-NC	0.8438	35.20	41.91	0.0716	
Freundlich isotherm					
	R^2	**$Q_{e\ exp}$ (mg/g)**	**$Q_{e\ mod}$ (mg/g)**	**K_F [(mg/g) (L/mg)^n]**	**n**
25H-NC	0.9465	41.60	41.18	17.4915	0.2212
0.2K-NC	0.9515	35.20	33.80	9.3313	0.3197

	25H-NC	**0.2K-NC**
C_o (mg/L)	**R_L**	**R_L**
10	0.29031	0.58266
20	0.16980	0.41109
30	0.11999	0.31758
40	0.09278	0.25873
50	0.07562	0.21828
60	0.06383	0.18876
70	0.05521	0.16628
80	0.04865	0.14858
90	0.04348	0.13429
100	0.03930	0.12251

6.2.6. The significant role of adsorbent modification/functionalization

Table 6.5. depicts the adsorption capacities of different carbon nanomaterials that have been modified and used for the sequestration of Cr(VI) from the solution. A direct comparison is almost impossible due to the differences in the experimental design.

Overall the oxidation of the adsorbents with H_2O_2 and KOH led to performance enhancement of the adsorbent. The 25H-NC and the 0.2K-NC returned adsorption capacities of 41.18 mg/g and 33.80 mg/g respectively. These data are significantly higher than those found for the pristine OLNCs (26.53 mg/g; Table 6.5.). Other modification techniques such as pyrolysis, decoration with CNTs, and treatment with

cetyl trimethyl ammonium bromide (CTAB) returned lower adsorption capacities. However, the grafting of carbon nanofibers (CNFs) with amine groups showed a higher adsorption capacity.

Table 6.5: Comparison of carbon rich adsorbents with different treatment

Adsorbent	Modification	pH	Qe (mg/g)	Isotherm	Kinetics	Reference
CNOs	Pristine	2	26.53	Langmuir	PSO	[23]
AC	CNTs	2	9.00	*	*	[36]
Biomass	Pyrolysis	1.5	6.08	Langmuir	PSO	[37]
CNTs	CTAB	4.5	27.70	Langmuir	*	[38]
25H-NC	H_2O_2	2	41.18	Fruendlich	PSO	Current study
0.2K-NC	KOH	2	33.85	Fruendlich	PSO	Current study

*Not reported

6.2.7. Adsorbent regeneration

Adsorbent regeneration is an important parameter in measuring the effectiveness of an adsorbent. This was done by desorbing the adsorbate from the surface of the adsorbent and the results are presented in Figure 6.7. The adsorption experiments were conducted using the method described in section 3.1.5.

After the adsorption experiments, the adsorbent and adsorbate were separated by centrifugation, followed by rinsing the adsorbate with deionised water several times to remove unbound adsorbate ions. This was followed by rinsing with HNO_3 and ethanol to re-protonate and regenerate the surface. The adsorbent was then dried for 24 h in an oven at 100°C. The adsorbent was cooled to room temperature and introduced into a solution of 0.1 M NaOH as a desorbing agent.

Both adsorbents were studied over four cycles of adsorption/desorption, indicating that the adsorbents could be reused more than four times. It could be noted that the sequestration of Cr(VI) was close to 100% for all cycles of desorption. This trend was observed for both adsorbents, moreover, as the adsorption cycles were increased the sequestration of Cr(VI) increased. This was attributed to the positive effects of the reagents used in the process (NaOH: desorbing agent), HNO_3 and ethanol (protonation and regeneration) [36].

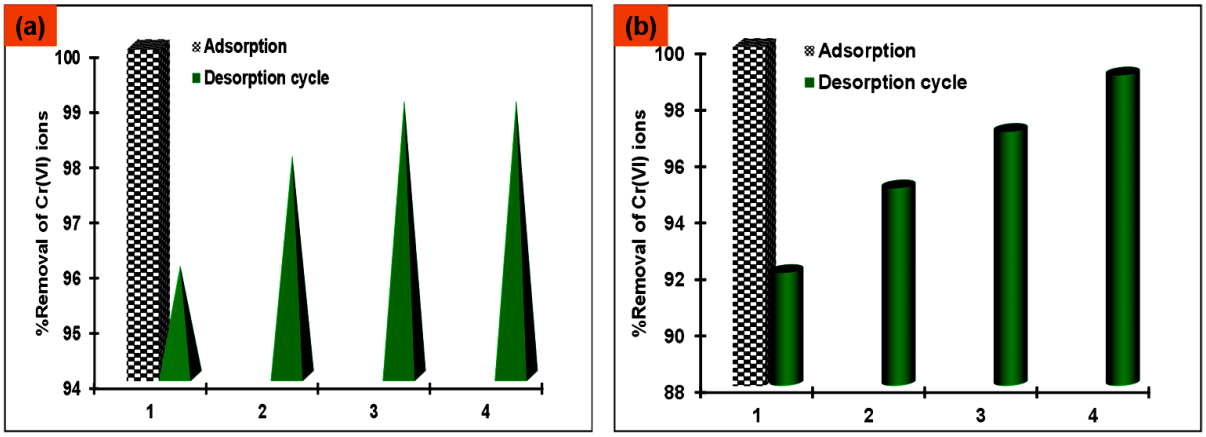

Figure 6.7: Regeneration of 25H-NC (a) and 0.2K-NC (b) [V = 10 mL, t = 24 h, m = 0.025 g,].

6.2.8. Competitive removal

One of the unique attributes of a good adsorbent is its capability to adsorb multiple adsorbates or pollutants. This is referred to as the effect of coexisting ions or competitive sequestration/adsorption. The sequestration of Cr(VI) by the oxygen-functionalised adsorbents was evaluated in the presence of methyl orange (MO). This was done by following an already described method (section 3.1.7.), with the difference being that the Cr study was performed in the presence of 10 mg/L of methyl orange (MO). The MO was selected as the coexisting ion due to the synergistic use of Cr(VI) and MO in the textile and clothing industries [24].

It could be seen from Figure 6.8a that the sequestration of Cr(VI) was slightly decreased by the presence of MO, for both adsorbents. This was attributed to the nature of both adsorbates being anionic and that they would compete for similar adsorption sites [37]. The Cr(VI) and MO would compete for the oxygen-functionalized adsorbents which had adequate active sites to accommodate both anions. This resulted in an adsorption efficiency of more than 95% for both adsorbents.

The adsorbents were regenerated and reused for the sequestration of MO using a method described in section 3.4. Both the adsorbents were regenerated five times and gave good data (Figure 6.8b). The ability to desorb the MO from the

surface of the adsorbents showed that the methyl orange was not degraded to less harmful products, but only adsorbed on the surface of the adsorbents [24].

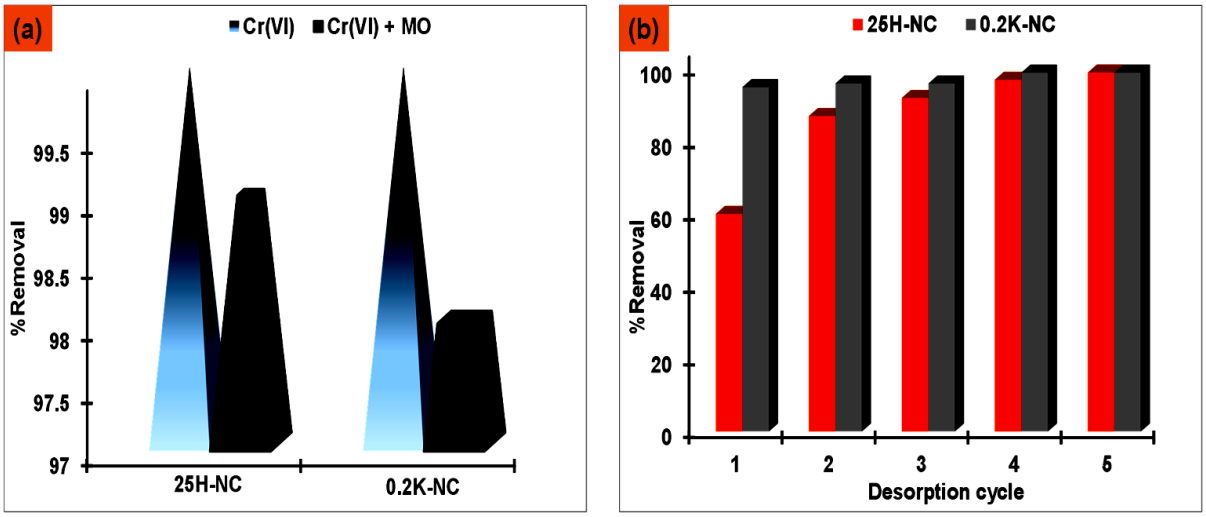

Figure 6.8(a & b): Effect of co-existing ions (a) and desorption cycles (b).

6.3. Conclusions

Metal-free OLNCs have been functionalised with oxygen moieties by using KOH and H_2O_2 respectively to enhance the Q^o_{max} of pristine OLNCs for the sequestration of Cr(VI) ion in a singular matrix and binary matrix with methyl orange. The adsorbents treated with H_2O_2 showed a higher Q^o_{max} of 41.18 mg/g (25H-NC) than the 33.80 mg/g for the 0.2K-NC, significantly higher than the 26.53 mg/g (pristine). This was attributed to the possibility of the 25H-NC having more active sites as a result of higher surface area. The addition of methyl orange as a coexisting anion slightly decreased the sequestration of Cr(VI) for both adsorbents, due to the completion of active sites.

Be that as it may, both adsorbents were recycled four times for the sequestration of the Cr(VI) ion and five-time for methyl orange. Indicating that the functionalised adsorbent had the potential for the selected adsorbate to return more than 90% adsorption efficiency after four and five cycles of being used respectively.

The experimental data was better described by the PSO kinetic model and the Freundlich adsorption isotherm. Indicating chemisorption on the heterogeneous surface of the respective adsorbents.

Therefore, the functionalization with oxygen groups played a vital role in increasing the adsorption capacity of OLNCs. Resulting in adsorbents that have great potential in the sequestration of Cr(VI) and MO anions.

6.4. References

[1] T. Oki, S. Kanae, Global hydrological cycles and world water resources, Science (80-.). 313 (2006) 1068–1072. https://doi.org/10.1126/science.1128845.

[2] A.R.K. Gollakota, V. Subbaiah Munagapati, C.M. Shu, J.C. Wen, Adsorption of Cr(VI), and Pb(II) from aqueous solution by 1-Butyl-3-methylimidazolium bis(trifluoromethyl sulfonyl)imide functionalized biomass Hazel Sterculia (Sterculia Foetida L.), J. Mol. Liq. 350 (2022) 118534. https://doi.org/10.1016/j.molliq.2022.118534.

[3] J.F. Amaku, S. Ogundare, K.G. Akpomie, C.U. Ibeji, J. Conradie, Functionalized MWCNTs-quartzite nanocomposite coated with Dacryodes edulis stem bark extract for the attenuation of hexavalent chromium, Sci. Rep. 11 (2021) 1–15. https://doi.org/10.1038/s41598-021-92266-0.

[4] World Health Organization, Guidelines for drinking-water quality, 2008. https://doi.org/10.1016/S1462-0758(00)00006-6.

[5] N.D. Shooto, Removal of lead(II) and chromium(VI) ions from synthetic wastewater by the roots of harpagophytum procumbens plant, J. Environ. Chem. Eng. 8 (2020) 104541. https://doi.org/10.1016/j.jece.2020.104541.

[6] O.B. Nchoe, T.D. Ntuli, M.J. Klink, F.M. Mtunzi, V.E. Pakade, A comparative study of acid, base and Fenton-like reagent treated biomass for Cr(VI) sequestration from aqueous solutions, Water Environ. Fed. 93 (2020) 370–383. https://doi.org/10.1002/wer.1421.

[7] M. Moyo, V.E. Pakade, S.J. Modise, Biosorption of lead(II) by chemically modified Mangifera indica seed shells: Adsorbent preparation, characterization and performance assessment, Process Saf. Environ. Prot. 111 (2017) 40–51. https://doi.org/10.1016/j.psep.2017.06.007.

[8] V.E. Pakade, N.T. Tavengwa, L.M. Madikizela, Recent advances in hexavalent chromium removal from aqueous solutions by adsorptive methods, RSC Adv. 9

(2019) 26142–26164. https://doi.org/10.1039/c9ra05188k.

[9] M. Lesaoana, R.P.V. Mlaba, F.M. Mtunzi, M.J. Klink, P. Edijike, V.E. Pakade, Influence of inorganic acid modification on Cr(VI) adsorption performance and the physicochemical properties of activated carbon, South African J. Chem. Eng. 28 (2019) 8–18. https://doi.org/10.1016/j.sajce.2019.01.001.

[10] Y. Patiño, E. Díaz, S. Ordóñez, Performance of different carbonaceous materials for emerging pollutants adsorption, Chemosphere. 119 (2015) S124–S130. https://doi.org/10.1016/j.chemosphere.2014.05.025.

[11] X. Yang, Y. Wan, Y. Zheng, F. He, Z. Yu, J. Huang, H. Wang, Y.S. Ok, Y. Jiang, B. Gao, Surface functional groups of carbon-based adsorbents and their roles in the removal of heavy metals from aqueous solutions: A critical review, Chem. Eng. J. 366 (2019) 608–621. https://doi.org/10.1016/j.cej.2019.02.119.

[12] L. Hlungwane, E.L. Viljoen, V.E. Pakade, Macadamia nutshells-derived activated carbon and attapulgite clay combination for synergistic removal of Cr(VI) and Cr(III), Adsorpt. Sci. Technol. 36 (2018) 713–731. https://doi.org/10.1177/0263617417719552.

[13] P. Mente, V. Mashindi, T.N. Phaahlamohlaka, T.N. Monyatsi, R.P. Forbes, N.J. Coville, Oxidation of Benzyl Alcohol Using Cobalt Oxide Supported Inside and Outside Hollow Carbon Spheres, ChemistryOpen. 10 (2021). https://doi.org/10.1002/open.202000312.

[14] O. Mkhari, T.D. Ntuli, N.J. Coville, E.N. Nxumalo, M.S. Maubane-Nkadimeng, A comparison of fluorescent N-doped carbon dots supported on the surface of hollow and solid carbon spheres, and solid silica spheres, Diam. Relat. Mater. 118 (2021) 108500. https://doi.org/10.1016/j.diamond.2021.108500.

[15] M. Mofokeng, L.N. Nthunya, L. Gutierrez, P. Matabola, S. Mishra, E.N. Nxumalo, Perflurooctyltriethoxy silane and carbon nanotubes-modified PVDF superoleophilic nanofibre membrane for oil-in-water adsorption and recovery, J. Environ. Chem. Eng. 8 (2020) 104497. https://doi.org/10.1016/j.jece.2020.104497.

[16] P. Dong, T. Maneerung, W.C. Ng, X. Zhen, Y. Dai, Y.W. Tong, Y.P. Ting, S.N.

Koh, C.H. Wang, K.G. Neoh, Chemically treated carbon black waste and its potential applications, J. Hazard. Mater. 321 (2017) 62–72. https://doi.org/10.1016/j.jhazmat.2016.08.065.

[17] B. Shaku, T.P. Mofokeng, T.H. Mongwe, N.J. Coville, K.I. Ozoemena, M.S. Maubane-Nkadimeng, Physicochemical Properties of Nitrogen Doped Carbon Nano-onions Grown by Flame Pyrolysis from Grapeseed Oil for Use in Supercapacitors, Electroanalysis. 32 (2020) 2946–2957. https://doi.org/10.1002/elan.202060383.

[18] U.O. Aigbe, O.A. Osibote, Carbon derived nanomaterials for the sorption of heavy metals from aqueous solution: A review, Environ. Nanotechnology, Monit. Manag. 16 (2021) 100578. https://doi.org/10.1016/j.enmm.2021.100578.

[19] A.T. Hoang, S. Nižetić, C.K. Cheng, R. Luque, S. Thomas, T.L. Banh, V.V. Pham, X.P. Nguyen, Heavy metal removal by biomass-derived carbon nanotubes as a greener environmental remediation: A comprehensive review, 2022. https://doi.org/10.1016/j.chemosphere.2021.131959.

[20] A.V. Ramya, R. Thomas, M. Balachandran, Mesoporous onion-like carbon nanostructures from natural oil for high-performance supercapacitor and electrochemical sensing applications: Insights into the post-synthesis sonochemical treatment on the electrochemical performance, Ultrason. Sonochem. 79 (2021) 105767. https://doi.org/10.1016/j.ultsonch.2021.105767.

[21] R.A. Venkatesan, M. Balachandran, Novel carbon nano-onions from paraffinum liquidum for rapid and efficient removal of industrial dye from wastewater, Environ. Sci. Pollut. Res. 27 (2020) 43845–43864. https://doi.org/10.1007/s11356-020-09981-w.

[22] M.B. Seymour, C. Su, Y. Gao, Y. Lu, Y. Li, Characterization of carbon nano-Onions for heavy metal ion remediation, J. Nanoparticle Res. 14 (2012) 1–14. https://doi.org/10.1007/s11051-012-1087-y.

[23] T.D. Ntuli, T.H. Mongwe, L.L. Sikeyi, O. Mkhari, N.J. Coville, E.N. Nxumalo, M.S. Maubane-Nkadimeng, Removal of hexavalent chromium via an adsorption coupled reduction mechanism using olive oil derived carbon nano-onions, Environ. Nanotechnology, Monit. Manag. 16 (2021) 100477.

https://doi.org/10.1016/j.enmm.2021.100477.

[24] C. Hu, Y.C. Chu, Y.R. Lin, H.C. Yang, K.H. Wang, Photocatalytic dye and Cr(VI) degradation using a metal-free polymeric g-C_3N_4 synthesized from solvent-treated urea, Polymers (Basel). 11 (2019) 1–14. https://doi.org/10.3390/polym11010182.

[25] L.L. Sikeyi, T.D. Ntuli, T.H. Mongwe, N.W. Maxakato, E. Carleschi, B.P. Doyle, N.J. Coville, M.S. Maubane-Nkadimeng, Microwave assisted synthesis of nitrogen doped and oxygen functionalized carbon nano onions supported palladium nanoparticles as hybrid anodic electrocatalysts for direct alkaline ethanol fuel cells, Int. J. Hydrogen Energy. 46 (2021) 10862–10875. https://doi.org/10.1016/j.ijhydene.2020.12.154.

[26] A. Makhongoana, B.J. Matsoso, T.H. Mongwe, N.J. Coville, D. Wamwangi, M.S. Maubane-Nkadimeng, The role of oxygen in a carbon source (castor oil versus paraffin oil) in the synthesis of carbon nano-onions, Nanotechnology. 32 (2021). https://doi.org/10.1088/1361-6528/abd0b1.

[27] T.H. Mongwe, B.J. Matsoso, B.K. Mutuma, N.J. Coville, M.S. Maubane, Synthesis of chain-like carbon nano-onions by a flame assisted pyrolysis technique using different collecting plates, Diam. Relat. Mater. 90 (2018) 135–143. https://doi.org/10.1016/j.diamond.2018.10.002.

[28] D. Park, Y.-S. Yun, J.H. Jo, J.M. Park, Mechanism of hexavalent chromium removal by dead fungal biomass of Aspergillus niger, Water Res. 39 (2005) 533–540.

[29] D. Park, S.R. Lim, Y.S. Yun, J.M. Park, Reliable evidences that the removal mechanism of hexavalent chromium by natural biomaterials is adsorption-coupled reduction, Chemosphere. 70 (2007) 298–305. https://doi.org/10.1016/j.chemosphere.2007.06.007.

[30] M. Kragović, M. Stojmenović, J. Petrović, J. Loredo, S. Pašalić, A. Nedeljković, I. Ristović, Influence of Alginate Encapsulation on Point of Zero Charge (pH_{PZC}) and Thermodynamic Properties of the Natural and Fe(III)-Modified Zeolite, Procedia Manuf. 32 (2019) 286–293. https://doi.org/10.1016/j.promfg.2019.02.216.

[31] Y. Ho, G. McKay, Pseudo-second order model for sorption processes, Process Biochem. 34 (1999) 451–651.

[32] H.N. Tran, S.J. You, A. Hosseini-Bandegharaei, H.P. Chao, Mistakes and inconsistencies regarding adsorption of contaminants from aqueous solutions: A critical review, Water Res. 120 (2017) 88–116. https://doi.org/10.1016/j.watres.2017.04.014.

[33] E. Worch, Adsorption Technology in Water Treatment: Fundamentals, Processes, and Modeling, 2nd rev. e, De Gruyter, 2012. https://doi.org/https://doi.org/10.1515/9783110715507.

[34] V.E. Pakade, T.D. Ntuli, A.E. Ofomaja, Biosorption of hexavalent chromium from aqueous solutions by Macadamia nutshell powder, Appl. Water Sci. 7 (2017) 3015–3030. https://doi.org/10.1007/s13201-016-0412-5.

[35] D. Kratochvil, B. Volesky, Advances in the biosorption of heavy metals, Trends Biotechnol. 16 (1998) 291–300. https://doi.org/10.1016/S0167-7799(98)01218-9.

[36] K.G. Akpomie, F.A. Dawodu, K.O. Adebowale, Mechanism on the sorption of heavy metals from binary-solution by a low cost montmorillonite and its desorption potential, Alexandria Eng. J. 54 (2015) 757–767. https://doi.org/10.1016/j.aej.2015.03.025.

[37] L. Dong, J. Liang, Y. Li, S. Hunang, Y. Wei, X. Bai, Z. Jin, M. Zhang, J. Qu, Effect of coexisting ions on Cr(VI) adsorption onto surfactant modified Auricularia auricula spent substrate in aqueous solution, Ecotoxicol. Environ. Saf. 166 (2018) 390–400. https://doi.org/10.1016/j.ecoenv.2018.09.097.

Chapter 7: Photocatalytic degradation of methyl orange by onion-like nanocarbon/TiO_2 nanocomposites under solar radiation

Abstract

Waste cooking oil is an environmental pollutant that has been used as a precursor for the synthesis of onion-like nanocarbons (OLNCs) using flame pyrolysis. The OLNCs were added to TiO_2 to form TiO_2/OLNC nanocomposites through hydrothermal treatment. The TiO_2/OLNCs ratio was varied by increasing the mass of the OLNCs (10, 20, 30, and 50 mg) whilst the mass of TiO_2 (100 mg) was kept constant at molar ratios of 1:2, 1:4, 1:6, and 1:10. The surface area of the photocatalysts increased with an increase in the mass of OLNCs. The nanocomposites were applied in the photocatalytic degradation of methyl orange. The photocatalysts showed a degradation rate trend of TC-10 > TC-20 > TC-30 > TC-50 > TiO_2. A similar trend was observed from the first-order kinetic rate data. The degradation rate of methyl orange was improved by adding 5% H_2O_2. The OLNCs were responsible for increased photocatalytic activity with the OLNCs acting as an electron acceptor while the TiO_2 acted as an electron donor. The enhanced catalytic behaviour was achieved by hindering the recombination of e^-/h^+ in the composite.

7.1. Introduction

Throughout the ages, photocatalysis has proven to be an effective method to degrade organic dyes in aqueous solutions. The utilization of photocatalysts for the degradation of dyes offers the advantages of using renewable energy sources such as solar energy. This can lead to the complete mineralization of the dye with decreased production of toxic substances as by-products [1].

The photocatalytic dye degradation reaction typically uses semiconducting metals as photocatalysts, in advanced oxidative processes. These catalysts include TiO_2 [2], Fe_2O_3 [3], ZnO [4], WO_3 [5], and ZnS [6], to name a few. However, TiO_2 remains the most used semiconductor due to its environmental friendliness [2], high chemical stability [7], and high photocatalytic activity in the organic dye photodegradation

process [8]. Pure titania, typically in the anatase phase, remains one of the most widely used semiconducting materials for the photodegradation of dyes. [9]. [10]. However, the use of TiO_2 comes with shortcomings that include rapid electron-hole recombination, a wide band gap energy, particle aggregation, and difficulties in photocatalyst-solution separation.

To mitigate these challenges, doping with anionic/cationic species has been widely explored [11]. Another cost-effective route is the use of carbon-rich substrates to either dope, cover or interact with the TiO_2. The use of carbon-rich materials as substrates is due to their high surface area and surface functional groups. Such properties make the adsorption of carbon materials to the surface of metal oxides feasible, leading to the immobilization of TiO_2 nanoparticles on the surface of the carbon material. An added benefit of using carbon-rich materials is that they have electron transfer (donor or acceptor) properties [12]. There are two prevailing (complementary) schools of thought on how to improve the use of semiconducting materials as photocatalysts, (i) harvesting of visible light, and (ii) decreasing the rate at which the generated hole (h^+) and electrons (e^-) recombine [13]. Carbon materials can potentially satisfy both requirements.

Carbon materials such as carbon spheres [14], carbon fibres, carbon nanotubes [15], and activated carbon [16] are attractive as an additive to semiconducting metal oxides to form photocatalytic nanocomposites. For example, a carbon nanotube/TiO_2 composite was applied as a photocatalyst for the degradation of Direct Red 23 and Direct Red 31 in the presence of H_2O_2. It was reported that the dye was adsorbed to the surface of the composite through the carbon nanotubes (CNTs) functional groups. This was followed by dye degradation due to a light-induced reaction of the TiO_2 particles. The degradation of the dye was increased by the addition of H_2O_2 due to the H_2O_2 being activated on the surface of the CNTs to generate $^{\bullet}OH$, free radicals [17].

Many studies have been reported on the synthesis of carbon-TiO_2 materials. The carbon-rich materials are typically synthesized by methods that include chemical vapour deposition [18], hydrothermal carbonization [19], and arc discharge [20]. However, the use of such methods requires sophisticated instruments that have a high

energy consumption drawback. An alternative simple method to make carbons for use in the composites is via flame pyrolysis. Here any carbon source can be used, including waste materials such as waste cooking oil, to produce onion-like nanocarbons (OLNCs) [21]. OLNCs are related to the family of carbon fullerenes [22]. They have a graphitic core, abundant surface functional groups, moderate porosity and can have an inner cavity [23]. Park et al. reported that the use of OLNCs with semiconducting composite materials enhanced the harnessing of visible light by narrowing the bandgap of the semiconducting materials and creating surface energy traps which decreased the recombination reaction [1].

In this study anatase, TiO_2 has been added to OLNCs to form photocatalytic nanocomposites for use in the photodegradation of a model complex, methyl orange. Zhang et al. reported that the combination of OLNCs and TiO_2 as photocatalysts was highly effective in the degradation of rhodamine B. This was attributed to the ability of the OLNCs to decrease the band gap of TiO_2 and foster the decrease of the recombination of photo-generated electrons and holes [13]. OLNCs have shown the potential to be used in the photocatalytic process but have not been widely used. The difference with the OLNCs reported in this study is that they were synthesized from waste cooking oil as a carbon source.

Methyl orange (MO) was chosen as a model dye for the study as many studies have been done on this dye, and this allows for a comparison of the use of OLNCs with other carbons. This was done by comparing pristine TiO_2 with TiO_2/OLNC nanocomposites made with varying ratios of the TiO_2-OLNC. In this study waste cooking oil has been applied as a carbon source for the synthesis of the OLNCs. For methodology and instrumentation please refer to Chapter 3

7.2. Results and discussion

7.2.1. Powder X-ray diffraction spectroscopy

The powder X-ray diffraction (PXRD) peaks of all the materials are shown in Figure 7.1. As it could be observed, only the TiO_2 peaks are seen as the carbon is amorphous

and in a low concentration. The diffraction peaks for all the nanocomposites showed peaks at the correct 2θ degree values for the expected planes of the anatase phase of TiO_2 (JCPDS Card No. 78-2486). Similar patterns have been reported in the literature for OLNCs/TiO_2 nanocomposites [24]. The main peak for anatase, the (I 0 1) peak, showed a downshift for the TC-20, TC-30 and TC-50 composites. This coincided with peak broadening and decreased peak intensities for all the composites relative to the TC-10 composites. This could be attributed to crystal growth hindrances as the mass of the OLNCs was increased resulting in lattice defects and poor crystallization [25].

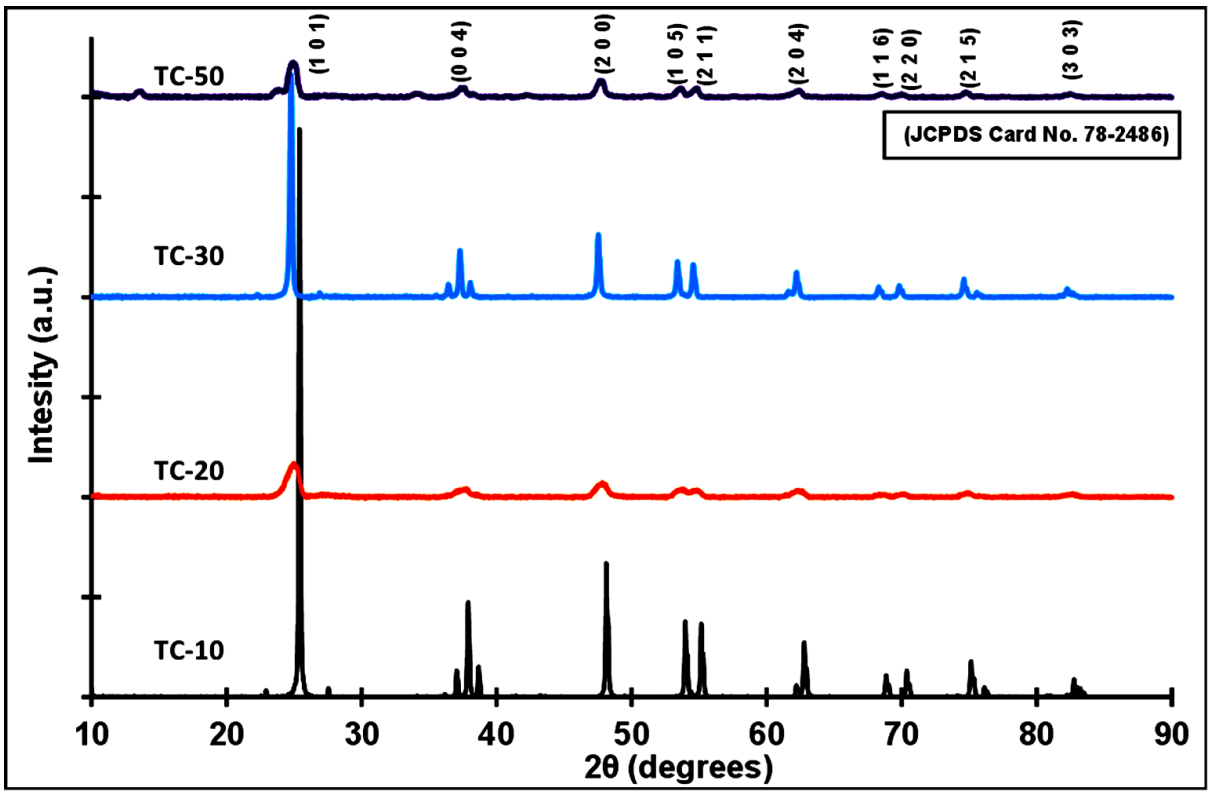

Figure 7.1: PXRD patterns of anatase TiO_2 phase for TC-10, TC-20, TC-30, and TC-50.

7.2.2. Thermogravimetric and differential thermal analysis

Figure 7.2. shows the thermal decomposition steps for the photocatalysts as the mass of the OLNCs was increased from 10 to 50 mg. From Figure 7.2(a), two major weight loss steps could be seen for all the materials. The first weight loss took place at around 100°C and is attributed to the evolution of moisture, and contributed 3% to 6% (TC-

50, 5%; TC-30, 3%; TC-20 4%; TC-10; 6%) of the weight loss for the respective photocatalysts. The second major weight loss took place at 478°C (TC-50), 480°C (TC-30), 561° (TC-20), and 500°C (TC-10) corresponding to 36%, 27%, 25%, and 13% weight loss for the respective materials, and is attributed to the decomposition of organic material due to the carbon oxidation process [13]. The DTA thermograms give a clearer picture of the decomposition steps that all the nanocomposites underwent (Figure 7.2b). The remaining residue was TiO_2 and the analysis data confirmed the approximate TiO_2/OLNC ratios. The composites with the lower OLNCs content (TC-20 and TC-10) showed higher thermal stability than the composites with higher OLNCs content. However, pristine OLNCs (from our previous study) showed higher thermal stability (ca. 650°C) than the as-synthesized TiO_2/OLNCs [21]. The hydrothermal treatment in the presence of NaOH affected the thermal stability of all of the nanocomposites [26].

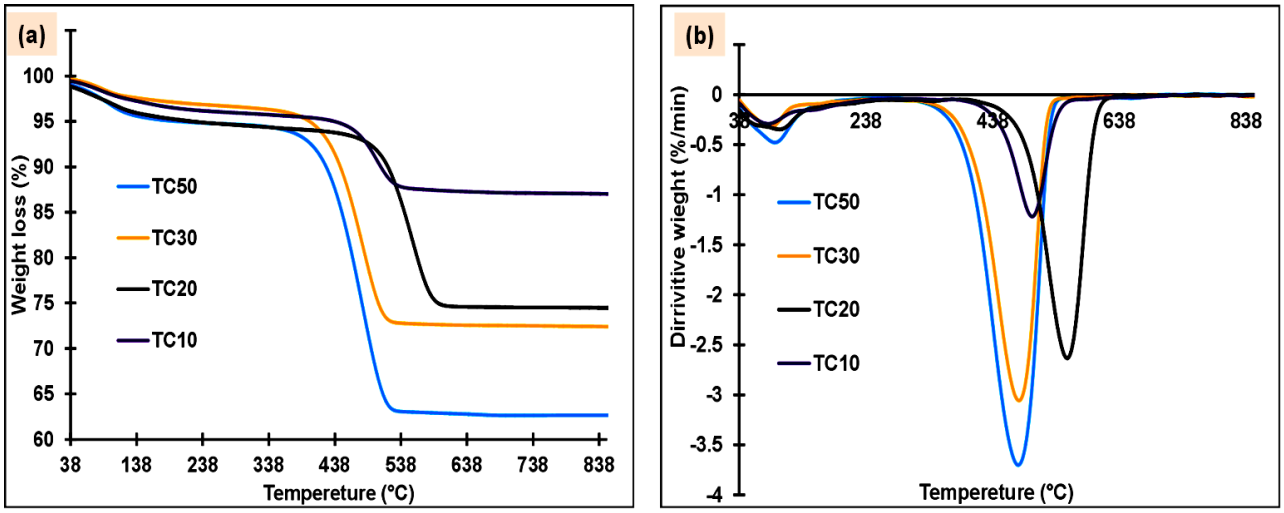

Figure 7.2: TGA (a) and DTA (b) thermograms for the TC-50, TC-30, TC-20, and TC-10 nanocomposites.

7.2.3. Morphological characteristics and BET analysis

The SEM micrographs for the TC-50, TC-30, TC-20, and TC-10 nanocomposites are shown in Figure 7.3. An irregular morphology could be observed in Figure 7.3(a, b) which was similar to that reported by Da Dalt et al. for multiwall carbon nanotube-TiO_2 composites [27]. On the contrary Figure, 7.3(c, d) showed quasi-spherical agglomerates consistent with the OLNCs morphology [28].

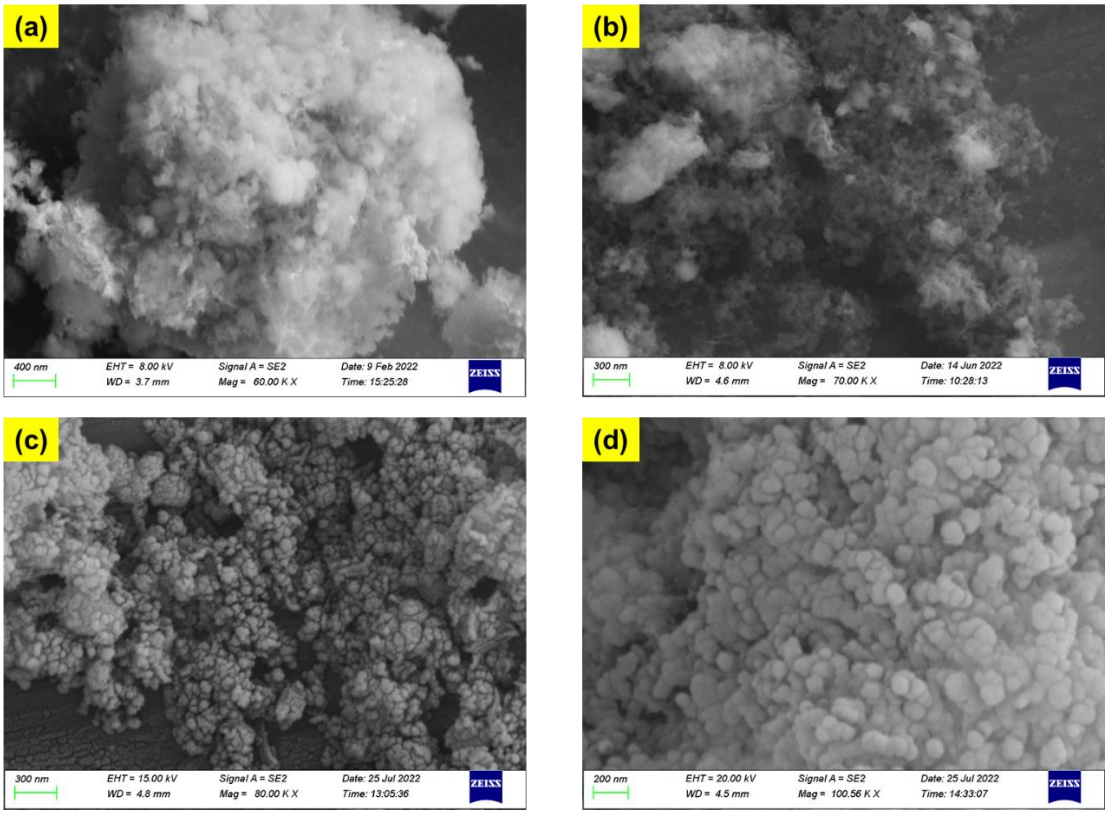

Figure 7.3: SEM micrographs for the TC-10 (a), TC-20 (b), TC-30 (c), and TC-50 (d) nanocomposites.

The TEM micrographs of all the nanocomposites are shown in Figure 7.4. The images showed that the material was quasi-spherical and multi-layered, and resembled that of an onion as seen from all the nanocomposites. This was consistent with the morphology reported by Sikeyi et al. [28]. It could be seen that as the mass of OLNCs increased, the shape of the TiO_2 became more irregular. The TC-50 material showed lumps of irregular spheres (Figure 7.4a). When the mass of OLNCs was decreased to 30 mg (TC-30) the morphology of the TiO_2 consisted of irregular spheres having a spider web connection (Figure 7.4b). The TiO_2 transformed into a tube-like nanostructure when the mass of the OLNCs was decreased to 20 mg (TC-20) (Figure 7.4c). Similar morphology was seen when the mass of the OLNCs was decreased to 10 mg (TC-10) (Figure 7.4d). Such a morphology of the TiO_2 is familiar to the titania made in alkaline media e.g. in synthesized TiO_2 (titanate) nanotubes [29]. Wang et al. reported that the conversion of anatase to titanate could be hindered by the presence of a carbon layer [30]. This may be the case in this study, as the occurrence of

nanotubes disappears in the material with higher carbon mass as seen in the TC-30 and TC-50 materials.

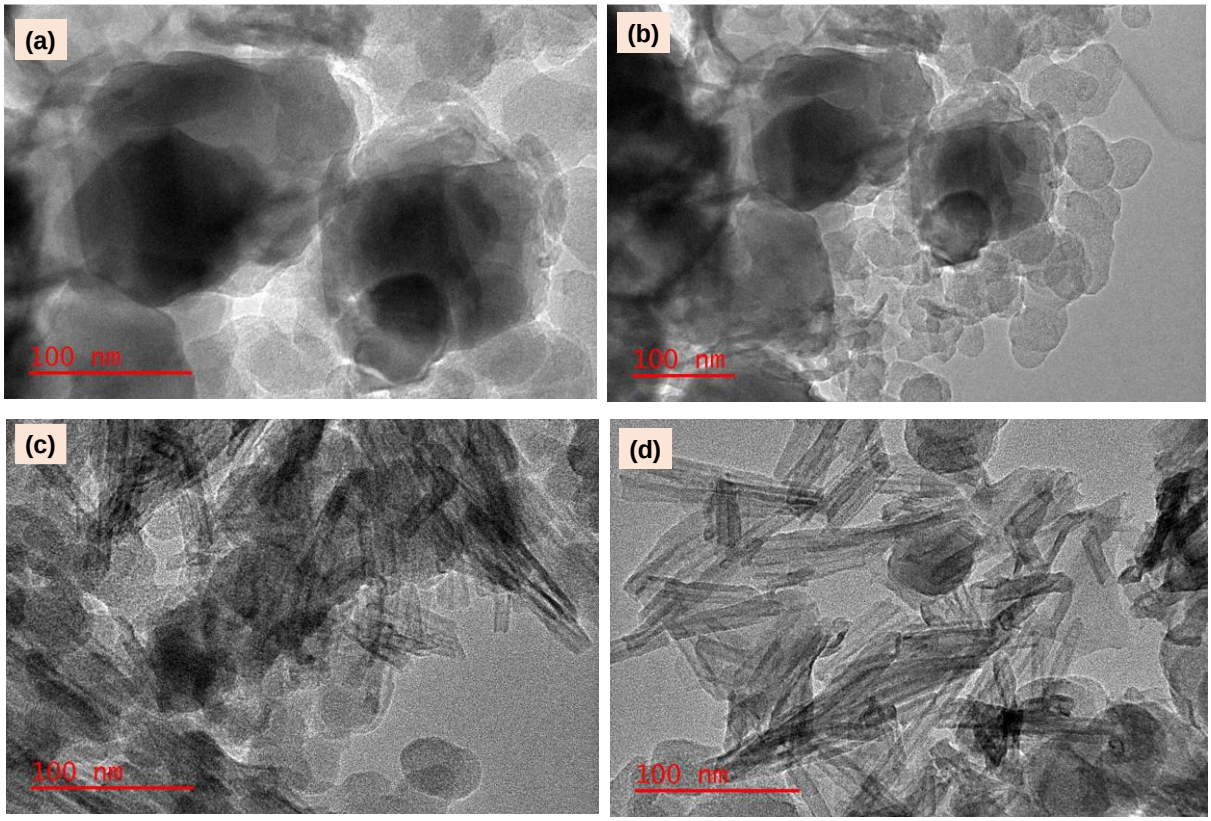

Figure 7.4: TEM micrographs for the TC-50 (a), TC-30 (b), TC-20 (c), and TC-10 (d) nanocomposites.

The surface area of the nanocomposites was considerably higher than that of pure TiO_2, in the order TiO_2 (7 m^2/g) < TC-10 (56 m^2/g) < TC-20 (69 m^2/g) < TC-30 (78 m^2/g) < TC-50 (120. m^2/g). This suggests that the addition of the OLNCs contributed to the increased surface area since OLNCs alone (80.89 m^2/g) [21] have a higher surface area compared to the as-prepared TiO_2 (Table 7.1). The pore volume and average pore size were also increased by the addition of the OLNCs but did not show any particular trend.

Table 7.1: BET parameters for TiO_2 and OLNCs/TiO_2 the nanocomposite

Adsorbent	Surface area (m^2/g)	Pore volume (cm^3/g)	Average pore size (nm)
TiO_2	7.6	0.02	7.58
OLNCs	81.8	0.080	4.20
TC-10	56.6	0.12	8.09
TC-20	69.8	0.19	10.80
TC-30	78.1	0.17	8.85
TC-50	120	0.28	9.43

7.2.4. Optical characteristics

The optical properties of the as-synthesized photocatalysts were studied using ultraviolet-visible spectroscopy (Figure 7.5.). It could be seen that as the mass of the OLNCs increased from 10 mg to 50 mg the absorption band shifted away from the visible region (Figure 7.5a). This gave the calculated bandgap energies of the photocatalysts in the order (TC-10: 2.0 eV) < (TC-20: 2.60 eV) < (TC-30: 2.80) = (TC-50: 2.80) (Figure 5b), all significantly lower than the bandgap of TiO_2 (~ 3.0 eV) [31]. The composite with a 10% mass to TiO_2 ratio (TC-10) showed a smaller bandgap (2.0 eV) than all the other materials, consistent with the bandgap of 2.094 eV reported by Zhang et al. for CNOs/TiO_2 composite with a 10% mass of TiO_2 [13].

The smaller bandgaps increase the probability of harvesting visible light and the formation of an increased number of photoexcited carriers for enhanced photodegradation activity [32]. Compared to TiO_2, the presence of the OLNCs contributes to the possibility of the recombination of holes and electrons. This is attributed to the presence of energy traps and optically active centres on the surface of the photocatalysts, due to the OLNCs [1].

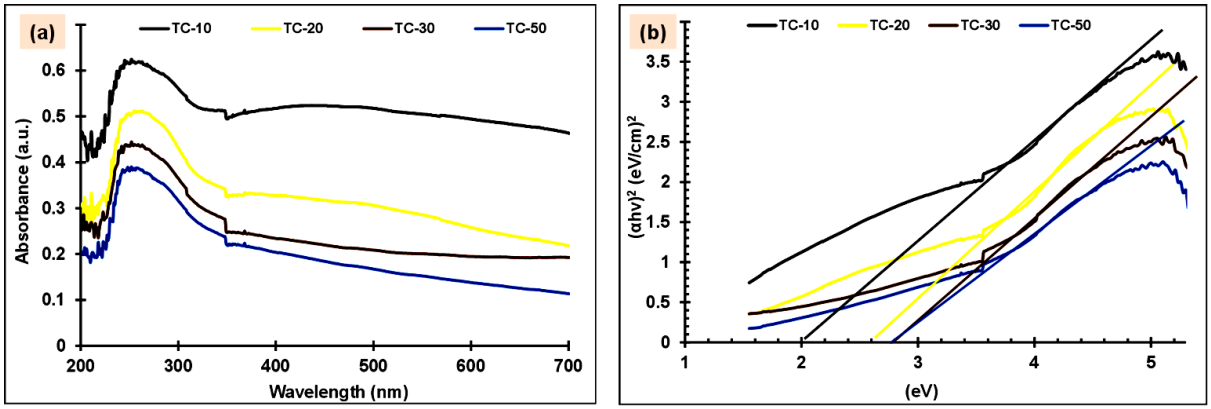

Figure 7.5: UV-Vis spectroscopy scanning (a) and bandgap energies (b) for the TC-50, TC-30, TC-20, and TC-10 photocatalysts.

7.2.5. Photocatalytic degradation of methyl orange

The photocatalytic degradation of MO was evaluated using TiO_2 and the TiO_2/OLNCs nanocomposites (Figure 7.6.). The reaction was first conducted in the absence of any photocatalyst, first in the dark for 30 min and then in light for 120 mins. Only a small amount of photodegradation of the MO (120 min) was observed in the absence of the OLNCs.

A similar experiment was performed with TiO_2 in the dark and an insignificant amount of MO was degraded. However, as expected, the TiO_2 catalyst was able to photodegrade the MO in light, with 44% of MO degraded after 120 min (Figure 7.6.). The photocatalytic degradation of MO was then carried out with the composites. When the experiment was carried out in the dark it was noted that all composites showed adsorption of the dye. Further, as the OLNC content increased the reaction also increased. This suggests that the carbon assists with the MO adsorption process [27]. This is in line with the increased surface area as the mass of OLNCs increased, as shown in Table 7.1.

However, the best photocatalytic result was found to be the composite with the lowest loading of OLNCs (Figure 7.6.). This suggests that two effects are at play: i) at low loadings the OLNCs enhance the conductivity but ii) at high loadings the carbon covers the active TiO_2 sites i.e. the OLNCs cover the photoactive sites of the TiO_2 resulting in a decreased light transmittance and charge transfer indicative that the surface area was not the major driving force to explain the photocatalytic degradation of MO [27].

Similar observations were made by Zhang et al. for the CNOs/TiO_2 composites used for the degradation of rhodamine B. It was reported that the composite that showed

the most effective photocatalytic activity was the composite with a 10% mass ratio of CNOs to TiO_2 due to enhanced separation of e^-/h^+ [13].

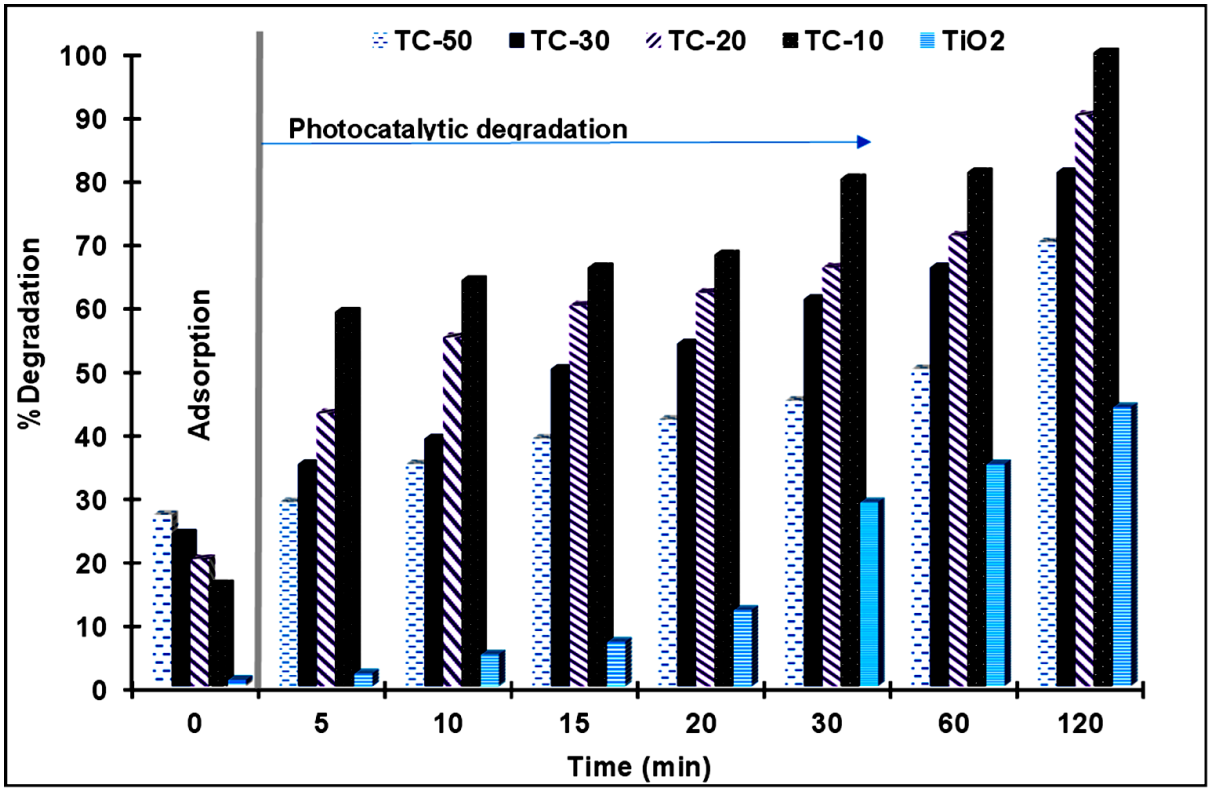

Figure 7.6: Photocatalytic degradation of MO using TiO_2, TC-50, TC-30, TC-20, and TC-10 photocatalysts

7.2.6. Kinetics

The kinetics of the photocatalytic degradation of MO using TiO_2 and its composites was evaluated (Figure 7.7; Table 7.2.). The experimental data fitted the first-order kinetic model. The nanocomposites showed an improved photocatalytic degradation of MO compared to TiO_2 alone. This was attributed to the enhanced absorptivity of the OLNCs, which created adsorption-coupled photocatalytic degradation synergy between the ONLCs and the TiO_2 [2]. As with the conversion data, the kinetic results followed the same trends viz. faster rates in the order 10 mg > 20 mg > 30 mg > 50 mg > TiO_2. This can be attributed to decreased electron-hole recombination due to the addition of OLNCs [27]. The TC-10 photocatalyst was selected for further study as it gave the best performance.

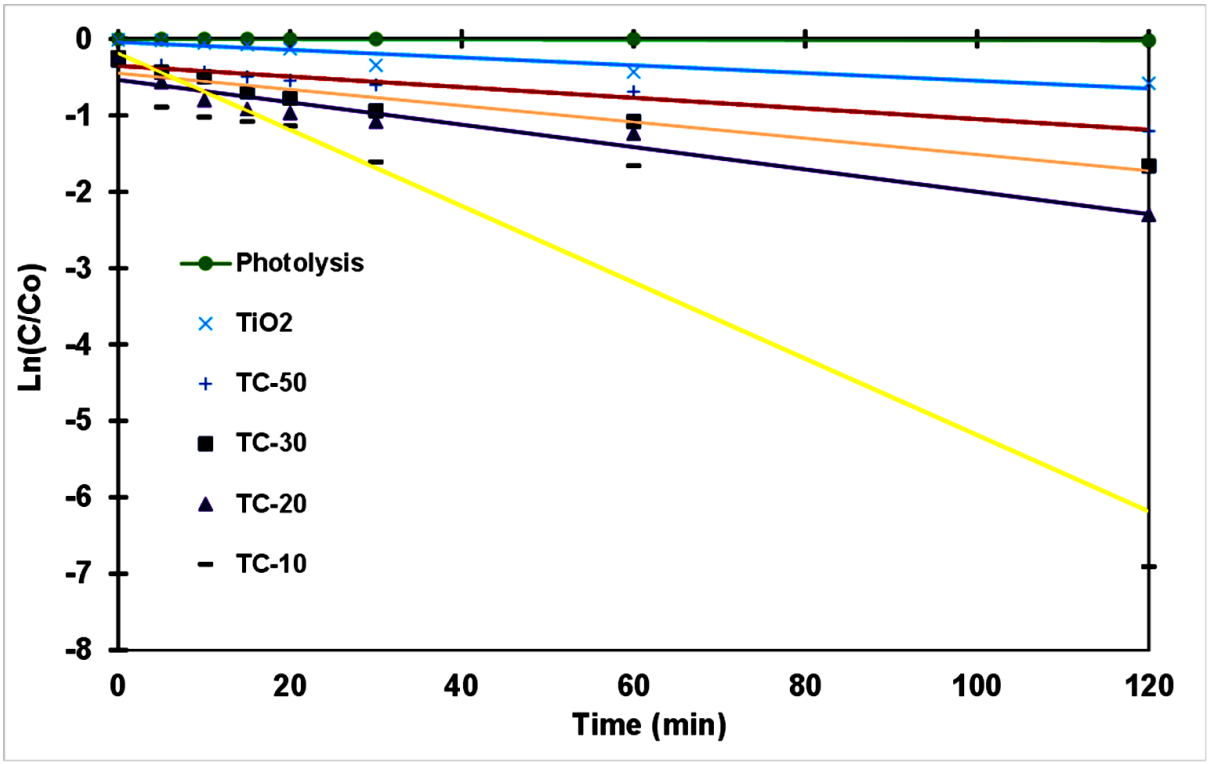

Figure 7.7: First order kinetics of the photocatalytic degradation of methyl orange

Table 7.2: Parameters for the first order kinetics for the photocatalytic degradation of methyl orange

Photocatalyst	Equations	R^2	k (min^{-1})
TiO_2	$Ln(C/C_o) = -0.0051X - 0.0395$	0.8745	0.005
TC-50	$Ln(C/C_o) = -0.007X - 0.3511$	0.9728	0.007
TC-30	$Ln(C/C_o) = -0.00106X - 0.4488$	0.9307	0.001
TC-20	$Ln(C/C_o) = -0.0146X - 0.5349$	0.9229	0.015
TC-10	$Ln(C/C_o) = -0.05X - 0.1861$	0.8975	0.050
TC-10 (H_2O_2)	$Ln(C/C_o) = -0.287X + 0.6119$	0.9002	0.287

The photocatalytic degradation of MO was investigated in the presence of 5% H_2O_2 (Figure 7.8.). It can be seen that complete degradation of MO was observed in 30 min of light radiation (Figure 7.8a) with a first-order kinetic rate of 0.287 min^{-1} (Table 7.2 and Figure 7.8b). The kinetic rate was 6 times faster than the 0.050 min^{-1} that took place in the absence of H_2O_2. The ability of H_2O_2 to decrease the electron-hole

recombination reaction is suggested to occur by harvesting the electrons and producing more hydroxyl radicals [33].

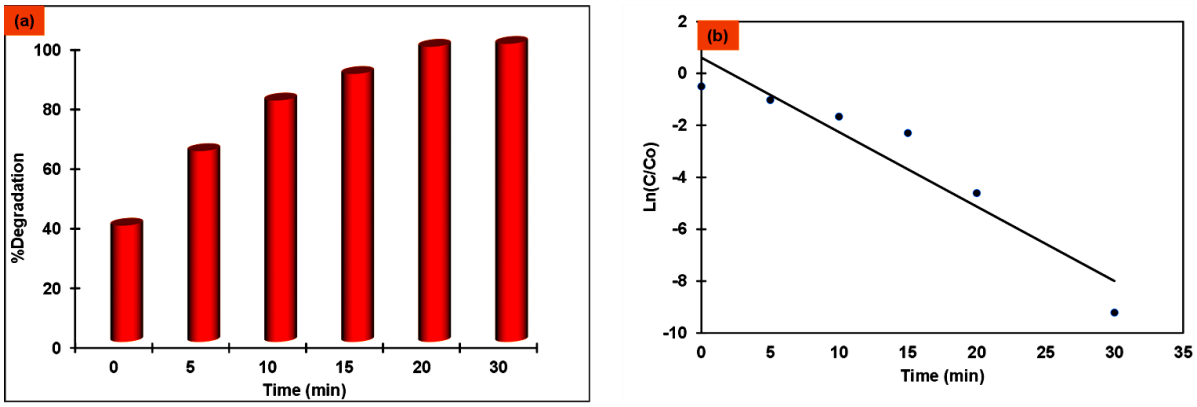

Figure 7.8: The photocatalytic degradation (a) and first-order kinetic curve (b) for the TC-10 photocatalyst in the presence of 5% H_2O_2.

7.2.7. Methyl orange speciation and the regeneration of the photocatalyst

Figure 7.9. shows the removal of MO by the TC-10 photocatalyst. The absorption spectrum depicts a maximum absorption peak at ~465 nm which decreased as the photocatalytic degradation progressed from 5 min to 120 min. The colour of the MO solution changed from orange to colourless. No new peaks were observed throughout the reaction, indicating that there was no formation of any chromophoric compounds [1].

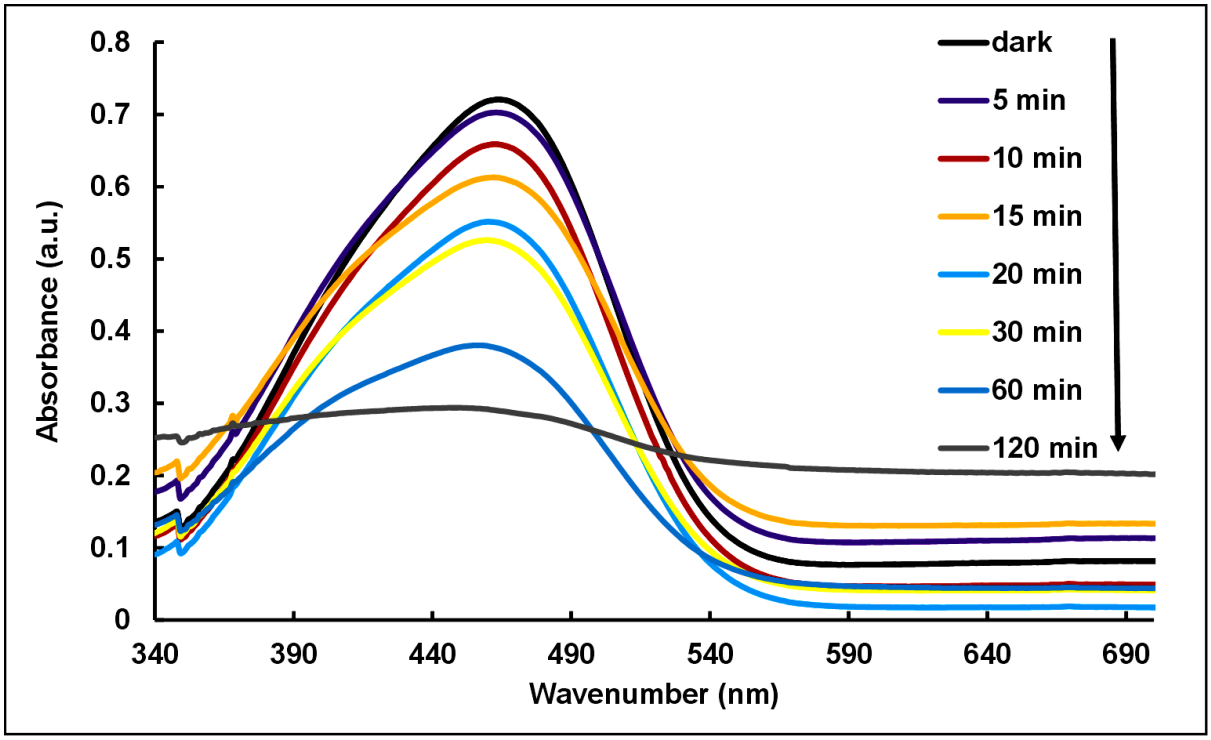

Figure 7.9: Absorption spectra of methyl orange as degraded by TC-10 over time

The photocatalyst's recyclability was evaluated by first conducting photocatalytic experiments for the degradation of MO for 120 min at neutral pH. Thereafter, the photocatalyst was separated from the solution by centrifugation. This was followed by rinsing the catalysts with 0.1 M NaOH and then boiling water to leach out any MO that may have been adsorbed on the surface of the photocatalyst. The photocatalyst was then dried at 60°C for 24 h and was reused in the photocatalytic degradation of more methyl orange. This process was performed 5 times with the results presented in Figure 7.10. The activity decreased with reuse 100% > 95% > 89% > 81% > 76%. This was attributed to the loss of mass each time it was reused [13].

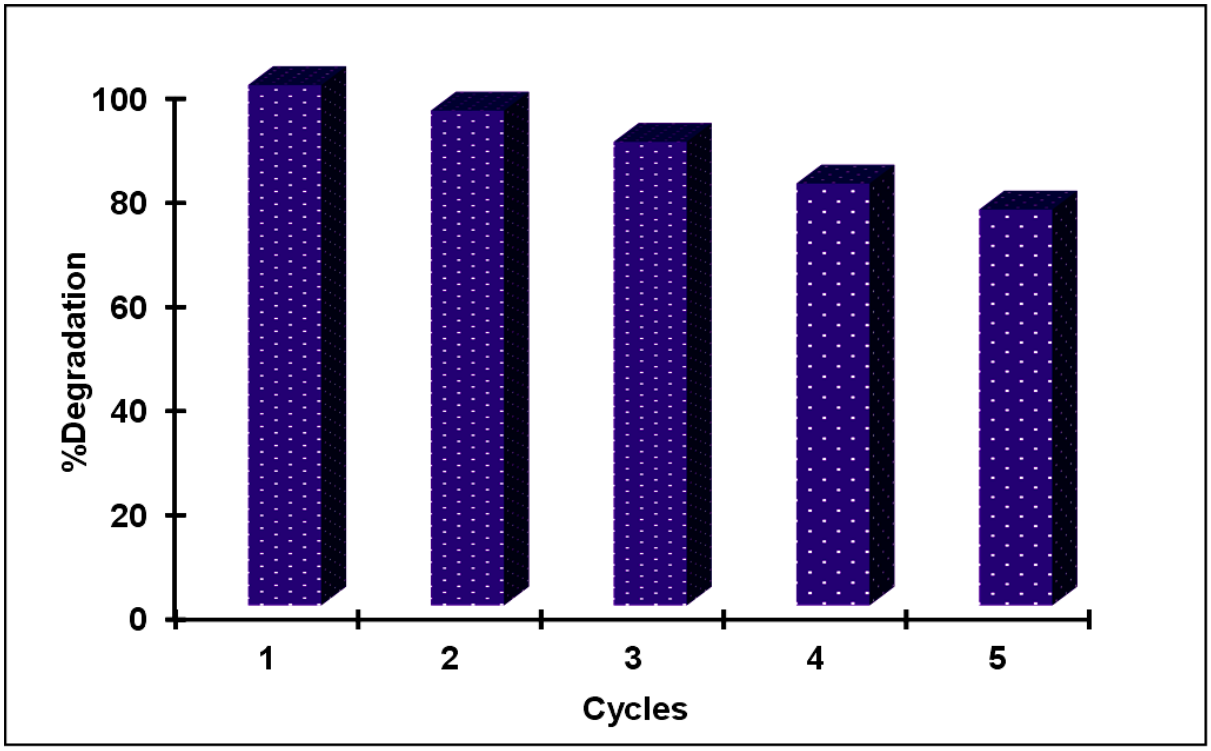

Figure 7.10: Regeneration of the TC-10 photocatalyst on 5 cycles of MO photocatalytic degradation.

7.2.8. Possible degradation mechanism

Figure 7.11 is an illustration of the proposed degradation mechanism of MO using the OLNCs/TiO_2 nanocomposite as a photocatalyst. The mechanism is based on the literature for similar carbon-TiO_2 composites [34] At first, the MO ions are adsorbed to the surface of the nanocomposite through the carbonyl groups [35]. This was followed by light irradiation and the photo generation of electrons (e^-). As the e^- migrates from the valence band (VB) to the conduction band (CB), holes (h^+) are created in the VB. The TiO_2 will then donate an e^- to the OLNCs thus preventing the rapid recombination of e^-/h^+. The e^- reacts with O_2 to form oxide radicals ($O2^{\bullet-}$) on the surface of the nanocomposite, simultaneously forming hydroxyl radicals ($^{\bullet}OH$) in the VB. Lastly, the respective radicals would degrade the MO. In like manner when the H_2O_2 gets irradiated it will produce free radicals that would play a role in the photodegradation of MO. The addition of H_2O_2 results in added free radicals leading to a more rapid degradation process.

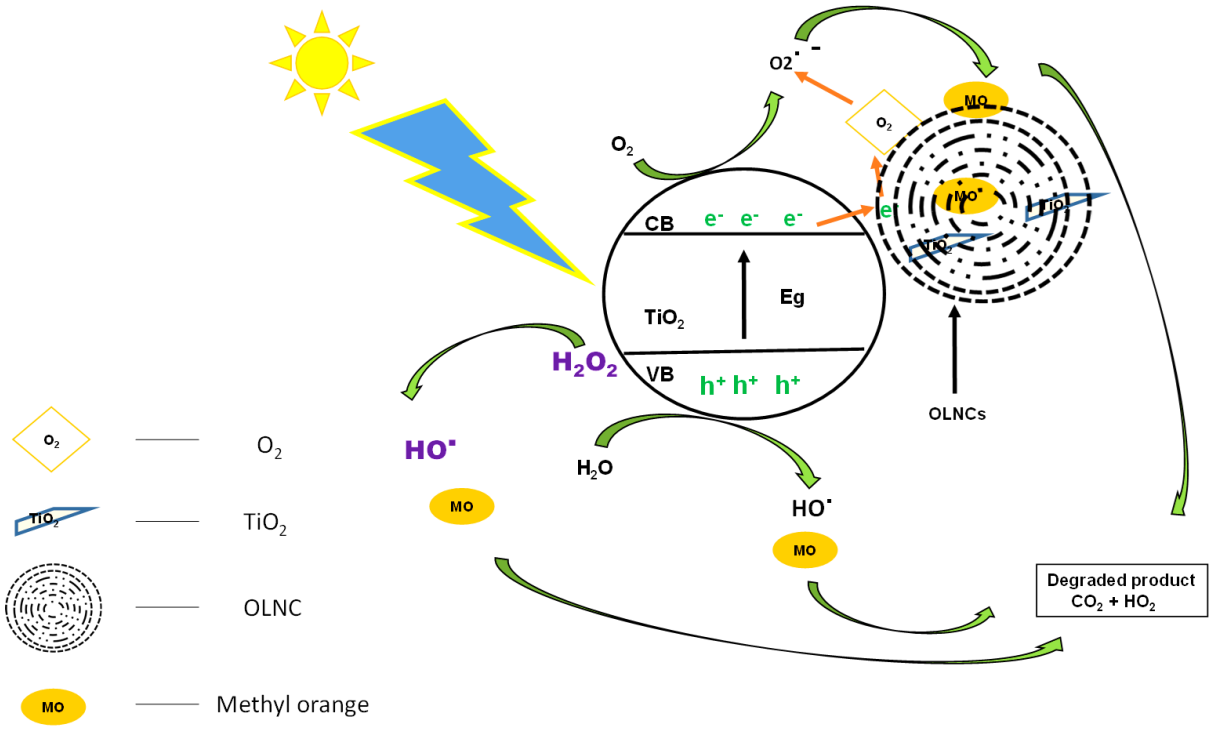

Figure 7.11: Schematic representation of MO degradation using OLNCs/TiO_2 photocatalyst

7.2.9. Comparison with other carbon/TiO_2 composites

A comparison of different carbon nanomaterials in composites with TiO_2 for the photocatalytic degradation of MO is presented in Table 7.3. A direct comparison is difficult due to differences in the experimental conditions used by the different workers. In the Table, different composites of TiO_2/carbon nanomaterials with different sources of carbon have been presented, carbon nanofibers [CNFs] of cellulose origin (TiO_2/CNF), graphitic carbon nitride (g-C_3N_4: TiO_2/g-C_3N_4), nitrogen-doped graphene quantum dots (N-GQDs) [N-GQD/TiO_2], carbon quantum dots (CQDs) [TiO_2/CQD], multiwall-carbon nanotubes (MWCNTs) [MWCNT/TiO_2] and OLNCs [TiO_2/OLNC].

In all cases, the combination of carbon/TiO_2 has proven effective in the removal of MO at low initial concentrations (10 to 40 mg/L). The adsorption of MO to the surface of the photocatalyst is important for the rapid degradation of the dye. For the selected composites adsorption of the dye by the TiO_2 alone was lower than in the composite materials. This was attributed to the active sites responsible for the adsorption of the dye. Resulting in a synergistic removal pathway of the dye with the dye adsorbed on the surface of the photocatalyst through carbon material. This is followed by the degradation of the dye molecules through the TiO_2. The synthesized composites of

TiO_2/OLNC proved to be comparable with other carbon/TiO_2-based photocatalysts. As it demonstrates 99.9% degradation of MO at 120 min significantly higher than all the presented composites. However, the TiO_2/CNF and the MWCNT/TiO_2 showed fewer reaction times of 30 min and 90 min respectively with the TiO_2/CNF having the lowest volume of MO solution (20 mL). The composites with the lowest degradation were the TiO_2/CQD and TiO_2/g-C_3N_4 at 39.1% and 55% respectively. This could be speculated as due to the generally low surface functional groups [36]. Therefore, along with a simple synthesis method of flame pyrolysis of waste cooking oil for making OLNCs. The TiO_2/OLNC composites show potential in the photocatalytic degradation of MO.

Table 7.3: Comparison of different carbon materials

Photocatalyst	Carbon source	C_O (mg/L)	Degradation (%)	Time (Min)	Volume (mL)	Reference
TiO_2/CNF	Nanocellulose	40	99.72	30	20	[37]
TiO_2/g-C_3N_4	g-C_3N_4	10	55	180	100	[38]
N-GQD/TiO_2	N-GQDs	10	95	120	50	[39]
TiO_2/CQD	CQDs	10	39.1	120	100	[40]
MWCNT/TiO_2	MWCNTs	15	97.4	90	150	[41]
TiO_2/OLNC	OLNCs	10	99.9	120	100	This study

7.3. Conclusion

The study has demonstrated the synthesis of OLNCs from the flame pyrolysis of waste cooking oil. This resulted in high-quality carbon nanomaterials that were used in TiO_2/OLNCs nanocomposites by varying the amount of OLNCs (10 mg, 20 mg, 30 mg, and 50 mg). The nanocomposites were effective in the photocatalytic degradation of MO compared to TiO_2 alone with the TC-10 material having the faster kinetic rate. This was attributed to a bandgap that was much narrow than that of TiO_2 and the adsorptive capacity of the photocatalysts through the OLNCs.

The addition of H_2O_2 greatly enhanced the photocatalytic activity of the photocatalyst due to the harvesting of electrons by the H_2O_2 thus, limiting recombination. No formation of chromophoric compounds was detected when the as-prepared

photocatalysts were applied in the degradation of methyl orange. Overall the TiO_2/OLNCs nanocomposites have the potential to be applied as photocatalysts for MO degradation. This was achieved by converting a waste material (waste cooking oil) to onion-like nanocarbons. That was able to decrease the bandgap of pure TiO_2 (3.0 eV) to (TC-10: 2.0 eV) < (TC-20: 2.60 eV) < (TC-30: 2.80) = (TC-50: 2.80). This allowed for the better photocatalytic activity for the nanocomposites than pure TiO_2, due to enhanced absorption of visible light and less recombination of e^-/h^+. The study has shown that nanocomposites of OLNCs/TiO_2 are a potential photocatalyst for the photocatalytic degradation of methyl orange.

7.4. References

[1] S.J. Park, G.S. Das, F. Schütt, R. Adelung, Y.K. Mishra, K.M. Tripathi, T.Y. Kim, Visible-light photocatalysis by carbon-nano-onion-functionalized ZnO tetrapods: degradation of 2,4-dinitrophenol and a plant-model-based ecological assessment, NPG Asia Mater. 11 (2019). https://doi.org/10.1038/s41427-019-0107-0.

[2] L. Xiong, D. Lan, H. Liang, L. Chen, Q. Wang, Grafting TiO_2 nanoparticles onto carbon fiber via “thiol-ene” click chemistry and its photodegradation performance for methyl orange, Mater. Lett. 211 (2018) 296–299. https://doi.org/10.1016/j.matlet.2017.10.028.

[3] G.K. Weldegebrieal, A.K. Sibhatu, Photocatalytic activity of biosynthesized α-Fe_2O_3 nanoparticles for the degradation of methylene blue and methyl orange dyes, Optik (Stuttg). 241 (2021) 1–15. https://doi.org/10.1016/j.ijleo.2021.167226.

[4] C. Belabed, A. Tab, B. Belhamdi, S. Boudiaf, B. Bellal, N. Benrekaa, M. Trari, Optical and dielectric properties of polyaniline-ZnO nanoparticles for enhancing photodegradation of organic pollutants, Optik (Stuttg). 248 (2021) 168066. https://doi.org/10.1016/j.ijleo.2021.168066.

[5] Y. Lun, S. Hu, F. Chen, Q. He, Y. Wang, W. Li, G. He, Highly enhanced photocatalytic property dominantly owing to the synergic effects of much negative Ecb and S-scheme heterojunctions in composite g-C_3N_4/Mo-doped WO_3, Colloids Surfaces A Physicochem. Eng. Asp. 642 (2022) 128682.

https://doi.org/10.1016/j.colsurfa.2022.128682.

[6] S. Ahluwalia, N.T. Prakash, R. Prakash, B. Pal, Improved degradation of methyl orange dye using bio-co-catalyst Se nanoparticles impregnated ZnS photocatalyst under UV irradiation, Chem. Eng. J. 306 (2016) 1041–1048. https://doi.org/10.1016/j.cej.2016.08.028.

[7] X.N. Yang, F.Y. Cui, Stability of Nano-sized titanium dioxide in an aqueous environment: Effects of pH, dissolved organic matter and divalent cations, Water Sci. Technol. 68 (2013) 276–282. https://doi.org/10.2166/wst.2013.165.

[8] J. Singh, A.K. Manna, R.K. Soni, Bifunctional Au–TiO_2 thin films with enhanced photocatalytic activity and SERS based multiplexed detection of organic pollutant, J. Mater. Sci. Mater. Electron. 30 (2019) 16478–16493. https://doi.org/10.1007/s10854-019-02023-3.

[9] F. Dziike, P.J. Franklyn, S.H. Durbach, M. Maubane, L. Hlekelele, Synthesis of radially aligned nano-rutile modified with Au and Ni for the photodegradation of methyl orange, Mater. Res. Bull. 104 (2018) 220–226. https://doi.org/10.1016/j.materresbull.2018.04.016.

[10] L. Liu, F. Pan, C. Liu, L. Huang, W. Li, X. Lu, TiO_2 Nanofoam-Nanotube Array for Surface-Enhanced Raman Scattering, ACS Appl. Nano Mater. 1 (2018) 6563–6566. https://doi.org/10.1021/acsanm.8b01566.

[11] T.T. Vu Nu, N.H. Thi Tran, P.L. Truong, B.T. Phan, M.T. Nguyen Dinh, V.P. Dinh, T.S. Phan, S. Go, M. Chang, K.T. Loan Trinh, V. Van Tran, Green synthesis of microalgae-based carbon dots for decoration of TiO_2 nanoparticles in enhancement of organic dye photodegradation, Environ. Res. 206 (2022) 112631. https://doi.org/10.1016/j.envres.2021.112631.

[12] A. Mahmood, X. Wang, G. Shi, Z. Wang, X. Xie, J. Sun, Revealing adsorption and the photodegradation mechanism of gas phase o-xylene on carbon quantum dots modified TiO_2 nanoparticles, J. Hazard. Mater. 386 (2020) 121962. https://doi.org/10.1016/j.jhazmat.2019.121962.

[13] Y. Zhang, W. Zhang, K. Yang, Y. Yang, J. Jia, Y. Liang, L. Guo, Carbon Nano-Onions (CNOs)/TiO_2 Composite Preparation and Its Photocatalytic Performance under Visible Light Irradiation, J. Environ. Eng. 146 (2020) 1–12. https://doi.org/10.1061/(ASCE)ee.1943-7870.0001662.

[14] P. Mente, V. Mashindi, T.N. Phaahlamohlaka, T.N. Monyatsi, R.P. Forbes, N.J. Coville, Oxidation of Benzyl Alcohol Using Cobalt Oxide Supported Inside and

Outside Hollow Carbon Spheres, ChemistryOpen. 10 (2021). https://doi.org/10.1002/open.202000312.

[15] T.P. Mofokeng, Z.N. Tetana, K.I. Ozoemena, Defective 3D nitrogen-doped carbon nanotube-carbon fibre networks for high-performance supercapacitor: Transformative role of nitrogen-doping from surface-confined to diffusive kinetics, Carbon N. Y. 169 (2020) 312–326. https://doi.org/10.1016/j.carbon.2020.07.049.

[16] V.E. Pakade, L.C. Maremeni, T.D. Ntuli, N.T. Tavengwa, Application of quaternized activated carbon derived from Macadamia nutshells for the removal of hexavalent chromium from aqueous solutions, South African J. Chem. 69 (2016) 180–188. https://doi.org/http://dx.doi.org/10.17159/0379-4350/2016/v69a22.

[17] N.M. Mahmoodi, Photocatalytic degradation of dyes using carbon nanotube and titania nanoparticle, Water. Air. Soil Pollut. 224 (2013). https://doi.org/10.1007/s11270-013-1612-3.

[18] C.M. Hussain, Carbon Nanomaterials as Adsorbents for Environmental Analysis, Nanomater. Environ. Prot. 9781118496 (2015) 217–236. https://doi.org/10.1002/9781118845530.ch14.

[19] O. Mkhari, T.D. Ntuli, N.J. Coville, E.N. Nxumalo, M.S. Maubane-Nkadimeng, A comparison of fluorescent N-doped carbon dots supported on the surface of hollow and solid carbon spheres, and solid silica spheres, Diam. Relat. Mater. 118 (2021) 108500. https://doi.org/10.1016/j.diamond.2021.108500.

[20] R. Sharma, A.K. Sharma, V. Sharma, Synthesis of carbon nanotubes by arc-discharge and chemical vapor deposition method with analysis of its morphology, dispersion and functionalization characteristics, Cogent Eng. 2 (2015). https://doi.org/10.1080/23311916.2015.1094017.

[21] T.D. Ntuli, T.H. Mongwe, L.L. Sikeyi, O. Mkhari, N.J. Coville, E.N. Nxumalo, M.S. Maubane-Nkadimeng, Removal of hexavalent chromium via an adsorption coupled reduction mechanism using olive oil derived carbon nano-onions, Environ. Nanotechnology, Monit. Manag. 16 (2021) 100477. https://doi.org/10.1016/j.enmm.2021.100477.

[22] B. Shaku, T.P. Mofokeng, T.H. Mongwe, N.J. Coville, K.I. Ozoemena, M.S. Maubane-Nkadimeng, Physicochemical Properties of Nitrogen Doped Carbon Nano-onions Grown by Flame Pyrolysis from Grapeseed Oil for Use in

Supercapacitors, Electroanalysis. 32 (2020) 2946–2957. https://doi.org/10.1002/elan.202060383.

[23] L.L. Sikeyi, T.D. Ntuli, T.H. Mongwe, N.W. Maxakato, E. Carleschi, B.P. Doyle, N.J. Coville, M.S. Maubane-Nkadimeng, Microwave assisted synthesis of nitrogen doped and oxygen functionalized carbon nano onions supported palladium nanoparticles as hybrid anodic electrocatalysts for direct alkaline ethanol fuel cells, Int. J. Hydrogen Energy. 46 (2021) 10862–10875. https://doi.org/10.1016/j.ijhydene.2020.12.154.

[24] A.K. John, S. Palaty, S.S. Sharma, Greener approach towards the synthesis of titanium dioxide nanostructures with exposed {001} facets for enhanced visible light photodegradation of organic pollutants, J. Mater. Sci. Mater. Electron. 31 (2020) 20868–20882. https://doi.org/10.1007/s10854-020-04602-1.

[25] S. Tong, J. Zhou, L. Ding, C. Zhou, Y. Liu, S. Li, J. Meng, S. Zhu, S. Chatterjee, F. Liang, Preparation of carbon quantum dots/TiO_2 composite and application for enhanced photodegradation of rhodamine B, Colloids Surfaces A Physicochem. Eng. Asp. 648 (2022) 129342. https://doi.org/10.1016/j.colsurfa.2022.129342.

[26] H. Chen, J. Wu, J. Shi, W. Zhang, H. Wang, Effect of alkali treatment on microstructure and thermal stability of parenchyma cell compared with bamboo fiber, Ind. Crops Prod. 164 (2021). https://doi.org/10.1016/j.indcrop.2021.113380.

[27] S. Da Dalt, A.K. Alves, C.P. Bergmann, Photocatalytic degradation of methyl orange dye in water solutions in the presence of MWCNT/TiO_2 composites, Mater. Res. Bull. 48 (2013) 1845–1850. https://doi.org/10.1016/j.materresbull.2013.01.022.

[28] L.L. Sikeyi, T.D. Ntuli, T.H. Mongwe, N.W. Maxakato, N.J. Coville, M.S. Maubane-Nkadimeng, Platinum Nanoparticles Loaded on Pristine and Boron Oxide Modified Carbon Nano-Onions for Enhanced Ammonia Electrooxidation in Alkaline Direct Ammonia Fuel Cells, J. Electroanal. Chem. 917 (2022) 116411. https://doi.org/10.2139/ssrn.3982297.

[29] J. Xiong, L. He, Influence of Na+content on the structure and morphology of TiO_2 nanoparticles prepared by hydrothermal transformation of alkaline titanate nanotubes, J. Exp. Nanosci. 12 (2017) 384–393. https://doi.org/10.1080/17458080.2017.1382734.

[30] X. Wang, H. Pan, X. Xue, J. Qian, L. Yu, J. Yang, Z. Zhang, Preparation and characterization of titanate nanotubes/carbon composites, Mater. Chem. Phys. 130 (2011) 827–830. https://doi.org/10.1016/j.matchemphys.2011.08.019.

[31] A. Fujishima, K. Honda, Electrochemical photolysis of water at a semiconductor electrode, Nature. 238 (1972) 37–40. https://doi.org/10.1038/238038a0.

[32] P. Khare, A. Singh, S. Verma, A. Bhati, A.K. Sonker, K.M. Tripathi, S.K. Sonkar, Sunlight-Induced Selective Photocatalytic Degradation of Methylene Blue in Bacterial Culture by Pollutant Soot Derived Nontoxic Graphene Nanosheets, ACS Sustain. Chem. Eng. 6 (2018) 579–589. https://doi.org/10.1021/acssuschemeng.7b02929.

[33] R. Rahmati, B. Nayebi, B. Ayati, Investigating the effect of hydrogen peroxide as an electron acceptor in increasing the capability of slurry photocatalytic process in dye removal, Water Sci. Technol. 83 (2021) 2414–2423. https://doi.org/10.2166/wst.2021.136.

[34] Y. Zhang, K. Hawboldt, L. Zhang, J. Lu, L. Chang, A. Dwyer, Carbonaceous nanomaterial-TiO_2 heterojunctions for visible-light-driven photocatalytic degradation of aqueous organic pollutants, Appl. Catal. A Gen. 630 (2022) 118460. https://doi.org/10.1016/j.apcata.2021.118460.

[35] S.S. Shah, T. Sharma, B.A. Dar, R.K. Bamezai, Adsorptive removal of methyl orange dye from aqueous solution using populous leaves: Insights from kinetics, thermodynamics and computational studies, Environ. Chem. Ecotoxicol. 3 (2021) 172–181. https://doi.org/10.1016/j.enceco.2021.05.002.

[36] H. Khojasteh, M. Salavati-Niasari, H. Safajou, H. Safardoust-Hojaghan, Facile reduction of graphene using urea in solid phase and surface modification by N-doped graphene quantum dots for adsorption of organic dyes, Diam. Relat. Mater. 79 (2017) 133–144. https://doi.org/10.1016/j.diamond.2017.09.011.

[37] G. qing Liu, X. jun Pan, J. Li, C. Li, C. lu Ji, Facile preparation and characterization of anatase TiO_2/nanocellulose composite for photocatalytic degradation of methyl orange, J. Saudi Chem. Soc. 25 (2021) 101383. https://doi.org/10.1016/j.jscs.2021.101383.

[38] Y. Zang, L. Li, Y. Xu, Y. Zuo, G. Li, Hybridization of brookite TiO2with g-C3N4: A visible-light-driven photocatalyst for As^{3+} oxidation, MO degradation and water splitting for hydrogen evolution, J. Mater. Chem. A. 2 (2014) 15774–15780. https://doi.org/10.1039/c4ta02082k.

[39] D. Pan, J. Jiao, Z. Li, Y. Guo, C. Feng, Y. Liu, L. Wang, M. Wu, Efficient separation of electron-hole pairs in graphene quantum dots by TiO_2 heterojunctions for dye degradation, ACS Sustain. Chem. Eng. 3 (2015) 2405–2413. https://doi.org/10.1021/acssuschemeng.5b00771.

[40] X. Zhang, Z. Li, S. Xu, Y. Ruan, Carbon quantum dot-sensitized hollow TiO_2 spheres for high-performance visible light photocatalysis, New J. Chem. 45 (2021) 8693–8700. https://doi.org/10.1039/d1nj00501d.

[41] K. Ouyang, S. Xie, X. Ma, Photocatalytic activity of TiO_2 supported on multi-walled carbon nanotubes under simulated solar irradiation, Ceram. Int. 39 (2013) 7531–7536. https://doi.org/10.1016/j.ceramint.2013.03.004.

Chapter 8: Removal of Cr(VI) and Cr(III) via adsorption-coupled photoreduction systems using iron oxide/onion-like nanocarbon composites

T.D. Ntuli, L.L. Sikeyi, T.H. Mongwe, O. Mkhari, C. Palet, N.J. Coville, E.N. Nxumalo, M.S. Maubane-Nkadimeng, Removal of Cr(VI) and Cr(III) via adsorption coupled photoreduction systems using iron oxide/onion-like nanocarbon composites

Abstract

The presence of hexavalent chromium (Cr(VI)) in wastewater remains a serious problem for the environment. Adsorption and photoreduction have become the most popular methodologies for the removal of Cr(VI) from water systems. However, both removal methods have limitations such as the formation of secondary toxins, low adsorption capacity and incomplete removal. Herein, we present a method for the elimination of Cr(VI), together with Cr(III) ions, using iron oxide nanoparticles/onion-like nanocarbons (OLNCs) as nanocomposites applied as both adsorbents and photocatalysts. The elimination of Cr(VI) and Cr(III) ions was achieved via a three-step process, based on (i) adsorption coupled reduction of Cr(VI) to Cr(III) ions on the surface of the nanocomposites, followed by (ii) photoreduction of the remaining Cr(VI) ions to Cr(III) aided by light radiation, and (iii) adsorption of Cr(III) ions on the nanocomposites. The as-synthesized nanocomposites were fully characterized by scanning electron microscopy, transmission electron microscopy, surface area analysis, thermogravimetric analysis and X-ray diffraction studies.

The optimum conditions for the adsorption coupled reduction experiments by using iron oxide/OLNCs (which acted both as adsorbent and photocatalyst) were pH = 4, with the experimental data explained by the Langmuir adsorption isotherm and by pseudo-second-order kinetic models. Photo-reduction experiments, using iron oxide nanocomposites, demonstrated the reduction of Cr(VI) in the first 20 min, followed by the adsorption of Cr(III) ions. The iron oxide/OLNCs as adsorbents/photocatalysts were reused 5 times with more than a 90% removal efficiency.

The overall results showed that the elimination of Cr(VI) and Cr(III) ions by using reusable iron oxide/OLNCs nanocomposites is feasible.

8.1. Introduction

Chromium has several oxidation states with hexavalent chromium [Cr(VI)] and trivalent chromium [Cr(III)] being the most stable in an aqueous environment [1]. Cr(VI) is more

toxic than Cr(III) due to its high mobility and oxidation state [2]. The World Health Organization (WHO) has placed Cr(VI) in group 1 of the list of environmental pollutants. The maximum limit of Cr(VI) in freshwater bodies is set at 0.05 mg/L [3].

Several methods have been developed for the adequate elimination of Cr(VI) ions from solutions. They include solvent extraction, ion exchange [4], chemical precipitation [5], membrane filtration [6], flocculation [7], coagulation [8], and the use of microorganisms [9]. However, the aforementioned methods come with limitations such as high consumption of electricity and chemicals, membrane fouling, electrode corrosion, and the generation of toxic sludge and secondary pollutants [10].

Adsorption and photoreduction are attractive methodologies for the elimination of Cr(VI) ions. In particular, carbon-rich materials that include biomass [11], pine biomass waste [12] and polymers [13] have been used as adsorbents in adsorption processes.

The elimination of Cr(VI) ions by carbon-rich adsorbents has been reported to involve an adsorption-coupled reduction mechanism. In this process, the Cr(VI) ions are reduced to Cr(III) ions due to the presence of electron donor groups on the surface of the adsorbent (Park et al., 2005). However, low adsorption capacity, incomplete removal and extended contact time between adsorbent and adsorbate remain a challenge in the elimination of Cr(VI) ions [15]. In an alternative strategy, metal oxide nanoparticles such as ZnO [16], TiO_2 [17], and Fe_2O_3 [17] have been applied as photocatalysts for the reduction of Cr(VI) ions to Cr(III) ions. However, the Cr(III) ions remain in the solution which has the potential to generate secondary pollution. This suggests that if the two procedures, using both metal oxides and carbon are combined, a new type of catalyst to address the Cr pollution problem may be found. This would involve the elimination of both Cr(VI) ions and Cr(III) ions from the solution by the use of adsorption and photocatalysis simultaneously.

To achieve this, we have used onion-like nanocarbons (OLNCs) obtained from the flame pyrolysis of waste cooking oil as the carbon source. The OLNCs were combined with iron oxide nanoparticles to form nanocomposites that could act as both adsorbents and photocatalysts, to be applied in the elimination of Cr(VI) from the solution. The type of OLNCs used was chosen based on our previous work [18] as the OLNCs surface contains carbonyl groups for Cr ion coordination. The iron oxide was chosen due to its facile reduction of Cr(VI) to Cr(III) [19]. As will be seen the iron oxide

nanoparticles/OLNC nanocomposites accelerated the reduction of Cr(VI) and the adsorption of Cr(III) ions on the surface of the catalyst. For methodology and instrumentation please refer to Chapter 3

8.2. Results and discussions

8.2.1. BET and thermal analysis

Table 8.1. gives the surface area, pore volume, and average pore size of the nanocomposites in comparison to the pristine OLNCs and iron oxide nanoparticles alone. It can be seen that after the OLNCs were incorporated with the iron oxide nanoparticles the surface area, pore volume, and average pore size decreased. The decrease in surface area was attributed to the low surface area that comes with metal oxides and the possibility of the OLNCs being blocked by the iron oxide nanoparticles [20]. When compared to the iron oxide nanoparticles the surface area of the nanocomposites was larger, attributed to the increased surface area of OLNCs.

Table 8.1: BET parameters for the nanocomposites

Adsorbent	Surface area (m^2/g)	Pore volume (cm^3/g)	Average pore size (nm)
Iron oxide	1.48	0.0060	16.9
OLNC	81.8	0.080	4.20
FeC-25	5.07	0.015	12.0
FeC-50	9.96	0.027	10.7
FeC-100	10.9	0.032	11.4
FeC-170	15.5	0.047	12.0

TGA (Figure 8.1a) and DTA (Figure 8.1b) analyses were performed on all the nanocomposites. Two major weight loss peaks were observed in all the samples. The first decomposition step was observed at temperatures less than 150°C (Figure 8.1a and 1b) due to the evolution of moisture with weight losses of 16% (FeC-25), 6% (FeC-50), 20% (FeC-100), and 18% (FeC-170); see Figure 8.1a. The second major decomposition step took place at temperatures between 250°C and 650°C (Figures 1a and 1b) attributed to the oxidation of surface moieties, dihydroxylation, and decomposition of the graphitic core of the OLNCs. The second decomposition step resulted in weight losses of 44% (FeC-25), 40% (FeC-50), 40% (FeC-100), and 50%

(FeC-170); see Figure 8.1a. The residual weight percent for all the nanocomposites was attributed to the iron oxide.

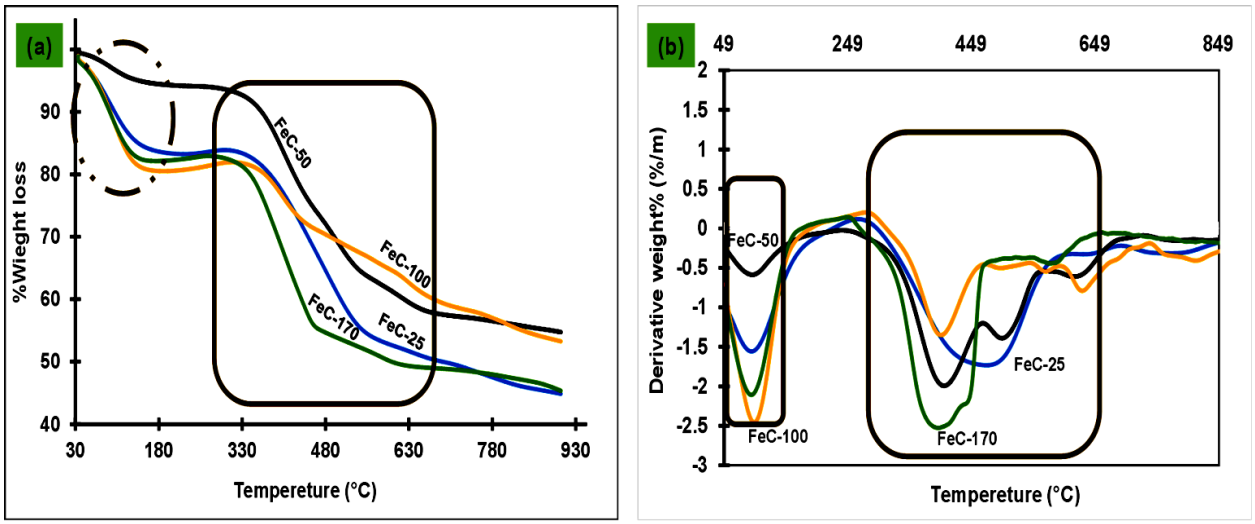

Figure 8.1: TGA (a) and DTA (b) thermograms for the FeC-25, FeC-50, FeC-100, and FeC-170 nanocomposites

8.2.2. SEM and TEM micrographs

Figure 8.2. depicts SEM micrographs for the FeC-25, FeC-50, FeC-100, and FeC-170 photocatalysts or nanoadsorbents. The SEM micrographs show that the morphology of the nanocomposites consisted of quasi-spherical materials that were closely packed and had a similar morphology to that seen for the pristine OLNCs [18]. Furthermore, SEM images show that the synthesis process did not damage the structure of the OLNCs.

Figure 8.3. depicts the TEM micrographs for FeC-25, FeC-50, FeC-100, and FeC-170 nanocomposites. The nanocomposite showed a typical morphology of OLNCs that is represented by multiple layered materials. Such a morphology was similar to that of pristine OLNCs derived from waste cooking oil, as seen in Figure 8.4a. The micrographs for the nanocomposites and the pristine OLNCs were compared to that of the iron oxide nanoparticles. The nanoparticles formed clusters closely packed with a shape resembling dots, as can be seen in Figure 8.4b. A clear distinction in the morphology of the nanocomposites, iron oxide particles and the OLNCs could not be easily seen due to the clustered nature of the materials. However, from the micrographs of the iron oxide nanoparticles, it could be seen that the multilayer

morphology of the OLNCs was not observable (Figure 8.4b). The slight difference between the micrographs of the nanocomposites and the pristine OLNCs was the appearance of black dots as seen in Figure 8.3. The black dots were assumed to be the iron oxide nanoparticles since they are not present in the micrograph of the pristine OLNCs (Figure 8.4a).

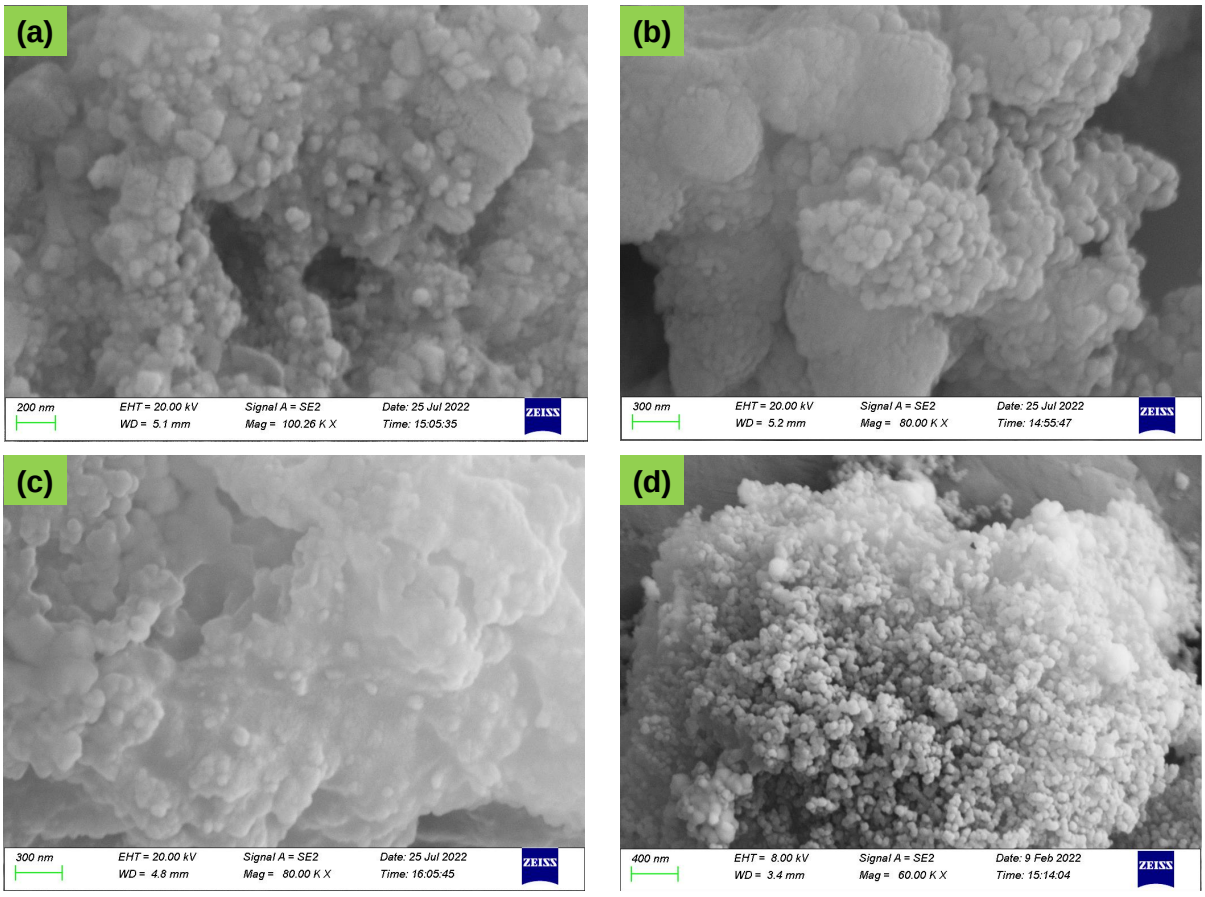

Figure 8.2: SEM micrographs for the (a) FeC-25, (b) FeC-50, (c) FeC-100, and (d) FeC-170 nanocomposites

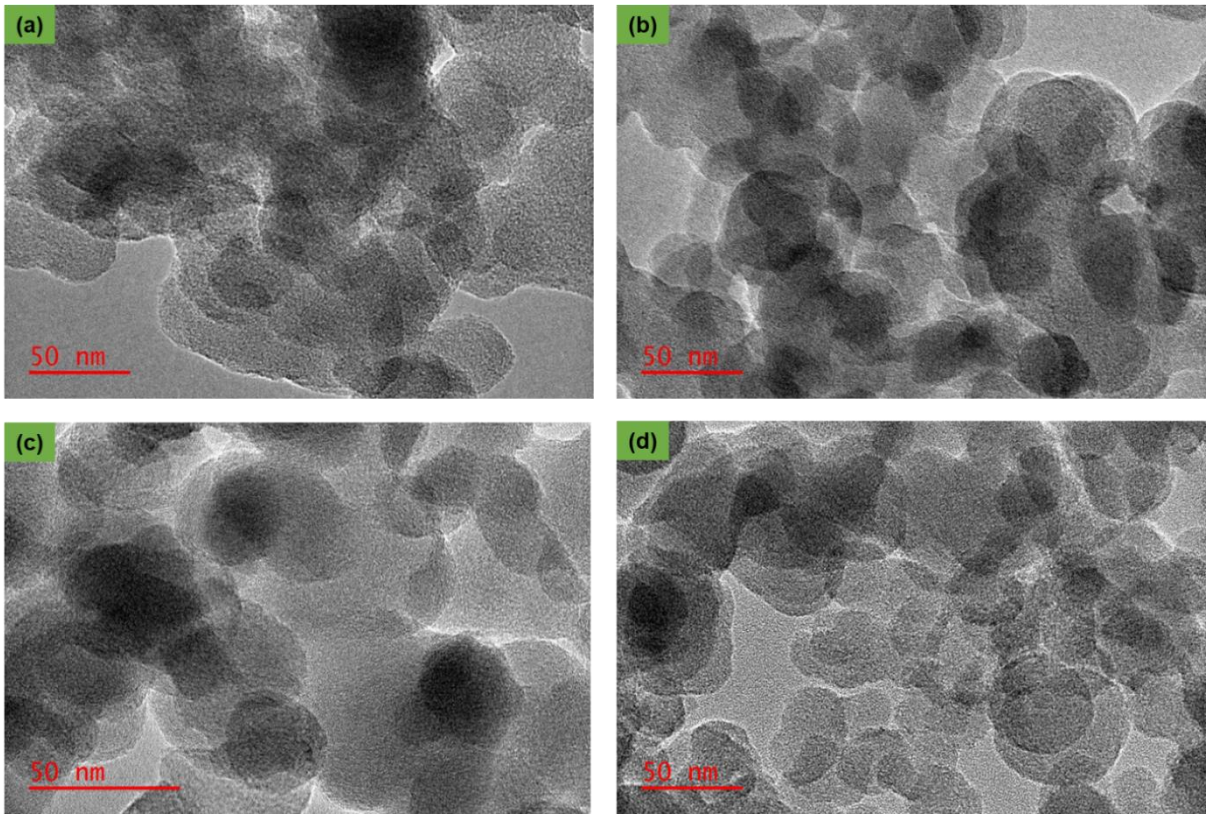

Figure 8.3: TEM micrographs for the (a) FeC-25, (b) FeC-50, (c) FeC-100, and (d) FeC-170 nanocomposites

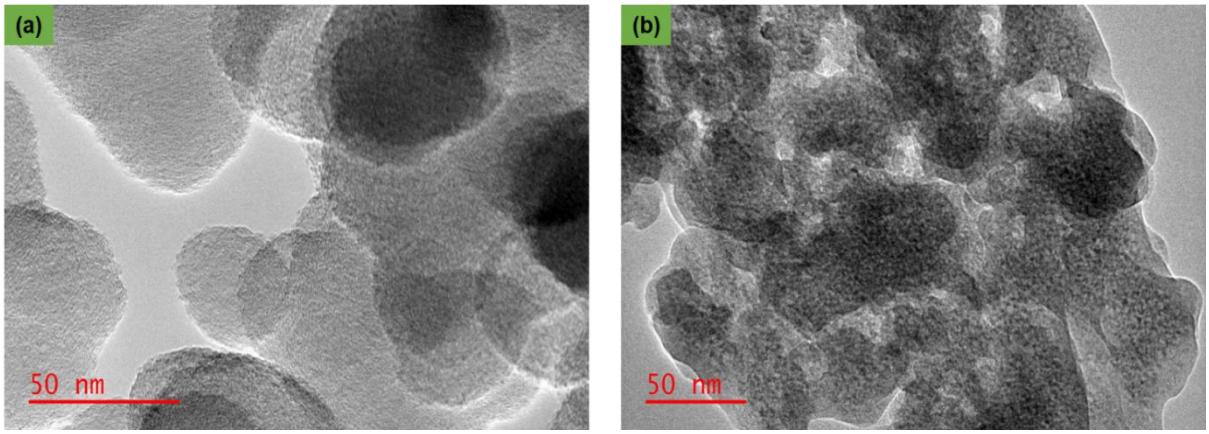

Figure 8.4: TEM micrographs for pristine OLNCs (a) and iron oxide nanoparticles (b)

8.2.3. PXRD patterns for the FeC nanocomposites

The X-ray diffraction spectra for the nanocomposites are displayed in Figure 8.5. The presence of magnetite (Fe_3O_4) and hematite Fe_2O_3) were present as part of the nanocomposites in all the materials, as shown by the diffraction peaks at approximately 2θ = 20°, 28°, 32 -33°, 37°, 39°, 40°, 46°, 47° and 54°, corresponding to the (1 1 1), (2 2 0), (2 2 1), (3 1 1), (4 0 0), (1 0 4), (1 1 3), (0 2 4) and (4 2 2)

planes respectively as indicative by the JCPDS no: 39-1346, 4-755, and 65-3107 files. (Jafari et al., 2015). It is to be mentioned that the peak at 2θ = 20° was not present in the FeC-25 spectrum. The XRD patterns for magnetite and hematite are close to each other thus, not easy to separate them [21]. The Debye-Scherrer's equation was used to compute the crystalline size (*D*) of the iron oxide nanoparticles using the tallest peak, as shown in equation 21:

$$D = \frac{0.9\lambda}{\beta cos\ \theta} \tag{21}$$

where: the wavelength was represented by λ (Cu Kα, with λ = 0.15418 nm), the full width at half maximum (FWHM) of the intense peak was represented by β (rad) and the Braggs angle was represented by θ (rad). The average crystalline size of the nanocomposites was calculated to be 7.64 nm (FeC-25), 4.39 nm (FeC-50), 8.44 nm (FeC-100), and 5.44 nm (FeC-170).

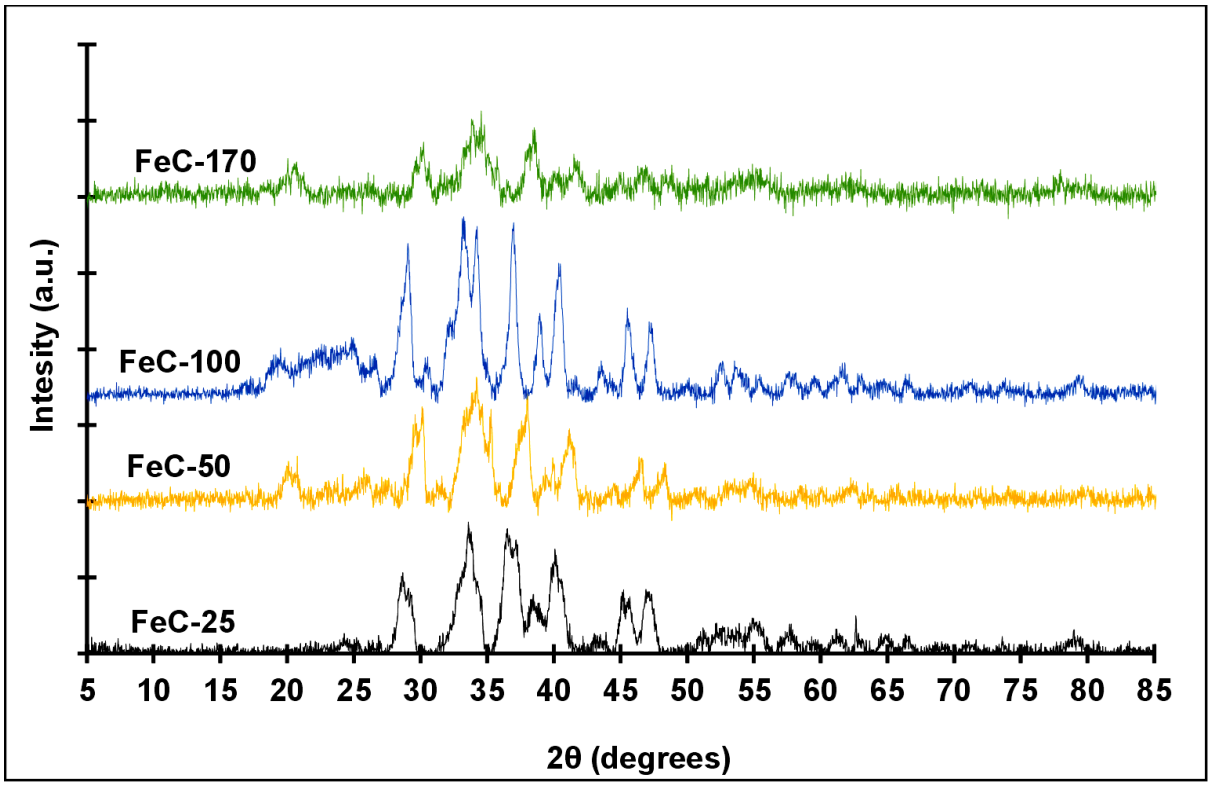

Figure 8.5: PXRD spectra for the FeC-170, FeC-100, FeC-50, and FeC-25 nanocomposites

8.2.4. Effect of the amount of OLNCs and solution pH

Authors such as Zhang et al. and Park et al. have used iron oxide-derived adsorbents for the removal of Cr(VI) ions. They reported that the optimum pH was pH = 4 [22,23]. Therefore, pH = 4 was selected to test the removal of Cr(VI) ions using the nanocomposites by varying the amount of OLNCs in the iron oxide/OLNCs nanocomposites with the results displayed in Figure 8.6a. When the iron oxide was used alone, it showed a 17% Cr(VI) ion removal, which is attributed to the ability of iron oxide to reduce Cr(VI) to Cr(III).

It can be seen that the removal of Cr(VI) ions increased with the increase of OLNCs content, as follows: FeC-25 (49%) < FeC-50 (64%) < FeC-100 (75%) < FeC-170 (88%). This was attributed to an increased number of carbonyl groups present in the OLNCs that could act as the active sites in the removal of Cr(VI) ions and electron donor groups for the reduction [19]. Compared to our previous study of the removal of Cr(VI) ions using pristine OLNCs. The nanocomposites showed faster removal at 49% > in 180 min than the 96% for pristine OLNCs in 720 min attributed to the influence of iron oxide [18].

Only the FeC-100 and FeC-170 composites were used in subsequent experiments since they showed the highest removal percentages.

8.2.5. Effect of pH

The initial solution pH is one of the most influential parameters in an adsorbent-adsorbate interaction.

The removal of Cr(VI) ions was tested by varying the solution pH using the FeC-100 and FeC-170 nanocomposites with results shown in Figure 8.6b. For the FeC-100 adsorbent, it can be seen that the highest removal took place under acidic conditions. This is probably due to the competition for active sites between the OH^- ions and the oxyanions of Cr(VI) resulting in surface repulsion under alkaline conditions Shooto et al. 2020 reported a similar trend when using plant roots for the removal of Cr(VI) ions [24].

However, the FeC-170 adsorbent shows that the solution pH does not impact the removal of Cr(VI), showing 100% removal efficiency throughout the pH range. This

can be attributed to the synergistic effect between the OLNCs and the iron oxide nanoparticles, where OLNCs can also give electrons for the reduction of Cr(VI) to Cr(III) as iron nanoparticles [25].

To check for the possible reduction of Cr(VI) to Cr(III), both ions were monitored throughout the checked pH range (Figure 8.6c) at a short experiment time. Experiments during 60 minutes were run to be able to measure Cr(III) before its adsorption onto the nanocomposite, even the removal percentage decreased as seen in Figure 8.6d (comparing with longer experiment at 180 minutes collected in Figure 8.6b). This removal efficiency decreases with the pH increase at a shorter time probably can be due to electrostatic attraction under acidic conditions and repulsion in alkaline conditions of chromium with the nanocomposite's sites. It has been well reported that carbon material with electron donor groups can reduce Cr(VI) to Cr(III) [11,26]. This resulted in synergistic adsorption coupled reduction mechanism, where the obtained Cr(III) ions can be adsorbed to the surface of the nanocomposites through the carbonyl groups, as previously reported [26].

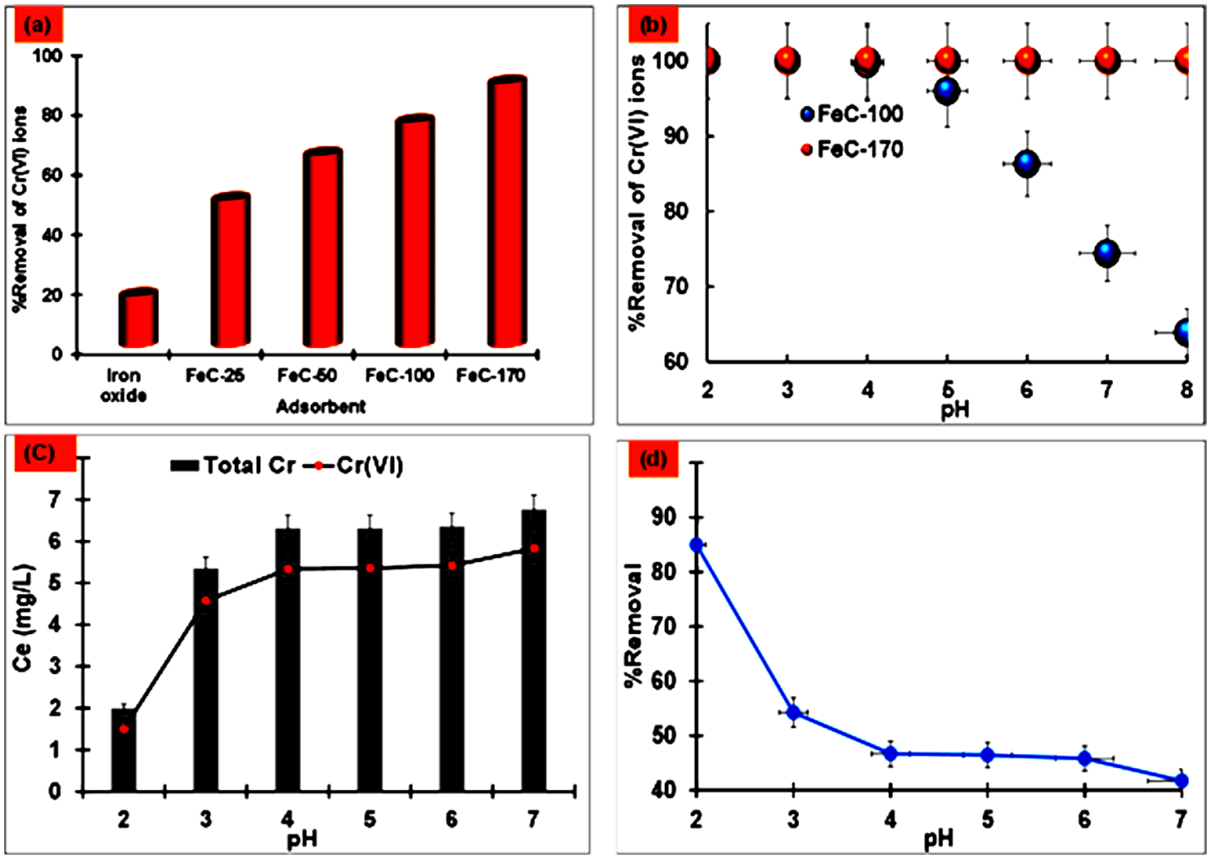

Figure 8.6: Influence of nanocomposite iron oxide OLNCs and pH on the chromium removal percentage and/or the adsorbent capacity: a) nanocomposite materials based on iron oxide

OLNCs; b) pH for FeC-100 and FeC-170 at 180 min; c) determination of the chromium speciation against pH at 60 min for FeC-170 (Cr(VI) and Cr(III) ions determination in solution), and d) pH for FeC-170 at 60 min, Experimental conditions: C_O = 10 mg/L of Cr(VI), V = (5 mL at 60 min and 1 mL at 180 min), 10 mg of adsorbents, and pH range from 2 to 8 (just pH= 4.0 for Figure 8.5a).

8.2.6. Effect of contact time and kinetics

The influence of the contact time between the adsorbent and the adsorbate was determined (1 to 180 min) using the FeC-170 nanocomposite (Figure 8.7). It could be observed that as the time increased the removal efficiency increased until equilibrium was reached [27]. The removal trend was separated into two steps. (i) a rapid reaction within 20 min where a high mass transfer was reached (around 96%) [28]. (ii) a slower step (20 min to 120 min) as equilibrium is reached. Similar results have been previously noted for the removal of Cr(VI) ions by different chemically treated biomass [29].

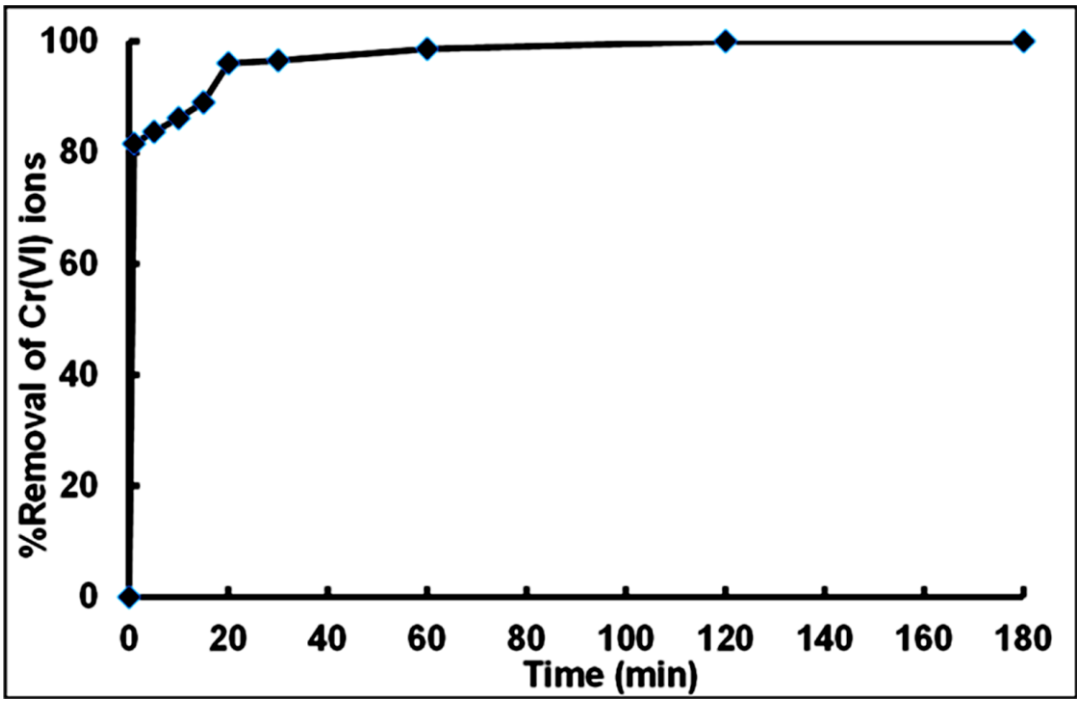

Figure 8.7: Influence of the contact time on the removal of Cr(VI) ions using FeC-170 adsorbent. Experimental conditions: C_O = 10 mg/L of Cr(VI), V = 1 mL, 10 mg of FeC-170, and pH 4.0.

Attempts were made to fit pseudo-first-order (PFO) and the pseudo-second-order (PSO) linear and nonlinear models to the data for the first 20 min of the interaction. The PSO kinetic model fitted the experimental data for both 20 min (see supplementary data Figure 8.8 (c and d) and Table S8.1) and 180 min data (Figure

8.8 (a and b) and Table 8.2). Interestingly studies by Ho and McKay and Tran et al. previously suggested that the PFO kinetic model best fitted their studies [30,31]. This behaviour could be attributed to a chemisorption mechanism [31] for the chromium (VI) adsorption onto the FeC-170 adsorbent. Attempts to model the data by using a nonlinear adjustment to both the PFO and PSO models (not presented) did not give a better fit to the data (Table 8.2).

The adsorbent showed rapid removal of Cr(VI) ions as indicated by the rate constant value (k_2 = 1.17 g/mg x min) and the initial adsorption rate value (h = 1.17 mg/g x min) (Table 2). This was attributed to the availability of active sites and the ability of the nanocomposite to reduce Cr(VI) ions to Cr(III) ions followed by adsorption of Cr(III) ions as discussed in section 8.2.5.

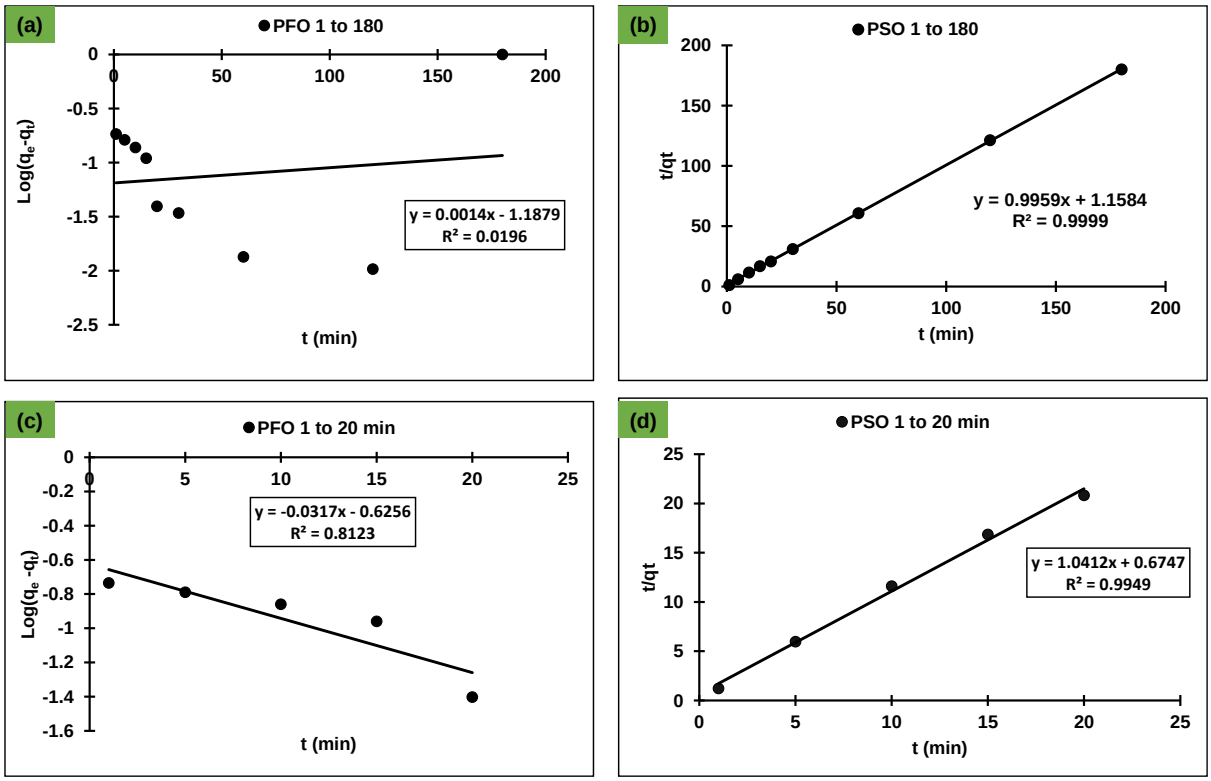

Figure 8.8: Linear plots of the PFO and PSO models (a and b) from 1 to 180 and (c and d) from 1 to 20 min for the FeC-170 nanocomposite

Table 8.2: Kinetic parameters for the PSO and PFO models.

PSO model				
	R^2	q_e (mg/g)	k_2 (g/mg x min)	h (mg/g x min)
Linear	1.00	1.00	1.17	1.17
Nonlinear	0.956	0.910	1.00	0.912
PFO model				
	R^2	q_e (mg/g)	k_1 (1/min)	
Linear	0.350	9.67	0.00250	
Nonlinear	0.814	1.00	0.115	

8.2.7. Effect of initial adsorbate concentration and isotherm modelling

The initial adsorbate (Cr(VI)) concentration [C_O (mg/L)] was evaluated from 1 to 150 mg/L and the results are presented in Figure 8.9a. It was observed that as the initial adsorbate concentration was increased that the removal efficiency decreased (91% chromium removal). This is attributed to the adsorbate-to-adsorbent active site ratio being lower at lower chromium solution concentration, resulting in an expected high removal efficiency [32]. As expected, the adsorption capacity [q_e (mg/g)] increased as the initial adsorbate concentration was increased [32].

The non-linear forms of the Langmuir adsorption isotherm [33] and the Freundlich adsorption isotherm [34] were selected to adjust the obtained experimental data. The model profiles are presented in Figure 8.9b with the model parameters collected in Table 8.3. It can be seen that at high equilibrium concentrations (C_e; mg/L) the isotherm plots did not reach saturation. This indicates that the active sites of the adsorbent are not fully occupied by the adsorbate ions [35], as demonstrated by the removal efficiency of 91% (Figure 8.9a).

The R^2 values for the Langmuir and the Freundlich model were closer to one and the experimental data was close to both models. This cloud indicates that the removal of Cr(VI) ions was through both the monolayer surface coverage and heterogeneous surface coverage. The maximum adsorption capacity (Q_{max}, mg/g) for both isotherms

was found to be 17.8 mg/g (Langmuir) and 11.1 mg/g (Fruendlich) is 17.75 mg/g. The Langmuir equilibrium constant (K_L: 0.1814 L/mg) relays to the adsorbate-adsorbent affinity and the (K_F: 6.21 (mg/g)/(mg/L)^n) is the Freundlich constant [30].

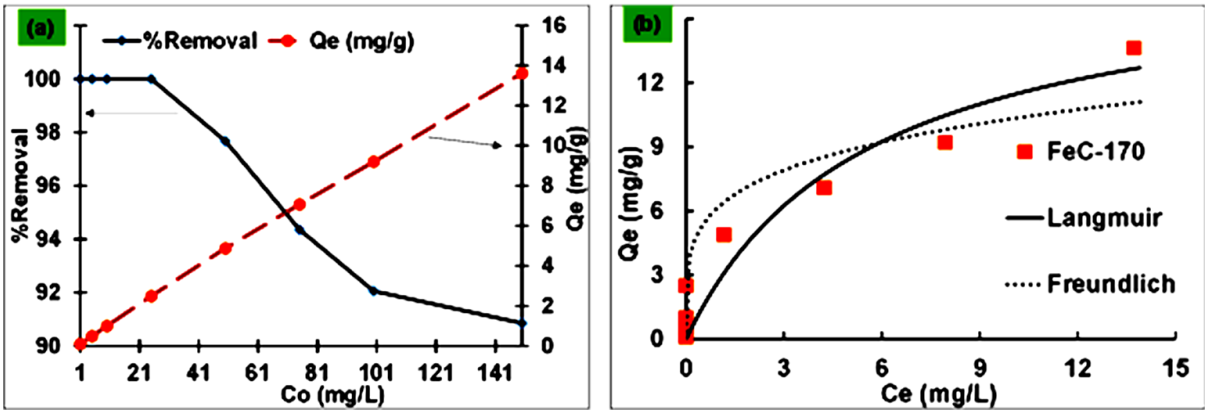

Figure 8.9: Plots for the (a) removal vs adsorption capacity and (b) adsorption isotherms. Experimental conditions: pH 4.0, V = 1 mL, and 10 mg of FeC-170, and time of the experiment is 180 min.

Table 8.3: Parameters for the adsorption isotherms

Langmuir isotherm				
Adsorbent	**R^2**	**Q_{max} (mg/g)**	***K_L (L/mg)***	
FeC-170	0.916	17.8	0.181	
Freundlich isotherm				
Adsorbent	**R^2**	**Q_{max} (mg/g)**	***K_F [(mg/g) (L/mg)^n]***	**n**
FeC-170	0.884	11.1	6.21	0.221

8.2.8. Comparison of the adsorption capacities of the nanocomposites

Different adsorption capacities for the removal of Cr(VI) ions by various adsorbent systems are collected in Table 8.4 and compared with the ONLC nanocomposites studied in this work. It is to be noted that a direct comparison does require the use of the same experimental conditions, such as adsorbent mass, adsorbate volume, initial concentration range, temperature, and time to mention a few. These vary from one study to the next (table 8.4). However, the adsorption capacity can be used to compare the effectiveness of an adsorbent.

It can be seen from Table 8.4 that the removal of Cr(VI) ions is typically carried out using acidic to neutral pH values. This is due to the electrostatic attraction between the adsorbate and adsorbent. As the adsorbent is mostly protonated and the adsorbate sites are in the anionic form at this pH range, carboxylic acid groups are considered the major sites of adsorption [12]. In all cases, the experimental data can be explained by the Langmuir isotherm model, suggestive of the importance of monolayer surface coverage. The adsorption capacity of the FeC-170 adsorbent was comparable with the other adsorbents (Table 8.4). The chitosan-iron oxide adsorbent returned the highest adsorption capacity of 92.04 mg/g, and the reason for this outlier could provide a direction for future studies using the OLCNs.

Table 8.4: Adsorption capacity for Cr(VI) removal by different nano-based adsorbents.

Adsorbent	Treatment	pH	Qe (mg/g)	Isotherm	Reference
Fe_3O_4	None	4	8.67	Langmuir	[22]
Chitosan	Fe_2O_3	4	14.45	Langmuir	[23]
Pinecone	Fe_3O_4	3	15.24	Langmuir	[36]
Chitosan	Iron oxide	5	92.04	Langmuir	[37]
Activated carbon	Fe_3O_4	3	5.76	Langmuir	[38]
Biochar	ZnO	5 - 8.5	43.84	Langmuir	[39]
Biochar	Iron	2	11.13	Langmuir	[40]
Pine/TiO_2	TiO_2	4	12.80	Langmuir	[12]
iron oxide/OLNC	OLNCs	4	17.75	Langmuir	This study

8.2.9. Photo-reduction of Cr(VI) to Cr(III)

A solar simulator was used as a source of light in the photo-reduction experiments. The impact of the source of light on a Cr solution without a catalyst is shown in Figure 8.10; only 0.64% of Cr(VI) ions were reduced to Cr(III) after 1 h, consistent with literature data [41].

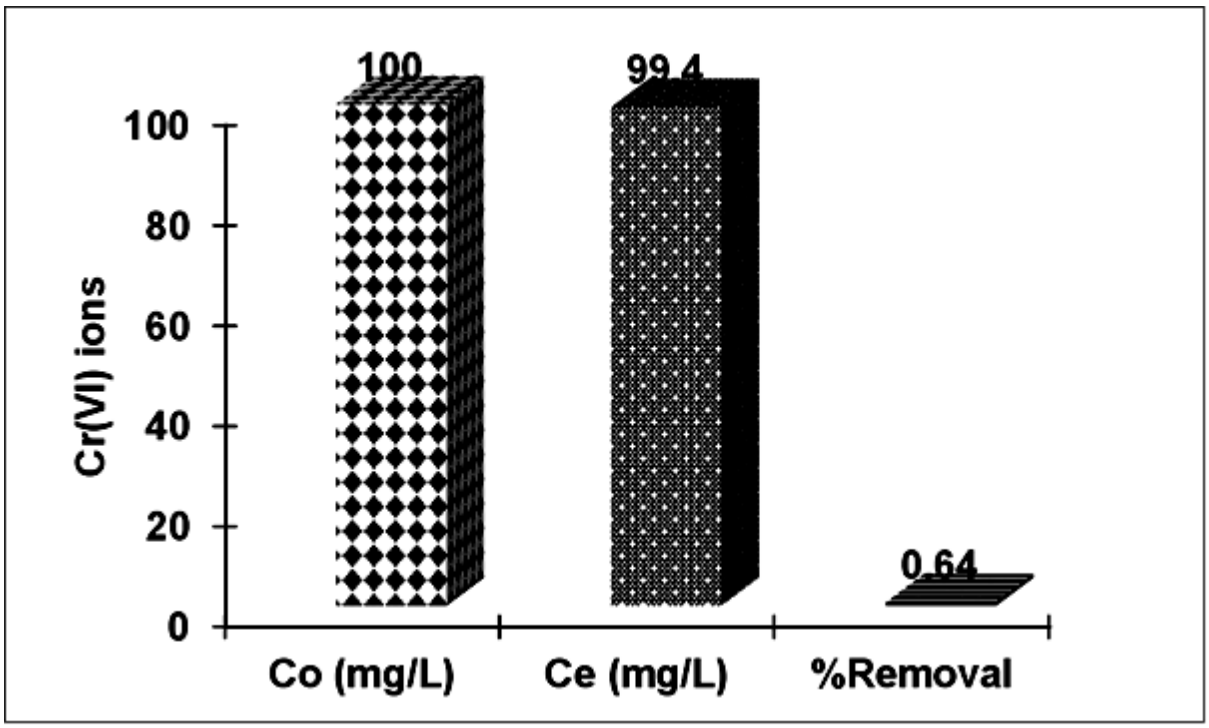

Figure 8.10: Photolysis experiments: the concentration of Cr(VI) in solution is represented against the initial and the equilibrium Cr(VI) concentration percentage and respect the removal percentage (data included onto the histograms). Experimental conditions: pH 4.0, V=1 mL, and 10 mg of FeC-170, and time of the experiment is 60 minutes.

The adsorption using the FeC-170 nanocomposite was studied under dark conditions for 30 min. In this case, an 86% reduction of Cr(VI) ions was observed, as shown in Figure 8.11a. This indicates that adsorption-coupled reduction is the principal driving force for the removal of the Cr(VI). This is attributed to the electron donor groups from the surface of the nanocomposites, as discussed in section 8.2.5.

The light-induced reduction of Cr(VI) ions to Cr(III) in presence of the nanocomposite was then studied. It was observed that the reduction of Cr(VI) ions under solar radiation is rapid (15 min; Figure 8.11b). This was significantly faster than the 180 min without light irradiation (see section 8.2.5).

Thus, the reduction of Cr(VI) to Cr(III) ions is attributed to both the electron donor properties of the nanocomposite and a photolysis effect. In other words, the reduced ability of the nanocomposite is improved under light irradiation. This can be explained as follows the OLNC act as a trapping agent for the generated holes limiting

recombination. It is to be noted that after 15 min the Cr(III) ions that were produced were subsequently adsorbed on the surface of the nanocomposite (iron oxide/OLNC).

The experiment was allowed to continue for another 30 min to monitor any desorption processes; none were observed. Furthermore, the resulting solution was tested for the presence of iron, and no iron was detected in the solution. The composite is thus stable during the adsorption-photoreduction experiments.

The nanocomposite photocatalyst was reused (5 times) and the efficiency decreased to 86% (Figure 8.11c). This is believed to be due to mechanical losses as it was necessary to filter the solution between cycles resulting in Fe-OLNC mass loss.

In summary, the incorporation of iron onto OLNCs resulted in photocatalytic nanocomposites that had a synergistic effect with a source of light assisting the removal of Cr(VI) ions. A simultaneous adsorption/reduction of Cr(VI) followed by adsorption of Cr(III) thus occurs in the process of chromium removal from wastewater.

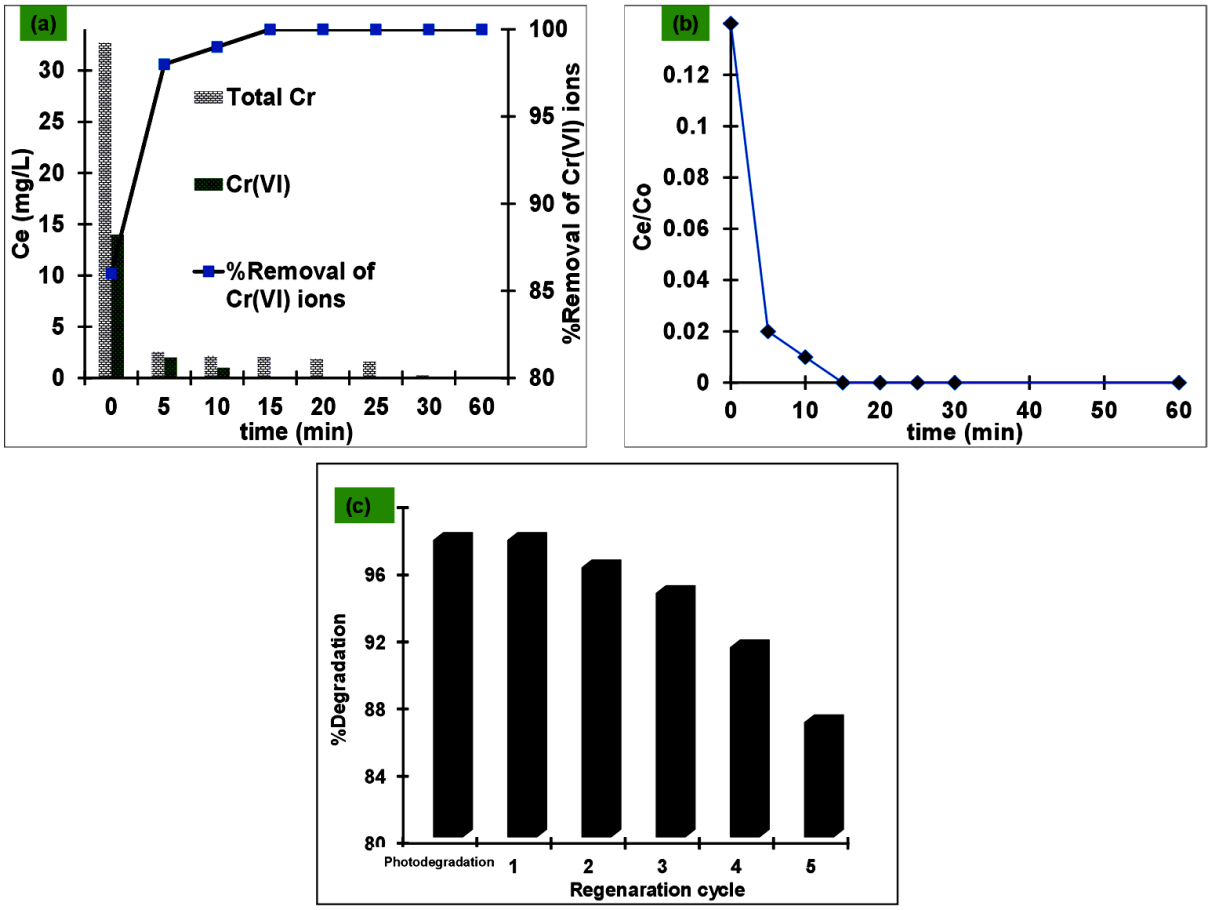

Figure 8.11: (a) The equilibrium concentration for Cr(VI) and total Cr, and the removal percentage of Cr(VI) ions against time; (b) Cr(VI) reduction rate against time, were C_e is the Cr(VI) concentration at any time and C_o is the initial Cr(VI) concentration; and (c)

8.3. Conclusions

Waste cooking oil was used as a starting material for the synthesis of OLNCs via the flame pyrolysis method. The iron oxide nanoparticles and the OLNCs were used to make nanocomposites. The nanocomposites were applied as adsorbents for the adsorption/reduction of Cr(VI) ions. The FeC-170 material gave the best results (pH range of 2 to 8), and data showed that the removal of Cr(VI) ions was driven by an adsorption-coupled reduction mechanism. Complete removal of Cr(VI) ions was observed in 120 min, with the experimental data explained by a PSO kinetic model and a Langmuir adsorption isotherm model with a maximum adsorption capacity of 17.75 mg/g.

The photocatalytic activity of the FeC-170 material was studied for Cr ion reduction or removal. A synergistic photocatalytic reduction of Cr(VI) ions to Cr(III) ions was found.

The reduction rate was rapid with complete reduction taking place in 15 min. The remaining Cr(III) ions in the solution were also adsorbed on the surface of the nanocomposite (FeC-170), through the aid of the OLCN carbonyl groups. Complete elimination of both Cr(VI) ions and Cr(III) ions took place in 30 min. The photocatalyst could be reused 5 times with good efficiency for chromium removal.

The nanocomposites made from iron oxide nanoparticles and the OLNCs showed potential as effective adsorbents and photocatalysts for the elimination of Cr(VI) ions and Cr(III) ions via an adsorption-coupled photoreduction process.

8.4. References

[1] U. EPA, Chromium compounds, Natl. Cent. Environ. Assessment, Off. Res. Dev. (2000) 639–700.

[2] S.A. Katz, H. Salem, The toxicology of chromium with respect to its chemical speciation: A review, J. Appl. Toxicol. 13 (1993) 217–224. https://doi.org/10.1002/jat.2550130314.

[3] World Health Organization, Guidelines for drinking-water quality, 2008. https://doi.org/10.1016/S1462-0758(00)00006-6.

[4] N. Kohila, P. Subramaniam, Removal of Cr(VI) using polyaniline based Sn(IV), Ce(IV) and Bi(III) iodomolybdate hybrid ion exchangers: Mechanistic and comparative study, J. Environ. Chem. Eng. 8 (2020) 104376. https://doi.org/10.1016/j.jece.2020.104376.

[5] G. Asgari, A. Sidmohammadi, A.R. Rahmani, M.R. Samargandi, H. Faraji, Enhancing photo-precipitation of Cr(VI) with sulfur dioxide radical: Mechanism, kinetic and energy consumption and sludge survey, Optik (Stuttg). 218 (2020) 164983. https://doi.org/10.1016/j.ijleo.2020.164983.

[6] Y. Zhang, X. Xu, C. Yue, L. Song, Y. Lv, F. Liu, A. Li, Insight into the efficient co-removal of Cr(VI) and Cr(III) by positively charged UiO-66-NH2 decorated ultrafiltration membrane, Chem. Eng. J. 404 (2021). https://doi.org/10.1016/j.cej.2020.126546.

[7] K. Lu, M. Gao, B. Sun, M. Wang, S. Wang, X. Wang, Simultaneous removal of Cr and organic matters via coupling Cr-Fenton-like reaction with Cr flocculation:

The key role of Cr flocs on coupling effect, Chemosphere. 287 (2022) 131991. https://doi.org/10.1016/j.chemosphere.2021.131991.

[8] T. Xu, Y. Zhou, X. Lei, B. Hu, H. Chen, G. Yu, Study on highly efficient Cr(VI) removal from wastewater by sinusoidal alternating current coagulation, J. Environ. Manage. 249 (2019) 109322. https://doi.org/10.1016/j.jenvman.2019.109322.

[9] B. Kullu, D.K. Patra, S. Acharya, C. Pradhan, H.K. Patra, AM fungi mediated bioaccumulation of hexavalent chromium in Brachiaria mutica-a mycorrhizal phytoremediation approach, Chemosphere. 258 (2020) 127337. https://doi.org/10.1016/j.chemosphere.2020.127337.

[10] A.U. Rajapaksha, R. Selvasembian, A. Ashiq, V. Gunarathne, A. Ekanayake, V.O. Perera, H. Wijesekera, S. Mia, M. Ahmad, M. Vithanage, Y.S. Ok, A systematic review on adsorptive removal of hexavalent chromium from aqueous solutions: Recent advances, Sci. Total Environ. 809 (2022) 152055. https://doi.org/10.1016/j.scitotenv.2021.152055.

[11] T.D. Ntuli, V.E. Pakade, Hexavalent chromium removal by polyacrylic acid-grafted Macadamia nutshell powder through adsorption–reduction mechanism: Adsorption isotherms, kinetics and thermodynamics, Chem. Eng. Commun. 207 (2019) 1–16. https://doi.org/10.1080/00986445.2019.1581619.

[12] J. Zhao, R. Boada, G. Cibin, C. Palet, Enhancement of selective adsorption of Cr species via modification of pine biomass, Sci. Total Environ. 756 (2021) 143816. https://doi.org/10.1016/j.scitotenv.2020.143816.

[13] S. Liu, T. Yu, M. Xu, M. Zhai, J. Peng, J. Li, Synthesis of novel aminated cellulose microsphere adsorbent for efficient Cr(VI) removal, Radiat. Phys. Chem. 125 (2016) 94–101. https://doi.org/10.1016/j.radphyschem.2016.03.019.

[14] D. Park, Y.-S. Yun, J.H. Jo, J.M. Park, Mechanism of hexavalent chromium removal by dead fungal biomass of Aspergillus niger, Water Res. 39 (2005) 533–540.

[15] V.E. Pakade, N.T. Tavengwa, L.M. Madikizela, Recent advances in hexavalent chromium removal from aqueous solutions by adsorptive methods, RSC Adv. 9

(2019) 26142–26164. https://doi.org/10.1039/c9ra05188k.

[16] E. Amdeha, R.S. Mohamed, A.S. Dhmees, Sonochemical assisted preparation of ZnS–ZnO/MCM-41 based on blast furnace slag and electric arc furnace dust for Cr(VI) photoreduction, Ceram. Int. 47 (2021) 23014–23027. https://doi.org/10.1016/j.ceramint.2021.05.015.

[17] Y. Li, J. Zhang, C. Zhan, F. Kong, W. Li, C. Yang, B.S. Hsiao, Facile synthesis of TiO_2/CNC nanocomposites for enhanced Cr(VI) photoreduction: Synergistic roles of cellulose nanocrystals, Carbohydr. Polym. 233 (2020). https://doi.org/10.1016/j.carbpol.2020.115838.

[18] T.D. Ntuli, T.H. Mongwe, L.L. Sikeyi, O. Mkhari, N.J. Coville, E.N. Nxumalo, M.S. Maubane-Nkadimeng, Removal of hexavalent chromium via an adsorption coupled reduction mechanism using olive oil derived carbon nano-onions, Environ. Nanotechnology, Monit. Manag. 16 (2021) 100477. https://doi.org/10.1016/j.enmm.2021.100477.

[19] S. Sathya, V. Ragul, V.P. Veeraraghavan, L. Singh, M.I. Niyas Ahamed, An in vitro study on hexavalent chromium [Cr(VI)] remediation using iron oxide nanoparticles based beads, Environ. Nanotechnology, Monit. Manag. 14 (2020) 100333. https://doi.org/10.1016/j.enmm.2020.100333.

[20] N.K. Park, J.D. Lee, T.J. Lee, S.O. Ryu, C.H. Chang, The preparation of a high surface area metal oxide prepared by a matrix-assisted method for hot gas desulphurization, Fuel. 84 (2005) 2165–2171. https://doi.org/10.1016/j.fuel.2005.06.010.

[21] T. Tuutijärvi, J. Lu, M. Sillanpää, G. Chen, As(V) adsorption on maghemite nanoparticles, J. Hazard. Mater. 166 (2009) 1415–1420. https://doi.org/10.1016/j.jhazmat.2008.12.069.

[22] J. Zhang, S. Lin, H. Meiling, S. Qing, X. Liancu, Adsorption Properties of Magnetic Magnetite Nanoparticle for Coexistent Cr(VI) and Cu(II) in Mixed Solution, Water. 12 (2020) 1–13.

[23] J.E. Park, J.-H. Shin, W. Oh, S.-J. Choi, J. Kim, C. Kim, J. Jeon, Removal of Hexavalent Chromium(VI) from Wastewater Using Chitosan-Coated Iron Oxide

Nanocomposite Membranes, Toxics. 10 (2022) 98. https://doi.org/10.3390/toxics10020098.

[24] N.D. Shooto, Removal of lead(II) and chromium(VI) ions from synthetic wastewater by the roots of harpagophytum procumbens plant, J. Environ. Chem. Eng. 8 (2020) 104541. https://doi.org/10.1016/j.jece.2020.104541.

[25] Z. Pan, X. Zhu, A. Satpathy, W. Li, J.D. Fortner, D.E. Giammar, Cr(VI) Adsorption on Engineered Iron Oxide Nanoparticles: Exploring Complexation Processes and Water Chemistry, Environ. Sci. Technol. 53 (2019) 11913–11921. https://doi.org/10.1021/acs.est.9b03796.

[26] D. Park, S.R. Lim, Y.S. Yun, J.M. Park, Reliable evidences that the removal mechanism of hexavalent chromium by natural biomaterials is adsorption-coupled reduction, Chemosphere. 70 (2007) 298–305. https://doi.org/10.1016/j.chemosphere.2007.06.007.

[27] A.T. Hoang, S. Nižetić, C.K. Cheng, R. Luque, S. Thomas, T.L. Banh, V.V. Pham, X.P. Nguyen, Heavy metal removal by biomass-derived carbon nanotubes as a greener environmental remediation: A comprehensive review, 2022. https://doi.org/10.1016/j.chemosphere.2021.131959.

[28] M.C. Qhubu, L.G. Mgidlana, L.M. Madikizela, V.E. Pakade, Preparation, characterization and application of activated clay biochar composite for removal of Cr(VI) in water: Isotherms, kinetics and thermodynamics, Mater. Chem. Phys. 260 (2021) 124165. https://doi.org/10.1016/j.matchemphys.2020.124165.

[29] O.B. Nchoe, T.D. Ntuli, M.J. Klink, F.M. Mtunzi, V.E. Pakade, A comparative study of acid, base and Fenton-like reagent treated biomass for Cr(VI) sequestration from aqueous solutions, Water Environ. Fed. 93 (2020) 370–383. https://doi.org/10.1002/wer.1421.

[30] H.N. Tran, S.J. You, A. Hosseini-Bandegharaei, H.P. Chao, Mistakes and inconsistencies regarding adsorption of contaminants from aqueous solutions: A critical review, Water Res. 120 (2017) 88–116. https://doi.org/10.1016/j.watres.2017.04.014.

[31] Y.S. Ho, G. McKay, The Kinetics of Sorption of Basic Dyes from Aqueous

Solution by Sphagnum Moss Peat, Can. J. Chem. Eng. 76 (1998) 822–827. https://doi.org/10.1002/cjce.5450760419.

[32] T.A.H. Nguyen, H.H. Ngo, W.S. Guo, J. Zhang, S. Liang, Q.Y. Yue, Q. Li, T. V. Nguyen, Applicability of agricultural waste and by-products for adsorptive removal of heavy metals from wastewater, Bioresour. Technol. 148 (2013) 574–585. https://doi.org/10.1016/j.biortech.2013.08.124.

[33] I. Langmuir, The adsorption of gases on plane surfaces of glass, mica and platinum., J. Am. Chem. Soc. 40 (1918) 1361–1403. https://doi.org/doi: 10.1021/ja02242a004.

[34] H. Freundlich, Über die Adorption in Lösungen, Z Phys.Chem. 57 (1906) 385–471.

[35] M. Moyo, V.E. Pakade, S.J. Modise, Biosorption of lead(II) by chemically modified Mangifera indica seed shells: Adsorbent preparation, characterization and performance assessment, Process Saf. Environ. Prot. 111 (2017) 40–51. https://doi.org/10.1016/j.psep.2017.06.007.

[36] A. Pholosi, E.B. Naidoo, A.E. Ofomaja, Batch and continuous flow studies of Cr(VI) adsorption from synthetic and real wastewater by magnetic pine cone composite, Chem. Eng. Res. Des. 153 (2020) 806–818. https://doi.org/10.1016/j.cherd.2019.11.004.

[37] J. Lu, B. Li, W. Li, X. Zhang, W. Zhang, P. Zhang, R. Su, D. Liu, Nano iron oxides impregnated chitosan beads towards aqueous Cr(VI) elimination: Components optimization and performance evaluation, Colloids Surfaces A Physicochem. Eng. Asp. 625 (2021) 126902. https://doi.org/10.1016/j.colsurfa.2021.126902.

[38] M.C. Qhubu, P.N. Nomngongo, V.E. Pakade, Exploring the Iron Oxide Functionalized Biobased Carbon-silica-polyethyleneimine Composites for Hexavalent Chromium Removal from Dilute Aqueous Solutions, Water. 13 (2021) 1–20.

[39] J. Yu, C. Jiang, Q. Guan, P. Ning, J. Gu, Q. Chen, J. Zhang, R. Miao, Enhanced removal of Cr(VI) from aqueous solution by supported ZnO nanoparticles on biochar derived from wastewater hyacinth, Chemosphere. 195 (2018) 632–640.

https://doi.org/10.1016/j.chemosphere.2017.12.128.

[40] K. Qiao, W. Tian, J. Bai, J. Zhao, Z. Du, T. Song, M. Chu, L. Wang, W. Xie, Synthesis of floatable magnetic iron/biochar beads for the removal of chromium from aqueous solutions, Environ. Technol. Innov. 19 (2020) 100907. https://doi.org/10.1016/j.eti.2020.100907.

[41] S.L. Wang, C.C. Chen, Y.M. Tzou, C.L. Hsu, J.H. Chen, C.F. Lin, A mechanism study of light-induced Cr(VI) reduction in an acidic solution, J. Hazard. Mater. 164 (2009) 223–228. https://doi.org/10.1016/j.jhazmat.2008.07.145.

Chapter 9: Conclusions

Conclusions

Onion-like nanocarbons (OLNCs) have been respectively synthesized from the flame pyrolysis of vegetable cooking oil (olive oil) and waste cooking oil. The OLNCs from olive oil as a carbon source was treated with 10% and 25% H_2O_2 and 1 M and 2 M KOH. The pristine OLNCs and the chemically modified OLNCs were applied in the removal of Cr(VI) ions.

The morphological characteristics of the OLNCs from olive oil resembled that of an onion being quasi-spherical, having multiple layers with cavities at the centre and closely packed together with an average diameter of 46 ± 5 nm. The surface of the OLNCs consisted mainly of carbon, oxygen and hydrogen functional groups. The material was applied in the removal of Cr(VI) ions from solutions in singular and complex matrices with Cu(II) and Ni(II) ions.

The optimum conditions for the removal of Cr(VI) ions were found to be at pH = 2, C_O = 10 mg/L, mass = 0.025 g, and T = 25°C. The XPS data showed the presence of Cr(III) on the surface of the OLNCs after the removal of Cr(VI) ions indicative of an adsorption-coupled reduction removal mechanism. This was supported by the kinetic data that was better explained by the pseudo-second-order kinetic model indicating the possibility of chemisorption. The experimental data fitted well with the Langmuir adsorption isotherm showing that the removal of Cr(VI) ions was via a monolayer surface coverage.

The removal of Cr(VI) ions using the OLNCs as an adsorbent in the presence of Cu(II) and Ni(II) ions did not negatively affect the removal of Cr(VI) ions, returning 98% removal efficiency. The removal efficiency of Cu(II) and Ni(II) ions was 87% and 35% respectively. The OLNCs was reused three times and returned a removal efficiency of 99% for the Cr(VI) ions. The thermodynamic data showed that the removal of Cr(VI) ions was favourable, spontaneous, exothermic and involved an associative mechanism. Thus, the OLNCs from olive oil synthesized without the aid of a metal catalyst showed potential in the application of Cr(VI) ions removal from solutions.

The OLNCs were treated with different concentrations of KOH (0.1 M and 0.2 M) and H_2O_2 (10% and 25%). The characterization results showed that the morphology of the chemically treated materials H_2O_2 (10H-NC and 25H-NC) and KOH (0.1K-NC and 0.2K-NC) was similar to that of the pristine OLNCs. The chemically treated materials

retained their structure having multiple layers closely packed together showing a quasi-spherical nature with cavities at the central point. The chemically treated adsorbents had carbonyl and hydroxyl groups on their surface. The material was applied for the removal of Cr(IV) ions from solutions.

The 10H-NC and 25H-NC adsorbents showed higher removal efficiency than the 0.1K-NC and 0.2K-NC adsorbents. This was attributed to a higher surface area and increased oxygen content. The 10H-NC and 25H-NC adsorbents showed higher removal efficiency from pH 2 to pH 8 compared to the use of pH 2 for the 0.1K-NC and 0.2K-NC adsorbents. This was attributed to the influence of the pH_{PZC} which was at pH 7.2 (10H-NC) and 7.4 (25H-NC) for the H_2O_2 treated adsorbents and pH 3.9 (0.1K-NC) and pH 3.2 (0.2K-NC) for the KOH treated adsorbents.

For further comparative and removal mechanism studies involving the Cr(VI) ions, removal studies on 25H-NC and 0.2K-NC were selected. The kinetic data for both the adsorbents was in agreement with the PSO kinetic model, a possible indication that the rate-limiting step could be chemisorption. The 25H-NC absorbent showed more rapid removal of Cr(VI) ions than the 0.2K-NC adsorbent. With the initial adsorption rate (h) = 0.1508 (mg/g x min), rate constant (k_2) = 0.0092 (g/mg x min) at an equilibrium time of 360 min for the 25H-NC adsorbent. This can be compared to h = 0.0622 (mg/g x min), k_2 = 0.0042 (g/mg x min) at an equilibrium time of 1440 min for the 0.2K-NC. This was attributed to the increased surface area and oxygen groups associated with the 25H-NC adsorbent.

The Fruendlich adsorption isotherm fitted the experimental data for both adsorbents indicating that the removal pathway for the Cr(VI) ions took place at the heterogeneous surface for both adsorbents. Due to an increased number of active sites the 25H-NC adsorbent showed maximum adsorption capacity (Q_e) = 41.18 mg/g compared to Q_e = 33.80 mg/g for 0.2K-NC. Both adsorbents showed R_L and n values that were greater than zero and less than 1 indicating that the removal of Cr(VI) ions by both adsorbents was favourable and spontaneous.

Both adsorbents were applied in mixed matrices containing both Cr(VI) ions and methyl orange; both adsorbents showed more than 97% removal of both adsorbates. Both adsorbents were reused 5 times indicating that the chemically treated OLNCs had the potential to be applied in the removal of Cr(VI) ions and methyl orange.

The use of pristine and chemically treated OLNCs was shown to have potential in the removal of Cr(VI) ions from the solution. One of the contributing factors was the

presence of oxygen moieties on the surface of the OLNCs. This was increased by the oxidative treatment of the OLNCs using H_2O_2. Therefore, the OLNCs from olive oil were compared with OLNCs from waste cooking oil.

The OLNCs from waste cooking oil showed similar characteristics to those from olive oil. This included their average size diameter (41 nm), surface area (60–85 m^2/g), onion-like structure, quasi-spherical shape, and presence of carbonyl and hydroxyl functional groups. The waste cooking oil OLNCs showed a higher oxygen content than those from olive oil. This was attributed to the waste oil cooking process that involved hydrogenation and oxygenation.

The optimum conditions for the removal of Cr(VI) ions from the solution using waste cooking oil-derived OLNCs were found to be at pH = 2, t = 360 min, and C_O = 10 mg/L. The maximum adsorption capacity (Q^0_{max}) was found to be 47.62 mg/g, with the h = 2.074 (mg/g x min). Thus, the waste cooking oil OLNCs showed improved removal capabilities relative to the OLNCs made from olive oil. This was attributed to the additional oxygen content as a result of the oxygenation and hydrogenation process that took place during the cooking process.

The study has indicated the potential of converting waste cooking oil to adsorbents that have the capability of removal of Cr(VI) ions from the solution thus, putting value to waste. The OLNCs from waste cooking oil was used for further experiments. The desorption of methyl orange from the surface of the OLNCs showed that the dye was not degraded to less harmful compounds but rather it was adsorbed onto the surface of the OLNCs. Therefore the OLNCs were incorporated with TiO_2 nanoparticles for the formation of TiO_2/OLNCs nanocomposites. These materials were then applied as photocatalysts in the photocatalytic degradation of methyl orange. This was done by varying the mass of the OLNCs (10, 20, 30, and 50 mg) whilst keeping the mass of TiO_2 (100 mg) constant and the photocatalysts were labelled as follows TiO_2, TiC-10, TiC-20, TiC-30, and TiC-50.

It was found that after incorporating the OLNCs with TiO_2 nanoparticles, the OLNCs retained their distinct features. This included their quasi-spherical shape and multiple concentric layers. The TiO_2 phase was found to be that of anatase, as depicted by their PXRD spectral planes. The bandgap energy of the pure TiO_2 was found to be 3.0 eV while the incorporation of the OLNCs had an impact by decreasing the bandgap in the order (TiC-10: 2 eV) < (TiC-20: 2.60 eV) < (TiC-30: 2.80 eV) = (TiC-50: 2.80 eV). In summary, an increase in the mass of the OLNCs gave a bandgap increase.

All the synthesized photocatalysts (TiO_2, TiC-10, TiC-20, TiC-30, and TiC-50) were applied in the photocatalytic degradation of methyl orange. The degradation percentage of the TiO_2 was found to be 44%. This was significantly lower than found for the nanocomposites, TiC-10 (99.9%), TiC-20 (90%), TiC-30 (81%), and TiC-50 (70%). This was attributed to a narrower bandgap and improved adsorption of methyl orange indicating that the dye could be readily degraded.

However, the photocatalyst with the highest amount of OLNCs (TiC-50) had the lowest degradation rate due to the OLNCs blocking the photoactive sites, with the TiC-10 having the highest degradation rate. This was increased by 6 times by the addition of 5% H_2O_2 presumably due to the production of radical groups and a decreased electron/hole recombination. The photocatalyst (TiC-10) was reused five times indicating its potential in the photocatalytic degradation of methyl orange.

The role of the OLNCs was explored further by incorporation with iron oxide nanoparticles. This was achieved by varying the mass of the OLNCs (25, 50, 100, and 170 mg) whilst maintaining the mass of the iron oxide constant at 100 mg. As anticipated, the morphological characteristics of the OLNCs resembled an onion showing multiple layers with a quasi-spherical shape. The surface area of the iron oxide nanoparticles was 1.48 m^2/g and the surface area of the composites was found to be: 5.07 m^2/g (FeC-25), 9.96 m^2/g (FeC-50), 10.86 m^2/g (FeC-100), and 15.48 m^2/g (FeC-170). The PXRD spectra showed the presence of both magnetite (Fe_3O_4) and maghemite (Fe_2O_3). The average crystalline size of the composites was calculated to be 7.64 nm (FeC-25), 4.39 nm (FeC-50), 8.44 nm (FeC-100), and 5.44 nm (FeC-170).

All the materials were applied in the removal of Cr(VI) ions and showed removal percentages in this order iron oxide (17%) < FeC-25 (49%) < FeC-50 (64%) < FeC-100 (75%) < FeC-170 (88%). This was due to the increased surface area and increased adsorption active sites as the amount of the OLNCs was increased. The kinetic data was better explained by the PSO kinetic model for the first 20 min of the reaction. An indication of chemisorption as a possible removal path was found for the Cr(VI) ions. The R^2 values for both the Langmuir and Fruendlich adsorption isotherms were close to unity. This indicated that the removal of Cr(VI) ions was through monolayer surface coverage and heterogeneous surface coverage.

The photocatalytic reduction of Cr(VI) to Cr(III) was conducted under light irradiation. The complete reduction took place in 15 min of light irradiation and this was aided by

the reduction ability of iron oxide and the electron donor groups from the OLNCs. This was followed by the adsorption of Cr(III) ions through the carbonyl groups from the OLNCs. After 30 min of irradiation, no Cr(VI) ions or Cr(III) ions were detected in the solution, and this indicated the synergy between iron oxide nanoparticles and the OLNCs derived from waste cooking oil. The photocatalyst was reused 5 times retaining 86% efficiency after the fifth cycle of reuse.

Generally, the OLNCs synthesized via the flame pyrolysis of vegetable cooking oil showed that they could be used as adsorbents for singular and binary pollutants. This was due to their surface functional groups. The ability of the OLNCs to reduce Cr(VI) to Cr(III) is advantageous because Cr(III) is less toxic than Cr(VI). This was due to its ability to act as an electron donor. The OLCNs showed a comparable Q^{o}_{max} with other carbon nanomaterials thus, making them a possible adsorbent for the adsorption process.

In composites with TiO_2 and FeOx nanoparticles, they showed great promise when combined with OLNCs to remove pollutants [(Cr(VI) and MO] via photocatalytic removal of Cr(VI) and MO. Their ability to act as an electron acceptor in composites is partly due to the decrease in the band gap of semiconductors and the decrease in the rate of e^-/h^+ recombination, resulting in improved photocatalysis.

In summary, the OLCNs have shown that carbon that can be synthesized without the use of a metal catalyst, with limited consumption of energy and chemicals, and without the use of high-temperature instruments has been used in wastewater treatment. An added advantage is that the OLNCs can be synthesized by using waste cooking as a carbon source. Thus, the study has shown that waste material can be used for the adsorption, reduction, and photocatalytic removal of organic and inorganic pollutants.

Appendix: *Supplementary data*

Chapter 4

Table S4.1: XPS elemental ID and quantification, BET analysis and point of zero charge (pH_{PZC})

Material	Name	Peak BE	Atomic %
OCNO	C1s	284.1	88.2
	O1s	532.3	11.8
Surface area	**Pore volume**	**Pore size**	**pH_{PZC}**
81.8 m^2/g	0.08 cm^3/g	4.2 nm	5.2

Table S4.2: Langmuir separation factor (R_L) for the adsorption of Cr(VI) ions on OCNO,s

Initial concentration C_o (mg/L)	R_L value
10	0.276
20	0.16
30	0.113
40	0.09
50	0.071
60	0.06
70	0.051
80	0.046
90	0.04
100	0.037

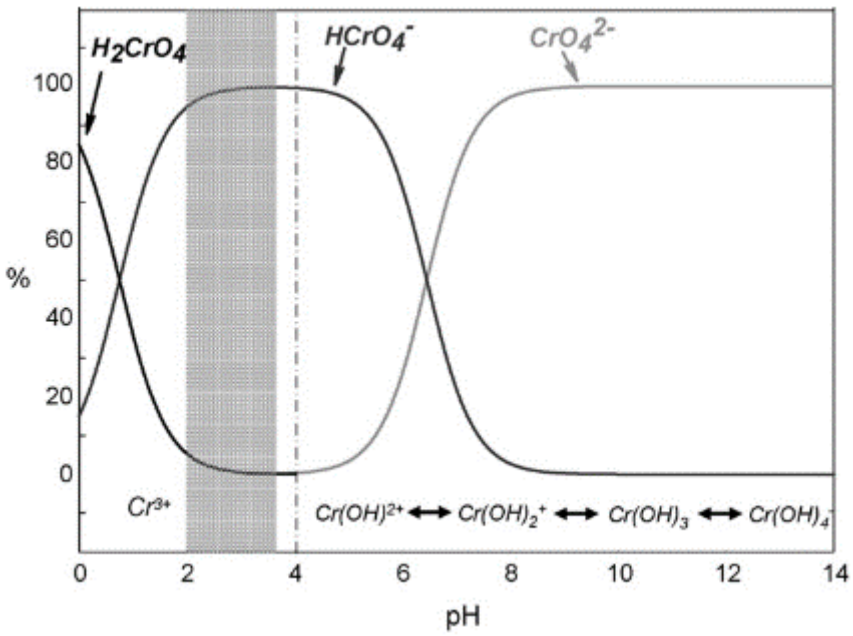

Figure S4.1: Speciation distribution diagram of Cr(III) and Cr(VI) in aqueous systems [49]

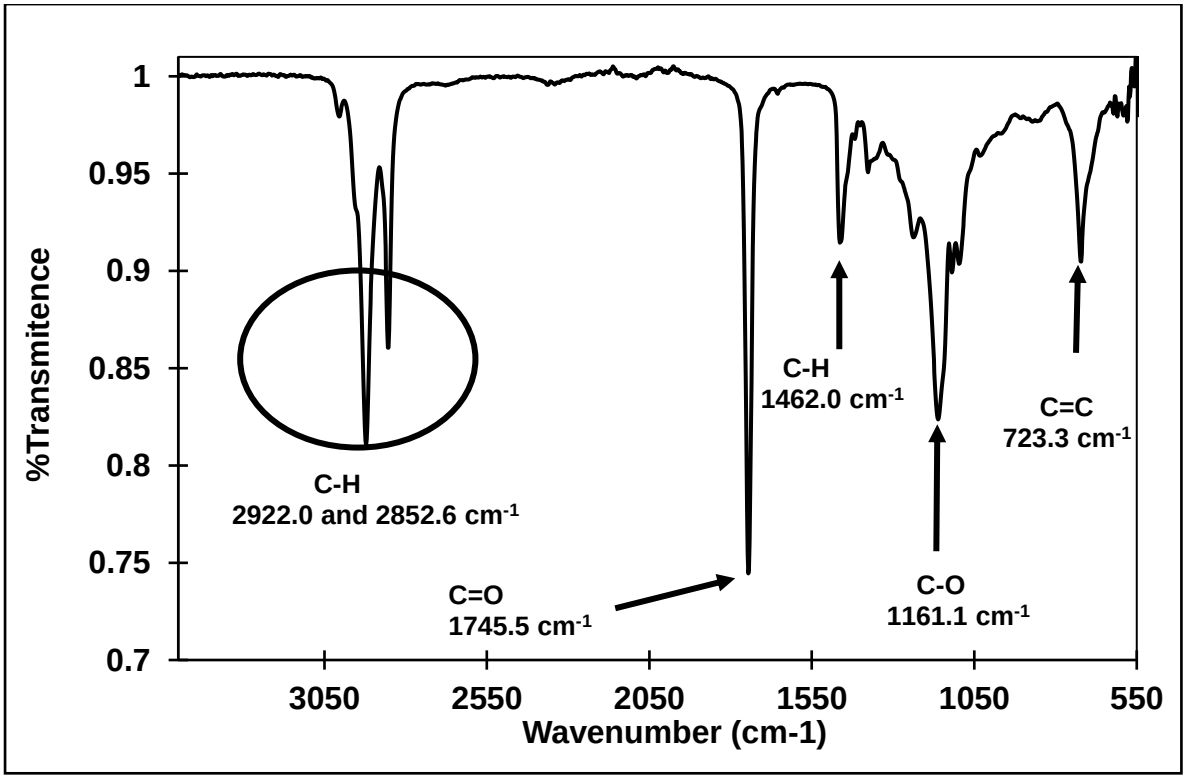

Figure S4.2: FTIR spectra of olive oil

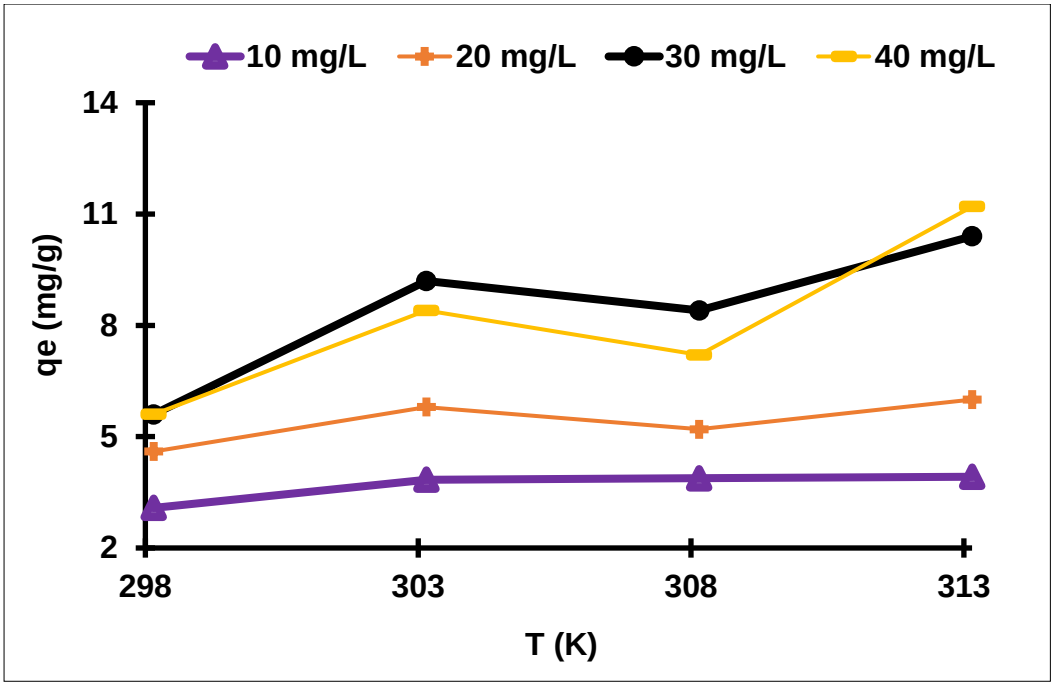

Figure S4.3: Effect of reaction temperature at the different initial concentrations for the removal of Cr(VI) ion by OCNOs.

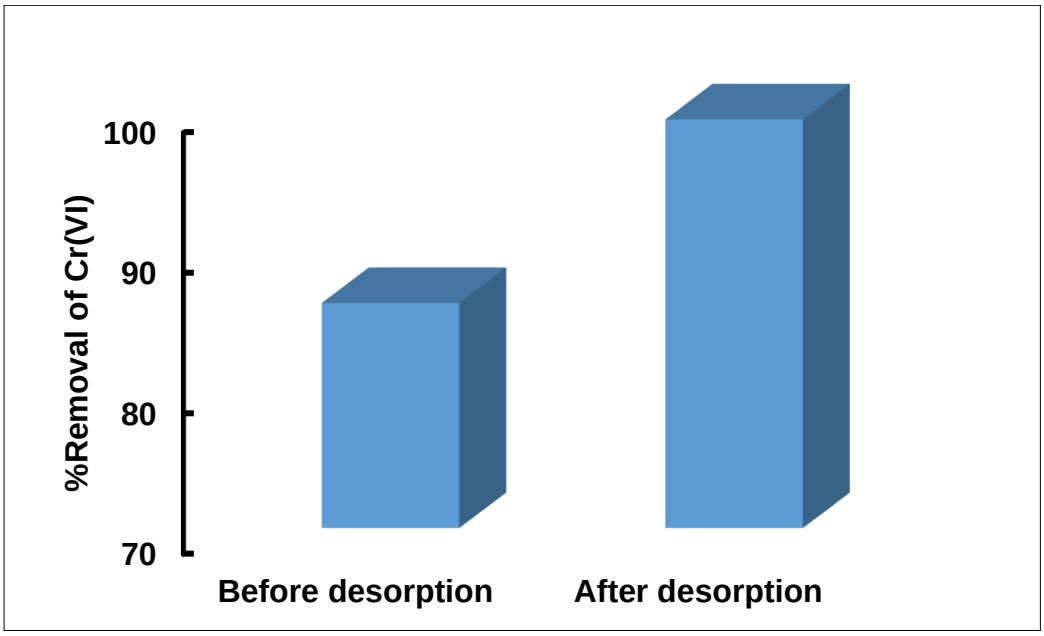

Figure S4.4: The regeneration of OCNOs using NaOH as a desorption solution.